Mapping Riparian Vegetation Functions Using Remote Sensing and Terrain Analysis

Leo Lymburner

Submitted in total fulfilment of the requirements of the degree of Doctor of Philosophy

December 2005

Department of Civil and Environmental Engineering

University of Melbourne

Abstract

Land use practices over the last 200 years have dramatically altered the distribution and amount of riparian vegetation throughout many catchments in Australia. This has lead to a number of negative impacts including a decrease in water quality, an increase in sediment transport and a decrease in the quality of terrestrial and aquatic habitats. The task of restoring the functions of riparian zones is an enormous one and requires spatial and temporal prioritisation. An analysis of the existing and historical functions of riparian zones and their spatial distribution is a major aid to this process and will enable efficient use of remediation resources. The approach developed in this thesis combines remote sensing, field measurement and terrain analysis to describe the distribution of five riparian zone functions: sediment trapping, bank stabilization, denitrification, stream shading and large woody debris production throughout a large semi-arid catchment in central Queensland. Each function is described in terms of an index that is derived by modifying published algorithms that describe these functions so that they can be calculated with spatial data. Each index describes on a scale of zero to one how active each function is at any location within the catchment, and, how the changes in the distribution and structure of riparian vegetation since European settlement have impacted on each function. Each riparian function index was calculated using biophysical attributes of the riparian vegetation and the dimensions of the adjacent stream channel. Each attribute was either measured in the field, or calculated from pre-existing data, and then linked to a classification of spatial data. This research uses recent developments in terrain analysis and image processing in combination with remote sensing imagery that is matched to the spatial and temporal scales of riparian zone phenomena. The parameters required to calculate the riparian function indices were reliably predicted, based on an independent set of field data.

The results of the riparian function indices indicate that there has been a large decrease in the sediment trapping capacity in 1500 hectares of riparian zones that are located on slopes >2% due to heavy grazing and land clearing in the riparian zone. There is also an increased risk of bank erosion with 25% of lower order stream banks devoid of any riparian vegetation. Removal of vegetation from the floodplain and riparian zones of higher order streams has also lead to a 50% reduction in the denitrification potential of riparian soils, and has removed the potential for future large woody debris recruitment from 2500 hectares of 3rd and 4th order stream bank. Stream bank clearing has also lead to an increase in the amount of sunlight reaching the surface of over 80% of 4th and 5th order streams, however 6th order streams are in relatively good condition with only 8% not receiving shade from woody vegetation. The approach developed in this thesis provides new insight into the spatial distribution of riparian zone functions throughout large catchments. It differs from previous approaches by enabling analysis that allows the user to select key riparian functions for an application and by using input data that can be obtained for large catchments in a cost effective manner.

Declaration

This is to certify that

(i) *the thesis comprises only my original work toward the PhD*

(ii) *due acknowledgement has been made in the text to all other material used,*

(iii) *the thesis is less than 100 000 words in length, exclusive of tables, maps, bibliographies and appendices.*

Leo Lymburner

Acknowledgements

The author wishes to thank Amanda Lymburner for her unswerving love and support throughout this thesis. The author would also like to acknowledge the feedback and guidance provided by the three supervisors, Peter Hairsine, Jeff Walker and Alex Held. My trusty field assistant Gavin Peck and Cameron Dougall were both invaluable in providing physical and moral support during long hot days on the Nogoa floodplain. There are also a number of other people who have provided me with valuable feedback on various ideas developed in this thesis including Kit Rutherford, Jacky Croke, John Quinn, Glenn Newnham, Ron de Rose, Paul Daniel, Chris Carroll, Tim McVicar, Tim Ellis and Alice Brown.

Alan Marks also provided valuable input both in terms of providing me with satellite imagery and by providing me with a unique perspective on the whole PhD process. I'd also like to thank Stephanie and Julian Lymburner for providing me with love and support during my formative years. I would also like to thank the staff of the Queensland Department of Natural Resource and Mines at Emerald for providing contacts and data. Finally, thanks go to my cat Zebbie for assistance in typing up this manuscript.

The authour would particularly like to thank the Cooperative Research Centre for Catchment Hydrology for the scholarship that supported this research, and for providing a valuable forum for vigorous discussions about the important science and management issues that relate to riparian zone science.

Table of Contents

List of Figures

List of Tables

List of Symbols

γ: bulk density

θ: angle

λ: number of trees per hectare

μ: average

ρ: density of water

σ: sediment density

ψ: ground cover coefficient

ω: unit stream power

Ωcr: stream power at which re-entrainment begins

a: amount of sunlight

B: blockage ratio

BH: bank height

c: material cohesion

c_r: material cohesion due to tree roots

C_{rad}: canopy radius

CSA: cross sectional area

CW: channel width

E: solar constant

F: Available stream power

g: acceleration due to gravity

I: number of sediment settling classes

K: dimensionless flow path factor

N: dimensionless stability factor

n: Manning's roughness coefficient

$NDNE$: number of denitrification events

OS: offset between top of bank and first tree

PFC: percentage foliage cover

PR: proportion of riparian vegetation

Pwh: probability of a waterhole

q: water flux per unit width

Q: discharge

Q_{bf}: bankfull discharge

R: hydraulic radius

S: slope

V: velocity

TH: tree height

v: settling velocity

$wood_A$: the volume of wood per hectare

WSC: water soluble carbon

x: soil depth range

List of Acronyms

ASTER: Advanced Spaceborne Thermal Emission and Reflection Radiometer

ANZECC: Australian and New Zealand Environment and Conservation Council

BRI: Bank Reinforcement Index

DN: Denitrification

DNI: Denitrification Index

LWD: Large Woody Debris

LWDI: Large Woody Debris Index

MODIS: Moderate Resolution Imaging Spectroradiometer

NDVI: Normalized Difference Vegetation Index

RVEW: Riparian Vegetation East West

SOC: Soil Organic Carbon

SR: Simple Ratio

SRTM: Shuttle Radar Topography Mission

SSI: Stream Shading Index

SSV: Stream Shading Vegetation

STI: Sediment Trapping Index

WHC: Water Holding Capacity

WSC: Water Soluble Carbon

Chapter 1 Introduction

1.1 Introduction

This thesis develops a methodology for assessing the impact of riparian vegetation on protecting waterways and their surrounding environment using a combination of satellite imagery, field data, terrain information, and stream channel characteristics. This is a pioneering cross disciplinary thesis on the use of spatial data for riparian assessment.

The native trees and grasses[1] beside rivers and streams (riparian vegetation) protect waterways and their surrounding environment: by reducing the amount of pollution entering the stream, and providing habitat for wildlife living next to and within the stream. To manage riparian vegetation effectively, and maximise the protection it affords, it is necessary to understand where in a catchment the riparian vegetation will provide the greatest protection. Fieldwork was carried out in the riparian vegetation and channels of streams and rivers within the study area to identify the existing riparian vegetation and stream channel characteristics. The satellite imagery and terrain information were used to extend these fieldwork observations to estimate what the riparian vegetation was like elsewhere within the study area.

The key outcome of this thesis is new information that 1. quantifies how riparian vegetation in different parts of the landscape is important in providing the following functions: sediment trapping, bank reinforcement, denitrification, large woody debris production and stream shading and 2. quantifies how changes to riparian vegetation since pre-European times have impacted on these five functions. This new information will enable the prioritisation of resources towards restoring riparian vegetation in critical areas, and ensuring the preservation of important pieces of riparian vegetation that are under threat by human activities.

1.2 The Functions Provided by Riparian Vegetation

At the catchment scale riparian vegetation provides the important functions described in Table 1.1. Although riparian vegetation only occupies a relatively small area of the landscape, its unique location at the interface between the terrestrial and aquatic environment means that it plays an important role in maintaining both the terrestrial and aquatic ecosystems. Human activity can impact on all of these riparian functions both directly and indirectly. Direct human impacts on riparian function include removal of riparian vegetation, damage to riparian vegetation by recreational vehicles, logging activities, grazing and land clearing. Indirect human impacts include weed invasion, feral animal activity, altered hydrologic regimes, increased salinity, altered fire frequency, and increased nutrient and sediment loads.

---

[1] Non-indigenous species can be deleterious, altering bank stability and leaf litter dynamics (Read and Barmuta, 1999).

Table 1.1 The functions performed by riparian vegetation and buffer strips

Function	Description
Hydrological functions	rainfall interception, hydraulic resistance to overland flow and floods
Geomorphic functions	sediment trapping, bank stabilization/reinforcement,
Geochemical functions	denitrification, trapping nutrients associated with fine particles
Terrestrial Ecological functions	habitat for various avian, mammalian, and herpetofauna, habitat corridors
Aquatic Ecological functions	providing shade for streams and waterholes, providing a source of food via litter fall, and providing habitat via root mats and large woody debris

The functions performed by vegetation in riparian zones are important because they combine to achieve the following outcomes:

- Providing large woody debris to the floodplain and to the stream channels. Large woody debris can have a number of positive influences including:
    - Providing hydraulic diversity, and thereby providing a range of in-stream habitats within close proximity (Marsh *et al*., 2001).
    - Providing visual protection from avian and piscatorial predation (Crook and Robertson, 1999).
    - Providing stable substrate for biofilms, and providing an egg laying site for a range of native fish species (Marsh *et al*., 2001).
    - Reducing near-bank flow velocities, and thereby increasing bank stability (Abernethy and Rutherfurd, 1998).
    - Playing an important role in floodplain geomorphology, leading to channel abandonment, and the formation of new waterholes (Tooth and Nanson, 2000).
- Reducing the amounts of sunlight reaching the stream surface. This can have the following positive influences:
    - Maintaining the trophic state of the stream, thereby reducing excessive algal growth (Sponseller *et al*., 2001).
    - Reducing fluctuations in stream temperature, and thereby reducing fluctuations in pH and dissolved oxygen, which in turn ensures a stable environment for aquatic organisms (Bunn *et al*., 1999).

- Reducing the amounts of sediment (both hillslope, and stream bank sediment) entering the stream network. This provides a range of benefits including:
    - Reducing the turbidity and hence improving the aquatic environment for native fish species (Crook and Robertson, 1999), and improving the quality of drinking water available to stock.
    - Reducing sedimentation of waterholes improving the aquatic environment for native fish species (Prosser *et al*., 2001).
    - Improving the lifespan of water reservoirs by reducing sediment inputs (Prosser *et al*., 2001).
    - Improving the quality of water leaving the river mouth and entering the receiving waters (either lakes or estuaries), with numerous benefits for these near-shore environments (Johnson *et al*., 1999).
- Reducing the amount of pollutants entering the stream network from adjacent land uses. This can produce a range of benefits including:
    - Reductions in the eutrophication of in-stream and receiving waters (Brodie and Mitchell, 2005).
    - Improved water quality for stock and human consumption, with benefits including improved human health outcomes (Agrawal *et al*., 1999; Basnyat *et al*., 1999).
    - Improved in-stream water quality with numerous benefits for the aquatic ecosystem, both in-stream, and in the receiving waters (Johnson *et al*., 1999).

1.3 Statement of Problem

The riparian vegetation functions listed above dominate in different parts of the catchment depending on the climate, terrain and flow characteristics of the catchment. However there is currently no means of quantifying where each process is important or quantifying how changes to riparian vegetation have impacted on these functions. Consequently, the spatial distribution of riparian functions and the pressures placed upon those functions by human activity remains a significant gap in knowledge.

Information about the spatial distribution of the ecological, geomorphic, hydrologic and geochemical functioning of riparian zones is needed from both a scientific and resource management perspective. Information about the distribution of riparian vegetation functions throughout a catchment is required from a scientific perspective to assist in designing experiments that will better quantify the catchment scale functions of riparian vegetation. This information can also be used to improve the representation of riparian vegetation functions within existing catchment-scale sediment and pollutant transport models such as SEDNET (Prosser *et al*., 2001).

Information about the spatial distribution of riparian vegetation, how that riparian vegetation functions, and how human activity can impact or improve these riparian functions is also required to inform catchment management decisions. To meet goals such as 'end of valley' reductions in sediment and pollutant loads, catchment managers need to know i) where planting or restoring riparian vegetation will have the greatest effect in reducing sediment and pollutant loads, and ii) where existing riparian vegetation is providing valuable sediment and pollutant buffering functions, and needs to be protected. Management decisions are currently limited by a paucity of such information. The approach developed in this thesis provides this information using recent developments in terrain analysis and image processing in combination with remote sensing imagery that is matched to the spatial and temporal scales of riparian zone phenomena.

1.4 Research Objective and Scope

The overall objective of this thesis is to develop a methodology that quantifies the multiple functions performed by riparian vegetation across large catchments. To meet this objective a number of key science questions are addressed:

1. Where within a large catchment is riparian vegetation functioning to trap sediment, stabilise banks, remove nitrate, provide shade and provide large woody debris?
2. How do these functions vary in terms of importance throughout the catchment?
3. How has the capacity of riparian vegetation to perform these functions changed as a result of European human activity?

The primary objective of this research was to address these questions by combining remote sensing and terrain analysis to describe the spatial and temporal distribution of riparian vegetation functions. The remote sensing and terrain analysis techniques used were developed with two main criteria in mind. First, that they represented the riparian vegetation dynamics at an appropriate spatial and temporal scale and second, that they could be applied in a cost-effective fashion to large (>10 000km^2) catchments. The approach described in this thesis could be applied to the riparian zones of other semi-arid catchments that are subject to grazing and cropping. However it is beyond the scope of this research to develop a generic methodology that could be applied to any riparian zone adjacent to any land use without modification.

1.5 Outline of Approach

The approach taken in this thesis was to identify the full range of riparian functions based on a review of the current literature. A subset of these functions have been described in the literature in terms of models or algorithms, which can be modified, based on a series of assumptions, into a series of riparian function indices that can be calculated using spatial data. This subset was constrained by the capacity to establish a statistical relationship between the parameters required to calculate the indices and a classification of spatial data. Consequently this thesis consists of the following steps.

1. Describe a series of riparian function indices (RFIs) that represent various riparian zone functions.
2. Identify the parameters required to calculate the riparian function indices (RFIs) and identify which classification of spatial data each parameter will be linked to.
3. Classify the spatial data (moderate spatial resolution satellite data, low spatial resolution multi-temporal data and digital elevation models).
4. Evaluate the reliability with which each parameter was predicted by their respective classifications using an independent set of field data.
5. Calculate the RFIs using the spatial parameters.
6. Evaluate the reliability of the RFIs based on the reliability of the parameters required to calculate each RFI.
7. Discuss the capacity for using the RFIs to inform riparian zone management decisions at the catchment scale.
8. Discuss the potential to incorporate the RFIs into existing catchment scale sediment and pollutant transport models.

These steps are shown in Figure 1.1 The methodology developed for mapping RFIs was undertaken in the Nogoa and Comet subcatchments of the semi-arid Fitzroy catchment in Queensland, Australia. The parameters used to calculate the RFIs in these catchments were either i) derived from field measurements at a series of locations, or ii) calculated from pre-existing datasets. The accuracy of the parameter extrapolation was validated by comparing the predicted parameters against observations made at an independent set of field sites. In addition to the field data collected as part of this research, stream channel cross-sections and stage height records supplied by the Queensland Department of Natural Resources and Mines, and stream channel geometry and riparian vegetation data from the State of the Rivers Reports (Henderson, 2000) were used to provide additional data about the vegetation structure, channel geometry and flow characteristics within the study area.

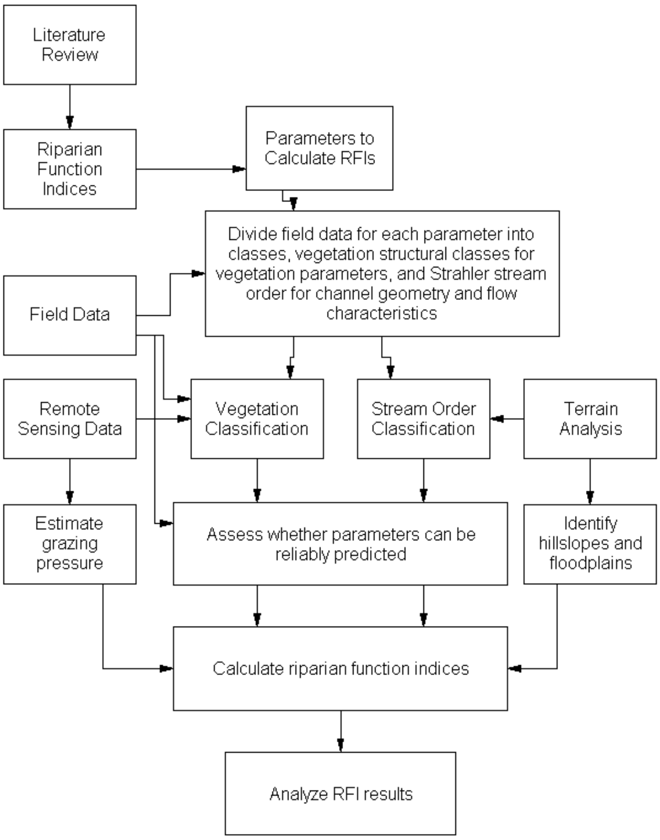

Figure 1.1 Flowchart showing research design

1.6 Thesis Organisation

The research embodied in this thesis is divided up into eight chapters. Chapter 2 identifies which riparian functions can be assessed using spatial data based on a review of the literature. An index for each riparian function that can be described using spatial data is also developed. These indices are calculated for a study area, which is described in terms of land use, climate, hydrology and vegetation in Chapter 3. Chapter 3 also describes the fieldwork that was undertaken to measure the parameters that are used to calculate the RFIs, and describes how the field data were processed and separated into calibration and evaluation datasets. These calibration and evaluation datasets are used in Chapter 4 to describe the range of values observed for each parameter in the field, and to assess the reliability with which each parameter could be predicted across the catchment. It was not possible to make direct measurements of some parameters required to calculate the RFIs. For these parameters it was necessary to use either pre-existing datasets or literature values, the suitability of which is also discussed in Chapter 4. Chapter 5 details the spatial data that were used to predict the parameters, with a brief description as to why certain data types were used, and the advantages and limitations of those data types. Chapter 5 also describes how the classifications used to predict the parameters were generated using remote sensing and terrain analysis, with some discussion of the methods used, and the difficulties encountered.

Chapter 6 presents the indices and their reliability assessment based on the reliability of the parameters. The index results are presented both as spatial maps, and as summary statistics in terms of the range of each index value observed for each Strahler stream order. The usefulness of the proposed methodology for understanding the contextual importance and impact of riparian functions, and the potential for application to other areas is discussed in Chapter 7. In addition, Chapter 7 describes the potential to combine indices to focus on specific catchment processes, and identify an integrated riparian management plan that can be tailored to meet catchment scale land management and water quality goals. The conclusions made about using remote sensing and terrain analysis to map riparian vegetation structure and function are contained in Chapter 8. This chapter also details the conclusions drawn from the analysis of the riparian function indices, and identifies areas for future research.

Chapter 2 Defining Riparian Function Indices

2.1 Introduction

This chapter describes how some of the hydrologic, geomorphic, biochemical and ecological functions of riparian zones can be quantified using indices. These indices are based on published verbal and numerical descriptions of each function. The process of defining each riparian function index (RFI) has a series of steps.

1. A physically-based, numerical description of a riparian function is identified from the current literature.
2. The numerical description of each function is modified into an index that can be calculated from parameters which can be predicted using spatial data, based on a series of assumptions.
3. Each index is defined in terms of how that riparian funtion has changed since pre-European times, and in terms of where within the catchment each function is most important.

The 'index' approach has been used in this thesis because it encapsulates the existing knowledge about riparian zone functions and allows information about the spatial distribution of these functions to be calculated from a series of classifications that are generated from satellite imagery and terrain analysis.

The functions performed by riparian vegetation operate at a range of temporal and spatial scales. The indices are constructed from studies in the literature that describe the process at a small (1-10 metres) scale. Each index is calculated using parameters that can be measured, or calculated at this small scale. The parameters are either measured in the field or calculated from the field data. Each parameter is then statistically linked[2] to one of three classification systems: a vegetation classification, an estimate of grazing pressure, or a stream order classification. A summary table of the parameters required to calculate the indices, and the classifications they are linked to is presented at the end of the chapter. There are two forms of each index. The local form, RFI_{local}, as seen in Equation (2.1), uses a local reference point that compares the existing riparian vegetation with the riparian vegetation that would have existed at the same location prior to European settlement. The global form, RFI_{global} as seen in Equation (2.2), uses a 'global' or catchment scale reference point that compares the function performed by the existing riparian vegetation with the maximum amount of that function being performed anywhere within the catchment at present.

---

[2] Described in detail in Chapter 4

2.1.1. RFI_{local}

The local form of each riparian function index is calculated by comparing the function of the existing riparian zone with a reference riparian zone.

$$RFI_{local} = \left(\frac{\text{Function performed by existing riparian zone}}{\text{Function performed by the riparian zone in 1780}} \right) \qquad (2.1)$$

The reference riparian zone is the riparian zone at that location prior to European settlement (referred to as 1780 vegetation by Carnahan (1989)). So if the riparian zone at a specific location has similar vegetation to that encountered at that location prior to European settlement, then the RFI_{local} will have a value of one. However, if the vegetation has been altered then the RFI_{local} will be less than one, and if all woody vegetation has been removed then some of the RFIs will have a value of zero. The RFI_{local} quantifies how the riparian function provided by a stand of vegetation at a particular location in the channel network has changed as the result of removal or alteration of riparian vegetation. Indices calculated based on a local reference point can be considered 'restoration' indices insofar as, with the right restoration practices, and time, every riparian zone throughout the stream network could theoretically attain an index value of one.

The use of a local reference presents some challenges in terms of knowing what the riparian vegetation was like at a certain location prior to European settlement. The map of 1780 vegetation presented by Carnahan (1989) is too coarse for the purposes of this thesis because it doesn't include the narrow strips of riparian vegetation that provide the functions that are of interest in this thesis. The vegetation maps contained in the Land Unit Series (Gunn *et al*., 1967) which were generated during land capability surveys carried out in the 1950s and 1960s are also to coarse for the purposes of this thesis, insofar as they describe the riparian vegetation of some of the larger rivers, but do not detail the distribution of the littoral vegetation. However their descriptions of the riparian vegetation encountered during their surveys are detailed and are contained in Gunn *et al.* (1967) and Story *et al.* (1967). Their descriptions have been simplified into a general description of the pre-European riparian vegetation that coincides with the vegetation classification system used in this thesis, which is based on the structural classification system described in Specht (1970) and described in detail in Section 3.3.

2.1.2. RFI_{global}

The behaviour of each riparian function at the catchment scale is captured by comparing the function performed by the existing vegetation at a location within the stream network with a 'global' reference value that represents the maximum amount of that function being performed anywhere within the catchment by current vegetation. The calculation of the 'global' RFI is shown in Equation (2.2).

$$RFI_{global} = \left(\frac{\text{Function performed by existing riparian zone}}{\text{Maximum function performed by existing riparian zone}} \right) \qquad (2.2)$$

The RFI_{global} index values represent a 'prioritization' or 'conservation' index because they identify areas within the catchment where certain stands of vegetation are performing the maximum amount of a function, and it is these stands of vegetation that are likely to be of high conservation value. RFI_{global} values close to one indicate areas where the process is most dominant within the catchment, and values close to zero indicate areas where the process is of lower importance. The RFI_{global} places the function performed by stand of vegetation into spatial context (at the catchment scale), whereas the RFI_{local} places the function performed by a stand of vegetation into a historical context.

The short term (yearly) temporal behaviour of the riparian zone functions is not explicitly described by the riparian function indices, however the parameters used to calculate the indices do encapsulate some of the temporal variability within the system. Consequently the index results need to be interpreted with an understanding of the different temporal scales at which each process operates.

Table 2.1 lists the riparian functions that are quantified using the RFI approach. These functions were chosen because they represent a cross section of the hydrological, geomorphic, biogeochemical and ecological functions performed by riparian vegetation. These functions were also chosen because published algorithms that describe these processes on a physical basis were suitable for modification into RFIs. The sediment trapping function of riparian vegetation is important because land use changes have lead to increased hillslope erosion in many areas throughout the world, and riparian buffers provide a valuable means of preventing sediment generated via hillslope erosion from entering into the river network (Deletic, 2001). The bank reinforcement capacity of riparian vegetation is important because stream bank erosion constitutes another major source of in-stream sediment, and maintaining/restoring riparian vegetation is one of the few aspects of bank erosion that can be directly managed (Abernethy and Rutherfurd, 1998). The potential for denitrification in riparian zone soils is of particular interest because it provides a mechanism whereby potentially harmful nitrate is converted into

Table 2.1. A list of the riparian function indices described in this chapter

Type of function	Riparian Function Index
Geomorphic	Sediment Trapping Index (STI)
	Bank Reinforcement Index (BRI)
Biochemical	Denitrification Index (DNI)
Ecological	Stream Shading Index (SSI)
	Large Woody Debris Index (LWDI)

atmospheric nitrogen gas and removed from the river network completely, potentially mitigating upslope or upstream pollution (Hill *et al*., 2000). The capacity of woody vegetation to provide large woody debris and shade to the stream channel are also important because they maintain the in-stream aquatic environment by maintaining the trophic state of the stream and providing a diverse range of habitats (Rutherford *et al*., 1997), in addition, large woody debris can alter in-stream hydraulics and rates of bank erosion (Gurnell *et al*., 2002). Each of these functions have been the focus of numerous previous studies at the stream reach and hillslope scale, and the distribution of these functions at a catchment scale in some previous studies, notably bank stabilization (Abernethy and Rutherfurd, 1998) and stream shading (Poole and Berman, 2001). However, to the authors knowledge, the approach developed in this thesis is unique in its use of remote sensing data that is matched to the spatial and temporal dynamics of riparian zone phenomena in combination with recent developments in terrain analysis and image processing to generate a suite of indices that describes the multiple functions performed by each stand of riparian vegetation throughout a large (>10 000km^2) catchment.

Understanding the spatial distribution of riparian vegetation capable of performing these functions, and understanding where within the catchment each process is most active is important. It is important because, while management activities can restore or maintain these functions, the cost of implementing these management actions is large, and the resources available are limited. Consequently it is important to identify exactly where particular management actions are likely to have the greatest effect in restoring or maintaining a specific function. This is particularly important in large catchments that drain into near-shore environments that are sensitive to sedimentation and eutrophication.

In addition to the indices listed in Table 2.1 a number of other RFIs were initially considered in this thesis. They were the pollutant trapping index, the overland flow interception index, the flood resistance index and the habitat fragmentation indices, as described in the Appendices. They are not considered further in this thesis due to difficulties associated with data collection, data processing, or index calculation.

2.1.3. Definitions

The term ‘riparian zone’ means different things to different people, and a comprehensive review of the different definitions of ‘riparian zone’ is contained in Verry *et al.* (2004). For the purposes of this thesis riparian vegetation is an inclusive term that refers to both littoral vegetation (vegetation within fifteen metres of the stream bank) and floodplain vegetation, as shown Figure 2.1. Littoral vegetation refers to vegetation immediately adjacent to the channel, and floodplain vegetation refers to vegetation on the floodplain. Similarly, the term ‘riparian zone’ refers to everything from the extent of historical flooding on one side of the valley to the extent of historical flooding on the other.

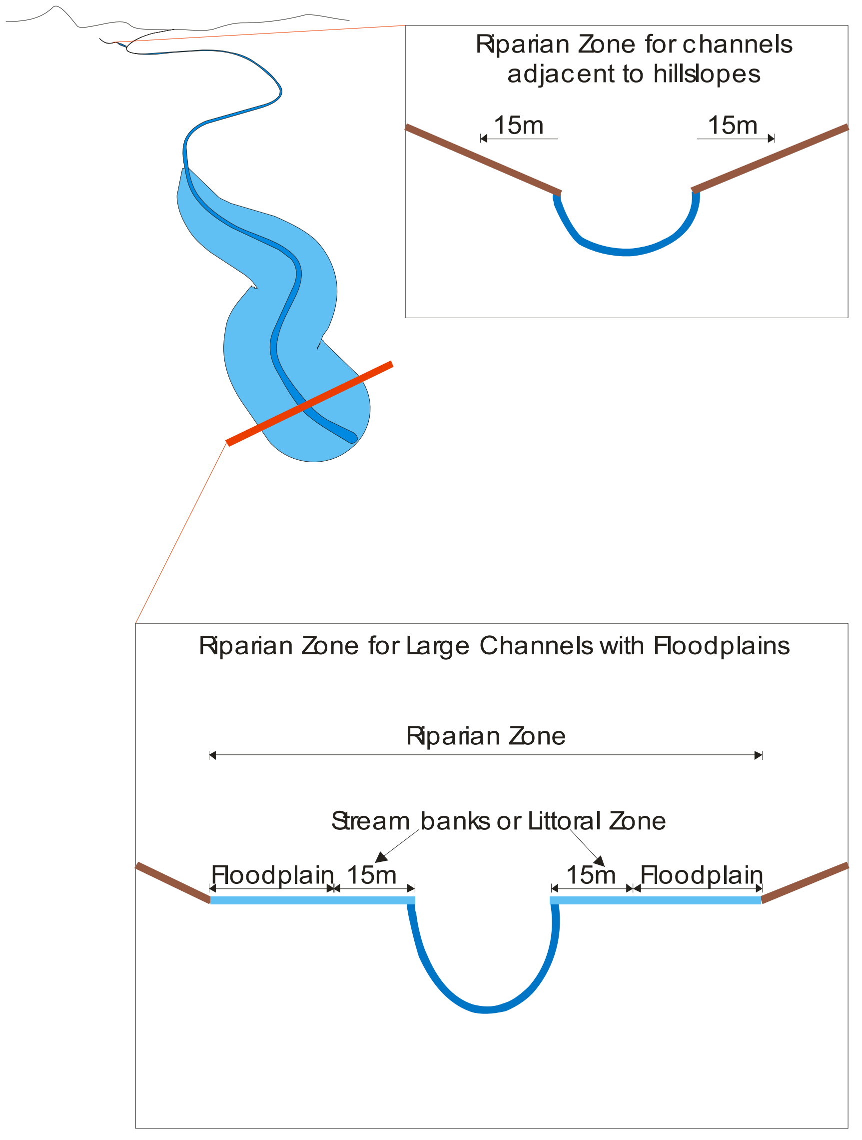

Figure 2.1 Two channel cross sections showing terminology used throughout this thesis.

For small streams the riparian zone and the littoral zone are synonymous, however on larger rivers the riparian zone contains both the littoral zones and the floodplains on either side of the channel. To avoid confusion, all areas within fifteen metres of the channel are referred to as littoral zones. Areas where hillslopes are drain directly into the channel and no floodplain is present the area within fifteen metres of the channel is referred to as hillslope littoral zones as shown in Figure 2.1. For larger rivers that have floodplains, the area fifteen metres either side of the channel is referred to as the floodplain littoral zone, and the floodplains are referred to as floodplains.

2.2 Sediment Trapping Index

Riparian zones act to buffer streams from sediment and pollutants carried by shallow overland flow from adjacent hillslopes (Vought *et al*., 1995; Loch *et al*., 1999; McKergow *et al*., 2003). The ground cover in riparian zones can act to trap sediment carried in overland flow. Numerous studies have shown that the reduction in flow velocity created by roughness elements in the overland flow path reduces the sediment transport capacity, which leads to the deposition of sediment (Prosser *et al*., 1995; Muñoz-Carpena *et al*., 1999; Carroll *et al*., 2000; Deletic, 2001; Rose *et al*., 2002). These studies are often based on field based studies or mathematical models that represent a vegetated filter strip. The efficiency of vegetated filter strips (VFS) in terms of trapping sediment is related to a number of factors including the length, slope, roughness (often expressed in terms of the roughness coefficient Manning's n) and infiltration rate (Hairsine and Rose, 1992a; Loch *et al*., 1999; Deletic, 2001; McKergow *et al*., 2003).

This function is important because it reduces the sediment and sediment-sorbed pollutant loads entering the streams, thereby improving the downstream water quality and increasing stream health. This function is also important because it reduces sediment exports from coastal catchments into near shore waters, thereby protecting estuaries and near-shore habitats from excessive sedimentation rates (Johnson *et al*., 1999). Consequently, information about the spatial distribution of the sediment trapping capability of existing riparian vegetation is of value.

Sediment transport happens at a range of micro-meso scales, from raindrop impact, aggregate breakdown, entrainment and re-entrainment at a scale of millimeters (Hairsine and Rose, 1992a) to the sheet and rill erosion processes operating at a scale of meters (Hairsine and Rose, 1992b). Sediment transport processes at this scale have been the focus of a number of studies (Hairsine and Rose, 1992a; Hairsine and Rose, 1992b) (Vought *et al*., 1995; Palis *et al*., 1997; Loch *et al*., 1999; McKergow *et al*., 2003). Data is not available at a catchment scale to drive sediment transport models that are based on millimetre scale sediment transport processes for each riparian zone, but the processes that operate at this scale can be represented in a sediment trapping index (STI). This index describes the sediment transport capacity of the current riparian zone in terms of a 'reference' riparian zone that contains a high amount of ground cover. The derivation of the STI from published sediment transport equations is described below.

Hairsine and Rose (1992a) presented Equation (2.3) for sediment concentration in shallow overland flow when the factor limiting sediment concentration is transport, rather than supply.

$$c_t = \frac{FK^{\frac{1}{m}} \dfrac{\sigma}{\sigma-\rho}}{\dfrac{1}{I}\sum_{i=1}^{I} v_i} \left[\rho S q^{1-\frac{1}{m}} - \frac{\Omega_{cr}}{g q^{\frac{1}{m}}} \right] \tag{2.3}$$

Where F is the available stream power, K is a dimensionless factor expressing flow path in the Manning's or Chezy equations, m is 5/3 or 3/2 depending on whether you use the Manning's or Chezy equations to describe kinematic flow, σ is the sediment density, ρ is the density of water, v_i is the settling velocity of sediment size class i, I is the number of sediment size classes, S is the slope, g is the acceleration due to gravity, q is the water flux per unit width and Ω_{cr} is the stream power at which re-entrainment begins.

This expression assumes that sediment transport is limited by the ability of overland flow to re-entrain the sediment. The transport limiting case has been chosen because the shallow overland flow and associated sediment entering the riparian zone is hill slope generated. Assuming that the shallow overland flow sediment carrying capacity is not supply limited, then the re-entrainment and transport of that sediment is only limited by the transport capacity of the flow. The hydraulically rough surface encountered in vegetated riparian zones reduces the sediment transport capacity of the flow, thereby enabling the riparian zones to act as sediment traps.

The sediment trapping index (STI) describes the sediment trapping capacity of the current riparian zone (STC^{current}) in terms of a 'reference' riparian zone that contains a high amount of ground cover ($STC^{\text{reference}}$) which can be calculated using

$$STI = \frac{STC^{\text{Current}}}{STC^{\text{Reference}}} . \tag{2.4}$$

The total flux of sediment passing through a unit width of the riparian zone, where width is measured parallel to the stream is the product of the overland flow transport potential per unit width (q) and the concentration at the sediment concentration at the transport limit c_t as described by Equation (2.3).

$$STC = qc_t \tag{2.5}$$

combining Equations (2.3), (2.4) and (2.5) gives

$$STI = \frac{\left\{ \dfrac{FK^{\frac{1}{m}} \dfrac{\sigma}{\sigma-\rho}}{\dfrac{1}{I}\sum_{i=1}^{I} v_i} \left[\rho S q^{2-\frac{1}{m}} - \dfrac{q^{1-\frac{1}{m}}\Omega_{cr}}{g} \right] \right\}^{\text{Current}}}{\left\{ \dfrac{FK^{\frac{1}{m}} \dfrac{\sigma}{\sigma-\rho}}{\dfrac{1}{I}\sum_{i=1}^{I} v_i} \left[\rho S q^{2-\frac{1}{m}} - \dfrac{q^{1-\frac{1}{m}}\Omega_{cr}}{g} \right] \right\}^{\text{Reference}}} \tag{2.6}$$

From Manning's equation we know that

$$K = \frac{S^{\frac{1}{2}}}{n} \tag{2.7}$$

where n is Manning's hydraulic roughness factor.

Equation (2.6) can be simplified using the following steps

1. By cancelling constant terms that are common to both the numerator and denominator, m the constant in the Manning's equation, ρ the density of water, σ the sediment density, and g the acceleration due to gravity.
2. Assume that the slope S in the riparian buffer strip hasn't changed due to the presence/absence of riparian vegetation, and is therefore common to both terms.
3. Assume that the runoff generated by the hillslope q hasn't changed. This assumption is likely to be violated in areas where cropping or grazing practices have altered the infiltration rate of the soil (Connolly *et al*., 1997). If the assumption that q hasn't changed is accepted, then the available stream power F will also remain unchanged.
4. Assume that the sizes of each sediment size class i is unchanged. This assumption will be violated if land use practices have altered the strength of the soil aggregates, and thereby altered the proportion of sediment in each size class, leading to an increase in the proportion of sediments in the finer sizes (Blair and Crocker, 2000).
5. A further assumption is that Ω_{cr} is constant. This is based on the assumption that the stream power threshold required to transport sediment is constant in both scenarios. If upslope land use practices lead to a reduction in soil aggregate strength, then Ω_{cr} may be lower because of the presence of smaller sediments in the sediment size distribution. If this was to occur then the assumption of constant Ω_{cr} would be violated, leading to potential overestimates, or underestimates in the value of STI depending on the nature of the land use change. The potential for land use change is not incorporated into the STI, so if all the other assumptions are accepted then the expression for STI can be described by

Based on these assumptions the expression for STI can be reduced to

$$STI = \frac{n_{rz}^{\text{Current}}}{n_{rz}^{\text{Reference}}}. \tag{2.8}$$

The Manning's n values used to calculate this index are described in Section 4.2.

The STI as described in Equation (2.8) assumes that the capacity of the riparian zone to trap sediment is dependent solely on the Manning's n of the riparian zone, irrespective of the magnitude or sequence of erosion events that may occur. Thus the capacity of the riparian zone to trap sediment without changing its hydraulic roughness is assumed to be limitless. This assumption may be violated when the riparian zone is very narrow in comparison to the contributing hillslope length or when time between events is insufficient to permit the vegetation to assimilate the sediment and grow back to reinstate hydraulic roughness (Karssies and Prosser, 1999).

The other assumption of the STI is that all overland flow leaving the hill slope passes through the riparian zone with its associated roughness characteristics. In practice, preferential flow pathways, such as roads, stock tracks and stock watering points enable overland flow to bypass riparian filters. The impact that these assumptions have on the reliability of the STI results is discussed in Section 6.2.

Overland flow from hill slopes travels down slope through riparian zones (Rustomji and Prosser, 2001). Thus, in small streams that are adjacent to hillslopes (coupled streams *sensu* Church (2002)), ground cover in the riparian zone filters overland flow entering the riparian zone from the adjacent hillslope. For larger streams with floodplains, the floodplains often separate the hillslope from the main channel. In these areas the slope S of the riparian zone is zero for both the actual and reference case, and Equation (2.3) predicts limited overland flow if the slope is close to zero. Consequently the STI is only calculated for riparian zones within the catchment that are both adjacent to hillslopes and adjacent to the channel (hillslope littoral zones as seen in Figure 2.1).

It is worth noting that riparian filter strips can be established in a relatively short time frame (months). This is important to keep in mind when comparing the STI to other riparian zone functions that can take considerably longer to re-establish.

2.3 The Bank Reinforcement Index

Littoral[3] vegetation reinforces stream banks by altering the hydrology and mechanical strength of the stream bank (McKenney *et al*., 1995; Abernethy and Rutherfurd, 1998; Abernethy and Rutherfurd, 2001). The following mechanisms strengthen the stream bank:

1. Canopy cover intercepts rainfall, thereby reducing rain splash and soil moisture levels;
2. Canopy cover also reduces soil desiccation and frost heave;
3. Evapotranspiration increases the matric suction of the soil[4], and;
4. Roots, both coarse and fine, increase the shear strength of the soil (Abernethy and Rutherfurd, 2001; Simon and Collison, 2002).

The weight of littoral vegetation increases surcharge on the littoral soil, this can either strengthen or weaken the bank depending on the circumstances. Under certain circumstances littoral vegetation can also act to weaken the bank, for example: flow concentration down plant stems and through soil macropores can create localised areas of high pore water pressure; and the increased surcharge of vegetation can lead to increases in shear stress (McKenney *et al*., 1995; Simon and Collison, 2002). Most authors report, however, that strengthening effects significantly outweigh the detrimental effects of littoral vegetation on bank stability (McKenney *et al*., 1995; Abernethy and Rutherfurd, 1998; Abernethy and Rutherfurd, 2001; Simon and Collison, 2002).

The dominance of the bank strengthening processes depends on the position in the catchment (Abernethy and Rutherfurd, 1998). The study of Abernethy and Rutherfurd (1998) describes the dominance of destabilising influences in the Latrobe catchment *i.e.* sub-aerial processes such as frost heave and soil desiccation dominate in the upper parts of the catchment; fluvial entrainment dominates the mid sections of the catchment and mass failure dominates the lower section of the catchment. Their study also describes how littoral vegetation protects stream banks from these bank erosion processes in different parts of the catchment.

The reduction in bank erosion afforded by littoral vegetation is particularly important because stream bank erosion is one of the three major sources of in-stream sediment (along with hillslope erosion and gully erosion) (Prosser *et al*., 2001), and can be the dominant source of in-stream sediment for some catchments (Prosser *et al*., 2001).

[3] The term 'littoral' here refers to woody vegetation immediately adjacent to the channel as shown previously in Figure 2.1, this is referred to by some other authors as riparian vegetation.
[4] This is of particular importance in semi-arid environments, where banks are often un-saturated, and the loss of matric suction is a leading cause of bank failure (Simon and Collison, 2002)

Stable stream banks area also important from an ecological point of view because they provide habitat for a range of species such as: the platypus (*Ornothorynchus anatinus*) (Serena *et al*., 1998); and various salmonid species (Armstrong *et al*., 2003).

In the latest version of SEDNET, Wilkinson *et al*. (2005) quantifies the impact of littoral vegetation on bank erosion using the *PR* parameter in Equation (2.9)

$$BE_x = Coeff \times Power \times \left(1 - PR_x\right) \times FloodplainFactor\,. \tag{2.9}$$

From Equation 15 in Wilkinson *et al.* (2005), where BE_x is the volume of bank material contributed to the stream link from bank erosion over a 100 year interval $Coeff$ is a variable used to account for reasonable maximum rates in stream links that have been subject to extensive clearing of littoral vegetation, or increased flow rate from inter-basin water transfers, $Power$ is the bankfull stream power, PR_x is the proportion of stream banks along stream link that have littoral vegetation present, and $FloodplainFactor$ is a factor that reduces the amount of bank erosion if the floodplain is less than 100 metres wide to account for the presence of rock (which would not contribute to bank erosion) in channels that lack a significant floodplain.

The PR_x parameter used by Prosser *et al*. (2001) and by Wilkinson *et al*. (2005) was calculated using a 100 metre resolution map of woody vegetation. For example if woody vegetation was present in 40 out of the 100 pixels adjacent to link L then the PR_x parameter would be calculated as 0.4. Whilst this level of detail was suitable for the national scale sediment transport modelling for which it was developed, higher spatial resolution satellite imagery allows us to map littoral vegetation in greater detail. Furthermore, higher spectral resolution enables the mapping of vegetation structure[5], which can in turn be used to describe the influence of littoral vegetation on bank erosion in greater detail as described below. Littoral vegetation reduces bank erosion via three mechanisms:

1. By reducing the amount of sub-aerial preparation;
2. By reducing the velocity of fluvial attack; and
3. By reducing the amount of mass failures by increasing the soil cohesion (Abernethy and Rutherfurd, 1998).

The relationship between vegetation structure and these three mechanisms is discussed below.

[5] The vegetation structural classification used in thesis is that described by (Specht; 1970)

Sub-Aerial Preparation

Sub-aerial preparation is a term that covers a range of processes, such as frost-heave, rain-drop impact, and bank/soil desiccation (Abernethy and Rutherfurd, 1998). Sub-aerial preparation is described by Abernethy and Rutherfurd (1998) as a second order effect in the overall gamut of bank erosion processes. Percentage foliage cover is an important control of many sub-aerial processes such as rainfall interception, and desiccation (Abernethy and Rutherfurd, 1998).

Percentage foliage cover is also strongly positively correlated with the number of trees per hectare (λ) (Adjusted $R^2 = 0.9$), Consequently, a reduction in λ, will coincide with a reduction in percentage foliage cover. The reduced percentage foliage cover will in turn reduce the amount of protection from sub-aerial preparation, leading to an increased likelihood of bank erosion. Therefore λ provides a rough approximation of the influence of littoral vegetation on the amount of sub-aerial preparation. The reason for using λ rather than percentage foliage cover is that λ strongly influences the other two erosion processes, as discussed below, and therefore provides a good parameter to approximate the influence of littoral vegetation structure on all three processes.

Fluvial Attack

Banks erode from fluvial attack when high velocity flows near the bank have sufficient force to mobilise the bank material, resulting in scour and in some cases undercutting the banks (Abernethy and Rutherfurd, 1998). Abernethy and Rutherfurd (1998) describe influence of littoral vegetation on fluvial attack in terms of the change in stream power ω that can be attributed to the presence of large woody debris (LWD). LWD is generated over time by woody littoral vegetation (Piégay and Gurnell, 1997; Gurnell *et al*., 2002; Montgomery and Piégay, 2003), and the presence of LWD in the channel reduces the stream power ω by reducing the flow velocity term, V, and reducing the hydraulic radius term, R. Stream power ω is given by

$$\omega = \rho gRVS \tag{2.10}$$

where ρ is the density of water (kg m^{-3}), g is the acceleration due to gravity (m s^{-2}) and S is the local energy slope (tan θ) from Equation 1 in Abernethy and Rutherfurd, (1998). The volume of LWD in the stream can be predicted as a function of λ as described in Section 2.6. To summarise, littoral vegetation with a high λ will generate a large amount of LWD into the adjacent channel, thereby reducing the amount of fluvial attack at the stream bank. In areas where littoral vegetation has been removed ($\lambda = 0$) the volume of LWD will diminish steadily over time, increasing the rate of fluvial attack in these locations. The relationship between ω and LWD volume is described in detail in the Appendices.

Bank Collapse

Bank collapse or mass failure occurs when the shear stress exceeds the shear strength of the material that makes up the stream bank. Littoral vegetation reduces the likelihood of bank collapse by increasing shear strength of the bank material via the presence of tree roots (Abernethy and Rutherfurd, 1998). The amount of bank reinforcement provided by tree roots is described as the variable c_r in terms of the relationship for the maximum depth of tension cracking $H_c^{'}$ in Equation 14 of Abernethy and Rutherfurd (1998) which is

$$H_c^{'} = \frac{2\left(c + c_r\right)}{3\gamma} N_S \qquad (2.11)$$

where: c is the material cohesion in kPa, c_r is the reinforcement provided by tree roots in kPa, γ is the bulk unit weight (kN m^{-3}), and N_S is the dimensionless stability factor.

Abernethy and Rutherfurd (2001) describe the spatial distribution at the individual tree scale of c_r values for two littoral tree species. The c_r for individual trees (c_{r_TREE}) were used to calculate bank average c_r values are calculated using Equation (2.12) as described below, this process is described in detail in the Appendices.

Calculating bank average c_r

To calculate the c_r value at any point along a stream bank where woody vegetation is present the c_{r_TREE} value is divided by the average distance between trees (*NND*) as shown in Equation (2.12).

$$c_{r\_BANK} = \frac{c_{r\_TREE}}{NND} \qquad (2.12)$$

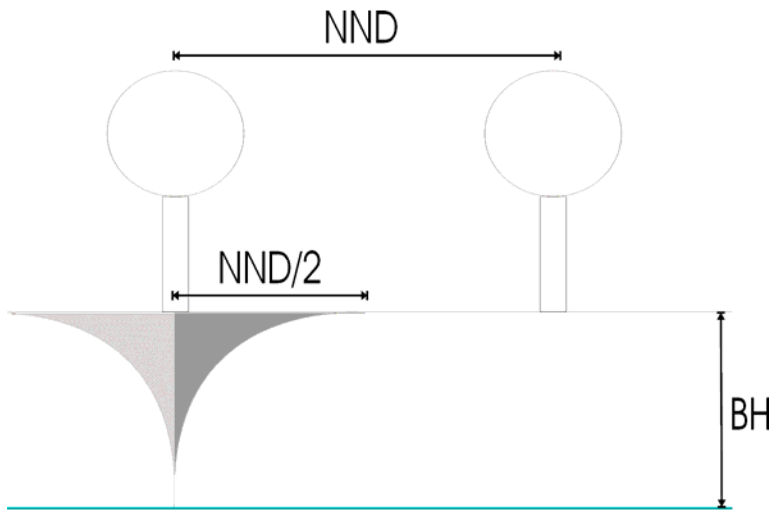

Figure 2.2 Graphical representation of the c_{r_BANK} calculations, BH is bank height, and the shaded area represents the portion of the stream bank reinforced by tree roots

The average distance to the nearest tree can be calculated using the nearest neighbour distance (*NND*). This distance is calculated based on the number of trees per hectare λ. From the equations listed on page 39 of Jupp and Lovell (2000) we know that *NND* is a function of the number of trees per hectare λ as described by

$$NND = \frac{1}{\sqrt{\lambda}} . \tag{2.13}$$

The use of the *NND* parameter to calculate the distance between trees along the edge of streams is based on the assumption that the average distance to the nearest tree is the same adjacent to the stream as it is elsewhere within the floodplain for vegetation of a given structural type. This assumption may be violated because the nearest neighbour statistics are affected by edge effects (such as those created by a stream bank).

Combining Equation (2.12) and Equation (2.13) and gives

$$c_{r\_BANK} = c_{r\_TREE} \times \sqrt{\lambda} . \tag{2.14}$$

So, as the number of trees per hectare increases, the probability of encountering tree roots in a stream bank increases, and the amount of tree roots that would be encountered, also increases. As a result of this, stream banks with littoral vegetation that has a high λ will have a higher shear strength, and will therefore be less prone to bank collapse, than those with low or zero λ.

Calculating the bank reinforcement index (BRI)

Based on the discussions above, the number of trees per hectare (λ) provides a reasonable approximation of the bank stabilizing effect of littoral vegetation for all three of the bank erosion processes discussed, insofar as areas with high λ will have more protection from erosion processes than areas with low λ or no littoral vegetation. Based on this the PR_x term in Equation (2.9) has been replaced by a normalized λ term such that

$$BE_x = Coeff \times Power \times (1 - \lambda_n) \times FloodplainFactor , \tag{2.15}$$

where λ_n is calculated using

$$\lambda_n = \frac{\lambda_{VT}}{\lambda_{MAX}} , \tag{2.16}$$

with λ_{VT} being the number of trees per hectare for vegetation type *vt* and λ_{MAX} is the maximum number of trees per hectare.

Quantifying changes in local bank erosion rates

To compare whether bank erosion rates at a given location have changed between the pre-settlement littoral zone conditions and the present, Equation (2.15) is substituted into Equation (2.1) to give the bank reinforcement index (BRI)

$$BRI_{local} = \frac{\left[Coeff \times Power \times (1 - \lambda_n) \times FloodplainFactor\right]^{\text{Current}}}{\left[Coeff \times Power \times (1 - \lambda_n) \times FloodplainFactor\right]^{\text{Reference}}} . \tag{2.17}$$

Equation (2.17) can be simplified based on a series of assumptions: If we assume that :

1. there are no inter-basin water transfers (Carroll pers com 2003);
2. that the maximum rate of bank erosion is not reached in either the current or reference case; and
3. that the bankfull stream power term *Power* is unchanged between the current and pre-settlement cases.

then the *Coeff* and *Power* terms cancel out. This is based on the assumption that land use changes upstream in the catchment haven't altered the rainfall-runoff characteristics of the catchment, and it ignores the impact that LWD may have on *Power* (although this influence of LWD is implicit within the λ_n term as discussed above). A further assumption is that at any given location the floodplain width remains unchanged between pre-settlement conditions and the current day.

If these assumptions are accepted then Equation (2.17) can be re-written as

$$\mathrm{BRI}_{\mathrm{local}} = \frac{\lambda_n^{\mathrm{current}}}{\lambda_n^{\mathrm{reference}}} . \tag{2.18}$$

Comparing bank erosion rates across the catchment

To identify locations throughout the catchment where bank erosion is likely to occur, and to identify locations where littoral rehabilitation would reduce the severity of bank erosion.

$$\mathrm{BRI}_{\mathrm{global}} = 1 - \left[\frac{\left[Coeff \times Power \times (1-\lambda_n) \times FloodplainFactor \right]^{\mathrm{Local}}}{\left[Coeff \times Power \times (1-\lambda_n) \times FloodplainFactor \right]^{\mathrm{Maximum}}} \right] \tag{2.19}$$

Assuming that there is no need to cap the maximum erosion rate using the *Coeff* term and that there are no interbasin transfers then Equation (2.19) can be simplified to

$$\mathrm{BRI}_{\mathrm{global}} = 1 - \left[\frac{\left[Power \times (1-\lambda_n) \times FloodplainFactor \right]^{\mathrm{Local}}}{\left[Power \times (1-\lambda_n) \times FloodplainFactor \right]^{\mathrm{Maximum}}} \right] \tag{2.20}$$

The values for $\mathrm{BRI}_{\mathrm{global}}$ also range between zero and one, values close to one indicate areas of stable banks, Whereas values close to zero indicate areas where bank erosion is most likely to occur, thereby identifying areas where riparian vegetation rehabilitation is likely to have the greatest impact in reducing in stream sediment loads.

2.4 The Denitrification Index

The denitrification index (DNI) has been developed in this project because it represents one of the important biogeochemical processes served by riparian zone vegetation, and it is important for maintaining the water quality for human and ecological purposes. Excessive amounts of nitrate have been linked to a range of negative human health impacts, and it is considered a carcinogen (Caraco and Cole, 2001). Excessive nitrogen loads also alter the trophic state of streams, leading to dramatic changes to the food web (Wilcock *et al*., 2002). Riparian zones can remove nitrogen from the soil and from groundwater in a variety of ways. Nitrogen can be removed via direct uptake by plants or via microbial denitrification.

Microbial denitrification is of particular interest, because the nitrogen is converted into gaseous forms of nitrogen N_2O and N_2, thereby removing the nitrogen from the riparian system completely. Microbial denitrification typically occurs when denitrifying bacteria are subjected to anaerobic conditions associated with inundation/submersion, and during this period use nitrate rather than oxygen to break down dissolved organic carbon (DOC) (Sigunga *et al*., 2002; Chen and MacQuarrie, 2004). This process is limited by a number of factors, including: the amount of DOC present and the contact time between the nitrate enriched water and the DOC. The concentration of nitrate can also limit this reaction. However nitrate concentration is not considered to be limiting in this thesis because in-stream nitrate levels in the study area (Section 3.2) are frequently above the upper limit set by the Australian and New Zealand Environment and Conservation Council (ANZECC) (Noble *et al*., 1997).

In humid areas, denitrification takes place when nitrogen enriched shallow groundwater enters the riparian zone from the adjacent hillslope, and then travels through the rooting zone of riparian vegetation towards the stream (Cirmo and McDonnell, 1997; Abdelouas *et al*., 1999; Gold *et al*., 2001; Flite III *et al*., 2001; Wilcock *et al*., 2002; Hill *et al*., 2004). There is also evidence to suggest that the denitrifying potential of riparian zones can be dramatically reduced if the groundwater can bypass the riparian root zone via gravel lenses (Burt *et al*., 1999), or via phreatic : hyporheic ground water exchanges below the root zone (Hill *et al*., 2000).

In semi-arid regions denitrification occurs via the same mechanism, but under different circumstances (Abdelouas *et al*., 1999, Schade, *et al*., 2002). In these regions denitrification is likely to occur when nitrogen enriched water enters the root zone of vegetation adjacent to the channel during the rising arm of the hydrograph, spends a period of time in the root zone, and then returns to the channel during the falling arm of the hydrograph (Schade *et al*., 2002). Denitrification can also occur when flow goes overbank, and water infiltrates into the floodplain (Caraco and Cole, 2001). This occurs when the flood duration is sufficient so that the dissolved oxygen levels drop to the point where microbes start to metabolise nitrate (Sigunga *et al*., 2002). Under these circumstance denitrification can occur at any location throughout the floodplain, if dissolved organic carbon is available (Hill *et al*., 2000), and provided that the soil remains wet enough for denitrification to occur. Studies of denitrification in semi-arid areas with vertisol soils (similar climate and soil type to those encountered in the study area of this research) have found that denitrification occurs when the water holding capacity (WHC) of the soil exceeds 60% for more than twenty hours and occurs rapidly when WHC exceeds 80% (Sigunga *et al*., 2002). Once WHC exceeds 60% there is a lag period of twenty hours whilst available oxygen is used up (Sigunga *et al*., 2002), after which denitrification begins to take place. In a study of vertisols from the Fitzroy catchment[6] , Powlson *et al.* (1988) found that 25% of denitrification took place in the first two days (after the initial lag) and all denitrification took place (*i.e.* available carbon supplies were consumed) within seven days. It is worth noting that a number of authors report incomplete denitrification (*i.e.* NO_3^- is reduced to N_2O rather than N_2) when WHC is less than 100% (Luo *et al*., 1998).

Previous authours have described the spatial distribution of denitrification at a range of scales via a number of methods including: direct observations (via piezometer nests and a variety of chemical tests) (Burt *et al*., 1999); numerical modelling of the chemical processes governing denitrification (Chen and MacQuarrie, 2004); 3 dimensional soil maps (Cosandey *et al*., 2003), by correlating land use within the riparian zone with nitrate concentrations at various points in the stream network (Basnyat *et al*., 2000), and by using wetted perimeter of the river channel to estimate the area available for denitrification (Bartkow and Udy, 2004). These methods were not suitable for this thesis because they were either developed in humid riparian zones (where denitrification take place under different circumstances as discussed above) or they required extensive datasets that are not typically available.

The DNI is calculated using the equations contained in Chen and MacQuarrie (2004), that have been simplified based on a series of assumptions. These equations have been manipulated as described below to calculate the amount of denitrification performed by the current riparian vegetation, as compared to the riparian vegetation at that location prior to European settlement. The index provides an estimate of denitrification potential rather than a figure in terms of kilograms of nitrogen per hectare per year for a particular stand of vegetation. The calculation of the DNI is detailed below, and contains a number of steps as follows.

1. Modify an existing denitrification model to account for the circumstances under which denitrification occurs in the study area.

---

[6] The Nogoa and Comet catchments that form the study area for this thesis are sub-catchments of the Fitzroy catchment.

2. Estimate the amount of water soluble carbon for riparian soils for both the current riparian zone, and pre-settlement.

3. Calculate the number of denitrification events that are likely to occur at any given location/soil depth.

Modifying an existing denitrification model

Equation (2.21) is taken from Equation 16 in Chen and MacQuarrie (2004) and is used to calculate the change in nitrate over time. It represents both nitrification and heterotrophic denitrification.

Comment [I1]: Hi Peter, you'll notice some inconsistencies with the NO3 superscripts (the minus sign is present in some cases and absent in others, this will be fixed prior to final submission)

$$\begin{aligned}\frac{d\left[\mathrm{NO_3^-}\right]}{dt} &= \mathrm{ratio}_1 k_2 X_1 F\left(X_1\right)\left[\frac{\mathrm{NH_4}}{\mathrm{K_{NH_4}}+\mathrm{NH_4}}\right]\times\left[\frac{\mathrm{O2}}{\mathrm{K_{O_2}}+\mathrm{O_2}}\right]\\ &-\mathrm{ratio}_3 k_4 X_2 F\left(X_2\right)\left[\frac{\mathrm{CH_2O}}{\mathrm{K_{CH_2O}}+\mathrm{CH_2O}}\right]\times\left[\frac{\mathrm{NO_3^-}}{\mathrm{K_{NO_3^-}}+\mathrm{NO_3^-}}\right]\times\left[\frac{\mathrm{K_{O_2I}}}{\mathrm{K_{O_2I}}+\mathrm{O_2}}\right]\end{aligned} \tag{2.21}$$

where ratio_1 is the mass ratio of $\mathrm{NO_3^-}$ to $\mathrm{NH_4}$, k_2 is the reaction rate constant for the conversion of $\mathrm{NH_4}$ to $\mathrm{NO_3^-}$, X_1 is the nitrifying biomass $F(X_1)$ is the biomass growth inhibition function as defined by Equation (2.22), $\mathrm{K_{NH_4}}$ is the ammonia half-saturation constant (M/L^3)[7], $\mathrm{K_{O_2}}$ is the oxygen half-saturation constant, ratio_3 is the mass ratio of $\mathrm{NO_3^-}$ to DOC, $\mathrm{CH_2O}$ represents the amount of dissolved organic carbon (DOC), X_2 is the heterotrophic biomass, $F(X_2)$ is the biomass growth inhibition function (same form as Equation (2.22)) for the biomass X_2, $\mathrm{K_{CH_2O}}$ is the DOC half-saturation constant (M/L^3), $\mathrm{K_{NO_3}}$ is the nitrate half-saturation constant, $\mathrm{K_{O_2I}}$ is the inhibition constant of oxygen (M/L^3).

$$F(X_1)+\frac{K_{X_1}}{K_{X_1}+X_1} \tag{2.22}$$

For the purposes of this index we are only considering denitrification. In which case Equation (2.21) can be simplified to express the process of denitrification as shown in Equation (2.23).

$$\begin{aligned}\frac{d\left[\mathrm{NO_3^-}\right]}{dt} &= -\mathrm{ratio}_3 k_4 X_2 F(X_2)\\ &\times\left[\frac{\mathrm{CH_2O}}{\mathrm{K_{CH_2O}}+\mathrm{CH_2O}}\right]\times\left[\frac{\mathrm{NO_3}}{\mathrm{K_{NO_3}}+\mathrm{NO_3}}\right]\times\left[\frac{K_{\mathrm{O_2I}}}{K_{\mathrm{O_2I}}+\mathrm{O_2}}\right]\end{aligned} \tag{2.23}$$

The DNI is calculated by comparing the current rate of denitrification with a reference rate. So the for soil depth range *x* the DNI takes the form shown in Equation (2.24).

---

[7] Mass per length cubed

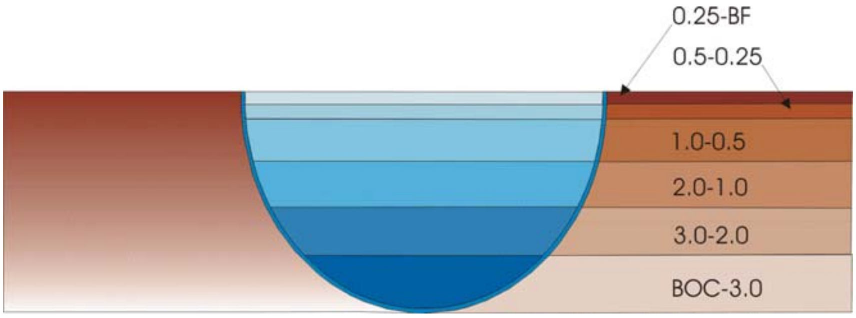

Figure 2.3 Channel cross section showing soil depth ranges (*x*)

$$\mathrm{DNI}_x = \frac{\int_{t_0}^{t_1}\left[\frac{d\left[\mathrm{NO}_3^-\right]}{dt}\right]_x^{\mathrm{Current}} \times NDNE_x^{\mathrm{Current}}}{\int_{t_0}^{t_1}\left[\frac{d\left[\mathrm{NO}_3^-\right]}{dt}\right]_x^{\mathrm{Reference}} \times NDNE_x^{\mathrm{Reference}}} \tag{2.24}$$

Where t_0 represents the time at which conditions in soil depth range *x* (values for *x* are 0-0.5m, 0.5-1m, 1-2m and 2m-3m and 3m - BOC where BOC is the base of the channel, and the soil depth 0 represents the top of the bank, as shown in Figure 2.3) become suitable for denitrification (*i.e* WHC exceeds 60% for more than twenty hours) and t_1 represents the time at which conditions are no longer suitable for denitrification, and if t_1 is greater than eight days (Powlson *et al*., 1988)then it is assumed all possible denitrification has occurred. $NDNE_x^{\mathrm{Current}}$ and $NDNE_x^{\mathrm{Reference}}$ represent the probability of conditions being suitable for denitrification to occur at soil depth *x* during any given year for the current and reference case respectively.

Calculations of $NDNE_x$ are contained in Section 4.4.4 If all terms are included, then Equation (2.24) can be re-written as Equation (2.25)

$$\mathrm{DNI}_x = \frac{\left[\int_{t_0}^{t_1}\left[-\mathrm{ratio}_3 k_4 X_2 F(X_2)\times\left[\frac{\mathrm{CH_2O}}{\mathrm{K_{CH_2O}}+\mathrm{CH_2O}}\right]\times\left[\frac{\mathrm{NO_3}}{\mathrm{K_{NO_3}}+\mathrm{NO_3}}\right]\times\left[\frac{K_{\mathrm{O_2I}}}{K_{\mathrm{O_2I}}+\mathrm{O_2}}\right]\right]_x^{\mathrm{Current}} \times NDNE_x^{\mathrm{Current}}\right]}{\left[\int_{t_0}^{t_1}\left[-\mathrm{ratio}_3 k_4 X_2 F(X_2)\times\left[\frac{\mathrm{CH_2O}}{\mathrm{K_{CH_2O}}+\mathrm{CH_2O}}\right]\times\left[\frac{\mathrm{NO_3}}{\mathrm{K_{NO_3}}+\mathrm{NO_3}}\right]\times\left[\frac{K_{\mathrm{O_2I}}}{K_{\mathrm{O_2I}}+\mathrm{O_2}}\right]\right]_x^{\mathrm{Reference}} \times NDNE_x^{\mathrm{Reference}}\right]}. \tag{2.25}$$

Equation (2.25) can be simplified greatly because Ratio$_3$, the mass ratio of NO_3^- to DOC, k_4 the reaction rate constant are common to both the numerator and denominator. If we assume that nitrate is not limiting in either the current or reference case then the term $\left[\frac{\mathrm{NO}_3^-}{\mathrm{K}_{\mathrm{NO}_3^-}+\mathrm{NO}_3^-}\right]$ cancels from both the top and bottom of Equation (2.25). Please note that this represents a scenario whereby remnant (or reference) riparian vegetation has unlimited nitrate supplied to its root zone, rather than representing the amount of denitrification that would have occurred prior to settlement (which would have been strongly limited by the small amount of naturally occurring nitrate). Furthermore if we assume that for a soil depth range *x* that the inhibition due to oxygen, represented by the term $\left[\frac{K_{O_2I}}{K_{O_2I}+O_2}\right]$ is the same in both the current and reference case, then that term also cancels. A further assumption is that the heterotrophic biomass X_2 available to metabolise the nitrate is constant for both the current and the reference case. This assumption is likely to be violated in areas where tree clearing in the past has resulted in a reduction of below-ground biomass over time, which is in turn likely to lead to a decrease in the amount of heterotrophic biomass. It is also assumed that the space available for growth of heterotrophic biomass, represented by the term K_{X1} in the $F(X_1)$ term (show previously in Equation (2.22)), is the same for both cases, and is not limiting in either. This assumption may be violated if land use practices have altered the bulk density of the soil. Under these assumptions and if the rainfall-runoff relationship upstream of the riparian zones is considered constant, and the river is unregulated (*i.e.* the frequency and duration of denitrification events at soil depth *x* haven't changed) then DNI can be calculated using Equation (2.26).

$$\mathrm{DNI}_x = \frac{\int_{t_0}^{t_{dry}} \left[\frac{\mathrm{CH_2O}}{\mathrm{K_{CH_2O}}+\mathrm{CH_2O}}\right]_x^{\mathrm{Current}}}{\int_{t_0}^{t_{dry}} \left[\frac{\mathrm{CH_2O}}{\mathrm{K_{CH_2O}}+\mathrm{CH_2O}}\right]_x^{\mathrm{Reference}}} \tag{2.26}$$

Where t_0 is the time at which soil moisture in depth range *x* exceeds 60% WHC, and t_{dry} is the time at which soil moisture falls below 60% WHC. On the other hand if the river is regulated then the frequency of denitrification events at soil depth *x* may be altered in which case the DNI_x is calculated using Equation (2.27).

$$\mathrm{DNI_x} = \frac{\int_{t_0}^{t_{dry}} \left[\frac{\mathrm{CH_20}}{\mathrm{K_{CH_20}}+\mathrm{CH_20}}\right]_x^{\mathrm{Current}} \times NDNE_x^{\mathrm{Current}}}{\int_{t_0}^{t_{dry}} \left[\frac{\mathrm{CH_20}}{\mathrm{K_{CH_20}}+\mathrm{CH_20}}\right]_x^{\mathrm{Reference}} \times NDNE_x^{\mathrm{Reference}}} \tag{2.27}$$

If we assume that the concentration of $\mathrm{CH_2O}$ or dissolved organic carbon is much less than the half saturation content $\mathrm{K_{CH_2O}}$, and we assume that for every denitrification event t_{dry} is greater than eight days (eight days being the sum of the twenty hours (approximately 1 day) lag between WHC exceeding 60% and denitrification beginning as described by Sigunga *et al.* (2002) and the seven days during which all available organic carbon is consumed as described by Powlson *et al*. (1988). Then the integration of the Monod equation calculates the amount nitrate removed from soil depth x is equal to the amount of dissolved organic carbon present at soil depth x at time zero multiplied by $ratio_3$, the mass ratio of NO_3^- to DOC. If these assumptions are accepted then Equation (2.27) can be re-written as

$$\mathrm{DNI}_x = \frac{WSC_x^{\mathrm{Current}} \times NDNE_x^{\mathrm{Current}}}{WSC_x^{\mathrm{Reference}} \times NDNE_x^{\mathrm{Reference}}} . \tag{2.28}$$

Where WSC_x^{Current} and $WSC_x^{\mathrm{Reference}}$ represent the amount of water soluble carbon (WSC)(kg m^{-3}) that would become dissolved organic carbon in the presence of water under current vegetation/land cover and reference vegetation cover respectively.

Having calculated DNI_x at every depth range x using Equation (2.28) it is now possible to calculate DNI using

$$\mathrm{DNI} = \sum_{\mathrm{x=BOC}}^{\mathrm{x=0}} \mathrm{DNI}_x . \tag{2.29}$$

2.5 Stream Shading Index

Vegetation that overhangs, or is immediately adjacent to a stream channel or waterbody provides shade for that waterbody. The shading function of riparian vegetation is important for two reasons: 1. it reduces fluctuations in water temperature, which in turn reduces fluctuation in dissolved oxygen and pH levels within the stream; and 2. it reduces the amount of light reaching the stream. The reduction in light levels can reduce the growth of filamentous algae and exotic macrophytes, thereby maintaining the existing trophic level of the benthos (Sponseller *et al*., 2001) and the stream (Bunn *et al*., 1999). Temperature and biochemical stability are also important for maintaining the ecological values of the stream both locally and downstream (Poole and Berman, 2001; Sponseller *et al*., 2001).

The stream shading function of riparian vegetation has been the subject of numerous studies (Sponseller *et al.*, 2001, Poole and Berman, 2001). Many of these studies report that the influence of shade on temperature stability is dependent on the position of the stream in the stream network, and the prevailing hydrologic conditions. For example riparian shading will have a large influence on small stream with small flow volumes, whereas riparian shading will have less of an influence on large streams, with large flow volumes. For larger streams, stream temperature is more dependent on the water temperature of tributary streams and hyporheic flows that contribute to the larger stream reach (Poole and Berman, 2001). Therefore quantifying the influence of riparian vegetation on stream temperature at the stream reach to catchment scale requires information about the spatial distribution of riparian vegetation, and the structure of that vegetation. In areas of low flow variability, the emphasis should be on quantifying the structure and distribution of vegetation adjacent to low order streams.

The importance of stream shading adjacent to high order streams increases in stream networks with high degrees of flow variability. This is because aquatic ecology becomes dependent on isolated waterholes and ponds in high order stream reaches when the water ceases to flow, and such isolated sites are particularly sensitive to the degree of thermal buffering provided by riparian vegetation (Pusey and Arthington, 2003). Consequently the spatial distribution of riparian vegetation capable of producing shade to high order streams is important, particularly for stream networks subject to highly variable flow volumes such as those found in semi-arid or drought prone regions.

A number of previous studies have described models that calculate the amount of sunlight reaching the stream surface in different environments, for example: Chen *et al*. (1998a) and Chen *et al.* (1998b) describe a radiative transfer model for the amount of sunlight reaching a stream in a montane region of north America.

The aim of the stream shading index (SSI) developed in this thesis differs to the stream shade model described in Chen *et al*. (1998a) and Chen *et al.* (1998b), because it estimates the importance of a stand of riparian vegetation in providing shade to the stream, rather than calculating the amount of sunlight reaching the stream surface. This is an important distinction because it means the index is calculated for a stand of vegetation, not for the body of water. This is consistent with the other RFIs that describe the role that riparian vegetation plays in certain functions, without comprehensively describing the function itself. Because the SSI has a different objective to previous stream shading studies, it has been calculated from basic principles using a simplfied channel geometry and canopy geometry as described in Figure 2.4. The calculations of stream shade geometry (as described in Figure 2.4) is based on the assumption that the water in the channel, and all waterholes are formed at the centre of the channel (*i.e.* the location of the thalweg is not accounted for in these calculations).

The amount of shade provided to the stream by riparian vegetation (SSV) was calculated for each canopy channel geometry combination using Equations (2.30) through to (2.46). Figure 2.4 is similar to Figure 3 p308 in Chen *et al.* (1998b) but differs in its description of channel geometry and the omission of a solar azimuth term (the reasons for omitting a solar azimuth term are discussed below).

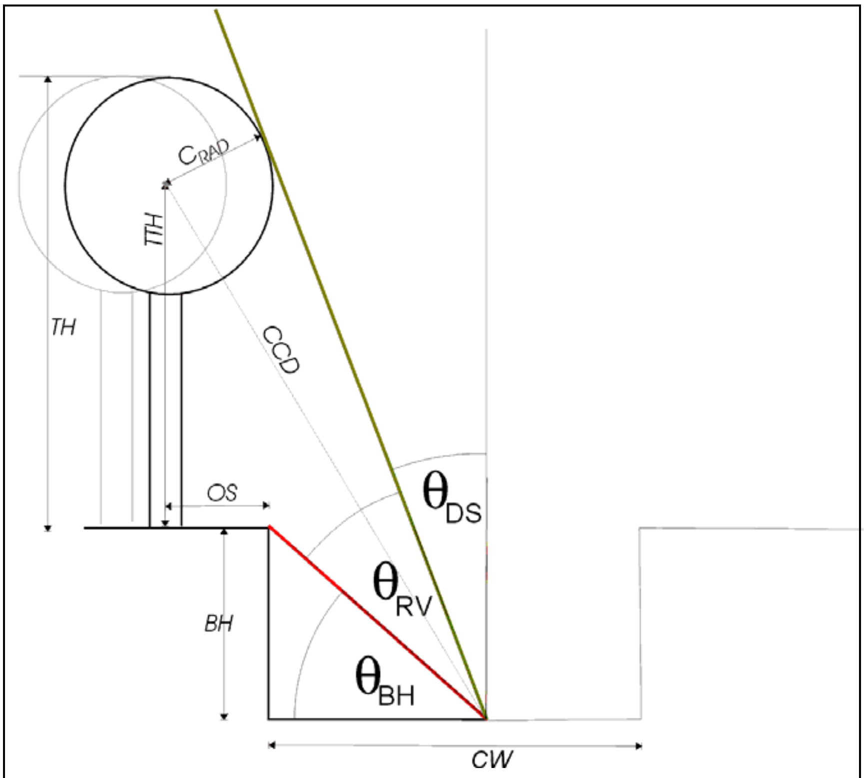

Figure 2.4 A simplified channel cross section with all the parameters used to calculate the SSI.

Figure 2.4 shows a simplified riparian cross section with a stream channel and riparian vegetation adjacent to the channel, where: *BH* is the bank height; *CW* is the channel width; *TH* is the tree height; C_{RAD} is the canopy radius; *TTH* is the tree trunk height, where $TTH = (TH - C_{RAD})$; *OS* is the offset distance between the top of the bank and the first tree trunk; *CCD* is the distance between the centre of the crown and the centre of the channel; θ_{RV} and θ_{BH} are the proportion of half the solar track occluded by riparian vegetation and the stream bank respectively, assuming a solar azimuth that tracks from 90°, directly overhead to 270° (which applies for the study area during summer time), and θ_{DS} is the proportion of the solar track during which sunlight reaches the stream surface unimpeded.

The simplified channel cross section shown in Figure 2.4 only represents half the solar track (90º) because the index is designed to describe the importance of a stand of riparian vegetation in providing shade to the channel. Assuming that the riparian vegetation doesn't overhang the entire channel (*i.e.* $\theta_{BH} + \theta_{RV} \leq 90^{\circ}$) then the importance of a stand of riparian vegetation in reducing the amount of sunlight reaching the stream can be calculated as θ_{RV} as described in Figure 2.4. The assumption that $\theta_{BH}+\theta_{RV} \leq 90^{\circ}$ applies to vegetation:channel geometries of high order streams observed in the study area.

To calculate the proportion of half the solar track occluded by stream bank the angle θ_{BH} is calculated as

$$\theta_{BH} = \arctan\left(\frac{BH}{CW/2}\right) \tag{2.30}$$

where $CW/2$ represents the centre of the channel. The proportion of the solar track that is occluded by riparian vegetation, represented by the angle θ_{RV} is calculated in Equations (2.31) through to (2.35).

$$\theta_{BH+TTH} = \arctan\left(\left(\frac{(BH+TTH)}{\left(\left(\frac{CW}{2}\right)+OS\right)}\right)\right) \tag{2.31}$$

Where θ_{BH+TTH} represents the angle taken from the horizontal to the top of the tree trunk. The portion of the solar track blocked by riparian tree height (rather than canopy overhang) is represented by the angle θ_{TTH}, which is calculated in Equation (2.32).

$$\theta_{TTH}=(\theta_{BH+THH}-\theta_{BH}) \tag{2.32}$$

To calculate the additional portion of the solar track blocked by the tree canopy the angle θC_{RAD}, it is necessary to calculate the distance from the midline of the stream to the top of the trunk CCD as shown in Equations (2.33) and (2.34) respectively.

$$CCD = \sqrt{(BH+TTH)^2+\left(\left(\frac{CW}{2}\right)+OS\right)^2} \tag{2.33}$$

$$\theta C_{RAD} = \arctan\left(\frac{C_{RAD}}{CCD}\right) \tag{2.34}$$

The portion of the solar track occluded by vegetation is taken as the sum of the angles of tree height, and canopy diameter as calculated in Equation (2.35).

$$\theta_{RV}=\theta_{TTH}+\theta C_{RAD} \tag{2.35}$$

The proportion of half the solar track where direct sunlight hits the stream surface θ_{DS} is calculated using

$$\theta_{DS} = \left(90^\circ - \left(\theta_{BH} + \theta_{RV}\right)\right) \tag{2.36}$$

To calculate the amount of shade provided by a stand of vegetation it is necessary to calculate how much direct sunlight is blocked by that stand of vegetation. From basic principles the amount of sunlight (a) reaching a horizontal surface is equal to the solar constant E multiplied by the cosine of the incident angle (θ)[8] as

$$a = E \times \cos\theta \tag{2.37}$$

If we ignore losses due to scattering, and diffuse radiation then the amount of sunlight reaching a horizontal surface over a period of time t_0-t_1 can be calculated using

$$a = E\int_{\theta_0}^{\theta_1} \cos\theta d\theta . \tag{2.38}$$

where θ_0 is the incident angle at time 0 and θ_1 is the incident angle at time 1. Taking the integral of Equation (2.38) produces

$$a = E\left[\sin\theta\right]_{\theta_0}^{\theta_1} \tag{2.39}$$

which is equal to

$$a = E\left(\sin\theta_1 - \sin\theta_0\right) \tag{2.40}$$

The time at which the solar angle is higher than the angle of the stream bank be equal to θ_{DS+RV}, and the time at which the solar angle is higher than the riparian vegetation be equal to θ_{DS} and the time at solar zenith (noon) be equal to θ_Z. Then the amount of sunlight reaching the stream if there is no riparian vegetation present is given by

$$a = E\left[\sin\theta_{DS+RV} - \sin\theta_Z\right] \tag{2.41}$$

and the amount of sunlight reaching the stream if there is opaque riparian vegetation present is given by

$$a = E\left[\sin\theta_{DS} - \sin\theta_Z\right] \tag{2.42}$$

So the amount of sunlight that reaches the stream when riparian vegetation is present, expressed as a proportion of the total that would otherwise reach the stream surface is calculated using

$$a = \frac{E\left[\sin\theta_{DS} - \sin\theta_Z\right]}{E\left[\sin\theta_{DS+RV} - \sin\theta_Z\right]} \tag{2.43}$$

Here the solar constant terms cancel, and the solar zenith terms cancel so that the amount of sunlight that reaches the stream *ripvegsun* expressed as a proportion of the total

---

[8] This ignores atmospheric attenuation.

amount of sunlight that would other wise reach the stream can be calculated using Equation (2.44).

$$ripvegsun = \frac{\sin\theta_{DS}}{\sin\theta_{DS+RV}} \tag{2.44}$$

Then the amount of shade provided by riparian vegetation (if it is considered opaque) can be calculated using

$$ripvegshade = 1 - ripvegsun \tag{2.45}$$

However the riparian vegetation is not opaque and the amount of shade provided by the riparian vegetation is directly proportional to the percentage foliage cover (PFC) assuming that the leaf angle distribution of the foliage is random then the amount of shade provided by a stand of vegetation can be calculated using

$$SSV = ripvegshade \times PFC\,. \tag{2.46}$$

Where *SSV* is the stream shading due to vegetation, and *PFC* is the percentage foliage cover, based on the assumption that there is more than one tree adjacent to the channel.

The SSI_{local} is calculated by comparing the amount of shade provided by the existing vegetation with the amount of shade provided by the vegetation encountered at that location in the catchment prior to settlement. If we assume that the channel geometry hasn't changed, since pre-settlement then the SSI_{local} can be calculated using

$$SSI_{local} = \frac{[SSV]^{\text{current}}}{[SSV]^{\text{reference}}}\,. \tag{2.47}$$

SSI_{global}

To calculate the SSI_{global}, an index that identifies the location in the stream network where vegetation has the greatest influence on the amount of stream shade, it is necessary to account for the impact of stream orientation on stream shade.

Stream orientation has an influence on the importance of a particular stand of vegetation in providing shade to the channel. For example a stand of vegetation located at the end of an east-west oriented stream will have a greater influence on the amount of sunlight reaching the stream than a stand of vegetation located at the end of a north-south oriented section of the stream network. This is because stands at the end of east-west oriented streams cast long shadows along the channel at low solar angles, whereas for north south oriented streams the shadows fall on the opposite bank rather than the channel (Figure 2.5). To account for this effect stands of vegetation the following steps were taken.

1. Calculate Equations (2.30) to (2.46) for a series of points starting at the centre of the channel, and then every 15 metres further from the bank as shown in Figure 2.6 A line of best fit was fitted to the points calculated in step 1, and the equation for that line identified, as shown in Figure 2.6

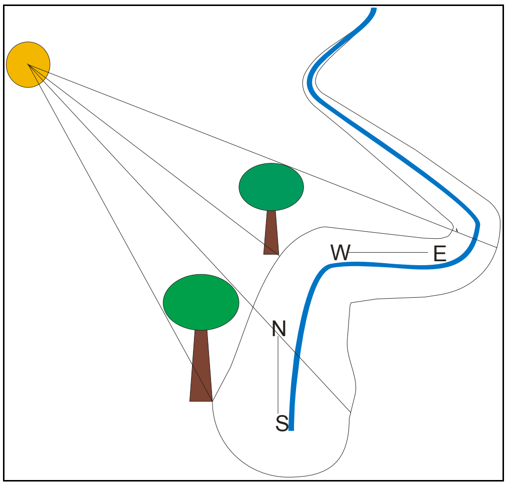

Figure 2.5 Different shade geometries for east-west, and north-south oriented streams

2. The amount of sunlight blocked from reaching the stream surface by riparian vegetation is calculated by integrating the equation identified in step 2 between the centre of the channel and the far bank as shown in Figure 2.5.

The line of best fit shown in Figure 2.6 is given by Equation (2.48)

$$SSV = 30.2DIST^{-1.8} \qquad (2.48)$$

where *DIST* is the distance in metres between the first point for which SSV is calculated

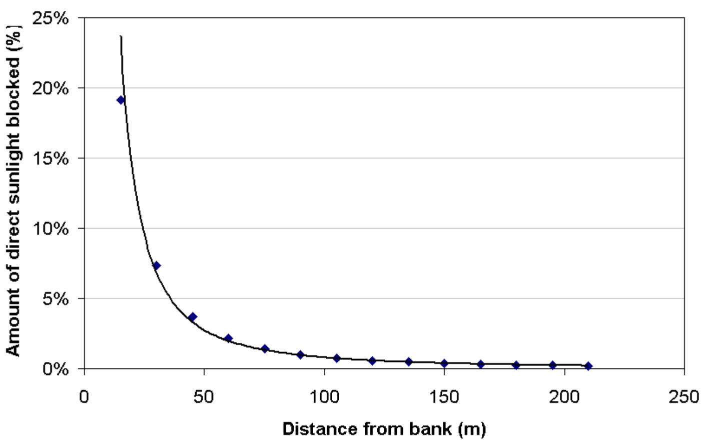

Figure 2.6 The amount of sunlight blocked by a stand of (closed forest) riparian vegetation on a bank adjacent to a long section of east-west flowing (4^{th} order) channel.

(the middle of the channel, as given by CW/2), and the bank at the end of that east-west oriented section of channel (hereafter referred to as *BEW*) as shown in Figure 2.5. More generally the amount of sunlight blocked by a stand of vegetation on an east west oriented section of stream (hereafter referred to as riparian vegetation east west (*RVEW*) can be described using Equation (2.49) calculated by integrating Equation (2.48) as shown in

$$SSV = aDIST^{b} \tag{2.49}$$

Where the coefficients *a* and *b* are calculated using the process described above for every vegetation type and stream order combination.

$$SSV_{RVEW} = \int_{CW/2}^{BEW} aDIST^{b} dDIST \tag{2.50}$$

Integrating Equation (2.50) gives

$$SSV_{RVEW} = \left[\frac{aDIST^{b+1}}{b} + f \right]_{CW/2}^{BEW} \tag{2.51}$$

where *f* is the constant of integration.

The $\mathrm{SSI_{global}}$ is calculated for each stand of riparian vegetation by comparing the SSV (calculated using either Equation (2.46) or Equation (2.51) depending on whether the stream is north-south or east-west oriented) value of the current riparian vegetation with that of maximum amount of shade provided by riparian vegetation anywhere in the catchment. The $\mathrm{SSI_{global}}$ also accounts for the probability of a waterhole forming at that location in the stream network as shown in Equation (2.52)

$$\mathrm{SSI_{global}} = \frac{SSV^{\mathrm{Current}} \times Pwh}{SSV^{\mathrm{Reference}} \times Pwh} \tag{2.52}$$

Where *Pwh* represents the probability of a waterhole forming at that location in the stream network *Pwh* is calculated as a function of Strahler stream order.

The simplifications made in calculating this index apply only to a relatively limited range of geographic locations. This is because the sun is assumed to have an azimuth angle of 90, which is true for areas between the tropics during mid-summer (*i.e.* the time when stream shading is likely to have the greatest impact on stream temperature). For areas outside the tropics solar azimuth angle would need to be included in the calculations of θ_{BH} and θ_{RV}.

The SSI also doesn't include variations in terms of flow height, the index is calculated for a canopy and channel geometry consistent with a waterhole located in the centre, and at the bottom of the channel. This is consistent with period of time when low water volumes will be sensitive to the shading influence of riparian vegetation. The θ_{BH} and θ_{RV} could be recalculated for other stage heights if required.

One of the important advantages of the SSI is that enables the identification of areas of woody vegetation that are providing shade to the stream. Conserving these areas is of importance because the process of regenerating riparian vegetation to provide stream shade can take many years before the stream shading levels are returned to those found in remnant riparian vegetation.

2.6 Large Woody Debris Index

Remote sensing technology provides an opportunity to map LWD loads via two different techniques. The first technique is to identify the LWD directly from the image. This approach requires high resolution imagery such as aerial photography or airborne scanner imagery. Previous studies using this technique to map LWD have reported mixed results. Aspinall (2002) reports a high degree of success mapping LWD using high spatial resolution (1-5 metre pixels) hyperspectral data, Wright *et al.* (2000) on the other hand report limited success using similar data, albeit with a different image analysis technique. High resolution hyperspectral data is well suited for studies of small areas of interest. However the acquisition, processing and analysis costs involved make such an approach prohibitively expensive for projects covering large areas. The approach is also limited by its reliance on the LWD to be visible from the air it is unable to identify LWD in cases where the LWD is submerged or beneath the forest canopy. The second approach is to use a statistical relationship between the volume of standing timber on a stream bank and the amount of LWD in the channel to predict the amount of LWD in the channel from a map of standing timber volumes. The map of standing timber volumes is based on a vegetation classification derived from remote sensing imagery. The second approach is used in this thesis.

The hydraulic influence of LWD is important from an ecological perspective, where the diversity in hydraulic conditions created by the LWD can lead to scours, increased pool width, a broader range of exposed substrate types, and areas of high, low and turbulent flow (Fetherston *et al*., 1995; Abe and Nakamura, 1996; Dudley *et al*., 1998; Wallerstein *et al*., 2001).

LWD is particularly important in the aquatic ecology of semi-arid areas, where highly variable stream flow can result in large rivers being reduced to a series of isolated water holes during dry periods. During such dry periods the waterholes act as refugia for the aquatic ecosystems of these rivers. Consequently the presence of LWD in waterholes is even more important to protect fish and other aquatic organisms from terrestrial predators (Crook and Robertson, 1999). The fact that some waterholes are initiated by the hydraulic effects of LWD (Knighton and Nanson, 2000) further emphasises the importance of LWD in semi-arid systems. Furthermore, when rivers in semi-arid (and other climatic) areas flood, LWD provides a velocity refuge (Crook and Robertson, 1999).

The statistical relationship between LWD and standing timber volumes used in this thesis is contained in Marsh *et al.* (2001). Marsh *et al.* (2001) described the correlation between *Eucalyptus* sp dominated riparian vegetation and LWD for Australian streams from a range of different climates (R^2 of 0.9). The correlation between the volume of standing timber on the stream bank and in-channel LWD.

$$LWD = 0.2 \times VEG_d - 0.054 \tag{2.53}$$

Where *LWD* is the volume of large woody debris per linear metre of stream bank (m^3 m^{-1}), and VEG_d is the density of standing timber on stream bank (m^3 m^{-1}). It is worth noting that these are unusual units. These units were used by Marsh *et al.* (2001) to remove the influence of stream width on the volume of LWD, so that irrespective of whether a stream is 20 metres or 100 metres wide, the bank top vegetation will still generate the same volume of LWD (Marsh pers com 2002). The conversion of the units of cubic metres of LWD per linear metre of bank (m^3 m^{-1}) used in Marsh *et al.* (2001) into the units of square metres of LWD projected in the channel cross-section (m^2 m^{-2}) used in Abernethy and Rutherfurd (1998) is contained in the Appendices.

Assuming that the LWD recruitment rates, have not altered since pre-settlement conditions then the $LWDI_{local}$ can be calculated using

$$LWDI_{local} = \frac{\left[wood_A\right]^{\text{current}}}{\left[wood_A\right]^{\text{reference}}} . \tag{2.54}$$

Where $wood_A$ is the volume of above ground woody biomass (m^3 m^{-1}). This assumes that any LWD generated by the vegetation prior to its being cleared is no longer present, which may not be true given that LWD generated by *Eucalyptus* sp. can be very dense[9], and consequently can take some time to decompose (Robertson *et al*., 1999). This also assumes that LWD density in the channel is solely a function of vegetation on the adjacent banks, and is not transported during flood events. For areas where Eucalyptus sp. is the dominant source of LWD, the LWD pieces are dense with only weak positive bouyancy and the transport capacity of the flow is low, these assumptions are reasonable (Marsh *et al*., 2001) . Care would need to be taken in applying this approach if the above conditions were not met.

---

[9] The term dense here refers to the density of the wood itself in kg m^{-3} rather than the density of LWD in the channel in terms of m^3 m^{-2}

$\mathbf{LWDI_{global}}$

From an aquatic ecology perspective, the functions provided by LWD *i.e.* hydraulic diversity, visual protection, velocity refugia, substrate for biofilm growth and egg laying sites, can all be represented by the blockage ratio *B,* as defined by

$$B = \frac{\left(LWD \text{ m}^2\right)}{\left(CSA \text{ m}^2\right)}. \tag{2.55}$$

Where LWD is the area of LWD projected into the stream flow expressed as m^2/m^2 rather than m^3/m^3).If we assume that the LWD are randomly oriented, then *B* represents surface available for biofilm to grow on, and also approximates the visual protection and velocity protection afforded by LWD. Substituting Equation (2.55) into Equation (2.2) gives

$$LWDI_{global} = \frac{\left[B\right]^{\text{Local}}}{\left[B\right]^{\text{Global}}}. \tag{2.56}$$

Where $\left[B\right]^{\text{Local}}$ is the blockage ratio calculated for the adjacent channel and $\left[B\right]^{Global}$ is the highest blockage ratio encountered anywhere within the catchment.

Established woody vegetation is required to generate LWD. Consequently riparian management strategies aimed at maintaining levels of LWD within stream networks fall into two categories, protection of existing vegetation that is capable of producing LWD, and LWD replacement. The protection of existing vegetation is the preferable management option, because LWD replacement, whilst effective (Gerhard and Reich, 2000) can be very costly to implement at large scales. Planting trees in riparian zones has the long term effect of generating LWD to the stream, however the timescales involved for trees to reach maturity and begin large wood generation are large (decades).

2.7 Chapter Summary

This chapter has developed a suite of indices that quantify key of the function performed by riparian zones. Each index was developed by modifying published algorithms that describe each riparian function on a physical basis. The algorithms were modified into indices based on a series of assumptions. The modifications were made so that each index can be calculated throughout large catchments using parameters that can be predicted using a classification of remote sensing data. These indices will provide us with new information about the multiple functions performed by riparian vegetation throughout a catchment. By combining this information with knowledge about the local hydrology and ecology, it will be possible to assess the importance of each function for any stand of riparian vegetation. This information enables catchment managers to make decisions about the allocation of resources for projects aimed at protecting and restoring riparian zones and the functions they perform.

Table 2.2. Summary of the parameters required to calculate riparian function indices

Index	Parameter
STI	Manning's *n*
BRI	The number of trees per area (λ), the volume of standing timber per area ($wood_A$), the average bank height for each stream order (*BH*), the average canopy diameter (C)
DNI	Percentage Foliage Cover (*PFC*), Number of denitrification events (*NDNE*) the volume of standing timber per area (wood$_A$)
SSI	Percentage Foliage Cover (*PFC*) Mean Tree Height (*TH*), Channel Dimensions (*CW* and *BH*), the average canopy diameter (C), Offset between top of bank and first tree (OS), Probability of a waterhole (*Pwh*)
LWDI	the volume of standing timber per area ($wood_A$), Channel Dimensions (*CW* and *BH*),

Each index is based on one or more parameters, and they are calculated for riparian zones in different parts of the landscape, the dominance of each process in different parts of the catchment is described in Chapter 5 in the context of the study area which is described in Chapter 3. Table 2.2 summarises the parameters required to calculate each index. Chapter 3 describes the catchment where this research was undertaken, and how the field data were collected. The ways in which these parameters were measured in the field or were calculated from the field data are described in Chapters 3 and 4 respectively. Chapter 4 also detials how these parameters were linked to the classifications that could be generated using remote sensing and terrain analysis.

Chapter 3 Study Site: The Fitzroy Catchment

3.1 Introduction

The riparian function indices developed in Chapter 2 were calculated for the Nogoa and Comet subcatchments of the Fitzroy catchment in Queensland, Australia. The Fitzroy catchment was chosen for use as a study area for three reasons. First, the sensitivity of the receiving waters, in this instance the Great Barrier Reef Marine Park, makes the need for riparian zone management particularly pressing. Second, the large scale of the catchment means that riparian zone management cannot be implemented simultaneously throughout the catchment, hence the need for a tool that enables identification of particular parts of the catchment where riparian zone management is likely to have the greatest effect. Third, the pressures placed on riparian zones in the Fitzroy, such as grazing in the riparian zone and cropping on the floodplains are found in many semi-arid and sub-humid catchments both in Australia and around the world.

The Fitzroy catchment is Australia's second largest (142 000km^2) seawards draining catchment. The catchment drains into the Great Barrier Reef Marine Park, and sediment transported out of the catchment has impacted on the reef during previous flood events (Hutchings *et al*., 2005). Consequently, there is a need to reduce the amount of sediment delivered by the Fitzroy river to protect sensitive near shore environments including the Great Barrier Reef (O'Reagain *et al*., 2005). One way of reducing the amount of sediment delivered by the Fitzroy river is to maintain and restore riparian zones within the catchment. To do this it is necessary to identify the sediment trapping and bank stabilizing capacity of the existing riparian vegetation within the catchment, thereby enabling the identification of areas where riparian vegetation needs to be restored. In addition to sediment trapping, riparian zones also perform a range of other important functions, as discussed previously in Chapter 2.

To calculate the RFIs developed in Chapter 2 it is necessary to know the spatial distribution of each parameter listed in Table 2.2. Existing vegetation maps do not describe the riparian vegetation in sufficient detail to enable the calculation of the RFIs, so field work was carried at thirty eight riparian zones throughout the study area to establish the relationship between vegetation structure (*sensu* Specht (1970)) stream order (Strahler, 1964) and the parameters listed in Table 2.2. The second half of this chapter describes the fieldwork in terms of the methods used to collect the various measurements, and the distribution of the field sites in terms of land use and stream order.

3.2 Description of Study Area

The study area of this research is the Fitzroy catchment in north-eastern Australia. Detailed fieldwork was performed in sections of the Nogoa and Comet sub-catchments of the Fitzroy catchment as shown in Figure 3.1. The RFIs listed in Chapter 2 were only calculated for the area indicated by the rectangle in Figure 3.1 (19 365 km^2). The analysis was limited to this area only because of a lack of a high resolution digital elevation model (DEM) for the whole catchment. The high resolution DEM was required for the calculation and analysis of the RFIs.

The climate in the study area is sub-tropical and semi-arid. There are three distinct seasons in the Nogoa and Comet Catchments as described in Gunn *et al.* (1977). The three seasons occur between May to August, September to December, and January to April.

During May to August the high pressure systems prevail, bringing fine clear days and cold nights. Temperatures range from maximums between 20°C and 25°C with minimums between 5°C and 10°C. This is the driest season with approximately 15% (between 75 and 100mm) of average annual rainfall received during this period. The rainfall during this period is associated with troughs that form between successive high pressure systems, and is of low intensity compared to the rainfall experienced during the other two seasons.

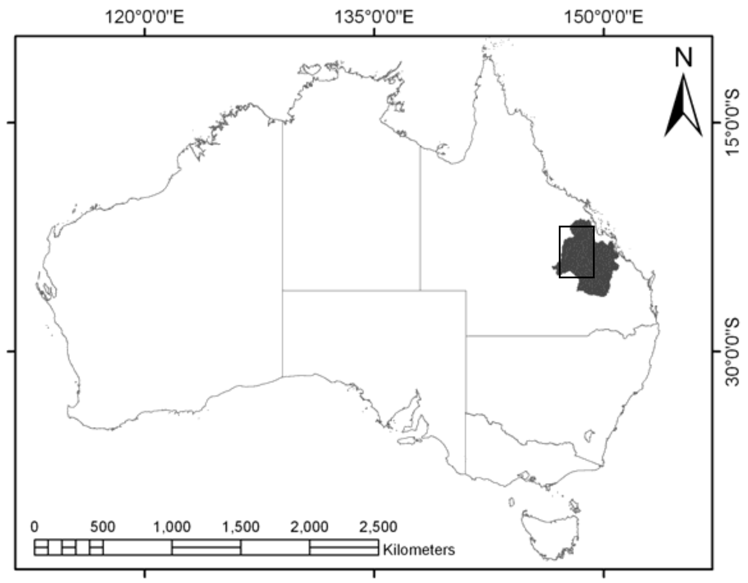

Figure 3.1 Location of the study area, catchment shown in grey and focus area shown by the black square

The period between September and December sees maximum temperatures increase rapidly to maximums between 27°C and 35°C and minimums between 8°C and 20°C, with up to 15 days in excess of 38°C. The dominant rainfall mechanism during this period is convectional storms, and the rainfall intensities associated with these storms can be very high. Rainfall during this period ranges between 175 and 200mm and represents approximately 30% of the average annual rainfall.

From January through to April the inflow of moist maritime air increases, and tropical cyclones will effect the catchment every other year on average. These cyclones and subsequent rain depressions deliver the largest proportion (55% or between 400 and 600mm, although event totals vary widely) of average annual rainfall, however this can all be delivered in one or two events. The rainfall intensities associated with these events are also very high, and are often associated with subsequent flood events. The area is subject to high levels of evaporation, between 1600-1900mm annually, and evaporation is greater than precipitation all year round. The variable rainfall and high evaporation rates have a large impact on the hydrology of the catchment(Gunn *et al*., 1967).

The whole river system was ephemeral prior to the installation of major irrigation dams such as Fairbairn reservoir (Noble *et al*., 1997), and unregulated sections of the stream network remain ephemeral. However, some of the larger streams flow for much of the year. For the purposes of this study a channel network was derived from a digital elevation model, both of which are shown in Figure 3.2. Sections of the stream network are classified using Strahler stream order after Strahler (1964) as shown in Figure 3.2.

First order streams have a contributing area of at least $5km^2$. The low order (1^{st} and 2^{nd}) streams are highly ephemeral, only flowing during and immediately after rainfall events. Higher order (3^{rd}-6^{th}) streams have a base flow component, but will cease to flow as the dry season progresses. As flow ceases throughout the stream network, waterholes form along higher order streams. The mean annual suspended sediment loads for the two catchments within the study area are 1 350 000 tonnes for the Nogoa catchment and 621 000 tonnes for the Comet catchment. These two catchments also have the highest mean annual suspended sediment concentration of all the sub-catchments in the Fitzroy basin with 2.03 g L^{-1} and 1.46 g L^{-1} in the Nogoa and Comet respectively (Values from local SEDNET modelling described in McKergow *et al*. (2005)).

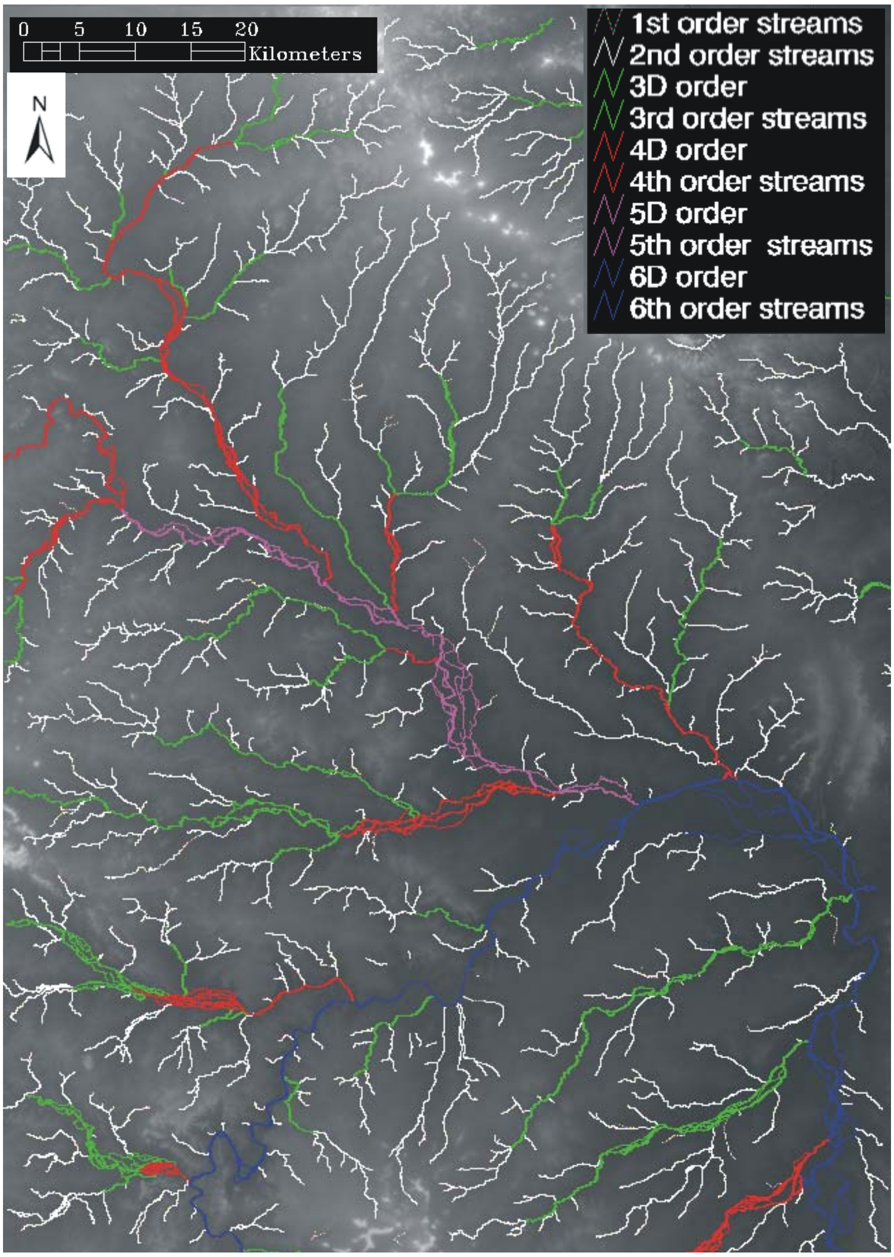

Figure 3.2 Channel network colour coded according to Strahler stream order

3.2.1. Vegetation Types

Vegetation in the study area is dominated by two genera, *Eucalyptus* and *Acacia*. The vegetation type and structure for the whole study area are described in detail in the land unit series contained in Gunn *et al*. (1977) and Story *et al*. (1967). The land unit descriptions are included here to provide the reader with an understanding of the lithology, terrain, soils, dominant genera and vegetation structure contained in the study area. The land units are not used in the calculation of the STIs because the spatial resolution of the land unit coverage is too low.

The upland land units encountered in the area are summarised briefly in Table 3.1. Low order (1^{st}, 2^{nd} and 3^{rd} order) streams drain through all of these land units. The floodplain and channel land units associated with higher order (4^{th} 5^{th} and 6^{th}) streams are described in greater detail in Table 3.2

Table 3.1 Brief description of all land units within the study area

Land Unit Nos.	Lithology	Terrain	Soils	Vegetation Structure	Dominant genera
1-38	Tertiary land surface	Hills, ridges, undulating terrain	Massive earths	Woodland or forest	*Eucalyptus* or *Acacia*
39-53	Tertiary weathered zone	Plains to undulating terrain	Cracking clays	Woodland or forest	*Acacia*
54-61	Quartz sandstone	Mountains and hills	Skeletal soils and texture contrast soils	Woodland or forest	*Eucalyptus Casuarina,* or *Calitris*
62-63	Metamorphic	Hills	Skeletal and texture contrast	Woodland or forest	*Eucalyptus*
64-75	Mixed sediments	Mountains and hills	Skeletal, texture contrast and cracking clays	Woodland or forest	*Eucalyptus*
76-82	Granite	Hills, rolling to undulating terrain	Skeletal and texture contrast	Woodland	*Eucalyptus*
83-90	Volcanics	Mountains and hills, rolling to undulating terrain	Humic massive earths cracking clays and texture contrast soils	Woodland or forest	*Eucalyptus*
91-102	Argillaceous sediments	Plains and undulating terrain	Texture contrast, dark brown, grey brown and cracking clay	Grassland woodland or forest	*Eucalyptus* or *Acacia* or *grassland*
103-111	Basalt	Elevated plateau, hills rolling terrain	Humic massive earths, cracking clays and skeletal soils	Grassland Forest or woodland	*Eucalyptus*
117-135	Described in detail in Table 3.2				

The most important feature of Table 3.1 is that all land units supported woodland or forest prior at the time of the survey, which was carried in the 1960s prior to the extensive land clearing schemes of the late 60s and 70s. The most important feature of Table 3.2 is that all floodplain classes support either woodland or open forest, and that littoral zones located on floodplains (listed as channels in the terrain category of Table 3.2) typically support open forest, with the exception of anastomosing sections of the channel network that sometimes support woodland adjacent to the channel. For the purposes of the calculating the RFIs the pre-European vegetation class distribution has been simplified to the following:

1. Low order (1st, 2nd, and 3rd) streams were surrounded by woodland;
2. The main channels of high order (4th, 5th and 6th) stream were surrounded by open forest; and
3. The floodplain and small channels on the flooplain supported woodland.

Note that this simplification of pre-European vegetation is on the conservative side. In other words, it will tend to under predict the amount of open forest and/or closed forest that may have been encountered in riparian zones prior to European settlement. The implications of these assumptions on the reliability of the RFIs are discussed in Chapter 7.

Table 3.2 Description of the floodplain and channel land units within the study area

Land Unit No.	Lithology	Terrain	Vegetation Structure	CW	BH
117-119	Alluvium coarse to medium texture	Sandy levees and drainage floors	Grassy Woodland	N/A	N/A
120-121	Alluvium	Broad levees and back slopes	Grassy Woodland	N/A	N/A
122	Alluvium	Channels	Open Forest	30-90 metres	3 to 10 metres
123-124	Alluvium medium to fine texture	Levees	Open Forest and Woodland	N/A	N/A
125	Alluvium fine textured	Plains associated with major streams	Woodland	N/A	N/A
127-130	Alluvium fine textured	Plains and drainage floors	Open Forest	N/A	N/A
131-132	Alluvium fine textured	Plains, terraces, back swamps	Open Forest or Tussock Grassland	N/A	N/A
135	Alluvium fine textured	Channels anastomosing or braided	Open Forest and/or Woodland	2-15 metres	1-8 metres

3.2.2. Land Uses

The land uses within the Fitzroy catchment are predominantly grazing, cropping (both dryland and irrigated) and mining. There are also areas of remnant native vegetation in the form of national parks and state forests. The distribution of each land use within the study area is shown in Figure 3.3

Within the grazing land use, some of the region is subject to 'treed grazing' where cattle graze beneath trees, indicating that the area has either not been completely cleared in the first place, or is experiencing some re-growth. The remaining catchment area is subject to grazing on cleared land. Some graziers will clear the majority of their land but leave shade trees scattered throughout paddocks. Some graziers are also in the practice of clearing most of the land but maintaining strips of riparian vegetation to provide shade for the cattle and provide some protection for the riparian zone. Graziers, whose properties abut or contain high order channels, often fence off the channel, although the distance between the edge of the bank and the fence varies widely. Despite the fact that these areas are fenced off, they are generally still subject to some level of grazing, particularly if feed levels elsewhere in the property are low (Carrol pers com 2002).

Dryland cropping practices vary within the study area as well, although it is difficult to ascribe proportions, because practices can change relatively quickly. The main variations in cropping practice are different cropping cycles, different tillage practices, and different stubble retention practices.

Traditional cropping cycles were typically summer sorghum followed by winter wheat, however many farmers are now using opportunity cropping, and will plant a crop (generally sorghum, wheat or sunflowers) that is appropriate for the season that the rain precedes. The tillage practices include conventional tillage, controlled traffic and zero till. The different tillage practices are often associated with different stubble retention practices, depending on the preferences of the farmer and the harvesting machinery used.

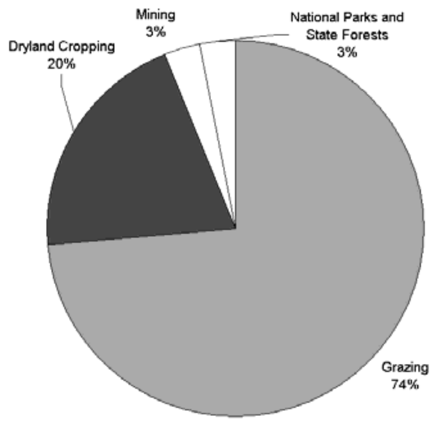

Figure 3.3 Proportions of different land uses in the Fitzroy catchment

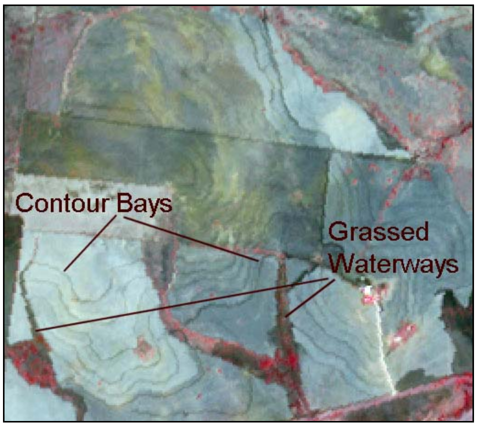

Figure 3.4 Satellite imagery showing erosion prevention measures

Crops such as wheat and sorghum typically generate relatively large amounts of stubble (although stubble retention practices will alter the amount left after harvest) and sunflowers generate very low amounts of stubble (irrespective of harvest method). An understanding of stubble/groundcover management practices within the study area is particularly important when assessing the importance of the STI throughout the catchment.

Many dryland cropping areas contain grassed waterways and in some locations riparian buffer strips. Many of these grassed waterways and buffer strips are relatively broad (in excess of 15 metres). Grassed waterways of these dimensions are required to capture hillslope generated sediment, because the rainfall events, whilst infrequent, can have very high rainfall intensities (up to 100mm an hour). The amounts of runoff, and associated sediment generated by such events necessitates relatively broad buffer strips. It is interesting to note that in some instances these buffer strips can be identified in the satellite imagery used in this project, as shown in Figure 3.4.

Irrigated cropping represents a relatively small proportion of the catchment, and the practice of laser levelling fields, and the associated irrigation networks essentially disconnects the irrigated cropping areas from many riparian processes (STI, BRI, ALWDI, SSI). However the location of irrigated cropping on the floodplain is important in terms of the DNI particularly in light of the very high nitrogen concentrations associated with some forms of irrigated cropping (Noble *et al*., 1997).

3.3 Field data

Fieldwork was carried out in the study area for a number of purposes:

1. To establish the relationship between field measurements of parameters (*i.e.* canopy dimensions, stream channel dimensions), and the classification schemes that would be used to spatially extrapolate those parameters (*i.e.* vegetation structural class, Strahler stream order) (as described in Chapter 4).

2. To verify the reliability with which these parameters could be spatially extrapolated (as described in Chapter 4).

3. To provide training and evaluation sites for the vegetation and land cover classification that is generated from the satellite imagery (as described in Sections 5.2).

This section describes where the fieldwork was carried out in terms of land use and stream order, it also describes the measurement techniques used in the field, and the limitations of these measurement techniques. This section details the breakdown of field sites into two sets used as a training set and a separate series that was used as an evaluation set (for the purposes of establishing and testing the relationship between various parameters and the classification schemes used to extrapolate them as described in Chapter 4).

3.3.1. Field Data Collection

The fieldwork was conducted from the 9th of October to the 22nd of November, 2002 during which period data was collected at 38 sites. The distribution of field sites in terms of land use and stream order are shown in Table 3.6. The uneven distribution of sites between land uses, and the low number of 2nd order streams sampled are the result of difficulties experienced accessing riparian zones. A single transect of measurements was made at each site, extending from one side of the riparian zone to the other at right angles to the channel. The edge of the riparian zone was identified via one of two methods:

1. The edge of riparian vegetation (i.e. vegetation on either side had been cleared).

2. A distinct break in slope indicating the end of the riparian zone/floodplain

A photo showing data being collected along a transect is shown in Figure 3.5 The transects varied in length from relatively short (45 metres) for the riparian zone of one particular 1st order stream up to quite long (790 metres) for the riparian zone (littoral and floodplain) of a 6th order stream).

A number of canopy and channel attributes were surveyed along each transect as described in Table 3.3. Many of the measurement techniques used in this study are identical to those described in The Australian Land and Soil Survey (McDonald *et al*., 1990). A thorough discussion of the limitations of these techniques is contained in the appropriate sections of McDonald *et al*. (1990). A brief description of the limitations is contained below.

Table 3.3 Description of survey techniques

Survey Type	Attribute measured	Measurement Technique	Units
Vegetation Survey[10]	Distance to tree from the start of the transect[11]	Tape transect	m
	Distance off the tape to the base of the tree[11]	Paced distance	m
	Diameter of tree at breast height[12]	DBH tape	cm
	Crown type (degree of openness) [11]	Visual estimate	%
	Tree Height[12]	Clinometer	m
	Canopy Width [11]	Paced distance	m
	Canopy Depth [12]	Clinometer	m
	Canopy Shape (spherical/ellipsoid/inverted triangle) [12]	Visual assessment	none
	Separation between one tree and the next (edge of canopy to edge of canopy) [12]	Paced distance	m
	Proportion of ground cover type[13]	Visual assessment	%
Channel Survey	Channel width	Tape and clinometer survey	m
	Bank Height	Tape and clinometer survey	m
Land Use	Land use adjacent to the riparian zone	Visual assessment	none
	Presence or absence of riparian fences	Visual assessment	none

This vegetation survey technique was used because it captures the vegetation structural parameters that influence canopy reflectance (Walker *et al.*, 1986) and allows for calculation of tree density using plotless techniques (Jupp and Lovell, 2002). There is potential for distance errors along the transect (*i.e.* the tree recorded at 7 metres from the start of the transect may only be 6.8 metres from the start of the transect) because tape tension is difficult to maintain. These errors are non-random, because they are likely to be larger further from the start of the transect. These errors would create problems for a project focussing on the location of individual tree crowns, but they are unlikely to cause errors in this project, where the smallest unit of riparian vegetation considered is 15 metres by 15 metres.

Pacing distances is a rapid way of collecting multiple distances, however it is relatively imprecise, particularly where terrain is rough or there are significant obstacles. Each person collecting paced distances needs to be calibrated to establish the relationship

---

[10] (McDonald *et al*., 1990)
[11] Measured for trees and shrubs
[12] Measured for trees only
[13] For every 5 metres of the transect the proportion of the following ground covers were recorded: bare soil; leaf litter, large woody debris, the riparian grasses

Figure 3.5 Data being collected along a transect.

between pace distance and metre distance. Both data collectors had a pace of 1± 0.1 metres, which leads to a random 10% error in paced distances.

The maximum paced distance measured was 15 paces, consequently the maximum error would be approximately 1.5 metres, which is considerably less than the pixel size (15 metres x 15 metres) of the satellite imagery used to generate the vegetation and land cover classification.

There are a number of error sources associated with using a clinometer to estimate tree height. Firstly assessing the location of the top and base of a canopy, particularly *Eucalyptus* canopies is subjective. If we consider a random error of ±2º this will lead to an error in height estimates of ±1.8 metres for a tree height measured 15 metres from the base of the tree. If the paced distance errors described above are included in the 15 metres then the errors in height measurements increase to ±2.5 metres. Both of these errors are random and are therefore likely to cancel each other out for sufficiently large sample sizes.

Visual assessment was used to measure canopy closure and percentage ground cover. It was also used to identify the land use adjacent to/within the riparian zone at the time of data collection, and to observe the presence/absence of fences. For the last two purposes visual assessment is logical and foolproof, there is however some limitations in using visual assessment for measuring canopy closure and percentage ground cover.

These limitations are based around the fact that any visual assessment is inherently subjective. A degree of objectivity was provided for the canopy closure measurements by using a reference sheet as shown in Figure 6 on page 71 of McDonald *et al.* (1990).

Repeatability was assessed for the ground cover measurement by comparing the ground cover percentages recorded by different field data collectors for the same stretch of transect (discrepancies between data collectors were random and were no greater than 10%).

The measurement errors associated with the tape and clinometer surveys made of channel dimensions will be combination of the errors associated with tape transects (based on the tension of the tape) and the errors associated with the clinometer survey.

3.3.2. Field Data Preprocessing

Prior to analysis, described in Chapter 4, the field data were sorted according to three criteria:

1. vegetation surveys were sorted according to vegetation structure;
2. percentage ground cover surveys were sorted according to adjacent land use; and
3. channel surveys were sorted according to stream order.

Changes in vegetation type (based on the dominant tree species in the overstory) were recorded for each transect wherever they occurred along the transect. For example at one site the dominant canopy species changed four times along the transect (Table 3.5). The change in vegetation type (based on dominant canopy species) was used to define subsections of each transect. The canopy and height measurements for each individual tree along these subsections were collated and used to identify the vegetation structure of that subsection.

An example of the results of this process for site 2 are shown in Table 3.5. The vegetation structural classes used in this study are based on the vegetation structural classification system described in Gunn *et al.* (1977). This system classifies vegetation structural types according to the height and canopy closure of the tallest stratum (Specht, 1970). Woody vegetation within the study area was predominantly tall (10m to 30m high) The vegetation classification described in Table 3.4 forms the basis for all subsequent analysis of riparian vegetation and vegetation structure. Because only tall (10 to 30 metres) vegetation was observed in the study area, the classes are referred to without the tall prefix, *i.e.* tall woodland as described in Table 3.4 will be referred to simply as woodland. The vegetation parameters (Table 3.3) for each of the subsections described in Table 3.5 were sorted according to vegetation structure. These measurements were used to calculate the range of vegetation parameters for each structural class.

Table 3.4 Summary of vegetation structural classes and abbreviations.

Class Name	Height of tallest stratum	Canopy Closure	Abbreviation
Tall Closed Forest	10 to 30 metres	100% to 70% (Dense)	TD
Tall Open Forest	10 to 30 metres	70% to 30% (Medium)	TM
Tall Woodlands	10 to 30 metres	30% to 10% (Sparse)	TS
Tall Open Woodlands	10 to 30 metres	10% to 1% (Very Sparse)	TV

An example of this process is shown in Table 3.5. It is important to note that some measurements, such as diameter at breast height (DBH) are made for every tree, whereas for others, such as percentage foliage cover, a single value is calculated for each section of the transect. The reason for this is that some measurements can be made for individual trees, *i.e.* each tree along the transect will have a separate DBH. Whereas the percentage foliage cover for a section of transect is calculated using the average canopy closure, average canopy radius and average intercrown gap (described in greater detail in Chapter 4), and these values are calculated using the individual canopy measurements and gap measurements for every tree in that section of the transect. The measurements made for each tree are listed in Table 3.3, the parameters calculated for each section of transect are percentage foliage cover (*PFC*), the number of trees per hectare (λ), the volume of standing timber per hectare ($wood_A$). The calculation of parameters from individual measurements is described in detail in Chapter 4.

The percentage of ground cover survey data were sorted according to the land use adjacent to the riparian zone, and used to calculate Manning's *n*. The channel width and

Table 3.5. Different vegetation types and structural classes and parameter measurements observed along a transect.

Distance Along Transect	Dominant overstory species	Structural class	DBH (cm)	PFC (%)
0-85	*Eucalyptus microtheca, and Acacia harpophylla*	Woodland	25, 31, 22… $\mu = 25$ σ=2.5, N=20	33
85-100	Channel			
100-163	*E. tesselaris, E. polycarpa*	Open Woodland	40, 55, 33… $\mu = 45$ σ=4.5, N=10	19
163-185	*E. tesselaris,*	Closed Forest	66, 40, 71… $\mu = 55$ σ=8.5, N=10	65
185-200	*Casuarina cunninghamiana, Melaleuca bracteata*	Closed Forest	69, 44, 81… $\mu = 65$ σ=7.5, N=8	71

Table 3.6 Distribution of Training and Validation Sites

Stream Order	Training Sites	Validation Sites
1st	11	7
2nd	3	1
3rd	7	3
4th	2	1
5th	1	0
6th	1	1
Land Use		
Grazing	15	8
Cropping	7	4
Crown Land	3	1

bank height parameters observed for each transect were sorted according to Strahler stream order. In this context the Strahler stream order represents a form of classification, and it is this classification that will be used to spatially extrapolate these parameters. These measurements were used to calculate average bank heights and channel widths for each stream order.

3.3.3. Training and Validation Sites

The field sites were divided into two subsets. The first set was used to establish a relationship between field observations and the classification schemes used to extrapolate the parameters. The second set was used to assess the predictive skill of this relationship. The sites were divided on a two thirds : one third basis into the training and validation subsets respectively (Table 3.6). The sites included in each subset were identified using a stratified random sampling technique. The stratification was based on stream order and land use, so that each set contained a two thirds : one third split of each stream order and each land use. In the event that there were an uneven number of sites, the extra site was placed in the training subset.

3.4 Chapter Summary

This chapter has described the study area that includes portions of the Nogoa and Comet catchments. The study area is described in terms of: climate, which is semi-arid; land use, which is predominantly grazing, dryland cropping with a small amount of irrigated agriculture; and vegetation which is dominated by *Eucalyptus* and *Acacia* species. Rainfall and consequently stream flow are both highly variable, with the entire stream network drying to a series of waterholes during periods of drought. The chapter also details when, where, how and why field data were collected, and describes how the field data were sorted prior to analysis, which takes place in Chapter 4.

Chapter 4 Riparian Zone Parameters

4.1 Introduction

To calculate the riparian function indices described in Chapter 2 for every stand of riparian vegetation in the study area it was necessary to predict the spatial distribution of the parameters required to calculate each index. Parameters, calculated from the field measurements (Chapter 3) were linked to vegetation/land cover or stream order classifications so that each parameter could be predicted for any given location within the study area. This chapter describes how field measurements of ground cover, vegetation, and channel characteristics were statistically summarized and linked to classifications of land use, vegetation and stream order, respectively. The statistical summaries of these field data *i.e.* average tree height or median channel width are the parameters used to calculate RFIs. An independent set of field data were used to assess whether observed parameter values were consistent with predicted parameter values. This chapter also describes the assumptions made in extrapolating each parameter.

Using maps to spatially predict attributes is an established practice in cartography and geographic information systems (GIS) (Bolstad; 2003). The practice enables a series of observations made at a range of locations to be linked to a classification scheme. By classifying a broader area with the same classification scheme it is then possible to estimate the attributes elsewhere within the area with a degree of confidence. One example of this practice is the use of aerial photography to spatially extrapolate soil characteristics as detailed in Gunn *et al.* (1977). Soil characteristics observed at a number of sparse points are linked to vegetation characteristics, and air photo interpretation is then used to describe the spatial extent of the vegetation characteristics, thereby inferring the spatial distribution of the underlying soils. There is significant potential for errors in this practice, and it is important to characterise the relationship between the attributes and the classification scheme used to extrapolate those attributes. It is also important to test the reliability of these extrapolations using an independent set of data.

The following parameters were not directly measured in the field, Manning's *n* of shallow overland flow, and the distribution of water soluble carbon with depth, these measurements were not collected because the instrumentation and fieldwork required to calculate these data for all of the riparian zone scenarios encountered in the study area would limit the practicality of applying this approach to other areas. For these parameters, the most suitable values were either identified from the literature, or calculated from third party datasets. Values from the literature and third party datasets were linked to, and extrapolated by, the relevant classification scheme. The applicability of the literature values for the study area is discussed for each literature derived value. The additional datasets used in this analysis are the channel cross sections, maximum daily stage height records and stage-discharge curves for all the stream gauging stations in the study area (Queensland Department of Natural Resources and Mines, and Bureau of Meteorology). In addition to this, the data collected as part of the State of the Rivers reporting (Henderson, 2000) were used to provide additional land use, vegetation and channel dimension data.

4.1.1. Statistical Analysis Applied to the Field Data

The data for each parameter that is linked to field data are subjected to a series of processing steps and statistical tests. These steps are as follows.

1. The measurements of each parameter collected during the field work were split up into classes
    a. Manning's *n* measurements were split up into land use classes.
    b. Vegetation measurements (tree height, DBH etc) were split up into vegetation structural classes.
    c. Bank geometry measurements (bank height and channel width) were split up according to Strahler stream order.
2. The distribution of each parameter in each class was characterised. This step was performed on all the field data in each class to assess whether parameter values were normally distributed. This step was done prior to separating the parameters into two groups because the sample size for some parameters was quite small ($N<15$). Parameters found to be normally distributed were represented using means and standard deviations, graphically represented by mean diamonds. Non-normally distributed data were represented using median and quartile values, graphically represented by box plots. This step was undertaken to establish the relationship between each parameter, and the classification scheme that was used to spatially extrapolate that parameter.
3. The parameter distribution of each class was compared with the parameter distribution of other classes. This step was performed to establish whether each class in the classification contained a significantly different parameter distribution, or whether there was some overlap between classes.
4. The parameter measurements were split into two groups: calibration (predicted) and validation (observed), and the summary statistics calculated for each group.
5. The predicted values were compared with observed values to assess whether the observed parameter values were significantly different from those predicted. For parameters with a normal distribution (identified in step 2) an un-paired *t* test was used to compare the predicted and observed values. For parameters that were not normally distributed the predicted and observed values were compared using a non-parametric Wilcoxon rank-sum test. Parameters that

have significantly different predicted and observed values are identified. The potential causes of this difference are discussed briefly, and the implications for indices calculated using this parameter are also discussed.

6. The summary statistics calculated from all the fieldwork data are used to assign parameter values to each classification.

A flow chart summary of these steps is contained in Figure 4.1 (H_0 is the null hypothesis, and H_1 is the alternative hypothesis).

Figure 4.1. Statistical tests applied to the field data to identify parameter values.

For parameters where stream gauging station data and/or State of the Rivers data were included in the analysis, these data were split evenly into the calibration and validation sets. This approach was taken to avoid errors due to different measurement techniques. The parameter value identified in the final (bottom) step of the flow chart is listed in a table at the end of the analysis for each parameter, and it is these values that are used to calculate the RFIs developed in Chapter 2. The level of statistically significant difference, is $\alpha = 0.05$ for all tests applied in this thesis.

4.2 Parameters Linked to a Land Use Map

4.2.1. Manning's n for Shallow Overland Flow

The Manning's *n* parameter described here refers to the resistance of partially-submerged elements subject to shallow overland flow. Literature values (Loch *et al*., 1999) for Manning's *n* of ground cover classes under these flow conditions, that correspond closely with the ground cover classes identified in the Fitzroy catchment are given in Table 4.1. The Manning's *n* for each 5 metres of a transect (n_{5M}) was based on a weighted average of the values listed in Table 4.1 where the weightings were based on the proportion of that ground cover over that 5 metres of the transect observed in the field data.

$$n_{5M} = \left(\left(P_{RG} \times n_{RG}\right) + \left(P_{BG} \times n_{BG}\right) + \left(P_{LL} \times n_{LL}\right) + \left(P_{BS} \times n_{BS}\right)\right) \quad (4.1)$$

where P_{RG} is the proportion of the riparian grass, P_{BG} is the proportion of buffel grass, P_{LL} is the proportion of leaf litter, and P_{BS} is the proportion of bare soil such that $P_{RG} + P_{BG} + P_{LL} + P_{BS} = 1$. Thus, for a 5 metre length of transect containing 60% buffel grass, 30% leaf litter and 10% bare soil, the Manning's *n* for that 5 m (n_{5M}) would be calculated as: $\text{Manning's } n_{5M} = \left((0.6 \times 0.28) + (0.3 \times 0.15) + (0.1 \times 0.08)\right) = 0.221$

Large woody debris (LWD) is considered as an obstruction to flow rather than a roughness element when calculating the Manning's *n* for this index and consequently was omitted from the calculation of the n_{5M} values. Thus, the proportion of ground cover used in Equation (4.1) is the proportion of the area that excludes the LWD. For example, if LWD had been present for 20% of a 5 metre section of the transect all the other

Table 4.1. Manning's *n* values for ground cover types

Ground Cover Class	Manning's *n* value (Loch et al. 1999)
Bare Soil (n_{BS})	0.08
Leaf Litter (n_{LL})	0.15
Leptochloa digitata, *Mnesithea rottboellioides*, *Arundinella nepalensis* (Riparian grasses[14]) (n_{RG})	0.20
Cenchrus ciliaris (Buffel Grass[15]) (n_{BG})	0.28

[14] Riparian grasses with an upright habit, generally with a lower amount of contact cover than buffel grass.
[15] Dense grass with a spreading habit, with a generally high amount of contact cover.

proportions would be divided by 0.8 so that the proportions summed to unity.

To enable the spatial extrapolation of Manning's *n* values across the landscape, a relationship between Manning's *n* values and a remotely sensed land surface coverage (either a land use map or a vegetation map[16]) was established. The n_{5M} values were related to land use because there was no systematic relationship between vegetation structure and n_{5M}. The n_{5M} values relate to the riparian zones adjacent to each land use, not the land uses themselves. This means that the land use adjacent to the riparian zone is used to infer land use and ground cover within the riparian zone.

The n_{5M} values for all of the sites (except the crown land sites) are shown in Figure 4.2 divided up into three land uses: heavy grazing; light grazing and cropping. The heavy grazing sites were identified based on observations in the field and subsequent analysis of the ground cover data. Figure 4.2 shows the combined distribution of n_{5M} according to land use. It is interesting to note that none of the outliers exceed a value of 0.2 for the heavy grazing sites, indicating that there are no areas of high grass cover at these sites. **Please note that classes that have different letters (as seen in** Figure 4.2**) are significantly different at the 95% confidence interval, this convention is used throughout this thesis.**

The Shapiro-Wilk test for normal distribution indicated that the distribution of n_{5M} values are normally distributed ($p<0.0001$) in each class (cropping, heavy grazing and light

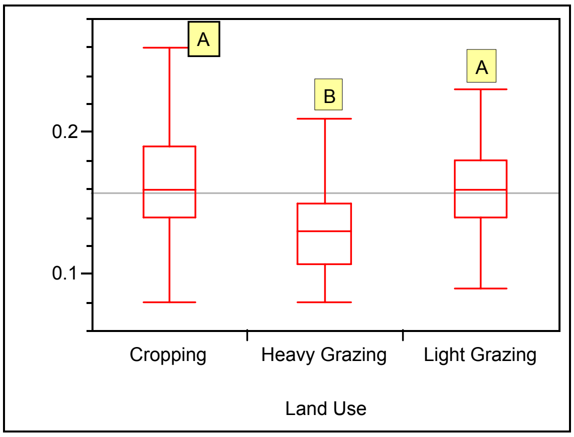

Figure 4.2. Distribution of Manning's n_{5M} values for each land use.[17]

[16] Direct remote sensing of the ground cover is not possible in many riparian zones because tree canopies prevent identification of different ground cover types.

grazing), so students t tests were used on all subsequent tests of n_{5M}. The 5 metre intervals over which ground cover was observed during the fieldwork represent a sample of a much larger population (where that population is the groundcover in riparian zones throughout the study area). For the purposes of this study it is assumed that distribution of the sample (cropping N= 235, light grazing N=400, heavy grazing N=270) is the same as the distribution of the population. The samples were compared using students t tests based on the following hypotheses,

$H_0\ \mu_{LU1} = \mu_{LU2}$

$H_1\ \mu_{LU1} \neq \mu_{LU2,}$

where μ_{LU1} and μ_{LU2} are the mean values for land use 1 and land use 2 respectively. These hypotheses were used to compare cropping with light grazing, cropping with heavy grazing, and light grazing with heavy grazing.

A bare soil class with the Manning's *n* contained in Table 4.1 was included in the land use/land cover map in addition to the three classes above. This class was included because bare soil can be identified adjacent to stream channels in the imagery, and irrespective of land use, bare soil immediately adjacent to the channel will not act as a sediment trap, but rather act as a sediment source.

The field data for the current study were collected in the dry season during a drought period, and consequently represent the lower end of the range of possible ground cover values (at the end of the wet season when grass cover is high the Manning's *n* for all riparian zones are likely to be higher). The temporal variability of the Manning's *n* and the other vegetation parameters is beyond the scope of this thesis. However this could be investigated further using multi-temporal remote sensing as detailed in Section 5.2.3.

Assumptions made in extrapolating the parameter

Assumption 1: Land use adjacent to a riparian zone is a reasonable predictor of Manning's *n* in the riparian zone.

Based on the statistics described in Table 4.1 this is a reasonable assumption at the time the field data were collected. This assumption is likely to be relatively stable over time unless riparian zone management changes. This is due to the fact that while total cover changes relatively quickly as plants grow and wilt the ground cover may change relatively slowly with the accumulation of litter, the growth of biological crusts and the expansion of plant basal area. There is also a causal mechanism for this relationship,

---

[17] The box plots in this chapter have the following format, the box is defined by the 25th to 75th percentiles of the data, the line inside the box is the median, and the whiskers are defined by the 10th and 90th percentiles, all data outside this range (outliers) are described by a black dot.

insofar as grazing within the riparian zone will directly influence the amount of ground cover and thereby the Manning's *n*.[18]

Assumption 2: The Manning's *n* values collected from the literature are reasonable estimate of Manning's *n* values for the ground cover types observed in the field.

The values used in this study were, to the authors' knowledge, the most suitable values available in the literature. The Manning's n_{5M} values could be adjusted in the future if more pertinent values (i.e. those based on observations in the study area) become available. The literature values were obtained from a flume-based study (Loch *et al*., 1999) of the sediment trapping efficiency of four types of filter strip. The four types of filter strip were dense paspalum(*Paspalum wettsteinii*), swamp grass (*Schoenus brevifolius*) leaf litter, and tree litter[19] receiving runoff from turn-out drains in pine forests in South Eastern Queensland. The site descriptions of each flume contained in Loch *et al*. (1999) were carefully examined to identify which sites were most similar to ground conditions observed in the field.

The influence of fencing off the riparian zones on ground cover and Manning's n_{5M} were also assessed and the results are shown in the Appendices. The influence of riparian fences was not pursued further in this thesis due to a lack of spatial data about the location of riparian fences.

Comparing predicted n_{5M} with observed n_{5M}

To assess whether land use was suitable for extrapolating Manning's *n* the average of the n_{5M} values recorded at validation sites were compared with the average of the n5M values at the calibration sites using unpaired students *t* tests.

The results at the 95% confidence interval are given in Table 4.2. Based on the comparison of the calibration and validation datasets the spatial extrapolation predicts the average n_{5M} of riparian zones adjacent light grazing accurately at the 95% confidence

Table 4.2 Results of statistical comparison of predicted and observed mean n_{5M} values.

Land Use	Cropping	Light Grazing	Heavy Grazing	Bare Soil
Null Hypothesis (H_0)	Reject	Accept	Reject	N\A
Trend	Cal>Val	No trend	Cal<Val	N\A
Value used to calculate STI	0.165	0.163	0.130	0.080

[18] Discussions with local farmers indicated that even where riparian zones were fenced off the riparian zones were subject to some grazing.
[19] Branches twigs and stumps resulting from logging

interval. For cropping areas the calibration data predicts higher n_{5M} values than those observed in the validation dataset. The most likely reason for these results is that some of the riparian zones adjacent to cropping are subject to light grazing when cattle are released onto the fields to graze on the stubble after crops have been harvested (Carroll pers com. 2003). If this practice occurred in more of the validation sites than the calibration sites then this would potentially explain the difference. For the heavy grazing class the values observed in the validation set were higher than those predicted from the calibration set. The reasons for this are unclear, although a larger sample size and data on stocking rate may provide insight into the cause of this discrepancy. It is worth noting that even though the n_{5M} observed at the heavy grazing validation sites were higher than predicted, they were still significantly lower ($p<0.001$) than the n_{5M} observed in the riparian zone adjacent to cropping and light grazing.

To calculate the sediment trapping index (STI) the Manning's n_{5M} values listed in Table 4.1 these values are entered into Equation (2.8). The results given in Table 4.2 mean that the STI values calculated for cropping and light grazing will be essentially the same. The STI values calculated for areas subject to heavy grazing will be lower than those calculated for the other two land uses. As a consequence of this the reliability of this index will depend on the capacity to discriminate areas subject to heavy grazing from areas subject to light grazing.

4.3 Parameters Linked to a Vegetation Structural Map

4.3.1. Percentage Foliage Cover (*PFC*)

The percentage foliage cover (*PFC*) of the tallest stratum is the proportion ground area covered by foliage. Calculating the *PFC* is a three step process as described in McDonald *et al*. (1990):

Step 1. Calculate the Crown Separation Ratio (C) as the ratio of the mean gap between crowns to the mean crown width given by

$$C = \frac{\text{Mean Gap}}{\text{Mean Width}} \tag{4.2}$$

Step 2. Calculate the Percentage Crown Cover (%CC) from a relationship with C (Penridge and Walker, 1988)

$$\%CC = \frac{80.6}{(1+C)^2} \tag{4.3}$$

Step 3. Calculate Percentage Foliage Cover (PFC) from CC by

$$PFC = \%CC \times \text{crown type} \tag{4.4}$$

Crown type is defined by the degree of canopy openness, as described in Figure 6 on page 71 of McDonald *et al*. (1990). To illustrate this two photos of different crown types are shown in Figure 4.3, where. The *PFC* data collected at all sites was sorted according to structural class and tested to see if the data were normally distributed.

Figure 4.3. the example on the left has a cover of 65% (low degree of canopy openness), and the example on the right has a cover of 30% (high degree of canopy openness)

The Shapiro-Wilk test for normal distribution indicated that the values are not normally distributed ($p = 0.328$), consequently non-parametric tests are applied to *PFC* values, and the median, rather than the mean *PFC* value is linked to the vegetation classification.

The *PFC* measurements made during the fieldwork represent a sample of a much larger population (where that population is the percentage foliage cover of each vegetation class throughout the study area). For the purposes of this study it is assumed that distribution of the samples in each class (Closed Forest N= 7, Open Forest N=11, Woodland N=50 Open Woodland N=13) is the same as the distribution of the population for each class. The small sample sizes for the closed forest, open forest and open woodland classes may

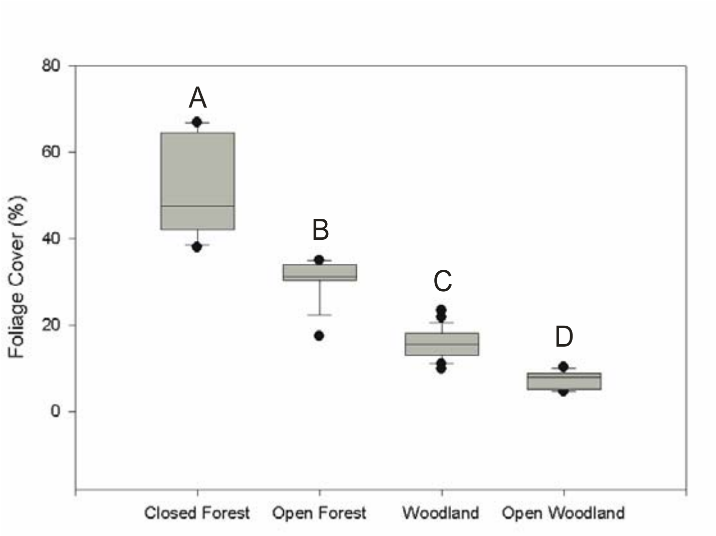

Figure 4.4 The distribution of *PFC* for each structural class (showing all outliers)

not fully characterise the population, and are insufficient to carry out conclusive statistical tests in the case of the two forest classes. However the samples collected for each class are consistent with the expectations in terms of the relative *PFC* values, in other words, the expected trend in *PFC*, closed forest>open forest>woodland>open woodland was observed in the majority of samples. The *PFC* for each 'calibration' transect segment were sorted according to structural class as shown in Figure 4.4 This relationship fits in with expectations insofar as areas with high degree of canopy closure have a high percentage foliage cover.

Each structural class is significantly different from the others, as indicated by the fact that each box plot has a unique letter.

Assumption 1. It is possible to discriminate canopy classes from satellite imagery.

This is a reasonable assumption because canopy closure affects the way light is reflected from the canopy, and previous studies have shown that it is possible to discriminate canopy classes from satellite imagery (Walker *et al*., 1986). This assumption is tested using a confusion matrix in Section 5.2.2

Assumption 2. That PFC is stable over time.

It is likely that *PFC* will change over time, particularly given that some tree species in the study area are deciduous. While the absolute values of *PFC* are likely to change over time, the relative values of the *PFC* are likely to stay the same (*i.e.* it is unlikely that a stand of vegetation identified as open woodland will develop a higher *PFC* than open forest. An extended fieldwork campaign involving additional data acquisition would be required to describe the temporal variability of *PFC*, and as such is beyond the scope of this thesis. Given that the *PFC* values are calculated for the end of the dry season, they represent the lower end of the *PFC* range that would be encountered in these riparian zones.

To assess whether the vegetation structural classification was reliably extrapolating *PFC* the median values recorded at validation sites were compared with the median of the *PFC* values at the calibration sites using a Wilcoxon Rank Sum tests to test the following hypotheses.

$H_0\ median_{cal} = median_{val}$

$H_1\ median_{cal} \neq median_{val}$.

Table 4.3 Results of statistical comparison of predicted and observed median *PFC* values.

Structural Class	Closed Forest	Open Forest	Woodland	Open Woodland
Null Hypothesis (H_0)	Sample to small	Sample to small	Accept	Accept
Trend	No trend	No trend	No trend	No trend
Value used to calculate SSI	48.9	30.7	15.6	8.2

These hypotheses were used to test every vegetation structural parameter, but are not shown for subsequent parameters in the interests of brevity. The results at the 95% confidence interval are shown in Table 4.3. These results indicate that observed values are not significantly different to the predicted values for *PFC* across the two woodland classes. Visual assessment of the predicted and observed values for the two forest classes shows similar values in both predictions and observations in each class, and the values for both classes fit in with expected trends closed forest>open forest>both woodland classes Based on this the vegetation structural classification can be used with confidence to predict *PFC* for woodland classes. There are insufficient data to assess whether *PFC* can be reliably predicted for the forest classes. However given that the same factors determine *PFC* in both woodland and forest vegetation classes (in this environment water availability), and that *PFC* directly influences the way vegetation reflects light (and thereby the signal received by the satellite) it is assumed for the purposes of this thesis that vegetation structure can be used to predict *PFC* for the forest and woodland vegetation classes.

The stream shading index (SSI) is the only index that uses the *PFC* parameter. The *PFC* parameters were collected towards the end of the dry season (October to November) and are likely to represent the lower end of possible *PFC* values. As a consequence of this the SSI calculated using these 'dry season' *PFC* values may underestimate the amount of shade provided by riparian vegetation for periods that support a higher *PFC*, such as those experienced at the end of the wet season. However this is unlikely to change the information provided by either SSI_{LOCAL} or SSI_{GLOBAL} because both indices are ratios and the relative difference between the *PFC* of any two vegetation types is likely to remain the same (*i.e.* a woodland will have a lower *PFC* than a closed forest irrespective of whether the PFC data are collected during the dry season, or at the end of the wet season).

4.3.2. Tree Height (*TH*)

Tree heights were measured using a clinometer as part of the field work as described in Section 3.3.2. The vegetation height refers to the height of the top of the canopy of the tallest strata as described in McDonald *et al*. (1990). The range of tree heights observed for each structural class is shown in Figure 4.5

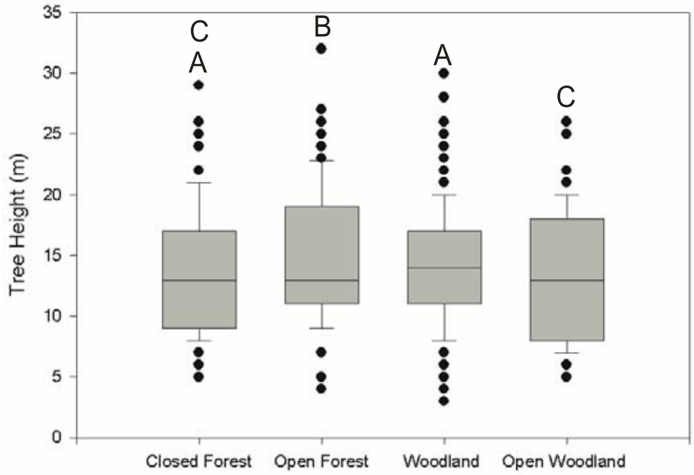

Figure 4.5. The distribution of tree heights for each height

The Shapiro-Wilk test indicated that tree heights were normally distributed ($p<0.0001$). Consequently average values are used to characterise this parameter, and the predicted and observed values are compared using unpaired students *t* tests. The open forest class is significantly taller than the other 3 classes, with overlap between the remaining 3 classes. The tree height measurements made during the fieldwork represent a sample of a much larger population (where that population is the height of individual trees in each vegetation class throughout the study area). For the purposes of this study it is assumed that the distribution of the samples in each class (Closed Forest N= 85, Open Forest N=106, Woodland N=718 Open Woodland N=107) is the same as the distribution of the population for each class.

To assess whether the vegetation structural classification was reliably extrapolating tree height the average values recorded at validation sites were compared with the average of the tree height values at the calibration sites using a series of unpaired student's *t* tests. The results at the 95% confidence interval are as shown in Table 4.4. These results indicate that the classification can be used to predict tree height for the two forest classes, but not for the two woodland classes. The reason why the observed tree heights were

Table 4.4 Results of statistical comparison of predicted and observed mean *TH* values.

Structural Class	Closed Forest	Open Forest	Woodland	Open Woodland
Null Hypothesis (H_0)	Accept	Accept	Reject	Reject
Trend	No trend	No trend	Cal>Val	Cal>Val
Values used to calculate SSI	13.4	14.7	13.7	12.5

significantly lower than predicted for the two woodland classes is unclear, although land clearing and regrowth may mean that some of the vegetation is not at climax, which could explain the height differences. The difference between the predicted and observed average value was less than 1 metre in the case of woodland and less than 3 metres in the case of open woodland. Whilst these discrepancies will result in different SSI values, the variation between SSI values (less than 1% of incoming solar radiation) is not of great concern. The stream shading index (SSI) is the only index that uses the tree height parameter. To calculate the SSI the canopy radius (C_{rad}) values listed in the following section are subtracted from the tree height (*TH*) values shown in Table 4.4 to calculate the tree trunk height (*TTH*) which is entered into Equation (2.31).

4.3.3. Canopy Radius (C_{rad})

The technique for measuring canopy radius is described in Section 3.3.1. The range of canopy radius measurements observed for each vegetation type is shown in Figure 4.6.

The Shapiro-Wilk test indicated that canopy radius (C_{rad}) values were normally distributed ($p<0.0001$). Consequently average values are used to characterise this parameter, and the predicted and observed values are compared using unpaired students *t* tests. The open woodland class is significantly taller than the woodland class, with no other significant differences. The C_{rad} measurements made during the fieldwork represent a sample of a much larger population (where that population is the canopy radii of trees vegetation class throughout the study area). For the purposes of this study it is

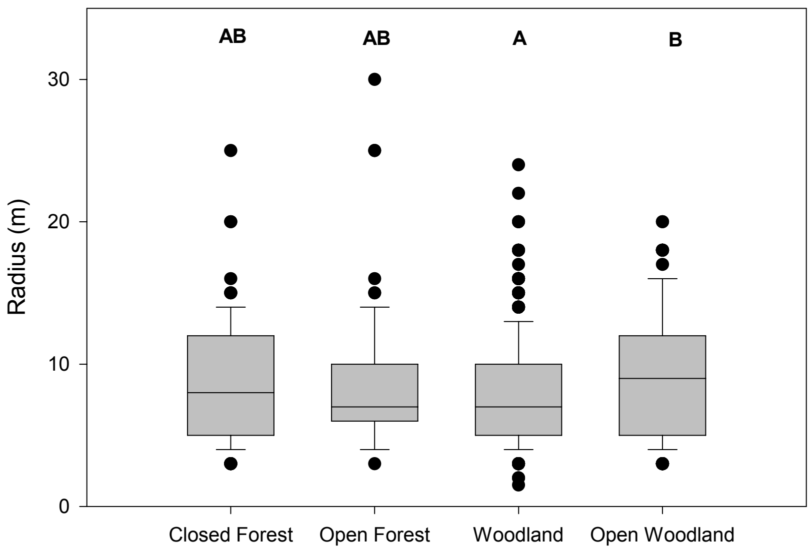

Figure 4.6 Canopy radii values for each vegetation class

Table 4.5 Results of statistical comparison of predicted and observed mean C_{rad} values.

Structural Class	Closed Forest	Open Forest	Woodland	Open Woodland
Null Hypothesis (H_0)	Accept	Accept	Accept	Reject
Trend	No trend	No trend	No trend	Cal>Val
Values used to calculate the SSI	8.4	8.8	7.8	9.3

assumed that distribution of the samples in each class (Closed Forest N= 85, Open Forest N=106, Woodland N=718 Open Woodland N=107) is the same as the distribution of the population for each class.

To assess whether the vegetation structural classification was reliably predicting C_{rad} the average values recorded at validation sites were compared with the average of the PFC values at the calibration sites using a series of unpaired student's *t* tests. The results at the 95% confidence interval are shown in Table 4.5 Based on these results the vegetation classification can be used to predict C_{rad} values for both forest classes and the woodland class. The reason for the difference between predicted and observed mean values for the open woodland class is unclear, however the clearing/regrowth scenario discussed briefly in the *TH* parameter may also apply to C_{rad}.

4.3.4. The Number of Trees Per Hectare (λ)

The number of trees per hectare λ is calculated from the field measurements of canopy radii and the distance between canopies using the method described in Jupp and Lovell (2000). The range of λ values calculated from the field data are shown in Figure 4.7.

The λ measurements made during the fieldwork represent a sample of a much larger population (where that population is the λ of each vegetation structural class throughout the study area). For the purposes of this study it is assumed that distribution of the samples in each class (Closed Forest N= 7, Open Forest N=11, Woodland N=50 Open Woodland N=13) is the same as the distribution of the population for each class.

The small sample sizes for the closed forest, open forest and open woodland classes may not fully characterise the population, and are insufficient to carry out conclusive statistical tests in the case of the two forest classes. However the samples collected for each class are consistent with the expectations in terms of the relative λ values, in other words, the expected trend in λ, closed forest>open forest>woodland>open woodland was observed in the majority of samples. The λ for each 'calibration' transect segment were sorted according to structural class as shown in Figure 4.4 This relationship fits in with expectations insofar as areas with high degree of canopy closure have a high λ.

The Shapiro-Wilk test indicated that the number of trees per hectare (λ) values were normally distributed ($p<0.0001$). However the small sample sizes render this test meaningless for the two forest classes. In the interests of performing robust statistical analysis, median values are used to characterise this parameter, and the predicted and observed values were compared using Wilcoxon Rank Sum tests. There were statistically significant differences between all vegetation structural classes, and λ values followed the expected trend of closed forest>open forest>woodland>open woodland.

To assess whether the vegetation structural classification was reliably extrapolating λ the average values recorded at validation sites were compared with the average of the *PFC* values at the calibration sites using a series of unpaired students *t* tests. The results at the 95% confidence interval are contained in Table 4.6. These results indicate that observed values are not significantly different to the predicted values for λ across the two woodland classes. Visual assessment of the predicted and observed values for the two forest classes found them to be similar values in both predicted and observed in each class, and the values for both classes fit with the expected trend of closed forest>open forest>both woodland classes Based on this the vegetation structural classification can be reliable be used to predict λ for woodland classes. There are insufficient data to assess whether λ can be reliably predicted for the forest classes. However it is assumed for the purposes of this thesis that vegetation structure can be used to predict λ for the forest and woodland vegetation classes.

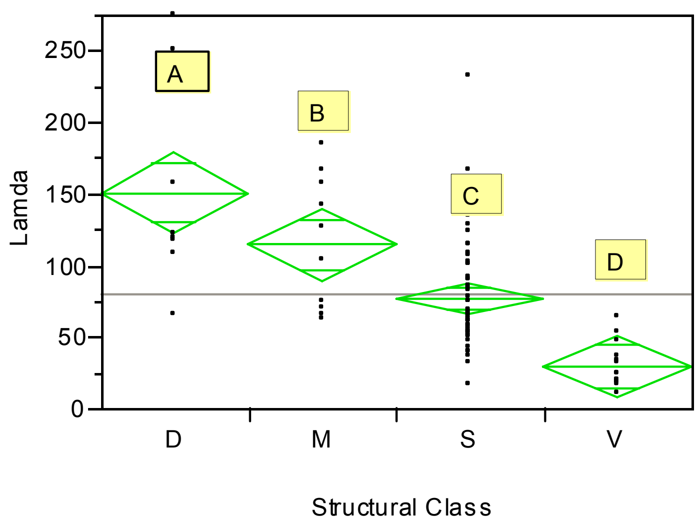

Figure 4.7 Distribution of λ values for each vegetation class, D, M, S and V stand for closed forest, open forest, woodland and open woodland respectively

Table 4.6 Results of statistical comparison of predicted and observed median λ values.

Structural Class	Closed Forest	Open Forest	Woodland	Open Woodland
Null Hypothesis (H_0)	Insufficient data	Insufficient data	Accept	Accept
Trend			No trend	No trend
Values used to calculate BRI, DNI	169	114	77	29

The bank reinforcement index (BRI) and denitrification index (DNI) are calculated using the parameter. The assumption that the vegetation structural classes can predict λ values for the two forest classes may lead to inaccuracies in the DNI and BRI values calculated for the two forest classes.

4.3.5. Aboveground woody biomass ($wood_A$)

The diameter at breast height (DBH) is used in conjunction with λ and vegetation height to calculate the volume of timber per hectare. This is based on the approach described in Jupp and Lovell (2000) for calculating basal area, with some modifications based on the assumptions described in Marsh *et al*. (2001). To calculate the volume of timber the following steps were taken:

Step 1 Calculate the DBH and height of each tree

Step 2 Multiply the height by the DBH to calculate the volume of wood per tree ($wood_T$) (this ignores any differences in branching habit between trees according to the assumptions described in Marsh *et al*. (2001))

$$wood_T = \left(\pi \times \left(\frac{DBH}{2} \right)^2 \right) \times TH \, , \qquad (4.5)$$

where *DBH* is the diameter at breast height in metres and *TH* is the tree height in metres.

Step 3 Multiply the volume of wood per tree by the number of trees (λ) per hectare to calculate the volume of wood per hectare ($wood_A$),

$$wood_A = wood_T \times \lambda \, . \qquad (4.6)$$

This process was performed for the $wood_T$ for each tree and the λ values for each vegetation structural subsection of each transect, and the results are shown in Figure 4.8.

The $wood_A$ measurements made during the fieldwork represent a sample of a much larger population (where that population is the $wood_A$ of each vegetation structural class throughout the study area). For the purposes of this study it is assumed that distribution of the samples in each class (Closed Forest N= 85, Open Forest N=106, Woodland N=718 Open Woodland N=107) is the same as the distribution of the population for each class. The results for each class are consistent with the expectations in terms of the relative $wood_A$ values, in other words, the expected trend in $wood_A$, closed forest>open forest>woodland>open woodland was observed in the majority of samples. The $wood_A$ for each 'calibration' transect segment were sorted according to structural class as shown in Figure 4.8.

This results are consistent with expectations insofar as areas with high degree of canopy closure have a high $wood_A$. The Shapiro-Wilk test indicated that the number of trees per hectare ($wood_A$) values were not normally distributed (p=0.8). Consequently median values were used to characterise this parameter, and the predicted and observed values were compared using Wilcoxon rank sum tests. There were statistically significant differences between all vegetation structural classes, and $wood_A$ values followed the trend of open forest>closed forest>woodland>open woodland. It is interesting to note that the volume of wood per hectare $wood_A$ is highest in the open forest class. This is due to the fact that trees in the open forest class had higher DBH and tree height values, counteracting the effect of λ on the $wood_A$ values.

To assess whether the vegetation structural classification was reliably predicting $wood_A$ the average values recorded at validation sites were compared with the average of the $wood_A$ values at the calibration sites using a series of unpaired student's *t* tests.

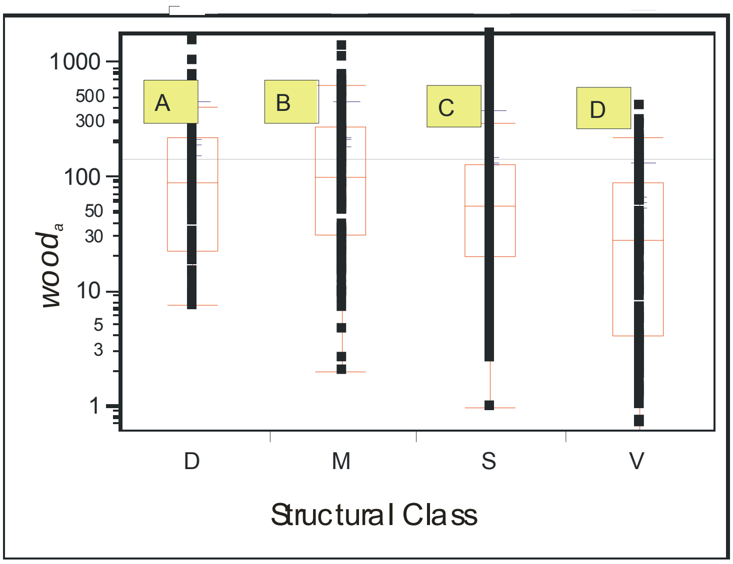

Figure 4.8The range of $wood_A$ values for each structural class, units are m^3 ha^{-1}.

Table 4.7 Results of statistical comparison of predicted and observed median $wood_A$ values.

Structural Class	Closed Forest	Open Forest	Woodland	Open Woodland
Null Hypothesis (H_0)	Accept	Accept	Accept	Accept
Trend	No trend	No trend	No trend	No trend
Values used to calculate LWDI (m^3 ha^{-1})	88	94	54	28

The results at the 95% confidence interval are listed in Figure 4.8. These results indicate that observed values are not significantly different to the predicted values for $wood_A$ across the all classes. Based on this the vegetation structural classification can be reliable be used to predict $wood_A$ for all classes. The large woody debris index (LWDI) and denitrification index (DNI) are calculated using the parameter $wood_A$.

4.3.6. Water soluble carbon (WSC_x)

The water soluble carbon parameter is required to calculate the denitrification index DNI. The amount of water soluble carbon (WSC) associated with each vegetation type was not measured directly during the field work. Consequently calculating the amount of WSC present in soil depth range x for either the current or reference condition requires three of steps.

1. Establish a relationship between a parameter measured during the fieldwork, above ground stem biomass ($wood_A$ kg ha^{-1})and the amount of soil organic carbon (kg ha^{-1}) for each vegetation class.
2. Calculate the amount of WSC based on the amount of soil organic carbon.
3. Describe the distribution of WSC with depth.

The relationship between above-ground stem biomass and soil organic carbon

In a study of plantation Eucalypts in Portugal, Kätterer *et al*. (1995) describes the relationship between above-ground stem biomass and soil organic carbon (SOC). The study explores the influence of irrigation and fertilisation on the distribution of fine roots and SOC. For the purposes of this thesis we use the figures for above-ground stem biomass and SOC from their control site, based on the assumption that the control site is most likely to represent natural conditions. Kätterer *et al*. (1995) reports the following figures for above-ground stem biomass and SOC respectively 9.3 kg m^{-2} and 0.15kg m^{-2}. If we assume that this relationship applies to the vegetation encountered in the study area of this thesis then SOC for any given vegetation type can be calculated using Equation (4.7).

$$SOC_{TOT} = 96 wood_A \tag{4.7}$$

Where SOC_{TOT} is the total amount of soil organic carbon (kg ha^{-1}) $wood_A$ is the above ground woody biomass (m^3 ha^{-1}). The climate and the soil type described by Kätterer *et al*. (1995) differ from those found in the study area, although both areas have relatively low (circa 600mm year rainfall), hence the relationship between above-ground stem biomass and SOC in the study area may differ from that described in Equation (4.7). However, to the authors knowledge, the relationship described in Equation (4.7) is the most applicable relationship between above-ground stem biomass and SOC available in the literature, given that it pertains to a species of the *Eucalyptus* genus, which is one of the dominant genera within the study area, which is growing in an area of relatively low rainfall.

Calculating the amount of water soluble carbon from the amount of soil organic carbon

It is possible to calculate the amount of WSC at a given soil depth if the amount of SOC at that depth is known using data contained (O'brien *et al*., 2003). In order to use these data, first it is necessary to calculate the amount of SOC at a given depth. If we assume that the SOC present in the soil is present as a result of root mortality and root exudates (Grayston *et al*., 1997), then the distribution of SOC with depth will be the same as the distribution of roots (this ignores leaf litter decomposition as a source of SOC for the surface soil layers, however this is dealt with in a subsequent section). The distribution of roots with depth was calculated as the parameter c_r in the Appendix. Assuming that roots capable of providing cohesion are also capable of providing SOC then the distribution of SOC with depth can be calculated using Equation (4.8).

$$\%SOC_x = \%c_{r_x} \tag{4.8}$$

Where $\%SOC_x$ is the percentage of the total SOC contained in soil depth range x, and $\%c_{r_x}$ is the percentage of the total c_r contained in the same soil depth range.

SOC can be broken down into two types (or pools) of carbon, labile, and recalcitrant. Labile carbon includes carbohydrates, proteins, whereas recalcitrant carbon consists predominantly of lignin, but also includes suberins, resins, fats and waxes (Rovira and Vallejo, 2002). The labile pool can be further broken down into two pools, labile I and labile II depending on whether the carbohydrates are masked by lignin (labile II) or not (labile I). A portion of the labile I pool is available as water soluble carbon (O'brien *et al*., 2003). As mentioned earlier, it is the WSC (*i.e.* the pool that can become DOC in the presence of water) that is of interest in terms of denitrification. Given that lignin biodegradation is hindered under anaerobic conditions (Rovira and Vallejo, 2002) (*i.e.* carbon from labile pool II is unlikely to be converted into WSC during the anaerobic conditions associated with denitrification events), it is probable that only the WSC is available to denitrifying bacteria during denitrification events.

Calculating the amount of water soluble carbon for soil depth *x*

In a study of that measured the distribution of WSC under a *Eucalyptus regnans* forest over various soil depths (O'brien *et al*., 2003) describes WSC as a fraction of SOC (measured as Walkley-Black organic carbon). Using the figures contained in (O'brien *et al*., 2003) the WSC fraction at depth *x* as a function of SOC_x can be calculated using Equation (4.9).

$$WSC_x = 0.01\mathrm{e}^{0.03SOC_x} \tag{4.9}$$

Equation (4.9) was formulated using the data for water soluble carbon and Walkley-Black organic carbon contained in Table 2 of O'brien *et al*. (2003). It was calculated by fitting a curve to the relationship between WSC with Walkley-Black organic carbon, using Walkley-Black organic carbon as the independent variable, and WSC as the dependent variable.

This approach ignores the temporal dynamics of the various carbon pools, because it describes WSC as a steady state function of vegetation structure (via $wood_A$). The authour acknowledges that the amount of WSC is likely to vary throughout the year, depending on generation rates by root mortality, root exudation rates, and consumption by fungi and bacteria under both aerobic and anaerobic conditions (Kätterer *et al*., 1995). However, in the absence of any other data, Equation (4.9) will be used to estimate the total amount of WSC available for denitrifying bacteria.

During flood events on semi-arid floodplain rivers, decomposing *Eucalyptus camaldulensis* leaf litter can generate up to 50 g DOC m^{-2} (Robertson *et al*., 1999), which will provide an additional input of WSC into the topsoil, water soluble carbon due to leaf litter WSC_{LL}. To account for this additional souce of WSC that is available to the topsoil, the WSC for the surface soil layer $WSC_{x=0.25}$ will be calculated using

Table 4.8 *%WSC_x* values for each vegetation structural class based on soil organic carbon only

Soil Depth Range (m)	Closed Forest	Open Forest	Woodland	Open woodland
0 to 0.25	58.10%	67.87%	11.43%	5.02%
0.25 to 0.5	14.73%	22.98%	1.70%	0.33%
0.5 to 1	4.39%	6.22%	0.81%	0.22%
1 to 2	1.28%	1.65%	0.38%	0.15%
2 to 3	0.53%	0.63%	0.22%	0.11%
3 to 4	0.28%	0.32%	0.15%	0.09%
4 to 5	0.18%	0.19%	0.11%	0.08%
5 to 6	0.13%	0.14%	0.09%	0.07%

Table 4.9 The proportion of pre-settlement WSC remaining in the soil at present.

Land Use	ψ	Reference
Light Grazing	1-WSC_{LL}	(Northup *et al.*, 1999; Dalal and Chan, 2001)
Heavy Grazing	0.5	(Holt, 1997)
Cropping	0.2	(Dalal and Chan, 2001)

$$WSC_{x=0.25} = WSC_x + WSC_{LL} \tag{4.10}$$

Where WSC_x is calculated using Equation (4.9) and WSC_{LL} is calculated using

$$WSC_{LL} = 50 \times \frac{PFC_{\text{current}}}{PFC_{\text{closed forest}}} \tag{4.11}$$

Where $PFC_{current}$ and $PFC_{closedforest}$ represent the percentage foliage cover (PFC) of the current vegetation and that observed in closed forest respectively. Based on the assumption that the pockets of closed forest observed during the fieldwork are capable of producing 50g DOC m^{-2}, and that litterfall volume is a direct function of percentage foliage cover (Francis and Sheldon, 2002).

The distribution of WSC shown in Table 4.8 (*i.e.* decreasing WSC with depth) is consistent that described by Liu and Sheu (2003). For areas no longer under native vegetation (*i.e.* areas that have been cleared for cropping or grazing) $WSC^{\text{Current}}_{x=0.25}$ was calculated as a percentage of the $WSC^{\text{Reference}}_{x=0.25}$ using Equation (4.12).

$$WSC^{\text{Current}}_{x=0.25} = \psi WSC^{\text{Reference}}_{x=0.25} \tag{4.12}$$

Where ψ represents the proportion of the original SOC remaining in the soil and the values for ψ are shown in Table 4.9. The ψ described for light grazing is based on the assumption that WSC (and thereby WSC) in the surface soil layer (x = 0.25) generated by root turnover and exudates don't change as a result of light grazing, which is consistent with the findings of other studies (Northup *et al.*, 1999; Evrendilek *et al.*, 2004). In the absence of tree cover, though there will be no WSC inputs from leaf litter.

It is assumed that areas that have been cleared for grazing or cropping have zero tree cover, and therefore generate no WSC in deeper soil layers (x >0.25), consequently the WSC amounts in these deeper soil layers is zero, this is consistent with the behaviour of SOC in cropping areas of semi-arid north eastern Australia described in Dalal and Chan (2001). It is also assumed that the areas cleared for grazing or cropping have been cleared for more than ten years. During which time SOC will have stabilized at these new levels (Dalal and Chan, 2001).

Residence time

The second factor that limits denitrification is residence time. Denitrification can occur rapidly when the nitrate comes into contact with WSC (Hill *et al*., 2000), however this is much evidence to suggest that limited contact time can reduce the amount of denitrification (Burt *et al*., 1999).

Residence time, for the purposes of this thesis, is defined in terms of the period of time that the watertable spends in one of the depth range x as previously described previously in. The temporal resolution of floodplain watertable records in the study area is very coarse (annual at best), making it very difficult to accurately assess the duration of the watertable at any specific height. River stage height is used in this thesis as a surrogate for watertable heights, based on the assumption that the water level in the river is equivalent to the watertable height in the adjacent riparian zone. This is consistent with the description of arid zone riparian denitrification as described in Schade *et al.*, (2002). This assumption is likely to be violated during periods of rapid change in the hydrograph, and is likely to be locally inaccurate depending on the hydraulic conductivity of the bank sediments and surrounding floodplain sediments.

If these assumptions are accepted, then the residence time of water within a certain depth range can be calculated as the proportion of time that the river is at or above a certain stage height if the channel geometry is known. For example the period of time that watertable is in depth range $x = 0.25$ is equal to the amount of time that the watertable is less than 25 centimetres below bankfull capacity.

Stage height records were available for thirteen gauging stations in the study area. Details of the gauging stations are contained in the Appendices. Because stage height records were not available for every section of the stream network a series of steps were taken to estimate the frequency and duration of events where the water table reaches soil depth range x at any part of the stream network. These steps are described below:

1. Calculate frequency and duration of the water table occurring in x, and the interval between events at every gauging station, analysing regulated period of the record separately to unregulated period if the river had become regulated at some point.
2. Calculate the average number of inundation events for each soil depth x $\left(NDNE_x\right)$ for each stream order for unregulated streams.
3. Calculate the average number of inundation events for each soil depth x for each regulated river reach $NDNE_x$ (assuming that all points down stream of the gauge have the same stage height characteristics as the gauge, until the stream joins a higher order stream).

4. Calculate the relative importance of denitrification on the floodplain rather than in the littoral zone by calculating the number of overbank flow events $NDNE_{OB}$, using records from all unregulated gauging stations to calculate the overbank frequency.

It is worth noting that gauging stations were all located on 3rd order or higher streams, consequently the stage height characteristics of 1st and 2nd order streams could not be calculated. Low order streams within the study area (described in Chapter 3) are typically highly ephemeral, flowing only for short periods during and immediately after rainfall events. As a result of this it is unlikely that the WHC in the riparian zones of low order, hillslope constrained, streams would exceed 60% for a long enough period for denitrification to occur.

Calculating the DNI for stands of floodplain vegetation requires some additional assumptions. The anastomosing river system in the study area (Section 3.2) makes it difficult to assign Strahler stream orders to various sections of the floodplain. Consequently, all floodplains are assigned the same overbank frequency. This assumption is likely to be violated at various points along the channel network depending on channel and floodplain geometry, and event magnitude, but is necessary in the absence of any additional data. As a consequence of this assumption the DNIlocal will show the change in long term average DN capacity, rather than the change in DN capacity for a specific event. A further assumption is that the entire floodplain[20] is inundated (*i.e* all floodplain vegetation is considered equal, irrespective of its elevation relative to the main channel), and is inundated for eight days (the period of time required for all DOC to be consumed as discussed earlier). Both of these assumptions are likely to be violated for a specific event, but these assumptions are necessary in the absence of any additional data. Soil organic carbon data was not available for vegetation and soil types found in the study region. Consequently the $wood_A$ parameter was used to estimate the total amount of amount of soil organic carbon SOC_{TOT} using Equation (4.7), from this SOC_{TOT} value for each vegetation class, the parameters $\%SOC_x$ and $\%WSC_x$ were calculated using Equations (4.8) and (4.9) respectively. The final values for $\%WSC_x$ are shown in Table 4.10.

It is interesting to note that open forest, rather than closed forest contains the highest $\%WSC_x$ value, reflecting the high above ground biomass values observed for open forest. If the organic carbon values identified from the literature are inconsistent with the actual organic values found in the field, then this will lead to spurious DNI results. This is why the DNI is normalized and provides a relative assessment (denitrification is more likely to be occurring in place A rather than place B) rather than an estimated value of the amount of denitrification (this stand of vegetation will remove a certain number

[20] The method for identifying floodplain extent is contained in Section 5.3.3

Table 4.10 *%WSC$_x$* values for each vegetation structural class

Soil Depth Range (m)	Closed Forest	Open Forest	Woodland	Open woodland
0 to 0.25	58.10%	67.87%	11.43%	5.02%
0.25 to 0.5	14.73%	22.98%	1.70%	0.33%
0.5 to 1	4.39%	6.22%	0.81%	0.22%
1 to 2	1.28%	1.65%	0.38%	0.15%
2 to 3	0.53%	0.63%	0.22%	0.11%
3 to 4	0.28%	0.32%	0.15%	0.09%
4 to 5	0.18%	0.19%	0.11%	0.08%
5 to 6	0.13%	0.14%	0.09%	0.07%

kilograms of nitrogen per year). The other important feature to notice is that the majority of the water soluble carbon is contained in the top 50cm of the soil, consequently the DNI (the only index to use this parameter) is highly sensitive to calculations of bankfull frequency.

4.4 Parameters linked to Strahler Stream Order

Using a series of channel cross sections to characterize hydraulic geometry relationships for a specific catchment is a recognised technique (Western *et al*., 1997). Traditionally hydraulic-geometry relationships use discharge Q (m^3 s^{-1}) to predict channel dimensions using Equations (4.13), (4.14) and (4.15) (Western *et al*., 1997; Ibbitt, 1997; Merritt and Wohl, 2003)

$$W = aQ^b \qquad (4.13)$$

$$D = cQ^f \qquad (4.14)$$

$$V = kQ^m \, , \qquad (4.15)$$

where W is the channel width in metres, D is the channel depth in metres, V is the flow velocity in metres per second, and $a, b, c, f, k,$ and m are numerical constants that are related by continuity such that $a \times c \times k = 1$ and $b + f + m = 1$.

Direct calculation of Q requires three parameters: catchment area, rainfall and the rainfall:runoff coefficient. For the purposes of this study it was not possible to calculate Q for all sections of the stream network. This was due to the fact that the catchment area parameter was not available for all links of the channel network. The reason for this is that the channel network derived from the digital elevation model was not spatially accurate for the purposes of this study and therefore required modification (this problem and associated solution is described in greater detail in Chapter 5). The process of re-digitising the channel network removed the catchment area parameters from re-digitised links. Consequently Strahler stream order was used to approximate catchment area, slope and Q for all links in the channel network. In addition the hydraulic geometry parameters bank height (*BH*) and channel width (*CW*) recorded at the field sites were combined with channel cross sections for each stream gauging station and State of the Rivers survey data. The combined data were used sorted according Strahler stream order to calculate the BH and CW parameters for each Strahler stream order.

The hydraulic geometry parameters were measured at the point where the width to depth ratio reached a minimum as described in Harvey (1969). The bank height parameter was calculated as difference in elevation between that at the top of the bank and that at the base of the channel. For multi-channel cross section the deepest channel was used to calculate bank height. Cross sections with no clearly defined channels were omitted from the analysis (both for bank height and channel width). If the two banks were of uneven height the lower bank was used to define bank height based on the methodology described in Harvey (1969). The bank height and channel width parameters can be seen in Figure 4.9.

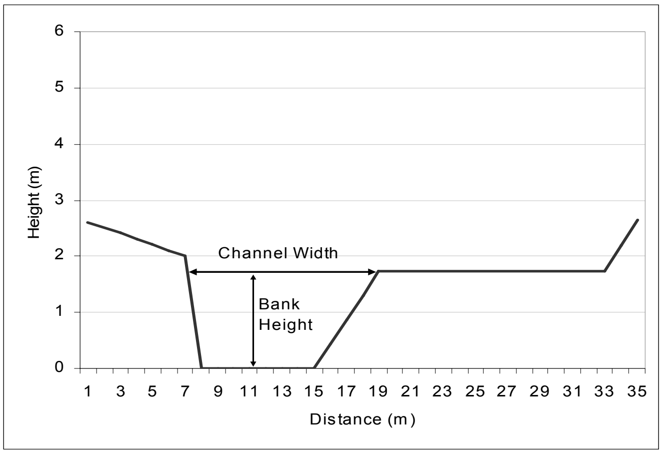

Figure 4.9 Definition of channel parameters

4.4.1. Bank Height (*BH*)

The bank heights observed in the field data, channel cross-sections recorded at stream gauging stations and the State of the Rivers data for each Strahler stream order are shown in Figure 4.10. The bank height (*BH*) measurements from all three data sources represent a sample of a much larger population (where that population is the bank height of each stream of a given Strahler stream order throughout the study area). For the purposes of this study it is assumed that distribution of the samples in each class (1st order N= 27, 2nd order N= 41, 3rd order N= 45, 4th order N= 20, 5th order N=6, 6th order N= 12) is the same as the distribution of the population for each class. The small sample sizes for 5th and 6th order streams may not fully characterise the population, and are insufficient to carry out conclusive statistical tests in the case of these two stream orders. However the samples collected for each class are consistent with the expectations in terms of the relative *BH* values, in other words, the expected trend in BH 6th order> 5th order> 4th order> 3rd order> 2nd order> 1st order was observed in the majority of samples. This is consistent with hydraulic geometry theory insofar as the higher the stream order (in this situation a proxy for catchment area) the higher the banks. The Shapiro-Wilk test indicated that the *BH* values were not normally distributed (p=0.7), consequently median values are used to characterise this parameter, and the predicted and observed values were compared using Wilcoxon rank sum tests. There were statistically significant differences between all stream orders.

To assess whether the stream order classification was reliably extrapolating *BH* the median values recorded at validation sites (in this case chosen at random from the three datasets, fieldwork, gauging station and State of the Rivers) were compared with the median of the *BH* values at the calibration sites using a series of Wilcoxon rank sum tests. The results at the 95% confidence interval are as shown in Table 4.11. It is worth noting that while the Wilcoxon rank sum test found no significant difference between observed and predicted median values for 5th order streams, the number of observations

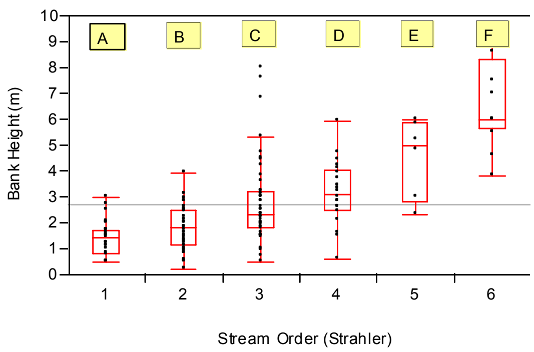

Figure 4.10 Bank Heights for each Strahler stream order.

Table 4.11 Results of statistical comparison of predicted and observed median *BH* values.

Structural Class	**1st order**	**2nd order**	**3rd order**	**4th order**	**5th order**	**6th order**
Null Hypothesis (H_0)	Accept	Accept	Accept	Accept	Insufficient data	Accept
Trend	No trend	No trend	No trend	No trend		No trend
Values used to calculate RFIs	1.4	1.8	2.3	3.1	5.0	6.0

is relatively low, and their were insufficient data to assess whether 5th order stream dimensions were being reliably predicted.

These results indicate that observed values are not significantly different to the predicted values for *BH* across the all classes except for 5th order streams. Given that the factors that determine hydraulic geometry (catchment area, rainfall and rainfall: runoff coefficient) are likely to be similar for 5th order stream channels, it is assumed for the purposes of this thesis that *BH* can be predicted as a function of stream order for 5th order streams. Based on this the Strahler stream order classification can be reliable be used to predict median *BH* for all stream orders. The stream shading index (SSI), bank reinforcement index (BRI) and denitrification index (DNI) are calculated using the parameter *BH*.

4.4.2. Channel Width (*CW*)

Channel width (*CW*) measurements were collected from three sources, the channel surveys collected during the field work, the channel cross-sections recorded at QDNRM stream gauging stations and the channel geometry measurements made at each of the State of the Rivers suvey locations. These *CW* data were sorted according to Strahler stream order are shown in Figure 4.10.

Table 4.12 Results of statistical comparison of predicted and observed median *CW* values.

Structural Class	**1st order**	**2nd order**	**3rd order**	**4th order**	**5th order**	**6th order**
Null Hypothesis (H_0)	Accept	Accept	Accept	Accept	Insufficient data	Accept
Trend	No trend	No trend	No trend	No trend		No trend
Values used to calculate BRI, LWDI and SSI	7.8	13	21.5	21.3	29.5	31

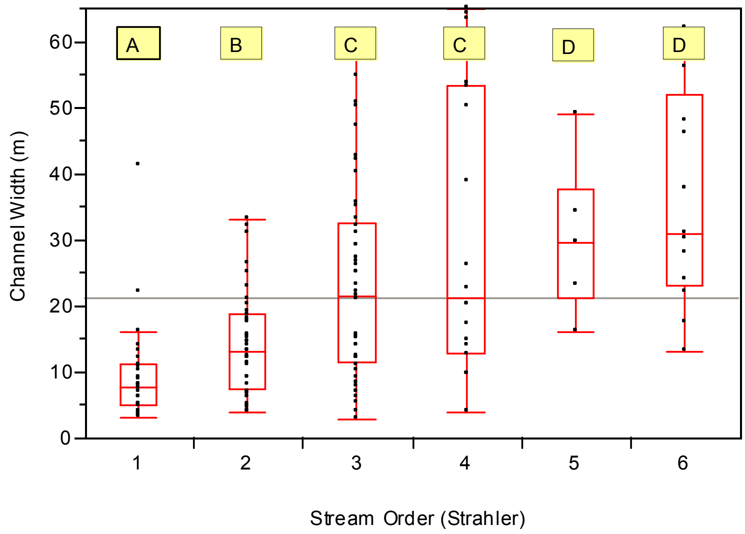

Figure 4.11 *CW*s for each Strahler stream order.

The *CW* measurements represent a sample of a much larger population (where that population is the channel width of each stream of a given Strahler stream order throughout the study area). For the purposes of this study it is assumed that distribution of the samples in each class (1^{st} order N= 27, 2^{nd} order N= 41, 3^{rd} order N= 45, 4^{th} order N= 20, 5^{th} order N=6, 6^{th} order N= 12) is the same as the distribution of the population for each class. The small sample sizes for 5^{th} order streams may not fully characterise the population, and are insufficient to carry out conclusive statistical tests for this stream order.

There is a large degree of variability in the channel widths observed for each class, and while in general the measurements are consistent with the expectations in terms of the relative *CW* values, in other words, the expected trend in *CW* is 6^{th} order>5^{th} order>4th order>3^{rd} order>2^{nd} order>1^{st} order, there is no significant difference between 3^{rd} and 4^{th} order streams or between 5^{th} and 6^{th} order streams at the 95% confidence interval. The increase of *CW* with increasing catchment area is consistent with hydraulic geometry theory insofar as the higher the stream order (in this situation a proxy for catchment area) the wider the channel. However the fact that there is no significant difference between channel widths for 3^{rd} and 4^{th} order streams and no difference between 5^{th} and 6^{th} order streams but will make the SSI less sensitive to Strahler stream order. The Shapiro-Wilk test indicated that the *CW* values were normally distributed for two stream orders but not for the remaining four. In the interests of conducting robust statistical tests on all classes, the Wilcoxon rank sum was used to compare the median values in all statistical tests applied to the *CW* parameter.

Table 4.13 OS values used to calculate the stream shading index (SSI)

	3rd	4th	5th	6th
Offset (m)	2.0	1.8	1.3	0.5
N	16	6	2	4

To assess whether the stream order classification was reliably extrapolating *CW* the average values recorded at validation sites (chosen at random from the three datasets, fieldwork, gauging station and State of the Rivers) were compared with the average of the *CW* values at the calibration sites using a series of Wilcoxon rank sum tests. The results at the 95% confidence interval are as shown in Table 4.11. It is worth noting that while the Wilcoxon rank sum test found no significant difference between observed and predicted median values for 5^{th} and 6^{th} order streams, the number of observations is relatively low. These results indicate that observed values are not significantly different to the predicted values for *CW* across the all classes, with the exception of the higher order streams where the number of values was to small for the statistical tests to be reliable. However the assumptions described for the factors determining *BH* also apply here, and based on this the Strahler stream order classification can be reliable be used to predict median *CW* for all stream orders.

4.4.3. Offset Between Top of Bank and First Tree (*OS*)

Comment [I2]: This parameter has only recently been included in the calculation of the SSI, figures will be included shortly. The underlying trend is that offsets become smaller for higher stream orders (the higher the stream order, the closer the tree to the top of the bank on average.

The offset between the top of the bank and the trunk of the first tree is one of the parameters used in calculating the SSI. Analysis of the offset values showed that they were related to stream order, and the median offset values for each stream order are contained in Table 4.13. There were no major assumptions made in measuring this parameter. In terms of extrapolating this parameter it is assumed that stream order is a reasonable predictor of offset, there is insufficient data to test this assumption. Table 4.13 only lists *OS* values for higher order streams, because it is these streams that are likely to support aquatic life in general, and it is along these streams where waterholes are most likely to form.

4.4.4. Number of Denitrification Events (*NDNE*)

Maximum daily stage height data collected at gauging stations within the study area were used to identify the frequency and duration events at each soil depth range *x* listed in Table 4.14 . This parameter is the $NDNE_x$ parameter used to calculate the (DNI). The number of denitrification (DN) events that occurred in any given *x* (*NDNEx*) were calculated by doing a visual assessment of the stage height record and counting the number of events that exceeded a given stage height, as shown in the figure below. Dotted blue line indicated bankfull stage height as seen in channel cross section in Figure 4.9. The coloured markers indicate the highest *x* where conditions were suitable for denitrification in any given event. To identify this height, the raw stage height data were processed to calculate the bank height at which the criteria for denitrification to start (inundation for more than 48 hours) and complete (inundation for more than 8 days). These heights were estimated by calculating the 2 day average and 8 day average of the raw (daily) stage height data.

The heights are shown as the DN_{start} and $DN_{complete}$ curves in Figure 4.13.

The DN start height, and DN complete heights were calculated using the average stage height for the previous 2 days and 8 days respectively. So for the example shown denitrification occurs throughout the stream bank on two occasions and the first DN

Table 4.14 *x* for each stream order

x	3rd	4th	5th	6th	Marker (colour, border)
0.25-Bank Full	Yes	Yes	Yes	Yes	Red, red
0.5-0.25	Yes	Yes	Yes	Yes	Yellow, red
1-0.5	Yes	Yes	Yes	Yes	Yellow, yellow
2 to 1	Yes	Yes	Yes	Yes	Yellow, blue
3 TO 2	Yes	Yes	Yes	Yes	Blue, blue
4 TO 3	Below BOC[21]	Yes	Yes	Yes	Not shown
5 TO 4	Below BOC	Below BOC	Yes	Yes	Not shown
6 TO 5	Below BOC	Below BOC	Below BOC	Yes	Not shown

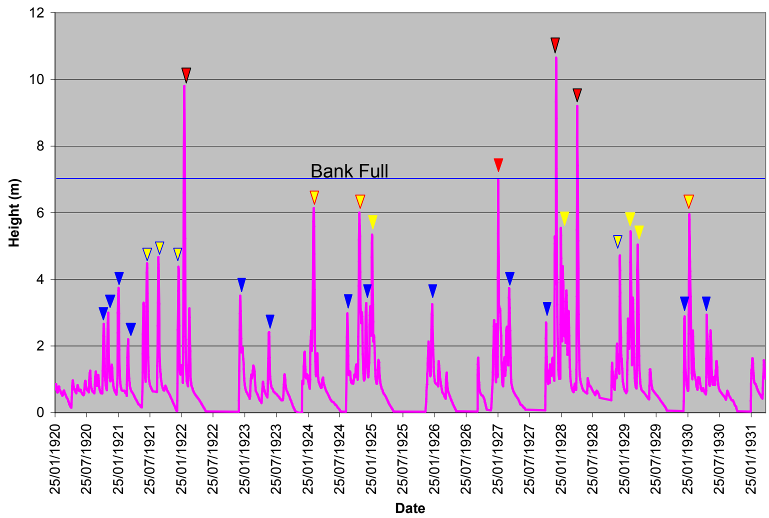

Figure 4.12 Daily stage height record with symbols indicating soil depth range x, x axis is day number from start of record and y axis is bank height in metres.

event did not last long enough for DN to be completed in the upper levels of the bank. The event counting technique shown in Figure 4.12 was applied to the DN complete timeseries, as shown in Figure 4.13 to calculate the number of DN events that ran to completion at each stage height ($NDNE_x$).

To compare DN complete timeseries calculated at different gauging stations it was necessary to identify a theoretical maximum number of DN events that could occur in any given year, thereby defining a theoretical maximum number for *NDNE* at any *x*. The theoretical maximum was calculated as a function of fine root dynamics of vegetation and climate as detailed below.

The constraints on the number of DN events due to fine root dynamics can be calculated by assuming that fine roots pursue a falling water table (Horton and Clark, 2001), and that the fine roots of Eucalyptus species will exude WSC, and die after a month (Katterer 1995). Under these conditions, one month after the water table has fallen past a certain height, the WSC in that zone (*x*) will have returned to the maximum amount of WSC encountered in that zone (WSC_{max}).

So if flood peaks are less than a month apart, then the WSC will not have regenerated in the root zone (*x*). The other factor that determines the theoretical maximum number of denitrification events is climate.

Given the climate in the Nogoa/Comet catchments, the following scenario is likely to provide the maximum number (3) of DN events, a flood event early in the wet season (late October/November), followed by a dry period (during which the water table falls

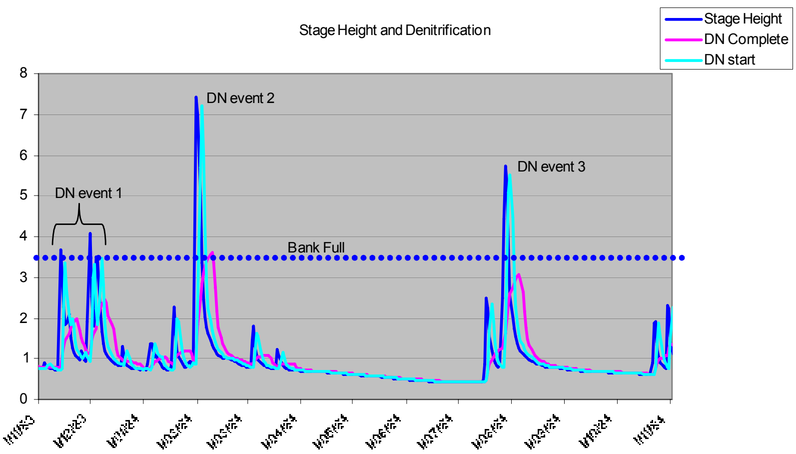

Figure 4.13 Stage height records and estimated DN start and complete curves

---

[21] BOC represents the bottom of the channel

and WSC is replenished down through the profile), another flood event late in the wet season (February) and a third event (associated with frontal rain in winter) in August. As shown in Figure 4.13. The peaks close together for DN event 1 are considered as 1 DN event because they are closer than one month apart, therefore the fine roots are unlikely to have grown, exuded and died (thereby replenishing the WSC) in the intervening period.This '3 events per year' scenario occurs quite frequently during wet periods (such as the 1970s) but has been less frequent in recent times.

The number of $DN_{complete}$ events at each soil depth range x is shown in Table 4.15 Note that the stage height has bankfull (depth = 0) as a common reference point to allow comparison between stage heights records colleted at gauging stations that have different 'bank full' heights.

4.4.5. Channel Slope (*S*)

The channel slope for each unaltered stream link (*S*) was calculated by the RiverTools ™ software as part of the channel network identification process. These data are shown in Figure 4.14. The *S* measurements calculated from the DEM (details of which are contained in Section 5.3.2) represent the entire population (where that population is the slope of each stream of a given Strahler stream order throughout the study area 1st order N= 673, 2nd order N= 300, 3rd order N= 139, 4th order N=66, 5th order N=115, 6th order N= 87. There is a large degree of variability in the slopes observed for each stream order, in general the measurements are consistent with the expectations in terms of the relative *S* values, in other words, the expected trend in *S* 1st order>2nd order>3rdth order>4th order>5th order>6th order is present in the data. However, there is no significant difference between 5th and 6th order streams at the 95% confidence interval (they both have very low median slopes).

This is consistent with hydraulic geometry theory insofar as the higher the stream order the lower the slope, but it reduces the difference between the BRI_{GLOBAL} values for stands of vegetation adjacent to high order streams.

Table 4.15 $NDNE_x$ for each stream order

	3rd	4th	5th	6th
0.25-BF	0.44	0.35	0.26	0.09
0.5-0.25	0.56	0.46	0.36	0.15
1-0.5	0.94	0.78	0.62	0.30
2 to 1	2.13	0.90	0.88	0.50
3 TO 2	1.13	1.72	0.80	0.63
4 TO 3		1.00	1.20	0.66
5 TO 4			1.00	0.96
6 TO 5				1.00

Table 4.16 Results of statistical comparison of predicted and observed median *S* values.

Structural Class	1st order	2nd order	3rd order	4th order	5th order	6th order
Null Hypothesis (H_0)	Accept	Accept	Accept	Reject	Accept	Accept
Trend	No trend	No trend	No trend	Cal<Val	No trend	No trend
Value used to calculate BRI_{global}	0.00421	0.00243	0.00146	0.00074	0.00041	0.00041

The Shapiro-Wilk test indicated that the *S* values were not normally distributed. Consequently the Wilcoxon rank sum was used to compare the median values in all statistical tests applied to the *S* parameter.

To assess whether the stream order classification was reliably extrapolating *S* the average values recorded at validation sites (chosen at random from the whole population) were compared with the average of the *S* values at the calibration sites using a series of Wilcoxon rank sum tests. The results at the 95% confidence interval are as shown in Table 4.16. These results indicate that observed values are not significantly different to the predicted values for *S* across the all classes except the 4th order streams.

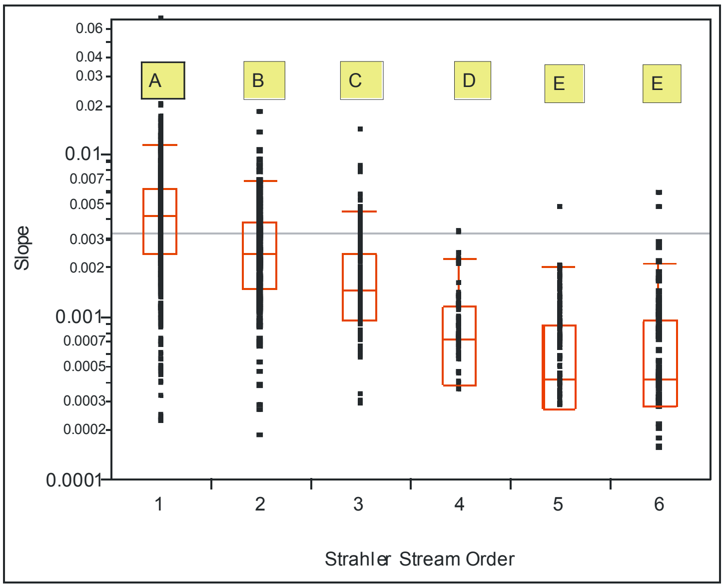

Figure 4.14 *S* values for each Strahler stream order.

The reasons for the difference between calibration and validation sets for the 4th order streams are unclear, as both samples were drawn at random and represent two halves of the entire population of channel slopes Based on this the Strahler stream order classification can be reliable be used to predict median *S* for most stream orders, and the median value off all 4th order streams will be assigned to the 4th order streams. The BRI_{GLOBAL} is calculated using the parameter *S* .

4.4.6. Stream Power (ω)

Unit stream power ω is used to calculate the bank reinforcement index (BRI) using Equation (2.15). ω for each Strahler stream order was calculated using a modified version of Equation (2.10) re-written as Equation (4.16)

$$\omega = \rho g \left(\frac{Q}{CW} \right) S \tag{4.16}$$

Where *Q* is bankfull discharge ($m^3 \ s^{-1}$), and *CW* is the channel width (m) and *S* is slope. Slope for each Strahler stream order was calculated as the average slope for streams of a certain order as listed in Table 4.16 Results of statistical comparison of predicted and

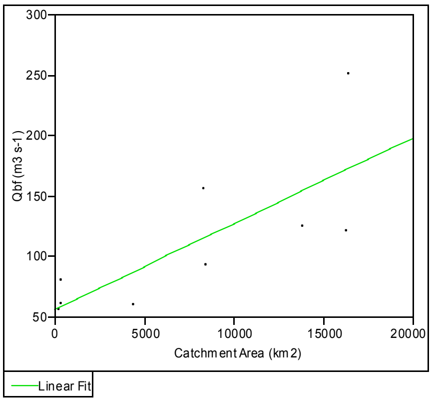

Figure 4.15 Correlation between Q_{bf} and catchment area

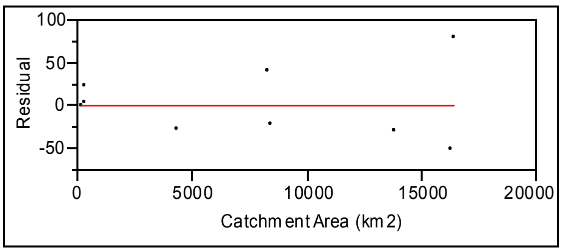

Figure 4.16 Residuals in the correlation between Q_{bf} and catchment area

Table 4.17 Q_{bf} values used to calculate RFIs

Stream Order	**1st order**	**2nd order**	**3rd order**	**4th order**	**5th order**	**6th order**
Q_{bf} value used	28.8	40.3	56.2	77.6	104.8	140.0
ω value used	152.20	73.75	37.42	26.41	14.28	18.15

observed median *S* values.. Values of *Q* were collected for each gauging station within the study area by looking at the stage-discharge curve and identifying the *Q* at bank full (Q_{bf}) values. To estimate Q_{bf} for each stream reach it was necessary to establish a relationship between catchment area and Q_{bf}. This was done using the same techniques as described in Young *et. al.* (2001) A linear model (Figure 4.15) provided the highest correlation coefficient. The correlation coefficient, adjusted for small sample size is R^2=0.52, the linear model fit has an F ratio value of 9.92, which is significant at the 95% confidence interval.

The residuals to this model fit are randomly distributed as shown in Figure 4.16. There are insufficient data to compare predicted and observed values, so the reliability of the Q_{bf} values will be untested in this thesis. To identify the Q_{bf} for each Strahler stream order (given that there were no gauging stations on low order streams) the average catchment area for each stream order were calculated from each stream link in the channel network (same population as used to calculate *S*). The linear model (Equation (4.17)) shown in Figure 4.15 was then used to calculate the Q_{bf} of links in each stream order. The *Qbf* for each stream order are listed in Table 4.17.

$$Q_{bf} = 56.1 + 0.0071 \text{Catchment Area} \tag{4.17}$$

By entering the values for *Qbf*, *S* and *CW* for each stream order into Equation (4.16) values for ω were calculated for each stream order as shown in Table 4.17. These values were used as the *POWER* term to calculate BRI_{GLOBAL} using Equation (2.20).

4.4.7. Probability of a Waterhole (*Pwh*)

The probability of a waterhole parameter *Pwh* is used to calculate the SSI_{GLOBAL} values according to Equation (2.52). To calculate the *Pwh* parameter the daily stage height records were processed using the following steps, periods of missing record were removed from the dataset, and then the number of flow days was subtracted from the length of record according to Equation (4.18).

$$ZFD = \text{period of record - flow days} \tag{4.18}$$

Where ZFD is the number of zero flow days and flow days are days when the stage height is greater than zero. The *Pwh* parameter is calculated for each gauging station using Equation (4.19).

$$Pwh = 1 - \left(\frac{ZFD}{\text{Period of record}} \right) \tag{4.19}$$

Table 4.18 *Pwh* values used to calculate RFIs

Stream Order	3rd order	4th order	5th order	6th order
Value used	0.5	0.6	0.8	0.9

The *Pwh* values for each gauging station were sorted according to stream order and an average *Pwh* for each stream order calculated, as listed in Table 4.18.

Strictly speaking these values represent how frequently the river flows, and are only an approximation of where waterholes are likely to form in the river network. However irrespective of whether waterholes form along each stream link of higher order streams, the riparian vegetation adjacent to theses channels will provide valuable LWD, and shade during the periods of time when they support aquatic life, and aquatic life is likely to persist for longer in higher order streams that have more frequent flow.

4.5 Chapter summary

This chapter established how the parameters that are required to calculate the riparian function indices were linked to classifications of land use, vegetation and Strahler stream order. Parameters were linked to these classifications via three mechanisms.

1. Statistical relationships between classifications and parameters were identified using field work.
2. Previously researched relationships between individual classes and parameters were identified in the literature.
3. Third party data such as stage height at stream gauging stations were analysed to provide addition parameters required to calculate the RFIs.

The parameters and their associated classifications are listed in Table 4.19. The parameter values listed in this chapter were entered into the RFI equations listed in Chapter 2 to calculate the RFIs for riparian zones in the study area. The results of these calculations are contained in Chapter 6, and the remote sensing and terrain analysis techniques used to generate the vegetation structural classification, the land use classification and the stream order classification are described in Chapter 5.

Table 4.19. Vegetation and stream channel parameters calculated from the fieldwork, and their associated spatial coverages.

Parameter	Spatial Coverage[22]	Data source	Riparian Function Index[23]
Manning's n for Shallow Overland Flow	Land Use Map	Field data and literature values	STI
Percentage Foliage Cover	Vegetation Structural Map	Field data	SSI, DNI
Vegetation Height	Vegetation Structural Map	Field data	SSI,
Volume of Wood	Vegetation Structural Map	Field data	LWDI, DNI
Number of trees per hectare	Vegetation Structural Map	Field data and literature values	BRI, DNI
Canopy Radius	Vegetation Structural Map	Field data	BRI, SSI
Soil Organic Carbon	Vegetation Structural Map	Literature values	DNI
Channel Depth	Strahler stream order	Field data	BRI, SSI
Channel Width	Strahler stream order	Field data	SSI
Number of Denitrification Events	Strahler stream order	Field data and third party data	DNI
Offset	Strahler stream order	Field data	SSI
Bank full discharge	Strahler stream order	Third party data	BRI
Channel slope	Strahler stream order	Terrain analysis	BRI
Probability of a waterhole	Strahler stream order	Third party data	SSI

[22] Details of all spatial coverages are contained in Chapter 5
[23] Details of the riparian function indices are contained in Chapter 2

Chapter 5 Spatial Distribution of Riparian Parameters

5.1 Introduction

To calculate the RFIs developed in Chapter 2 it was necessary to generate a series of classifications. The following classifications were used to predict the parameters described in Chapter 4 for every riparian zone throughout the study area:

1. A classification of the structural classes of woody vegetation and other land covers in riparian zones throughout the study area;
2. A channel network classification that accurately represented the location and dimensions of the stream and river channels;
3. A classification of grazing pressure that approximates the temporal dynamics of ground cover within the study area; and
4. A classification of the terrain that provides detailed information about the spatial distribution of hillslopes, alluvial soils and floodplains.

To generate these four classifications two sources of satellite imagery, and two digital elevation models were used. Each data source was subject to a different series of processing steps as shown in Figure 5.1.

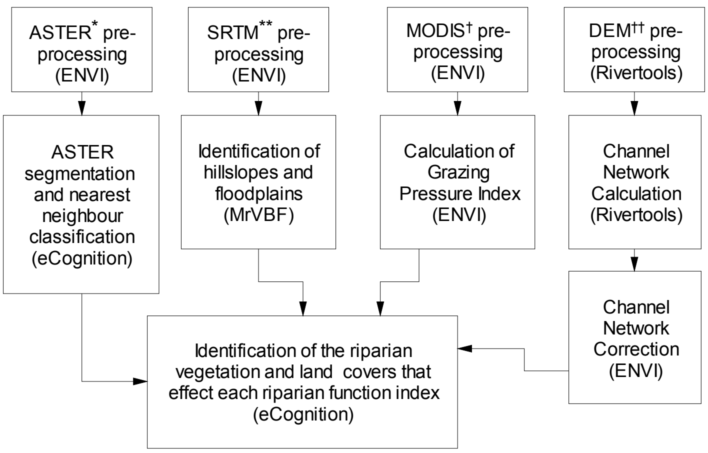

Figure 5.1 Spatial data and processing steps required to calculate the RFIs

* Advanced Spaceborne of Thermal Emmision and Reflection Radiometer (ASTER)
** Space Shuttle Radar Topography Mission (SRTM)
†Moderate Resolution Digital Imaging Spectrometer (MODIS)
†† 25 metre DEM derived from spot heights and contour lines

The rationale for choosing ASTER imagery and the pre-processing and classification applied to the ASTER imagery are contained in Section 5.2.1. The reasons for including the MODIS analysis and details of the processing steps applied to the MODIS data are contained in Section 5.2.3. The reasons why two different DEMs were used to generate the channel network classification and landscape classification, and the processing steps required to generate these classifications are contained in Section 5.3. The combination of all these classifications to generate the final coverages that were used to calculate the RFIs is contained in Chapter 6.

5.2 Remote Sensing of Riparian Vegetation and Land Cover

The use of remote sensing imagery to generate vegetation and land cover classifications has been the subject of numerous studies, ranging in scale from global (Running *et al.*, 1995) to species level classifications of individual tree crowns (Martin *et al.*, 1998). A common feature of vegetation classifications that have been generated using remote sensing is a choice of an appropriate resolution for the vegetation features being mapped.

A fundamental part of any vegetation classification derived from remote sensing is establishing a relationship between the vegetation structural characteristics of the vegetation, and the reflectance characteristics of the vegetation. The vegetation transect element of the fieldwork described in Section 3.3.1 is based on a methodology described in McDonald *et al*. (1990) that specifically aims to quantify the vegetation structural characteristics that effect the reflectance characteristics of the vegetation. Once this relationship between vegetation structural class and reflectance characteristics has been established for known areas, such as field sites, the vegetation structural class can be estimated for other areas within the remote sensing image by using an image classification algorithm to identify areas that have similar reflectance characteristics, and are therefore likely to contain the same vegetation structural class.

Areas of similar reflectance characteristics can be identified one of three ways, using classification algorithms that classify pixels based on their statistical properties such as nearest neighbour and maximum likelihood classifiers (Lillesand *et al*., 2004), or on their spectral properties, such as the spectral angle mapper algorithms (Kruse *et al*., 1993), or by using a geometrical optical model. A statistical classification algorithm was used because the different resolutions for visible near infra-red (VNIR) and short wave infra-red (SWIR) prevented the identification of unique spectra for each 15 metre pixel, thereby preventing the use of spectral properties. The construction of a geometrical optical (GO) model was beyond the scope of this thesis, due to the time and complexity associated with establishing a GO model for each riparian structural class encountered in the study area.

The use of remote sensing to map and monitor riparian vegetation has been the subject of a number of review papers (Muller, 1997; Congalton *et al*., 2002). Muller (1997) describes the specific needs of riparian vegetation mapping in terms of the need for relatively high spatial resolution to identify the narrow strips of riparian vegetation that occur along the steep environmental gradients that are encountered in the riparian zone. The steep gradients in terms of water availability encountered in the study area generate a number of narrow (less than 30 metres across) bands of woody riparian. Consequently the sensor used to map riparian vegetation needs to have sufficiently high spatial resolution to be able to capture these features, whilst simultaneously providing coverage of a large area.

Remote sensing has the capacity to deliver information about vegetation structure and type at a range of scales that are pertinent/useful/relevant to riparian zone studies. Airborne multi and hyperspectral scanners can provide high resolution (>1 metre) images of riparian zones, thereby enabling tree crown delineation, and potentially, species identification (Aspinall, 2002). It can also provide information about fine-scale riparian zone processes such as LWD size and distribution (Marcus *et al*., 2003) and channel geomorphology (Bryant and Gilvear, 1999). However, the resources required to collect and process airborne imagery are considerable, and the need for information about riparian zones at large catchment scales make the cost of airborne remote sensing prohibitive. Optical multi-spectral satellite imagery has been used in previous riparian zone studies to provide information at this larger scale (Basnyat *et al*., 1999; Goodrich *et al*., 2000; Congalton *et al*., 2002; Gutiérez *et al*., 2004). The advantage of multi-spectral satellite imagery is that it can provide coverage of large areas at relatively low cost. This is of particular importance when the catchment area is large, in this instance 19 365 km^2. The spatial resolution of multi-spectral satellites does provide some limitations, and these are discussed in more detail in the subsequent section.

The satellite imagery required by this project, to generate the vegetation and land cover classification needed to meet a series of criteria.

1. Spatial resolution high enough to discriminate the narrow strips of riparian vegetation and grassed waterways (pixel size less than 30 metres).
2. A relatively broad swath to capture the study area (19 365km^2) with a minimum of swaths (to reduce the amount of mosaicking and inter-swath comparisons).
3. Sufficient spectral resolution (particularly in the short wave infra red) to enable the discrimination of woody and non-woody vegetation, better differentiation between vegetation structural classes, and discrimination between stubble and bare soil.
4. Low cost, cloud free imagery available for the study area.

The sensor that was most suitable based on these criteria was the Advanced Spaceborne Thermal Emission and Reflection Radiometer (ASTER) sensor. Other sensors such as

SPOT, Ikonos and Quickbird provide higher spatial resolution, but the cost of data from these sensors can be prohibitive for projects that cover large areas. Landsat (TM and MSS) data were also available for the study area, but their larger pixel size limits their ability to distinguish narrow strips of riparian vegetation.

5.2.1. Advanced Spaceborne Thermal Emission and Reflection Radiometer (ASTER) Data

ASTER is a multispectral imager and covers a wide spectral region with 14 bands from visible to the thermal infrared with high spatial, spectral and radiometric resolution. The spatial resolution varies with wavelength: 15 m in the visible and near-infrared (VNIR), 30 m in the short wave infrared (SWIR), and 90 m in the thermal infrared (TIR). The spectral bandpasses of the VNIR, SWIR and TIR sensors is contained in Table 5.1. Each ASTER scene covers an area of 60 x 60 km.

All ASTER scenes were acquired as level 2 AST07 surface reflectance products, and consequently had been radiometrically, geometrically and atmospherically corrected. The atmospheric correction was performed by the data providers (NASA Distributed Active Archive Centre (DAAC)) using the MODRTAN 4 algorithm (Anderson *et al.*, 2000). Detailed information about the ASTER sensor is contained in the ASTER Users Handbook (Abrams et al. 2002). Imagery was reprojected using the geocoding information contained in the HDF files, so that the pixels were north oriented. This resulted in a small degradation in the image quality, but was necessary to enable files for the SWIR bands to be imported in the same spatial extent as the VNIR files. The small size of ASTER satellite scenes (3600km^2) relative to the study area (19 365 km^2) necessitated the analysis of multiple swaths. Analysis of multiple swaths necessitated two things, multi-date analysis and mosaicking. Multi-date analysis can present some

Table 5.1. The ASTER bandset, showing band number wavelength range and pixel size.

Spectral region	Band Number	Band Pass (μm)	Pixel Size (meters)
VNIR	1	0.52-0.60	15
	2	0.63-0.69	
	3	0.78-0.86	
SWIR	4	1.60-1.70	30
	5	2.145-2.185	
	6	2.185-2.225	
	7	2.235-2.285	
	8	2.295-2.365	
	9	2.360-2.430	
TIR	10	8.125-8.475	90
	11	8.475-8.825	
	12	8.925-9.275	
	13	10.25-10.95	
	14	10.95-11.65	

problems, particularly when the image acquisition dates are some time apart, and even more so when the images have been acquired during different seasons.

The 3 swaths of ASTER data used in this analysis were collected on 3 dates. The

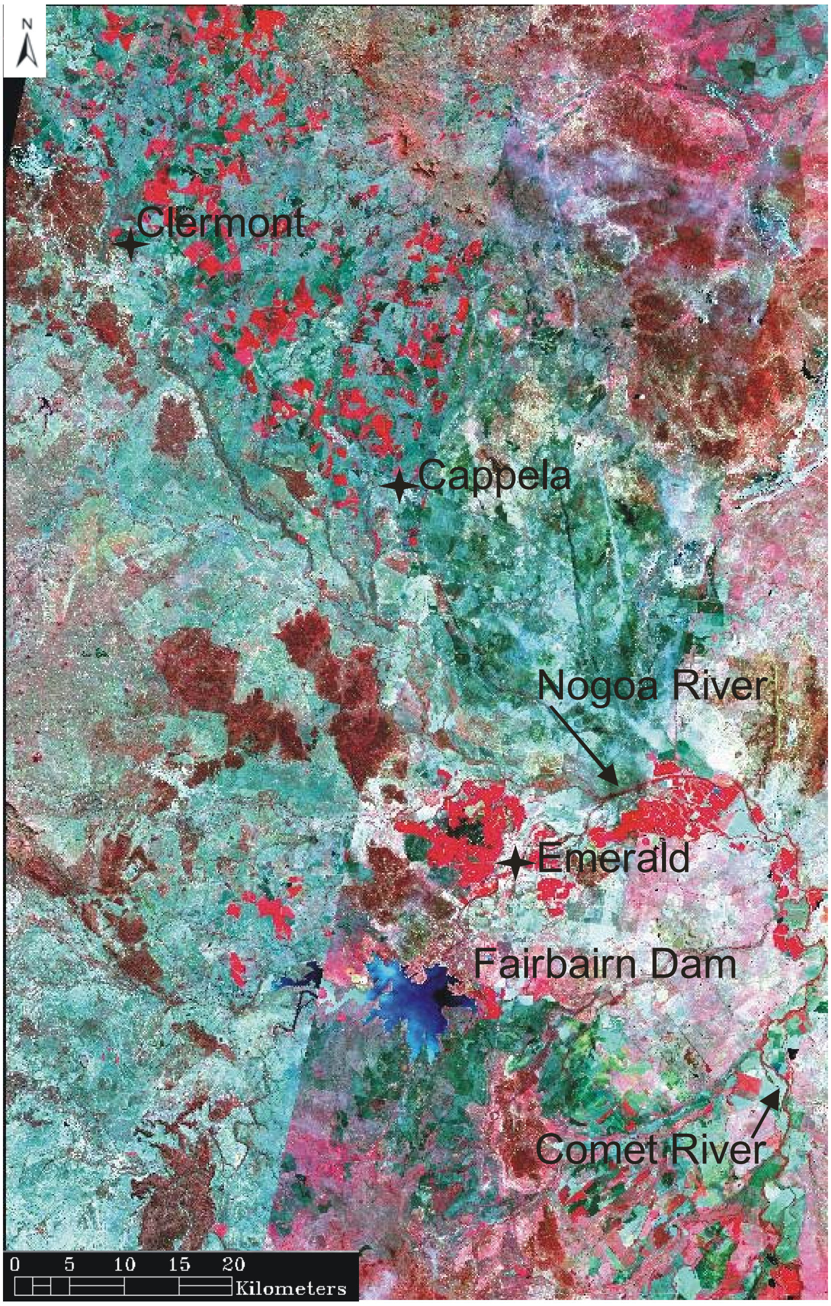

Figure 5.2 Mosaic of ASTER swaths for the study area

western most swath was collected on the 9th August 2000 (mid dry season), the central swath was collected on the 12 January 2002, and the eastern swath was collected on the 18th of January 2001 (both dates represent the early wet season) After reprojection the swaths were cropped to fit the extent of the 25 metre DEM. The result was three irregular shaped images as shown in Figure 5.7.

5.2.2. Riparian Vegetation and Land Cover Classification

Image Segmentation

One of the important aspects of the remote sensing/image processing research that was done in this thesis is the use of image segmentation software to generate the riparian vegetation classification and the land use classification. Image segmentation was chosen for the following reasons:

1. The definition of image objects, whose perimeter is described by a polygon, allows each polygon to be classified in terms of its 'context' within the image. This enables further classification of each polygon using queries related to the spatial, spectral and classification attributes of adjacent polygons. This in turn enables us to identify whether a given polygon is either (a). adjacent to a channel, (b). located on the floodplain, (c). located between the channel and a hillslope, or (d). some combination of the above. This was an important feature because the calculation of the RFIs requires information about the landscape context within which each structural class sits. For example, the statistical classifier applied to the reflectance data contained within the ASTER scene may classify a stand of vegetation as open forest. This stand of vegetation can then be further classified based on the fact that it is located on a floodplain (floodplain open forest) and is adjacent to the main channel of a 5th order stream (Littoral floodplain open forest on a 5th order stream) This capacity to classify polygons based on adjacent polygons and other data sources is used to further classify the basic vegetation and land cover class, as described in detail in Section 5.4.

2. Image objects can be generated from highest available resolution, and the objects can then be used to generate summary statistics for each object, both for the high resolution bands and for lower resolution bands. This is important in the context of this study because it enables short wave infra-red (SWIR) reflectance values (which have a larger pixel size than the visible near infra-red (VNIR) bands used to generate the image segments) to be included into the list of attributes used to classify each object. These attributes can also include non spectral data such as terrain features.

3. The pixel size is an artefact of the sensor and bares no relationship to any specific physical attributes on the ground, whereas image objects relate to

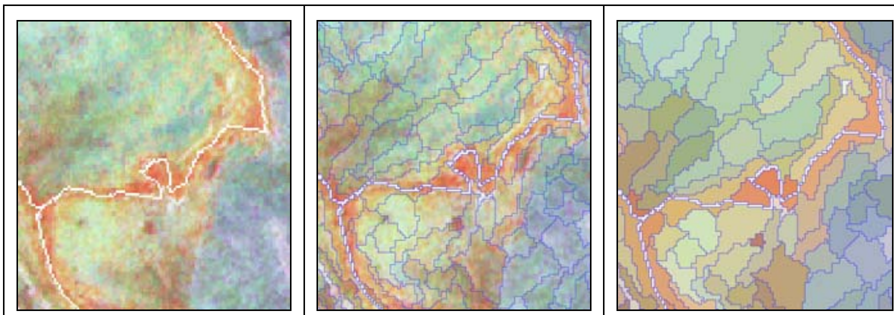

A B C

Figure 5.3 The process of image segmentation: A. raw ASTER data, B. polygons identified for areas with uniform spectral characteristics and C. Polygons showing average reflectance characteristics

specific physical attributes on the ground such as a paddock or a stand of trees. One of the important features of this approach is that the scale and the criteria used to generate image objects are defined by the user rather than the sensor. This was particularly important in this project because it allowed us to define image objects at a scale that corresponded to the narrow strips of riparian vegetation. The process of image segmentation is shown in Figure 5.3.

The process shown in Figure 5.3 uses two aspects of the image to generate the polygons. These two aspects are spectral uniformity and shape. Spectral uniformity is calculated using

$$h_{spectral} = \sum_{c} w_c \sigma_c . \qquad (5.1)$$

where w_c is the weight applied to that channel (or band) and σ_c is the standard deviation of pixel values in that band (from Equation 1 in the eCognition Users Guide). Using Equation (5.1) pixels will be clustered together to form polygons based on the spectral similarity between those pixels. The band weightings (w_c) used in the image segmentation are shown in Table 5.2. The rationale for these choices is as follows:

1. The strong emphasis the channel network (CN, described in detail in Section 5.3.2) remains intact and that polygons are formed on either side of the

Table 5.2 Bandset used to generate the image segmentation used to generate the riparian vegetation classification.

Layer	Segmentation Weighting
Channel Network (CN)	0.7
Vegetation Index (SR)	0.2
Visible and Near Infra Red (VNIR) bands	0.1

channel network;

2. The emphasis on the VI band was used to ensure that polygons were based on areas with a relatively uniform leaf area, and;

3. The emphasis on the VNIR bands ensure that polygons for non-vegetation targets formed were based on uniformity of all three bands.

Polygons identified using spectral uniformity alone can take on branched or fractal shapes. To reduce this effect a shape or compactness measure is applied. The shape parameter is calculated using

$$h_{compact} = \frac{l}{\sqrt{num\_pix}} \tag{5.2}$$

where l is the length of the perimeter of the polygon *num_pix* is the number of pixels contained within the polygon. The compactness of the polygons can be controlled by setting a maximum value for $h_{compact}$. Because of the highly irregular shape of many strips of riparian vegetation the $h_{compact}$ parameter was not used to constrain the riparian polygons. Consequently all polygons were formed based on the colour rather than shape of the stand of riparian vegetation. All of the bands used to generate the segmentation had 15 metre pixels.

The other parameter used for polygon generation is a scale parameter which determines the minimum number of pixels that will be considered for forming a polygon, *i.e.* the larger the scale parameter, the larger the polygons generated by the image segmentation algorithm. The optimal image scale for identifying riparian vegetation was 5 pixels, the results of these tests are shown in Figure 5.4, Figure 5.5 and Figure 5.6. Smaller scale parameters resulted in a large number of very small polygons that did not appear to relate to any specific image objects, and dramatically increased the time taken to perform any image processing steps, and larger scale parameters resulted in polygons that aggregated narrow strips of riparian vegetation (rather than leaving them as separate polygons) as shown in Figure 5.6. Further details of the image segmentation algorithms are contained in the Concepts and Methods chapter of the eCognition User Guide.

Another feature of riparian zones in remote sensing imagery is the presence of mixed pixels or 'mixels' at the interface between the edge of the riparian vegetation and the channel. Incorrect classification of these pixels can provide a misrepresentation of conditions immediately adjacent to the channel (a critical area for riparian zone assessment). Image segmentation avoids the incorrect classification of mixels and shade pixels by incorporating them into the adjacent image object. For example a mixel at the interface between the riparian vegetation and the channel would either be incorporated into the riparian vegetation polygon or the channel polygon, depending on the spectral properties of the pixel.

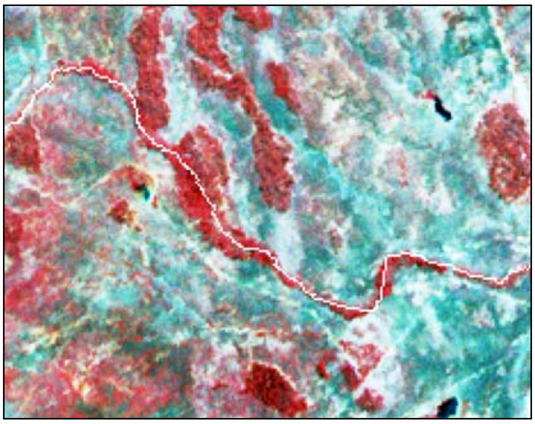

Figure 5.4 VNIR ASTER image of riparian zone surrounding a first order stream (digitised channel shown in white)

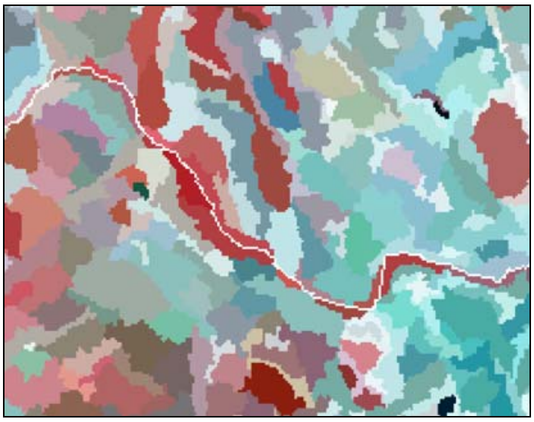

Figure 5.5 Scene segmented using an image object scale of 5 pixels, note that thin strip of riparian vegetation is preserved in the polygons (this resolution was used for image segmentation in this study).

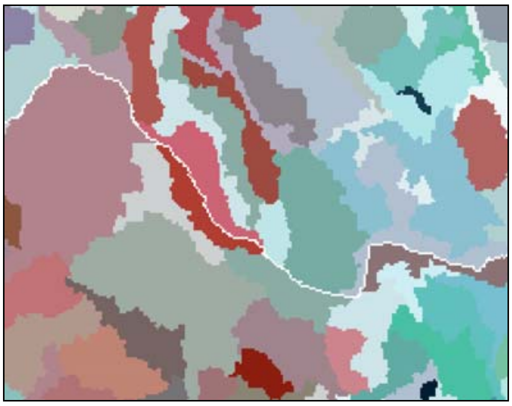

Figure 5.6 Scene segmented using an image object scale of 10 pixels, note that the thin strip of riparian vegetation is not captured at this scale of segmentation (this resolution was considered too coarse for the purposes of this study).

Image Classification

Image statistics (mean, standard deviation, range) for each of the bands shown in Table 5.3 were calculated for each polygon generated as per the previous section. The average value for each polygon was used as input into a nearest-neighbour algorithm to generate the vegetation and land cover classification. The vegetation indices used were a simple ratio (SR) of the red and near-infrared bands as described in (Lawrence, 1998), These bands were chosen based on the following rationale: the visible and near infra-red bands are useful for discriminating vegetation and other land broad land cover classes (Lillesand *et al*., 2004). Woody vegetation can be discriminated from non-woody vegetation using the short wave infra red wavelengths band 4, this is of particular importance given the spectral similarity between cropping areas with moderate leaf area and stands of open forest and closed forest in the visible and near infra-red bands.; The simple ratio was chosen because it is more sensitive to high leaf area index values than the normalized difference vegetation index (Huete *et al*., 1997), and identifying areas with similar leaf areas areas are likely to represent the same vegetation structural classes.

Training and Evaluation

The ASTER imagery was classified by selecting polygons of vegetation that had been visited and measured as part of the fieldwork described in Section 3.3. Because the vegetation structure was identified as part of the field data analysis, the vegetation structure at these polygons was known. Consequently these training polygons were used to seed (or train) the classification algorithm. This was done on the assumption that other polygons with the same vegetation structure will have the same spectral characteristics. For the non-woody vegetation classes, polygons were selected adjacent to the fieldwork sites (where the land use had been observed during fieldwork for this thesis), or via image interpretation and local knowledge.

The polygons (both woody vegetation and non-woody vegetation) selected in this fashion were used to seed the nearest neighbour classifier available in eCognition. The nearest neighbour classification algorithm was applied to the whole scene, and the classification accuracy was assessed using an independent set of evaluation polygons that were

Table 5.3. Bandset used to generate the vegetation structural classification

Band/Index	Band No./Index formula	Wavelength μm
VNIR	1	0.52-0.60
	2	0.63-0.69
	3	0.78-0.86
SWIR	4	1.60-1.70
SR	$\left(\frac{\text{Band3}}{\text{Band2}}\right)$	

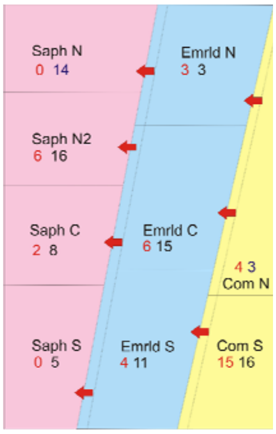

Figure 5.7 Swath and scene nomenclature for ASTER imagery covering the study area, the numbers shown in red represent the fieldwork sites which were used to train each classification, numbers shown in blue represent the State of the Rivers survey locations located in that scene (used as validation),[24]

selected based on the fieldwork as described in Section 3.3.1. The sites visited during the State of the Rivers (Henderson, 2000) survey were used to identify the evaluation polygons because the vegetation structure had been measured, thereby making them suitable locations to assess the reliability of a vegetation structural classification. Due to the file size limitations (200MB) of the image segmentation software eCognition™ 3.0 it was not possible to classify each satellite swath as an individual image. Consequently each swath was segmented into a series of scenes, four scenes for the western swath, and three scenes for the central swath and two scenes for the eastern swath as shown in Figure 5.7.

The distribution of training and evaluation sites used to calibrate and validate the riparian parameters[25] is shown in Figure 5.7 as blue (for calibration sites) and red (for validation sites). The large number and wide spatial distribution of the State of the Rivers survey sites made it possible to assess the accuracy of all scenes classified.

Most of the scenes in the study area have insufficient field sites within them to provide a large number of calibration sites, so in these instances polygons located in the overlap between swaths were used to seed (train) the classification of the adjacent swath as shown in Figure 5.7.

---

[24] The 'Saph' 'Emrld' 'Comet' prefixes refer to the swaths covering the towns of Sapphire, Emerald and the Comet River, N, C and S stand for North, Centre and South respectively

[25] The distribution of calibration/validation sites for the riparian parameters as described in Chapter 3 was chosen so that each land use, and stream order was equally represented in the calibration and validation datasets.

Table 5.4 Error Assessment Matrix for all scenes

User Class \ Sample	D	M	S	V	C	St	SD	SL	G	Sum	UA %
Closed Forest (D)	14	0	0	0	0	0	0	0	0	14	100
Open Forest (M)	0	29	1	0	0	0	0	0	0	30	97
Woodland (S)	0	8	97	2	0	1	0	0	0	108	90
Open Woodland (V)	0	0	2	31	0	0	0	0	0	33	94
Crops (C)	0	0	0	0	85	0	0	0	0	85	100
Stubble (St)	0	0	0	0	0	69	0	1	3	73	95
Bare Soil Dark (SD)	0	0	0	0	0	3	86	9	0	99	87
Bare Soil Light (SL)	0	0	0	0	0	1	2	60	0	63	95
Grassland (G)	0	0	0	0	1	2	0	0	68	71	96
Sum	14	38	100	33	86	76	88	70	71	576	
PA (%)	100	78	97	94	99	91	98	86	96		
Overall Accuracy	94%										
Khat stastic	0.928										

Based on this approach the classification accuracy values will be least reliable for Saph4, Emrld1 and Comet1 because there are relatively few validation sites in these scenes.

Classification Accuracy

The classification accuracy was assessed using a confusion matrix (Lillesand *et al.*, 2004). The individual confusion matrices for each scene are contained in the Appendices. The results are summarized in Figure 5.8. and Table 5.4.

The most obvious features of the confusion matrix (Table 5.4 are the high overall accuracy (94%) and the $\hat{K}$ statistic (0.928) which is significant at the 95% confidence interval, indicating that there are more polygons classified correctly than would be expected by chance alone. However there are a couple of features are worth noting. The producer’s accuracy for open forest is only 78% due to the fact that eight of the open forest polygons had been misclassified as woodland. Based on this the classification will tend to slightly underestimate the amount of open forest throughout the study area, which will in turn lead to errors in the RFIs calculated for these areas.

The high user accuracy (97%) for open forest however, means that any areas classified as open forest are being correctly identified. In addition to this there is some confusion between woodland and open woodland with 2 polygons of each class being misclassified as the other. Because the vegetation structural classes are based on a threshold of inter-crown distance as detailed in Section 3.3.2, it is not surprising that there is some confusion between structural classes either side of each threshold. In other words, a stand of open forest with a lower than average percentage foliage cover (PFC) may have

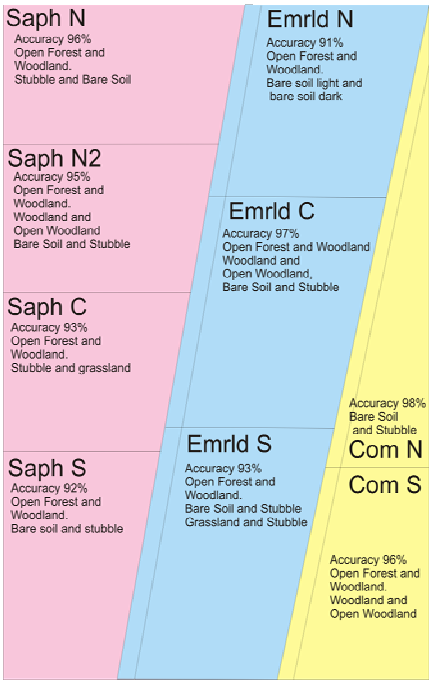

Figure 5.8 The classification accuracy of each scene

very similar reflectance characteristics to a stand of woodland that has above average PFC. It is important to note that the confusion between structural classes never bridged a structural class *i.e.* closed forest was never confused with woodland, nor open forest with open woodland. Furthermore, there is no confusion between the woody vegetation classes and the other land cover classes. This is very important in the context of the reliability of the RFIs, misclassification between similar vegetation structural classes may lead to small errors in the RFI values, but confusion between woody and non-woody vegetation would seriously impact on the reliability of the RFI values.

The implications of the classification errors for specific RFIs are discussed further in Chapter 6. If classification reliability at the individual polygon scale was of particular concern, then the classification stability statistics generated at a polygon level by eCognition would provide valuable information.

5.2.3. Moderate Resolution Imaging Spectroradiometer (MODIS) data

Describing the temporal dynamics of semi-arid landscapes and the riparian systems that exist within them requires the use of multi-temporal data (Hill, 2002). This is particularly true of phenomena that change rapidly over time such ground cover, and soil moisture dynamics in deep floodplain soils. To quantify these dynamics a preliminary analysis of The MOD13Q1 NDVI product (which is described in detail at http://edcdaac.usgs.gov/modis/mod13q1v4.asp) was performed in this thesis to i). estimate grazing pressure in areas without woody vegetation (used to calculate the STI as detailed below) and ii) estimate WSC dynamics for woody vegetation on located on the floodplain (used as a supporting evidence for the WSC parameter used to calculate the DNI as described in Section 7.3.3). Both sections of analysis are experimental, and would require additional fieldwork to validate the classification products generated through this analysis.

Grazing Pressure

The combination of moderate resolution data and low resolution multi-temporal data has been examined in previous studies (Hill *et al*., 1999). In particular multi-temporal data has been used to calculate grazing pressure in arid rangeland areas in a number of previous studies (Pickup, 1994; Pickup and Bastin, 1997; Pickup *et al*., 1998). In these studies, grazing pressure was calculated as a function of distance from a watersource. This was not possible in this thesis because the climatic conditions are semi-arid rather than arid, consequently the paddocks are much smaller, making it much more difficult to estimate grazing pressure as a function of distance. The estimation of grazing pressure from multi-temporal greenness data is based on the following theory. After a rainfall event, typically associated with the wet season (December through to February) areas that have been cleared of woody vegetation will green up rapidly and reach a maximum greenness between 6 to 8 weeks after the rainfall event, and then the greenness drops off as the vegetation senesces/cures (Archer, 2004). In areas that are not subject to grazing the vegetation cures at a certain rate, while in areas that are subject to grazing the greenness tends to fall more quickly than other areas because the grazing pressure is reducing the amount of green cover quicker than the curing process. The difference between curing and heavy grazing is most noticeable 8 to 10 weeks after the end of the growth period (*i.e.* after maximum greenness), as shown in Figure 5.9, and can be

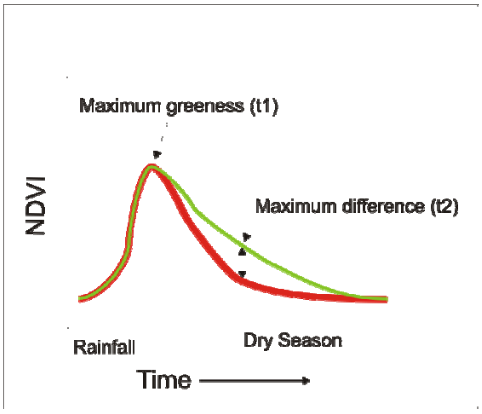

Figure 5.9 Theoretical greenness (NDVI) curves, green curve shows the NDVI response of ungrazed grassland and red curve shows the NDVI response to heavy grazing

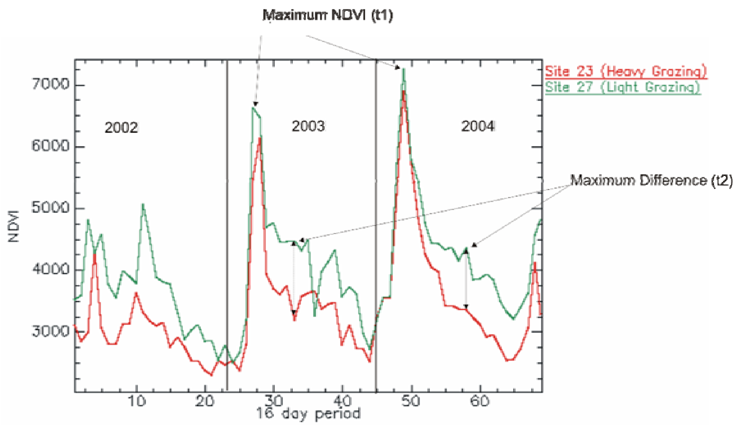

Figure 5.10 NDVI timeseries collected for areas subject to heavy and light grazing (as observed in the fieldwork)

calculated using the slope of the line between t1 and t2.

As the dry season progressed, and the grass became fully senesced, the greenness characteristics become increasingly similar. To assess whether the MODIS 16 day composited NDVI timeseries could be used to identify grazing pressure, the following steps were taken.

1. A subset of the land cover classification described in Section 5.2 was created that contained the land cover classes of stubble, bare soil light, bare soil dark, and grassland (all woody vegetation was excluded).
2. A further subset of that classification was taken so that only areas that were larger than one MODIS pixel (250metres x 250 metres) were included, so that any timeseries analysed represented areas that were devoid of woody vegetation.
3. NDVI timeseries were collected for grazing areas near field sites (*i.e.* places that had been visited during late 2002 where we could estimate grazing pressure based on visual observations) as shown in Figure 5.10

Note the similarity between Figure 5.10 and the theoretical greenness curves described in Figure 5.9. The time series for 2003 and 2004 shows the greatest similarity to the theoretical curve, (2002 was a drought year, with no distinct wet season) Consequently the 2002 data were not used to calculate the grazing pressure index (GPI).

To estimate grazing pressure using the NDVI time series the index described in Equation (5.3) is proposed.

$$\mathrm{GPI}=\left[\frac{\mathrm{NDVI}_{t1}}{\mathrm{NDVI}_{t2}}\right] \tag{5.3}$$

By dividing the maximum greenness observed at t1 (as shown in Figure 5.9) by the greenness observed for the same location at t2 weeks later (typically 8 weeks later), it is possible to estimate the drop in greenness over that period. For areas subject to heavy grazing $NDVI_{t2}$ will be much smaller than $NDVI_{t1}$ resulting in a large positive value for the GPI, whereas areas subject to light or no grazing will have $NDVI_{t2}$ that are only slightly smaller than $NDVI_{t1}$ resulting in a small positive value for the GPI. These calculations are shown with corresponding NDVI timeseries in Figure 5.12. The GPI was calculated for the 2 years of MODIS NDVI data when there was a wet season followed by the curing/grazing (*i.e.* 2003 and 2004 but not 2002) and an average GPI value calculated using the values for these two years.

So theoretically, any area that has a high GPI value has been subject to heavy grazing every year for two years. The range of GPI values observed in the study area is shown as a histogram in Figure 5.11, and high GPI values coincide with heavily grazed areas observed during the fieldwork (conducted in late 2002).

A series of regions of interest (ROIs) were generated by thresholding the GPI values (1-

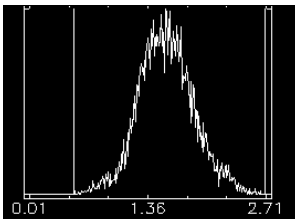

Figure 5.11 Histogram showing distribution of GPI values

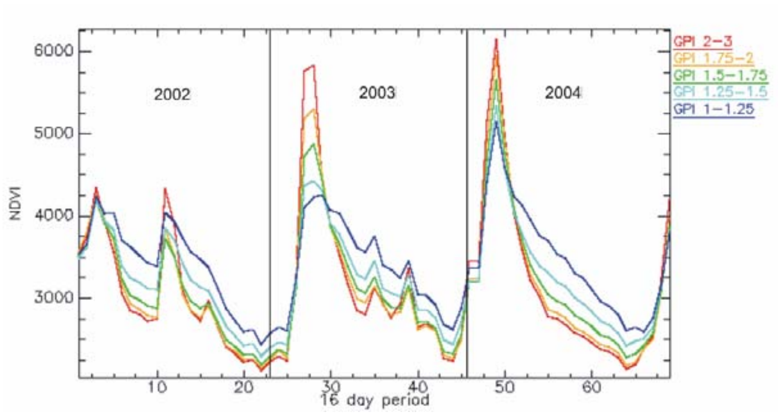

Figure 5.12 NDVI[26] timeseries for areas with different GPI values.

[26] Please note that the MOD13Q1 product is scaled between 0 and 10000 rather than 0 to 1

1.25, 1.25-1.5, 1.5-1.75, 1.75-2, 2-3, and the average time series for each region of interest is shown in Figure 5.12 NDVI25F timeseries for areas with different GPI values.

There is only a weak negative correlation between GPI and the roughness of the ground cover (Manning's n_{5m}) values observed in the field (high grazing pressure correlates with low ground cover), but this is hardly surprising given the difference in the scale of observation (*i.e.* field data collected every 5 linear metres as compared to a time series collected for an area covering 62500 square metres). Clearly, additional data would be needed to accurately characterise the relationship between GPI and ground cover over time. However for the purposes of this thesis (calculating the sediment trapping index) the GPI will be used as a crude estimate of grazing pressure. The GPI will be thresholded, with areas having a GPI_{2yr} >1.75 classified as heavy grazing, and GPI<1.75 classified as light grazing. This threshold value of 1.75 was based on estimates of grazing pressure made during the fieldwork *i.e.* sites classified as heavy grazing based on the field data described in Chapter 4 typically had GPI values >1.75. The approach described here is consistent with the theoretical relationship between grazing and groundcover dynamics described in Pickup (1994), and the simple analysis (histogram threshold of index results into two classes) technique is used because there are insufficient data to rigourously test the multi-temporal estimates of grazing pressure. In the future it would be desirable to validate this approach with additional stocking rate data and data quantifying the change in ground cover over time prior to using this information in a decision support capacity. An alternative means of estimating grazing pressure would be to integrate the area under the line of the NDVI timeseries to estimate the amount of biomass, and then identify areas that consistently had lower biomass, although this could be confounded by the pasture growth potential of different soils.

5.3 Terrain Analysis

5.3.1. Introduction

Digital terrain analysis was used in this research to generate two classifications: a classification of Strahler stream order, and a classification that separates the catchment into floodplains, hillslopes and plateaus. The use of terrain analysis has a long history in hydrology (Knighton; 1998). In terms of mapping riparian zones terrain analysis provides a critical adjunct to remote sensing because, while remote sensing can provide a classification of the conditions on the land surface, terrain analysis is required to place that classification in a hydrological context.

One of the advantages of using terrain analysis is that it enables identification of low order streams without riparian vegetation. These streams would be indistinguishable from the surrounding landscape in satellite imagery, and identifying these streams is essential for identifying the extent of the stream network that is without riparian vegetation.

Another advantage of the terrain analysis is that it can be used to identify floodplains. Floodplains can be identified using hydraulic models, but many hydraulic models are computationally intensive, and require extensive parameterisation to run accurately (Pickup and Marks, 2001). The terrain analysis tool MrVBF described in Gallant and Dowling (2003) enables the delineation of floodplains without the need to run hydraulic models. Terrain analysis is an essential adjunct to remote sensing in riparian mapping projects, because it places the riparian zones, and the vegetation observed in those zones into a broader landscape context. This enables hydrologic and hydraulic channel characteristics, such as flow duration, and channel dimensions to be approximated for the whole channel network.

Two DEMs were used in this thesis because each DEM was suitable for different purposes. The 25 metre DEM was generated by interpolating between spot heights and contour lines. For more hilly areas that contain some relief, such DEMs are well suited for identification of low order channels. However, the data available for low relief areas such as floodplains are very sparse, for example if the contour map used to generate the 25 metre DEM had a 10 metre contour interval and the floodplain has a very low slope, it can be many hundreds of metres or even kilometres between contour lines. Consequently all the heights between these contour lines are estimated heights based on whatever spline or kriging algorithm was used to interpolate between contour lines, thereby making it difficult to estimate the true extent of the floodplain. The spaceborne Shuttle Radar Topography Mission (SRTM) mission (Van Zyl, 2001) data on the other hand provides a spot height measurement for every 90 x 90 metre pixel, and, consequently the data about floodplain topography is much more dense. The 90 metre SRTM (DEM) is used in this thesis to calculate the extent of floodplains in the study area. The SRTM data was used in preference to the 25 metre data used to identify the channel network because the SRTM data contained far more detailed information in low relief and flat areas such as floodplains.

5.3.2. Channel Network Classification using a 25 metre DEM

Introduction

The DEM used in this component of the study was a 25 metre DEM derived from spot heights and contour lines (Queensland Department of Natural Resources Mines and Energy, 2001). The 25 metre DEM was chosen because a high resolution DEM is required to accurately identify the location of small 1st order streams that drain the greatest proportion (%) of the landscape. Knowing the accurate location of these first order streams is essential so that the land use and vegetation type adjacent to these low order streams can be identified.

The digital elevation model was used to generate a channel network based on Strahler stream order (seen previously in Figure 3.2), and this channel network was used to extrapolate channel dimensions (as described in Section 0) and hydrological parameters (as described in Section 0) , both of which are required to calculate the RFIs.

A number of previous studies have examined the possibility of using DEMs to define stream channel networks using flow accumulation algorithms (Martz and Garbrecht, 1992; Roth *et al*., 1996; Vogt *et al*., 2003). These studies propose a range of different algorithms for defining the channel network, including the D8 algorithm (Martz and Garbrecht, 1992) and D-infinity algorithm (Tarboton, 1997). The D-infinity algorithm was used in this research because it provides better estimates of flow direction in low relief areas (Tarboton, 1997).

The channel network defined by the D-infinity algorithm (with some manual adjustments as described in below) was used to spatially extrapolate the parameters which were used to calculate the BRI, DNI and SSI. One of the key advantages of using DEM derived channel networks to calculate the RFIs was that it enabled the identification of low order streams that had all of their riparian vegetation removed. These are often the areas at risk of sediment inputs from the adjacent hillslopes, and identifying these areas wouldn't be possible without a DEM.

DEM processing

Prior to application of the flow accumulation algorithm the DEM was pit-filled using RiverTools ™. Then the channel network was defined using a D-infinity flow algorithm (Tarboton, 1997) within RiverTools ™. The criteria used for channel initiation was a catchment area of 5km^2. This area threshold was chosen based on visual comparisons between the flow accumulation image and the ASTER imagery. The 5km^2 threshold coincided with the point at which many streams were visible within the imagery, usually via the presence of riparian vegetation associated with those streams.

The channel network accurately predicted the location of stream channels in high relief areas, but was ineffective in flat low relief areas such as floodplains. This phenomena can lead to an underestimation of the amount of riparian vegetation immediately adjacent to the channel, particularly for areas where the river formed an anastomosing channel network as seen in Figure 5.13 (many of the higher order streams within the study area anastomose extensively). To rectify this problem it was necessary to redigitize the channel network to correspond with the channel networks observed in the ASTER imagery, as seen in Figure 5.14.

This step was necessary in order to accurately assess the amount of riparian vegetation adjacent to the channel network.

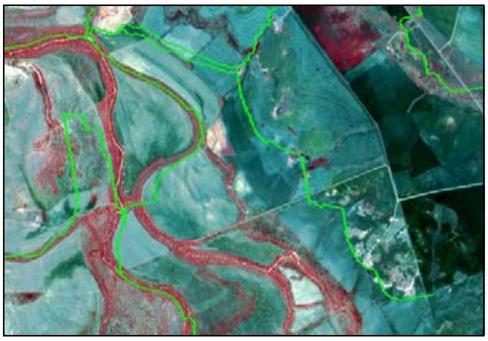

Figure 5.13 Channel network derived using the D-infinity algorithm (all stream orders are displayed as the same colour)

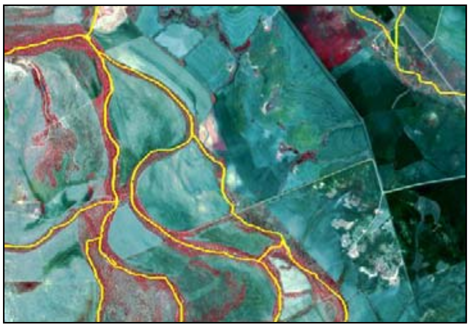

Figure 5.14 Channel network adjusted to match riparian zones observed in imagery.

As a consequence of the redigitizing, catchment area information was not available for each link. Whilst it is possible to recalculate the catchment area for each redigitized link, this is very time consuming, and can be very difficult for areas where the channel anastomoses, and consequently was not performed for this research. There is potential for future research in this area, particularly in relation to estimating channel geometry for anastomosing systems (DeRose pers com 2004). Consequently Strahler stream order was used as a surrogate for catchment area. Strahler stream order is an imperfect substitute for catchment area, because depending on catchment shape, two streams of the same Strahler order can have different catchment sizes.

Modification of Strahler stream ordering

The Strahler stream ordering system was originally designed to describe single channel stream networks (Knighton; 1998) and does not adequately characterise anastomosing river networks (Croke pers com 2005, DeRose pers com 2004). Whilst manually digitizing the channel network it became apparent that a modified version of the Strahler stream ordering system was required to represent the channel network encountered in the study area. The main problem that needed to be addressed were small channels located on the floodplains of high order streams, referred to as secondary and tertiary channels in (Knighton and Nanson, 2002) description of the Coopers Creek anastomosing floodplain.

These minor channels are important from both a pollutant transport point of view, and an ecological point of view. They play an important role in sediment/pollutant transport because they are closely coupled to the main channel, and will therefore have a high sediment/pollutant delivery ratio to the receiving waters. They are also important from an ecological point of view because they provide refugia for sections of the aquatic ecosystem during flood events, and often support important stages in the life cycle of various aquatic species as the floodwaters recede (Puckridge *et al*., 1998).

Visual assessment of the satellite imagery shows that these channels are significantly smaller than the main channel, and therefore are likely to have a different channel geometry to their more dominant 'parent' channels. However because these channels are located on the floodplain of high order streams, they are likely to have flow characteristics similar to the high stage events of the main channel. In other words, these smaller channels will start to flow when the main channel approaches and exceeds bank full flow (*Qbf*).

To account for these small channels on the floodplains of high order streams the following modification to the Strahler stream ordering system was developed. Streams of Strahler order 3 or above were considered as potential candidates for having these small channels (referred to as 'D' class channels hereafter). These 'D' class channels form part of a broader sub-classification of Strahler stream order, which was also developed in this thesis to describe anastomosing river systems. This sub-classification is shown in Figure 5.15 which contains the conceptual diagram of each channel class (A-D) and examples of each class from the study area. The sub-classes can be described as follows: Class A, single channel, with or without associated floodplain, and with no secondary channels; Class B, anastomosing channel network that forms when an Class A channel splits into 2 or 3 channels of approximately even size, with no clear dominance; Class C, single dominant channel with a floodplain (on which Class D channels are located); and Class D, small channels located on the floodplain of a high order stream, these channels separate from and reconnect to B or C class channels and are much smaller than the dominant channel on that floodplain.

For the purposes of the this thesis, where the channel network is used to predict the channel geometry and flow characteristics of any given channel in the stream network, Classes A, B and C are treated as being identical. In other words a 4th order stream will be assigned the same channel dimensions and flow characteristics irrespective of whether it is an A, B, or C class channel.

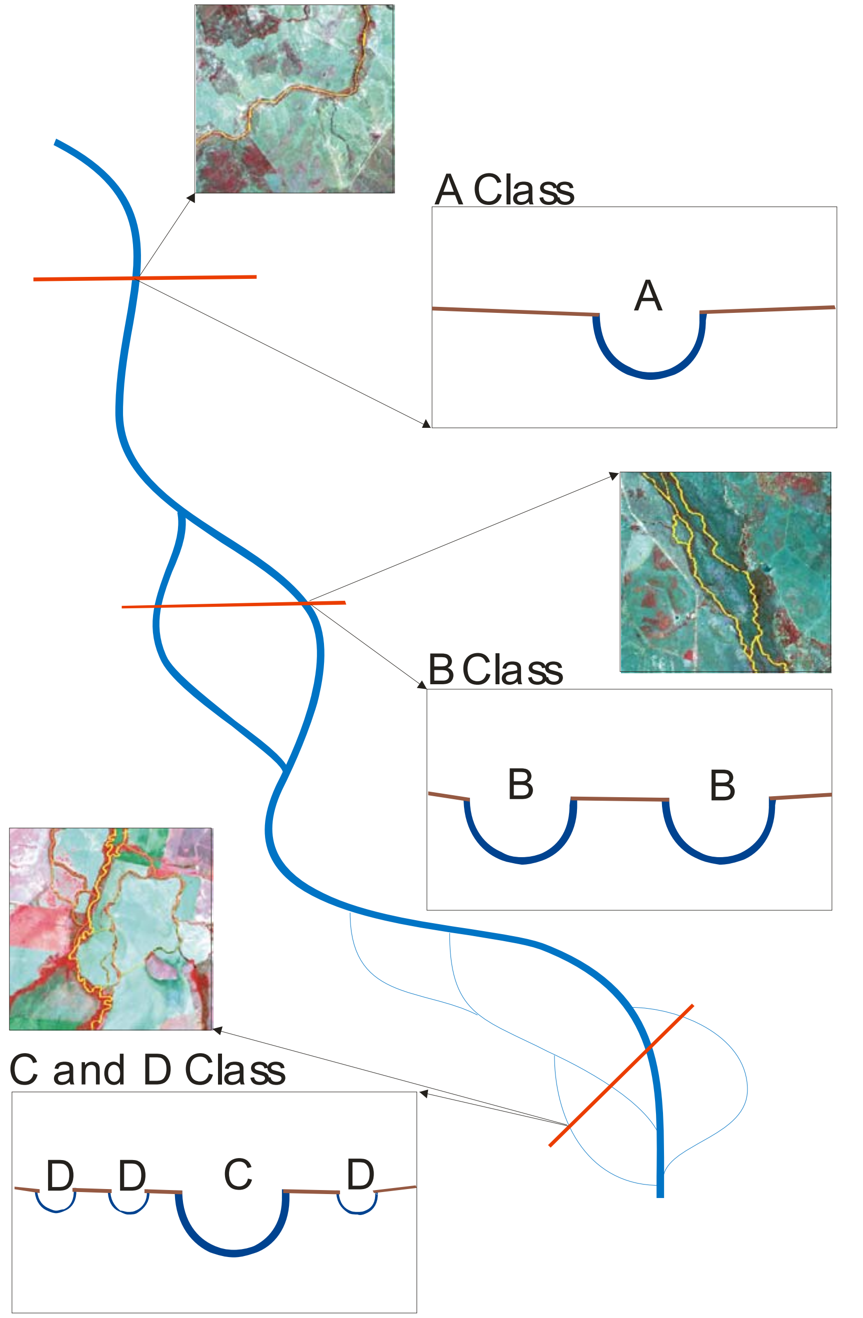

Figure 5.15 Definition of sub-classes for higher order stream channels

This assumption will lead to local inaccuracies in channel geometry, but quantifying the differences in channel geometry between A, B and C class channels for each stream order would require considerably more channel cross section data than was available for this research. This topic would provide an interesting avenue for future research, particularly if a methodology for assigning contributing catchment area to individual links in an anastomosing channel network was developed in conjunction with this data.

D class channels will have smaller channel width and bank height parameters and will have flow characteristics determined by the frequency of high stage events for their parent channel. For the purposes of nomenclature D class channels are referred to as *SO*D order so that a D class channel on the floodplain of a 3rd order stream is referred to as a 3D order stream. Similarly D class channels on 4th, 5th and 6th order streams are referred to as 4D, 5D, and 6D respectively. Due to a paucity of channel cross section information for these D class channels, their dimensions are estimated as a function of their 'parent' channel, as described by

$$\mathrm{CD}_{\text{D class channel}} = 0.33\mathrm{CD}_{\text{Parent C class channel}}\,. \tag{5.4}$$

Where $\mathrm{CD}_{\text{X class channel}}$ is the channel dimensions *BH* and *CW* for each channel class. Based on this the approximate dimensions of D class channels are shown in Table 5.5. These dimensions are consistent with the limited data available for D class channels, however additional data would be required to reliably predict the dimensions of these channels. Consequently the SSI, which is particularly sensitive to channel geometry is not calculated for these channels. The inclusion of these D class channels in the analysis of riparian zone vegetation distribution and function is important because it is an inclusive assessment of all littoral vegetation for each stream order, and will provide important insight into human impacts on the littoral zones of small channels that are closely coupled to high order streams.

The D class channels have the same bank full frequency as their parent channel, and will cease to flow once the river stage of the parent channel falls below the bottom of the D class channel. For example a 6C channel has a depth of 6 metres, and a 6D channel has a depth of 1.7 metres, so the D class channel will cease to flow when the stage height of the main channel falls below 4.3 (6-1.7) metres. Using this approach the $NDNE_x$ parameter for the D class channels is listed in Table 5.6. To calculate unit stream power (ω) for D class channels new values of *Qbf* were calculated for each stream order. The use of uniform channel geometry for C and D class channels does not reflect the natural complexity of distributive and contributive floodplain channels, which may begin and cease to flow at a range of stage heights, rather than one uniform stage height. High spatial resolution digital elevation models, would be required to fully characterise the hydrological connectivity of the main C class channel and the D class channels, but such data is not typically available.

Table 5.5 The channel dimensions of D class streams

	3D	4D	5D	6D
Channel Width (m)	4.3	7.2	7.1	9.8
Bank Height (m)	0.6	0.8	1.0	1.7

Table 5.6 The $NDNE_x$ of D class streams

Soil Depth (x)	3D	4D	5D	6D
0.25-Bank full	0.44	0.35	0.26	0.09
0.5-0.25	0.56	0.46	0.36	0.15
1-0.5	0.94	0.78	0.62	0.30
2-1	0	0	0	0.50

Consequently the approach used may be locally inaccurate in its description of how the floodplain channels fill and drain during high stage events, which would lead to local over and/or underestimates as the amount of denitrification occurring adjacent to D class channels. However the approach is the designed to approximate the behaviour of these D class channels, and will certainly identify where land cover / land use changes adjacent to D class channels have lead to a decrease in the large woody debris production, bank stabilisation and denitrification functions provided by woody riparian vegetation.

Calculating Qbf for D class channels

The bank full discharge (Q_{bf}) for D class channels Q_{bfD} was calculated using

$$Q_{bfD} = \left(\frac{CSA_D}{CSA_{PARENT}}\right) Q_{bfPARENT} \tag{5.5}$$

where CSA_D and CSA_{PARENT} are the cross sectional areas of the D class and parent channel respectively, because the channel dimensions of the D class channels were calculated as a function of the parent channel, the $\left(\frac{CSA_D}{CSA_{PARENT}}\right)$ term is the same value (0.11) for all stream orders. This is based on the assumption that both D class and the parent channel have the same slope and the same roughness, and therefore the have the same velocity, with differences in Q only due to differences in CSA. This is a crude assumption because it ignores potential differences between the slope of the main channel and the slope of smaller channels on the floodplain that may be distributive (lower slope than the main channel) or shortcuts across the floodplain that are only active at high stage (higher slope than the main channel). The BRI_{GLOBAL} values calculated for D class channels will be less accurate as a consequence of this assumption. If we assume that the slope (S) for both the D and parent channels is the same then substituting the values calculated using Equation (5.5) and the channel widths (CW) into Equation (4.16) , then the value for each D class channel are the values shown in Table 5.7. For the purposes of this thesis it is assumed that waterholes are more likely to form in the main channel rather than the D class channels. Consequently the *Pwh* parameter is not calculated for D class channels.

Table 5.7 The unit stream power (ω) of D class streams

	3D	4D	5D	6D
Unit stream power (ω) (Wm^{-2})	12.5	8.8	4.8	6.0

5.3.3. Landscape Classification Using Space Shuttle Radar Topography Mission (SRTM) data

DEM processing

Digital elevation models (DEMs) are grids where the value of each grid cell represents the height at that location (Bolstad; 2003). DEMs can take two forms a digital surface model (DSM) that contains non-terrain features such as trees, buildings, bridges and other structures. Digital terrain models DTMs (also referred to as 'bare earth' DEMs) on the other hand contain only terrain information, without the non-terrain features. The SRTM product is a digital surface model (DSM) rather than a digital terrain model (DTM). This is an important distinction in the context of this research because the 90m SRTM contains vegetation height information for dense riparian vegetation that creates 'ridges' adjacent to river channel as shown in Figure 5.16 on the following page. These artefacts exist because the radar signal is reflected by the woody structures within the tree, rather than the ground surface (Kellndorfer *et al*., 2004). When the multiresolution valley bottom flatness algorithm (Gallant and Dowling, 2003) is applied to the SRTM DSM the 'ridges' generated by the riparian vegetation create artefacts in the middle of the floodplain as shown in Figure 5.17. It is possible to convert a DSM to a DTM if the vegetation height (and the height of other non-terrain objects) is known for all points within the study area. Such data was not available for the study area, so the following approach was taken. A gamma filter as described in (Lopes *et al*., 1993) was applied using a large window size (9x9) to remove the radar speckle and to remove the small linear features such as the riparian vegetation 'ridges'. The gamma filter was chosen because it is a filter designed to remove high frequency speckle from radar data, without removing the detail of high frequency edges (*i.e.* the edges of the floodplain) (Lopes *et al*., 1993). The multi-resolution valley bottom flatness (MrVBF) algorithm described in Gallant and Dowling (2003) was chosen for this research because it is simple to use and was effective in identifying the landscape units required to analyse the RFIs. The MrVBF algorithm was then applied to the gamma filtered SRTM data and the results are shown in Figure 5.18.

It is interesting to note that the channel anastomosis described in the previous section occurred exclusively on floodplains identified by MrVBF. This is consistent with the fluvial geomorphology associated with anastomosis (Knighton, 1999; Church, 2002), but provides an interesting proof of concept.

A MrVBF threshold of 2.5 was used to identify floodplains in the study area. This value corresponds to slopes less than 2% when calculated for a 90 metre DEM. This threshold identified floodplain areas adjacent to high order channels within the study area as shown in Figure 5.19.

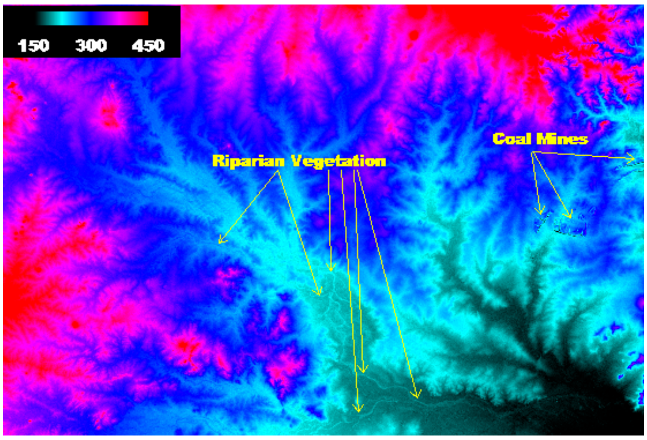

Figure 5.16 Raw SRTM data (values are height in metres)

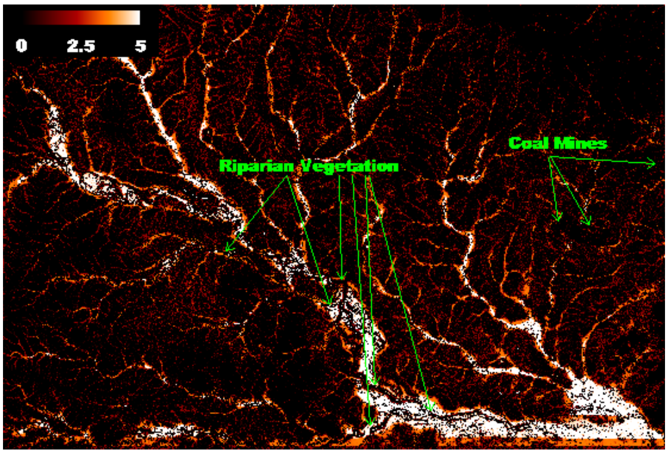

Figure 5.17 MrVBF results from raw SRTM data

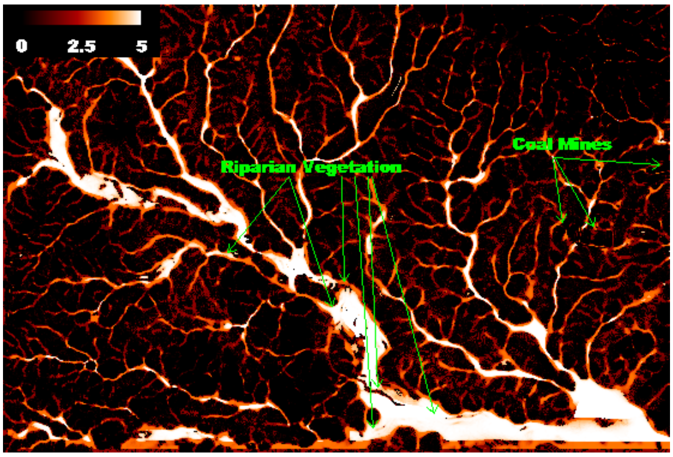

Figure 5.18 MrVBF values from gamma filtered SRTM data

For the largest rivers (6^{th} order channels on the Nogoa and Comet rivers) the channels were large enough to be detected by the radar data (the channels are less than 90 metres wide, but the channel geometry has different radar reflectance characteristics to the surrounding floodplain. As a consequence, the MrVBF algorithm calculates a value less than 2.5 because the overall slope within the channel pixel may be greater than 1. Areas where this phenomena occurred were easy to identify as they occur in the middle of the floodplain on high order streams. For the purposes of identifying floodplain vegetation those areas in the middle of the floodplain with MrVBF values less than 2.5 were included in the floodplain. The criteria for identifying these areas was that they were surrounded by values greater than 2.5 and were located on the floodplain of a high order stream. These criteria were also used to remove any residual vegetation effects that had not been removed by the gamma filter.

The MrVBF results were used to divide the landscape into two broad categories: 1. slopes >2% and 2. plains (slopes <2%). The MrVBF threshold value used to identify slopes and plains was 2.5. This value was chosen based on a visual comparison of the channel network and the MrVBF results, and a visual comparison of a soil GIS (Story *et al*., 1967) with the MrVBF results. The Multi-resolution ridge-top flatness (MrRTF) component of the algorithms described in Gallant and Dowling (2003) was not used, as there were no flat ridgetops contained within the study area.

This analysis was done to identify areas where hillslopes drained directly into riparian zones. This area is referred to as the ‘coupled region’ by Church (2002) indicating that the hillslopes are closely coupled to the channels. It is in these locations that shallow overland flow generated on the hillslope would pass through the riparian zone on its way to the stream. The depositional areas on the other hand are referred to by (Church, 2002) as the uncoupled zone, reflecting the fact that depositional areas of alluvium between the base of the hillslope and the channel have effectively decoupled the hillslope and the channel. It is in these depositional areas that floodplains and regional groundwater systems are likely to form. The identification of floodplains and hillslopes is important in calculating and analysing the results of the RFIs.

The results of the landscape segmentation are shown Figure 5.19. The areas identified using the MrVBF threshold are low slope areas made up of alluvial material. These areas may flood very infrequently, if ever, under the current climatic regime, so the term floodplain may be a little misleading. The implications of using this definition of a floodplain are discussed in the context of each index in Section 5.5.

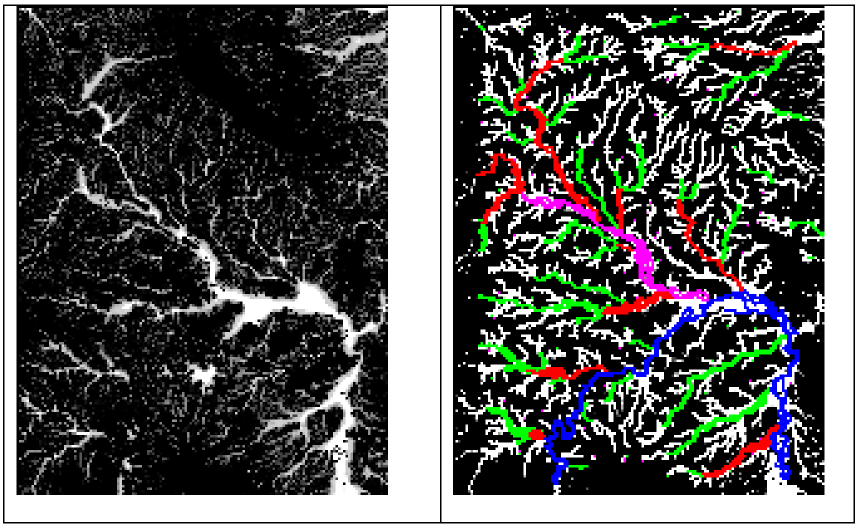

Figure 5.19 Raw MrVBF results for the study area and thresholded MrVBF showing channel network

5.4 Multi-Source Data Classification

To generate the GIS layer used to calculate the RFIs the following layers were combined: the land cover classification generated from the ASTER imagery (Section 5.2); the stream order classification (Section 5.3.2); the grazing pressure classification (Section 5.2.3); and the landscape classification (Section 5.3.3). This process was performed using eCognition ™ and involved the following steps:

1. Separating riparian vegetation and land cover from the rest of the landscape;
2. Identifying riparian zones that were located on hillslopes and those that were located on floodplains or depositional areas;
3. Classifying littoral (channel adjacent) stands of vegetation based on the stream order they were adjacent to; and
4. Classifying stands of littoral vegetation that were located on hillslopes based on whether they were adjacent to cropping, light grazing or heavy grazing.

To understand how these steps were undertaken requires a brief description of how eCognition classifies polygons. The polygons are generated as part of the image segmentation process as described in Section 5.2. These polygons can then be used to calculate statistics from other layers (which may differ in resolution to the 15 metre data used to generate the polygons). For example if a polygon that represents a stand of woodland vegetation is overlaid on top of the output of the MrVBF algorithm, then despite the fact that the MrVBF algorithm was calculated from 90 metre SRTM data, it is still possible to calculate minimum, maximum, mean and standard deviation of MrVBF values within that polygon. Polygons can also be classified based on their neighbouring polygons. For example the stand of woodland vegetation considered in the previous example can be classified based on the fact that it is adjacent to a stream channel, so rather than just being a woodland polygon, this polygon can now be classified as channel-adjacent woodland. If the adjacent channel was a 3rd order stream, then the polygon would be classified as floodplain woodland adjacent to a 3rd order stream. These polygon statistics, and adjacency rules were used to perform steps 1 through to 4 listed above.

The riparian zone was separated from the rest of the landscape by identifying every channel adjacent polygon, which are riparian by definition. In addition to this polygons that had a mean MrVBF value greater than 2.5 were classified as floodplain polygons, and were therefore included in the riparian class. All polygons that did not fit into either of the above categories were considered not to be riparian and were omitted from all further analysis. The distribution of riparian and not-riparian polygons is shown inFigure 5.20.

The riparian class shown in Figure 5.21was broken into 3 subclasses riparian zones located on hillslopes (polygon mean MrVBF <2.5) hereafter referred to as 'hillslope littoral', littoral zones on the floodplain (polygon mean MrVBF>2.5, and adjacent to the channel network) hereafter referred to as floodplain littoral and non-littoral floodplain vegetation (polygon mean MrVBF>2.5, and not adjacent to the channel network), hereafter simply referred to as floodplain. See Figure 5.21 for an example of each.

The hillslope littoral, and floodplain littoral classes shown in Figure 5.21 (in other words every stand of vegetation that was adjacent to the channel network), was then classified according the Strahler stream order of the adjacent channel. Stands of woody vegetation that fell into the hillslope littoral class shown in Figure 5.21, were classified based on their adjacent land use. So, if a stand of woodland located on a hillslope adjacent to a 1st

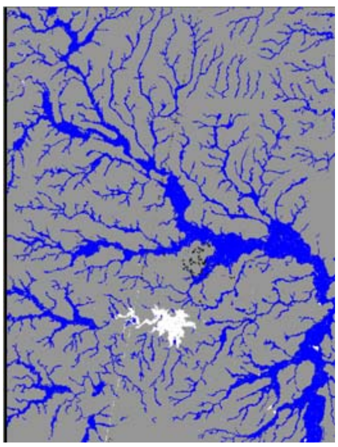

Figure 5.20 Riparian polygons shown in blue (white object is Fairbairn reservoir)

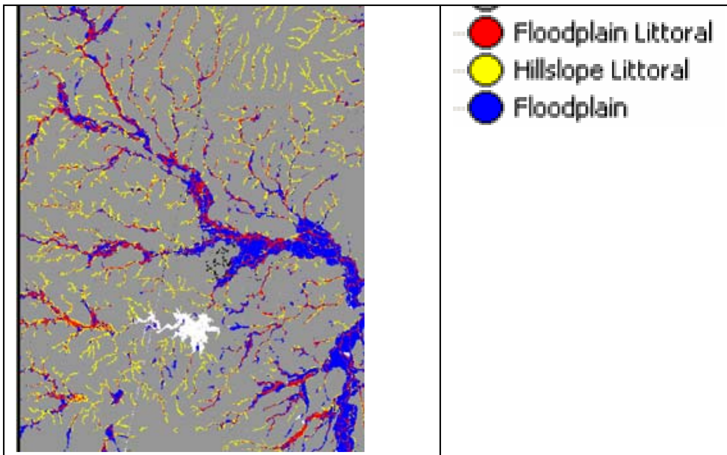

Figure 5.21 Distribution of floodplains and littoral zones

order stream was surrounded by heavy grazing, it was assumed that ground cover beneath the stand of woodland would also be subject to heavy grazing. This classification assumes that the groundcover beneath the woody vegetation canopy can be estimated based on the intensity of the grazing surrounding that stand of vegetation (as discussed previously in Section 4.2.

The final classification included all of the above steps so that all polygons in the image were classified into riparian or non riparian, hillslope or floodplain, adjacent to stream order X or not channel adjacent, and each channel adjacent polygon on a hillslope was classified according to grazing pressure. This classification was then used to calculate the RFIs.

5.5 Generation of Riparian Function Index Maps

Each RFI was calculated for the area in the landscape where the function that the RFI represents is likely to be important. For example, the stream shading index was only calculated for floodplain littoral vegetation on the main channel of higher order streams, because it is these sections of the channel network that support aquatic life. In other words, the SSI value of a stand of vegetation adjacent to a 1st order stream is irrelevant because these channels only flow during rainfall events, and consequently stands of vegetation adjacent to these channels do not provide shade for the aquatic ecosystem (they do however provide other important functions). The portion of the riparian zone used to calculate each RFI is detailed in the following Sections 5.5.1 through to Section 5.5.5.

5.5.1. Areas Used to Calculate the Sediment Trapping Index

The sediment trapping index (STI) was only calculated for all hillslope littoral polygons. The STI was calculated for these areas, because the hillslopes drain through these areas directly into the stream channel. Consequently the hillslope and the channel are closely coupled. In such areas, the presence of ground cover in the riparian zone will act to reduce velocity of shallow overland flow, thereby reducing its sediment transport capacity. In this setting, the sediment transport equations of Hairsine and Rose (2002) are applicable, thereby satisfying many of the assumptions made in calculating the STI (as discussed in Section 2.2). The vegetation and land use classification used to calculate the STI is shown in Figure 5.22. The red areas represent areas where bare soil (either light or dark) or crops are present in littoral hillslope polygons.

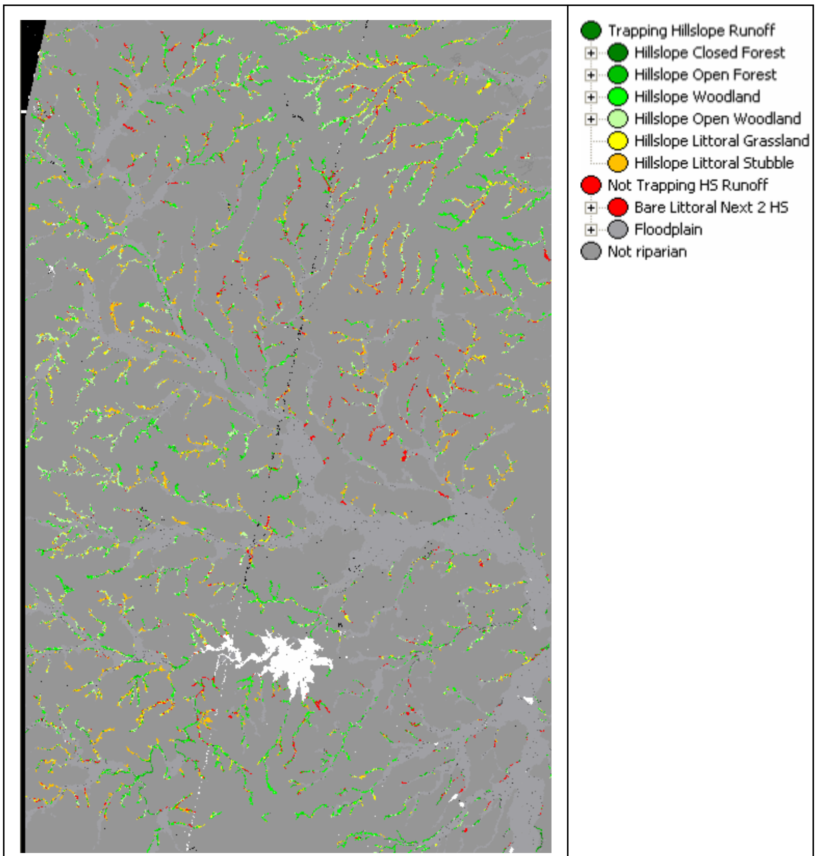

5.22 Riparian vegetation and land cover classification of hillslopes used to calculated STI

5.5.2. Areas Used to Calculate the Bank Reinforcement Index

The bank reinforcement index (BRI) is calculated for all channel adjacent polygons in the study area. The BRI is calculated for these riparian zones because bank erosion processes will be present throughout the catchment, and the presence or absence of woody vegetation on the stream bank may determine whether bank erosion takes place or not. The vegetation and land cover in this area is shown in Figure 5.23. The red areas represent all littoral zones (both hillslope and floodplain) that lack woody vegetation.

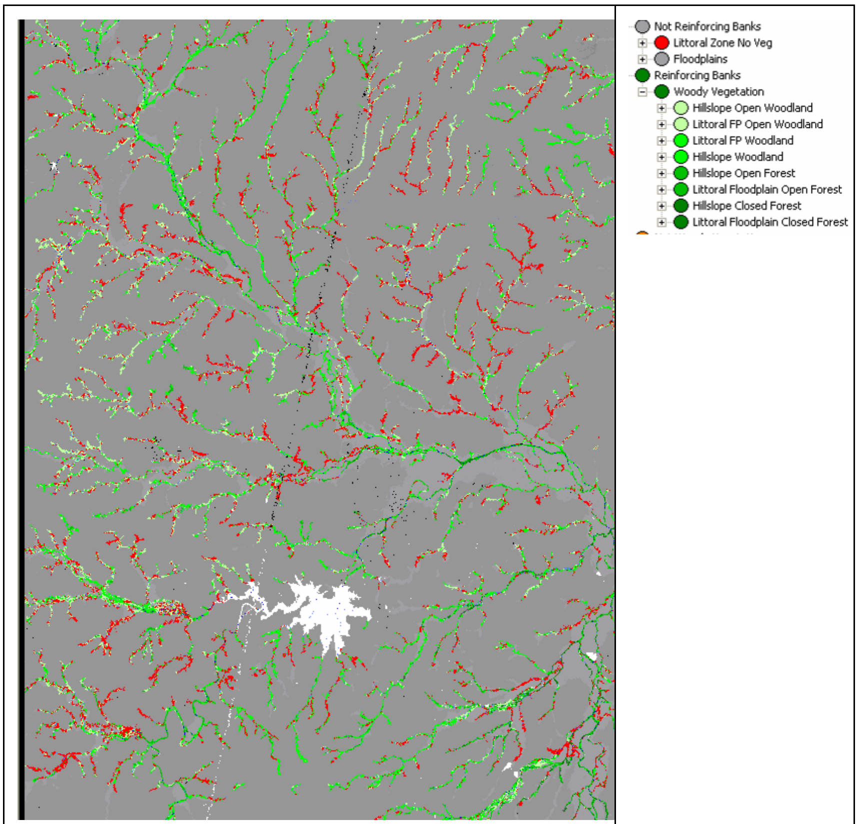

5.23 Riparian vegetation and landcover classification used to calculate BRI

5.5.3. Areas Used to Calculate the Denitrification Index

The denitrification index (DNI) is calculated for floodplain littoral polygons adjacent to 2nd to 6th order streams (including D class channels). The DNI is calculated for these areas, because it is in these areas where the conditions required for denitrification, namely, the root zone of the vegetation remaining saturated for more than 48 hours, are likely to be met. The vegetation and land use on the floodplain and the floodplain littoral zones is shown in Figure 5.24. The riparian zones of 1st order streams and higher order streams that are not located on floodplains are not included in the calculation of DNI because water is unlikely to remain in the root zone of these areas long enough for denitrification to occur. It is worth noting that nitrogen sources that were located in riparian zones (but not on floodplains) are included in the potential N sources class shown in Figure 5.24.

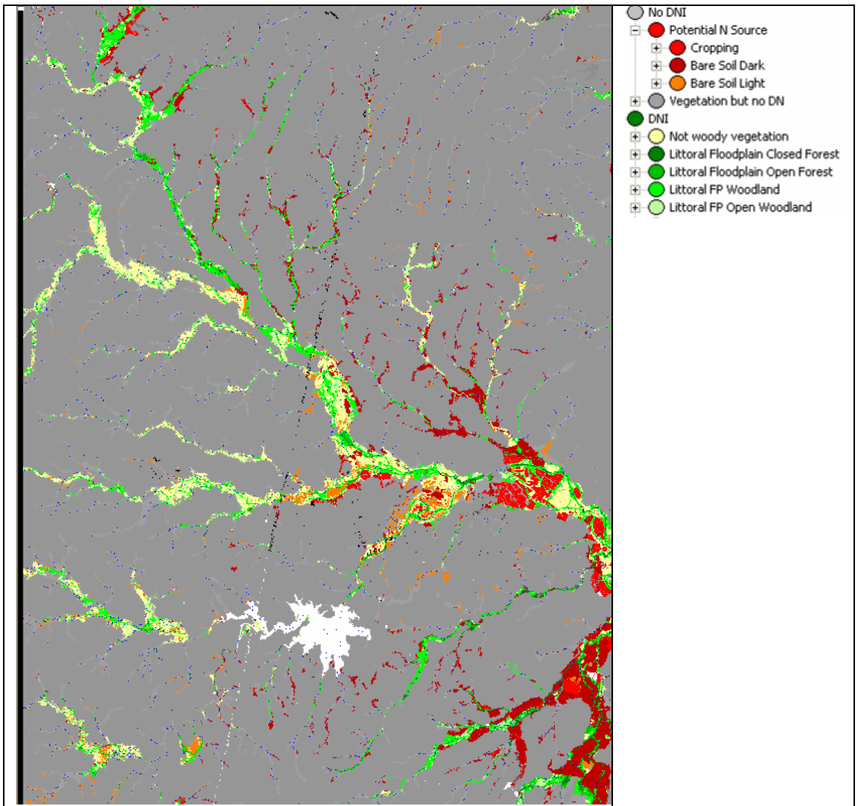

5.24 Riparian vegetation and land cover classification used to calculate DNI

5.5.4. Areas Used to Calculate the Stream Shading Index

The stream shading index (SSI) was calculated for floodplain littoral polygons adjacent to the main channel (excluding D class channels) of 3rd to 6th order streams. The vegetation in these areas is shown in Figure 5.25. The SSI is calculated for these areas, because it is in these areas that waterholes are likely to form during the dry season, and consequently the shading of these refugia for the aquatic ecosystem during dry periods is of great importance. During periods of higher flow the volume of water moving through the system will reduce the impact of solar radiation on water temperature (Poole and Berman, 2001). However under these higher flow conditions the velocity refuge and breeding habitat provided by LWD becomes more important. The areas shown in red represent floodplain littoral zones adjacent to higher order streams that are devoid of woody vegetation.

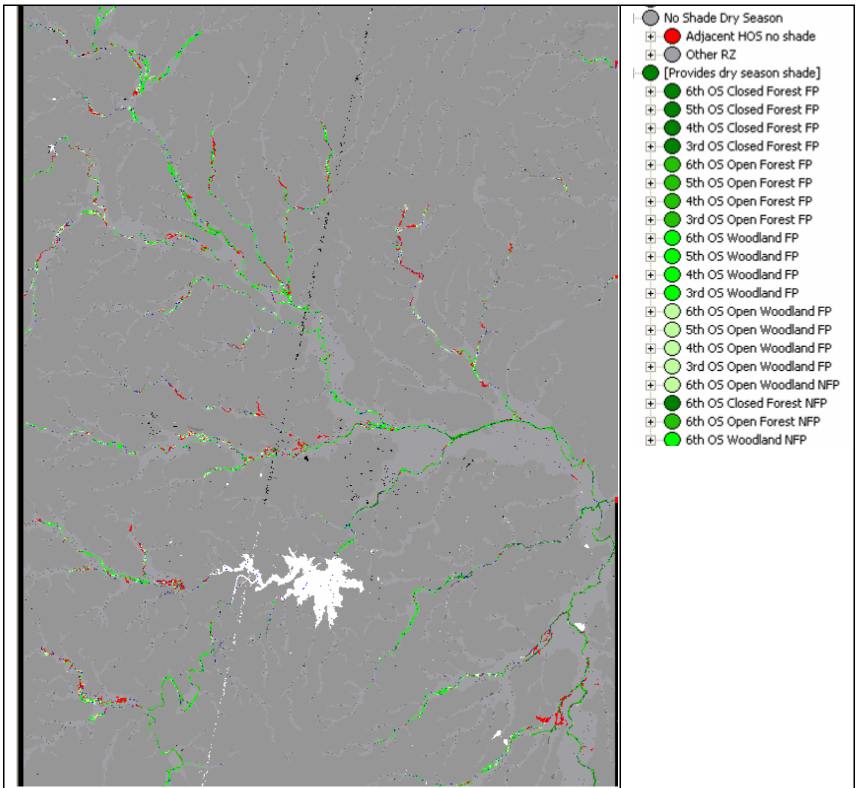

5.25 Riparian vegetation and land cover classification used to calculate SSI

5.5.5. Areas Used to Calculate the Large Woody Debris Index

The large woody debris index (LWDI) is calculated for floodplain and hillslope littoral polygons adjacent to 3rd to 6th order streams (including D class channels). The land cover and vegetation in these areas is shown in Figure 5.26. During flood events, water will fill both the main and D class channels of higher order streams, and LWD in these channels will provide a range of ecosystem services to fish species moving through the channel network during these times. The 1st and 2nd order streams were omitted from this analysis because they generally only flow during rainfall events and consequently don't contain water long enough to support aquatic life. It is possible that LWD entering the stream network in low order streams could be transported into higher order streams. However LWD transport is not considered to be a major process in the study area due to the combination of dense wood (which is less prone to transport because it doesn't float as well) and relatively low stream power.

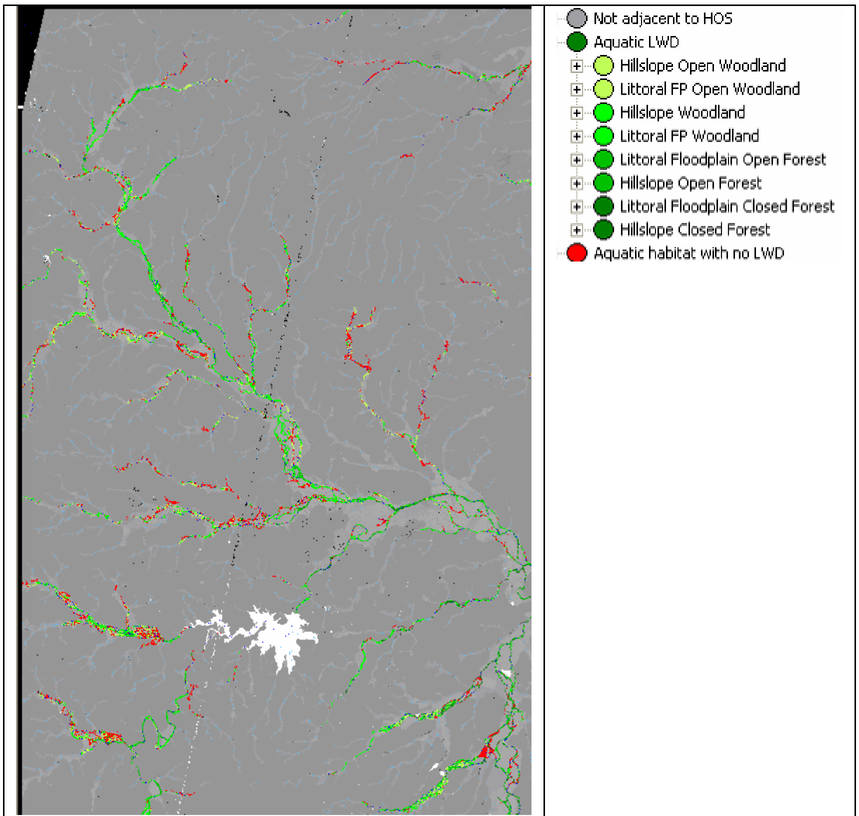

5.26 Riparian vegetation and land cover classification used to calculate LWD

5.6 Chapter Summary

This chapter describes the remote sensing and terrain analysis techniques that were used to spatially extrapolate the parameters described in Chapter 4. These parameters are required to calculate the riparian function indices (RFIs) developed in Chapter 2. The following classifications were generated from remote sensing data:

1. ASTER (multi-spectral 15 metre pixel) satellite imagery was used to generate a map vegetation structure and land cover which was used to extrapolate parameters listed in Table 2.2; and
2. MODIS (multi-temporal 16 day composite 250 metre pix) satellite imagery was used to estimate grazing pressure and thereby estimate the Manning's n_{5M} parameter used to calculate the STI.

These two maps were generated using an image segmentation package that enabled the identification of stands of riparian vegetation (rather than classifying individual pixels), and better discrimination of grazing and cropping land uses. The classification accuracy for the vegetation map was 94%. The implications of the classification errors on the index reliability are discussed in Chapter 6.

Terrain analysis was used in this chapter to define two classifications:

1. A channel network map was used to extrapolate channel geometry parameters, bank height and channel width, and the *NDNEx* values (used to calculate the denitrification index) and;
2. A landscape classification that was used to identify hillslopes and floodplains within the study area.

These four classifications were combined to generate a detailed classification of every polygon within the riparian zone, and this classification, in combination with the parameters described in Chapter 4 were used to calculate the RFIs as described in Chapter 6.

Chapter 6 Calculation and Results of Riparian Function Indices

6.1 Introduction

This chapter computes the riparian function indices (RFIs) described in Chapter 2 using the parameters (Chapter 4) predicted by the classifications (Chapter 5). The following results are presented for each index.

1. A table showing the RFI_{local} value for each vegetation/land cover class and stream order combination.
2. A map of the RFI_{local} for the whole study area.
3. A summary of RFI_{local} values for each stream order on a percentage basis.
4. A summary of RFI_{local} values on a hectare basis.
5. A table showing how RFI_{global} values were distributed (*i.e.* which stream order and vegetation class combination yielded the highest RFI_{global} value).
6. A summary of RFI_{global} values for each stream order on a percentage basis.
7. A summary of RFI_{global} values for each stream order on a hectare basis.

The RFI_{local} values describe changes in riparian functions at a local scale. In other words, the amount of a given function (for example stream shading) provided by the existing vegetation is compared with the amount of that function provided by the vegetation at that same location prior to European settlement. RFI_{local} values of 1 indicate that the current vegetation structure is the same as pre-settlement, and index values of zero indicate that all riparian vegetation has been removed. In the case of SSI and LWDI an RFI_{local} value of zero indicates that all woody vegetation has been removed, whereas for BRI, DNI and STI, an RFI_{local} value of zero indicates an area where *all* riparian vegetation, both woody and non-woody, has been removed (*i.e.* there is only bare soil or cropping immediately adjacent to the channel).

The RFI_{local} represents a 'restoration' index insofar as all areas within the stream network could be restored to a value of one. As mentioned earlier in Chapter 3, it is assumed for the purposes of this thesis that, prior to European settlement, woodland was present on all floodplains and in the littoral zones of low (1^{st} to 3^{rd} order streams) and minor floodplain channels (3D-6D) channels. The vegetation in the littoral zone of higher order (4^{th} through to 6^{th}) streams is assumed to have been open forest. This vegetation distribution is based on the description of riparian vegetation and land units contained in Gunn *et al.* (1967) and Story *et al.* (1967).

The RFI_{global} values, on the other hand, compare the function current riparian vegetation at a given location with the maximum amount of that function performed anywhere within the study area at the present time. This enables a stand of woodland providing shade to a 5th order stream to be compared with a stand of closed forest providing shade to a 4th order stream, because the combination of canopy geometry, PFC and channel geometry mean that closed forest adjacent to a 4th order channel blocks more sunlight from reaching the channel than any other vegetation and channel geometry combination. Consequently, the RFI_{global} values can be seen as a 'prioritization' index because values of 1 or close to 1 identify areas where the existing riparian vegetation is important for performing that particular function, and values of zero (particularly if they occur on the same stream order that yields a value of 1) indicate areas that are of high priority in terms of restoring that particular function. Note that STI_{global} values were not calculated because the sediment trapping capacity of the riparian zone is not a function of stream order (it is however, only calculated for littoral zones located on hillslopes, a scenario which occurs predominantly on lower order streams).

There is a brief discussion of each of these results identifying the key findings for each index, a more detailed discussion of the indices themselves is contained in Chapter 7.

6.2 Sediment Trapping Index

The STI was calculated using the average n_{5M} values for each land use as described in Section 4.2 and n_{5M} reference value used was the highest average n_{5M} observed at any site during the fieldwork. The*se* values were entered in the STI formula (Equation (2.8)) and calculated for the hillslope littoral zones as shown in Figure 5.22. The range of STI values for each land use are shown in Table 6.1, and the results of the STI calculation are shown in Figure 6.1.

Figure 6.1 shows a number of interesting features. The areas of bare soil (red) adjacent to the channel appear in the cropping areas within the image, and associated with heavy grazing (yellow). Catchment management strategies such as riparian fencing, lower stocking rates, or the installation of grass filter strips should be targeted at the red (highest priority) and yellow (high priority) areas to reduce the amount of sediment being delivered to the stream. Detailed STI results for an area in the top left of Figure 6.1 are shown in Figure 6.2 and Figure 6.3.

Table 6.1 STI values for each land use.

Land Use	STI
Cropping and Light Grazing	0.7
Heavy Grazing	0.5
Bare Soil	0.3

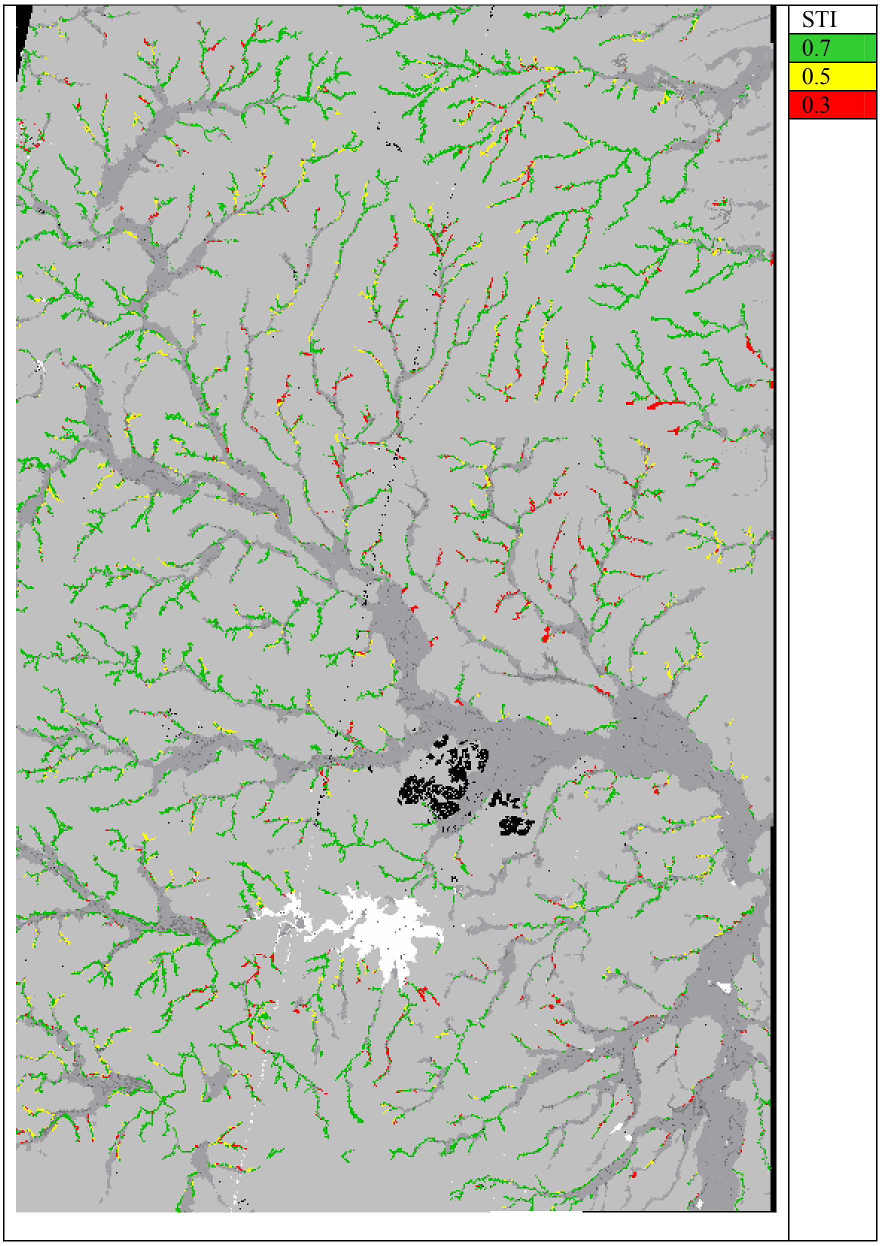

Figure 6.1 A map of the sediment trapping index for a section of the study area

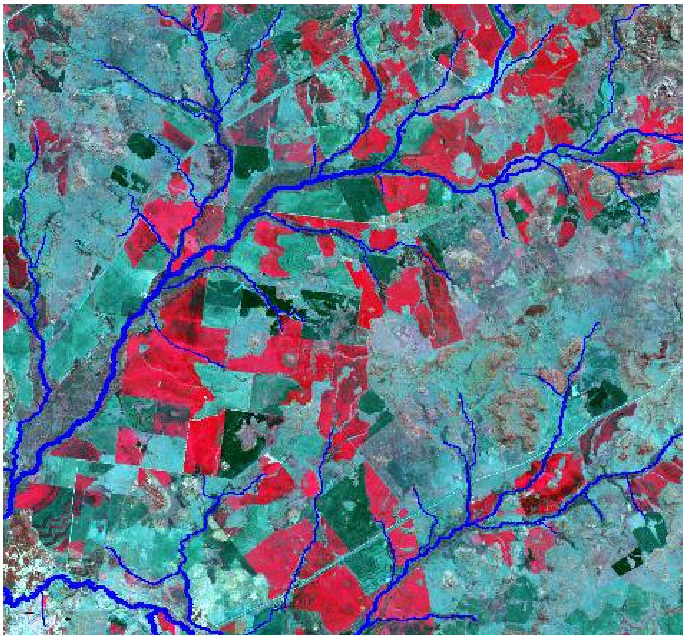

Figure 6.2 False colour image showing cropping and grazing areas

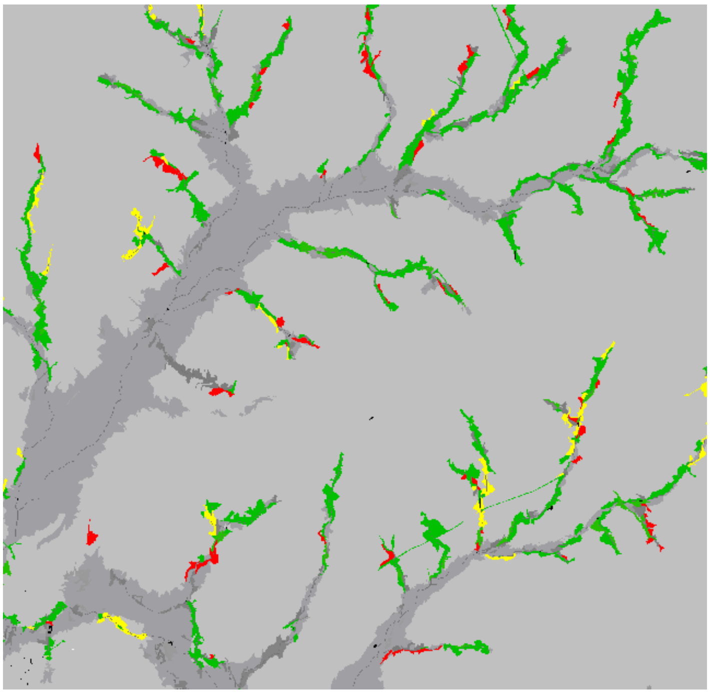

Figure 6.3 Detailed STI results

The results shown in Figure 6.1 were analysed by assessing the STI values within 15 metres either side of the stream network. These results were then sorted according to stream order as shown in Figure 6.5. The proportion of littoral zones located on hillslopes (*i.e* where the STI is calculated) is shown in Figure 6.4. As expected, the hillslope littoral zones form the majority of littoral zones adjacent to 1st order streams, and form an increasingly small proportion of littoral zones with increasing stream order. It is also interesting to note that the D class channels have a very low proportion (13%) of hillslope littoral zones, reflecting the fact that these channels are formed on floodplains and would only have hillslope littoral zones if the channels were located at the very edge of the floodplain.

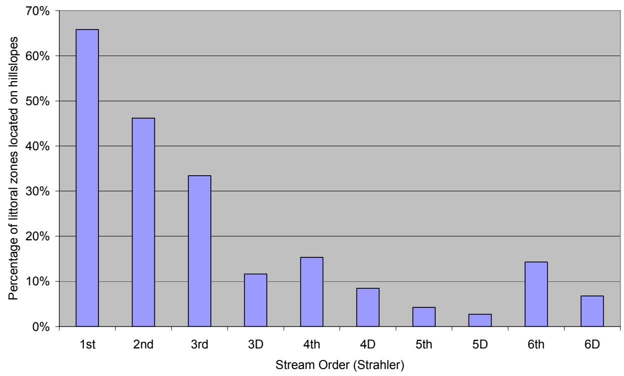

Figure 6.4 Proportion of hillslope littoral zones

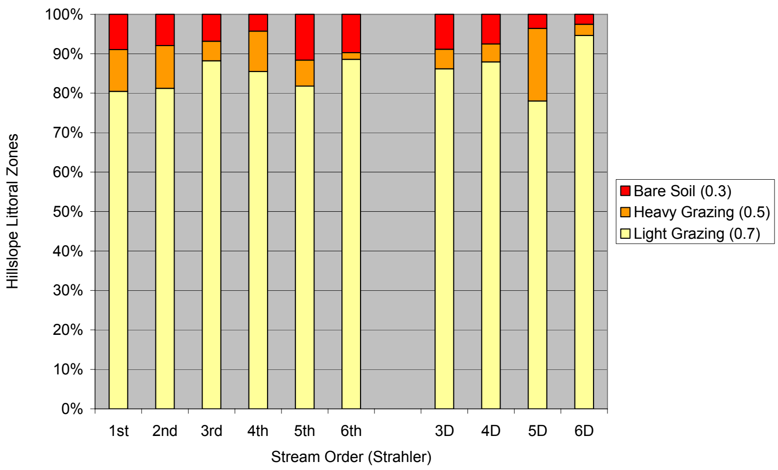

Figure 6.5 STI values for the littoral zones located on hillslopes

The results shown in Figure 6.5 indicate that there is bare soil in the littoral zones located on hillslopes for between 5 and 10% of the channel network across all channels, and between 3 to 15% of these zones are subject to heavy grazing These areas have the potential to deliver large amounts of sediment to the stream network during erosion events, and the areas adjacent to high order streams are of particular concern because these portions of the channel network will have a higher sediment delivery ratio to the receiving waters than lower order streams . Taking area into account in this analysis Figure 6.6, which indicates that over 1000 hectares of hillslope littoral zones on 1st order streams contain either bare soil or are subject to heavy grazing, thereby substantially reducing there capacity to trap sediment being carried by shallow overland flow. The same conditions exist next to 502 hectares of 2nd order streams and 156 hectares of third order streams, and it is these areas that would be of highest priority in terms of reducing the amount of sediment being delivered to the Great Barrier Reef. The management scenarios that could be applied to these areas are detailed in Chapter 7

Assumptions made in calculating the index

The assumptions made in extrapolating the parameters to calculate this index are described in Section 4.2 Additional assumptions made in calculating this index are as follows. That the area within 15 metres either side of the channel contains any riparian zone buffer. That all riparian buffer strips in the area are in excess of 15 metres in width. There may be riparian buffers that are less than 15 metres wide within the study area, and these areas would not be detected based on the spatial resolution of the ASTER data, however this limitation is not of great concern because less than 15 metres in width are likely to be ineffective in trapping sediment in a tropical rainfall environment (McKergow *et al.*, 2005). Furthermore, a number of landholders within the study area

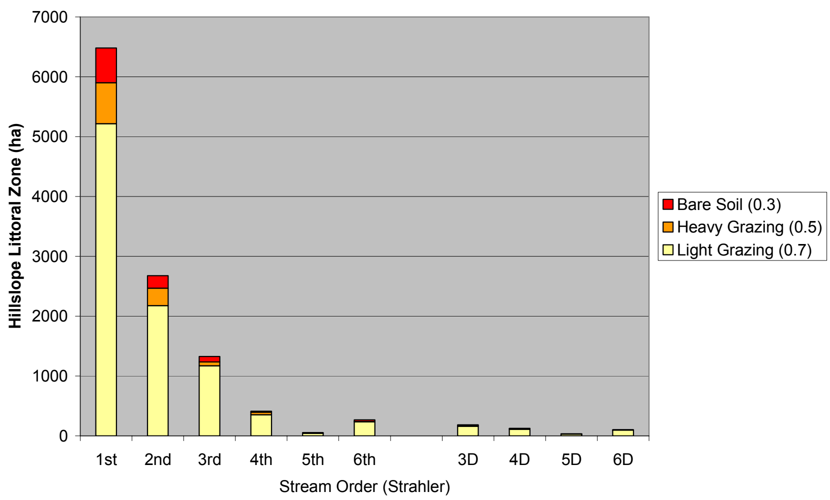

Figure 6.6 STI values in terms of hectares of littoral zone.

have adopted the practice of using grassed waterways, and the ASTER imagery can readily identify these features as seen previously in Figure 3.4.

Index Reliability

The STI is useful at a number of levels. At the most basic level the terrain analysis identifies hillslope areas within the catchment. These are the areas where hillslopes are closely coupled to the stream network (Church, 2002), and consequently, it is in these areas where riparian buffer strips will function as filters to hillslope generated runoff. The index is very reliable at this level, because the MrVBF algorithm (Gallant and Dowling, 2003) used to identify hillslope areas is relatively simple and robust.

By identifying areas of bare soil adjacent to the channel network in these hillslope areas the index further identifies potential sediment transport 'hotspots'. The index is reliable at this level because bare soil provides a unique spectral signature that can be discriminated from other land uses. However the proportion of bare soil (channel adjacent or otherwise) in a scene will depend on the image acquisition time relative to the cropping cycle. Imagery collected after an extended dry period would give the best estimate as to the maximum amount of bare soil within the catchment.

The index values calculated using the ground cover levels associated with different land uses are useful in that they identify the impact of land use on sediment transport potential. The grazing pressure index, calculated from MODIS NDVI data has been used to discriminate between heavy grazing and the cropping and grazing land use. This is an experimental index, and would require additional fieldwork to establish whether this technique is reliable in terms of identifying describing grazing pressure. The STI does not discriminate between cropping and grazing in terms of buffer efficiency. This is due to the fact that cover levels measured adjacent to each land use were very similar, which in turn may be due to the practice of subjecting cropping areas to light grazing after crops have been harvested (Carroll pers com 2003)

Another point worth considering is the difficulty associated in discriminating grassed waterways/buffer strips from dense stubble (both have the same spectral signature). Identifying all the grassed waterways throughout the study area would be possible, if a series of dry season images were analysed to identify persistent areas of stubble (i.e. areas that were not subject to cropping and/or periods of bare soil). However such analysis is beyond the scope of this thesis. Discrimination between grass waterways/buffer strips and stubble would provide information about the potential extent of bare soil adjacent to the channel after harvest.

6.3 Bank Reinforcement Index

The bank reinforcement index (BRI) is calculated for every polygon (both vegetation and non-vegetation) adjacent to the channel (*i.e.* all littoral zones) throughout the stream network for both floodplain and hillslope littoral zones. This is done by entering the λ values described in Section 4.3.4 into the BRI formula (Equation (2.18) The range of BRI values calculated for the study area are shown in Table 6.2 The BRI_{local} results is shown in Figure 6.7. Note that for the purposes of display and analysis the BRI_{local} values have been aggregated accorded to the cell colours shown in Table 6.2.

The areas shown as red in Figure 6.7 represent areas with no riparian vegetation. Stream banks in these areas are more likely to be unstable due to the absence of reinforcement provided by riparian vegetation (both woody and non-woody). Areas shown in orange indicate areas where grassland or stubble is present next to the channel. These areas have undergone a large decrease in the amount of bank reinforcement, and may be prone to bank erosion, based on observations in the field that non-woody vegetation did not provide adequate reinforcement to the banks 2nd order streams to prevent bank erosion, as shown in Figure 6.8. Consequently littoral zones of 2nd order or higher streams that have undergone a large decrease in the amount of reinforcement and are therefore likely to contain unstable banks in areas where the shallow rooting habit of the grasses does not stabilize higher banks (Figure 6.8). The riparian zones shown in yellow represent areas where forest or woodland have been replaced by open woodland, and the relatively low number of trees per hectare predicted for these areas means that there may be sections of the stream that are not reinforced by woody riparian vegetation.

The areas shown in lime green represent littoral zones on high order streams that currently contain woodland, and which would have supported open forest prior to settlement. These areas have undergone a slight decrease in the amount of bank reinforcement. Areas shown as dark green contain the same riparian vegetation now as they would have prior to European settlement, and are likely to have stable banks due to substantial reinforcement by riparian vegetation.

Table 6.2 BRI_{local} values for every vegetation type adjacent to different stream orders

	1st	2nd	3rd	3D	4th	4D	5th	5D	6th	6D
Closed Forest	2.2	2.2	2.2	2.2	1.5	2.2	1.5	2.2	1.5	2.2
Open Forest	1.5	1.5	1.5	1.5	1.0	1.5	1.0	1.5	1.0	1.5
Woodland	1.0	1.0	1.0	1.0	0.7	1.0	0.7	1.0	0.7	1.0
Open Woodland	0.4	0.4	0.4	0.4	0.3	0.4	0.3	0.4	0.3	0.4
No woody veg	0.1	0.1	0.0	0.1	0.0	0.1	0.0	0.1	0.0	0.0
Bare soil	0.0	0.0	0.0	0.0	0.0	0.0	0.0	0.0	0.0	0.0

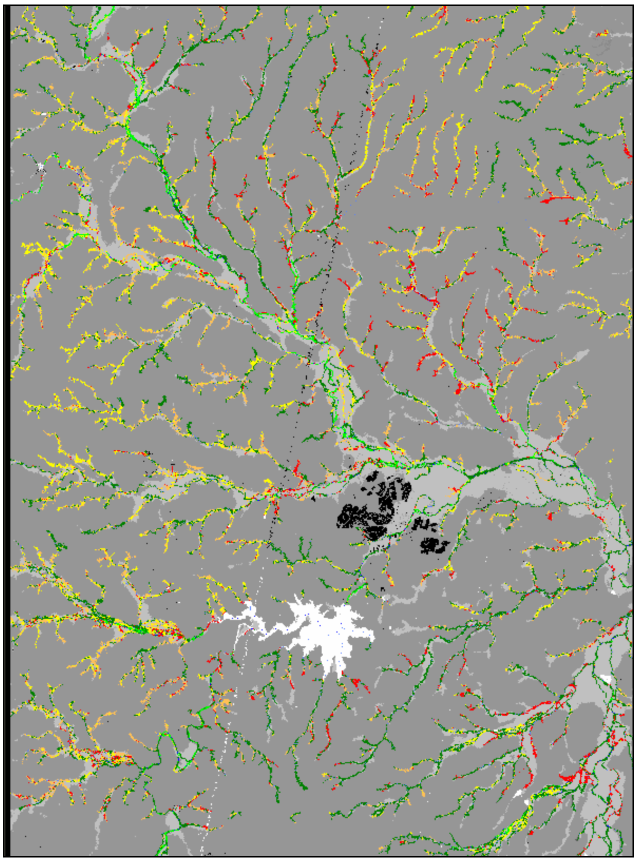

BRI value (change in amount of bank reinforcement)

BRI value	
>1 (No change)	
0.7 (Slight decrease)	
0.3-0.4 (Moderate decrease)	
0.1 (Large decrease)	
0 (No reinforcement)	

Figure 6.7 A map of the bank reinforcement index (BRI) for the study area.

Figure 6.8 A and B showing bank reinforcement by woody vegetation and an unstable bank with grasses at the same location on a 2nd order stream

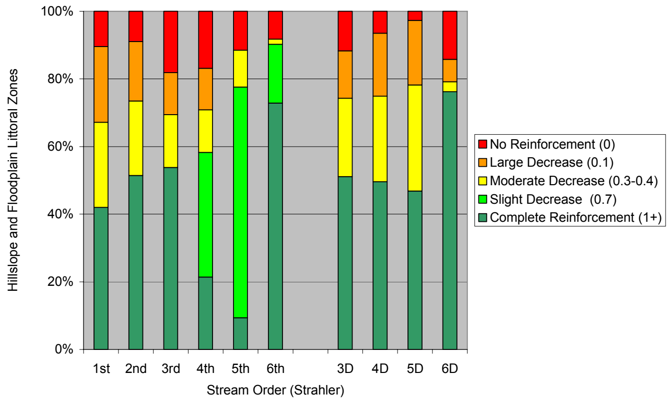

Figure 6.9 BRI$_{local}$ values for each stream order

There area number of interesting features to Figure 6.9. Over 25% of 1st, 2nd, 3rd and 4th order streams are without any reinforcement due to woody vegetation, and for the 2nd, 3rd and 4th order streams in particular, these areas will be prone to bank erosion. It is also worth noting that over 50% of 3rd 4th and 5th order D class channels have undergone a moderate or greater decrease in the amount of bank reinforcement.

Bank erosion in these D class channels is of particular concern because they are more closely coupled to high order streams, and therefore have a higher potential sediment delivery ratio. The proportion of the stream network that lacks any reinforcement (shown as red in Figure 6.9) is over 10% for 1st -5th order streams and nearly 20% of 3rd and 4th order streams, all of these areas will be highly prone to bank erosion. Plotting these results on a per hectare basis Figure 6.10 gives an indication as to the amount of stream restoration that would be required to improve bank stability within the study area.

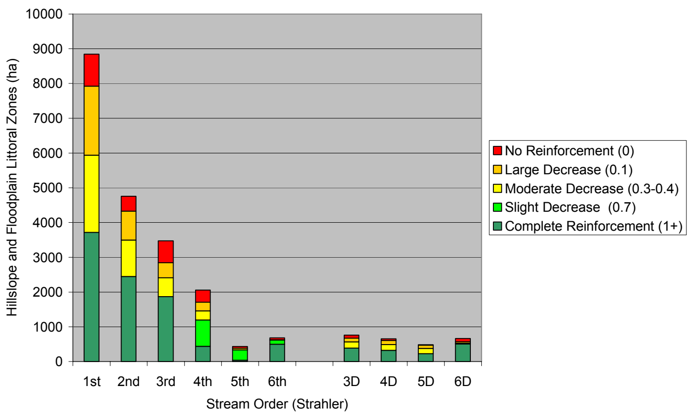

Figure 6.10 BRI$_{local}$ values for each hectare of littoral zone in the study area sorted by stream order.

There are 917 hectares of 1st order stream littoral zones that lack any reinforcement whatsoever, and a further 1988 hectares that are reinforced by grass only. There are stream banks that lack any reinforcement, and are therefore prone to erosion along 427 hectares of 2nd order streams, 631 hectares of 3rd order streams and 347 hectares of 4th order streams. The two highest stream orders have predominantly stable banks with only 50 hectares adjacent to 5th order streams and 56 hectares adjacent to 6th order channels lacking any reinforcement by woody vegetation. It is interesting to note that the D class channels adjacent to higher order streams all have over 100 hectares that lack reinforcement by woody vegetation.

Based on the results shown in Figure 6.10 there are large portions of the stream network that are prone to bank erosion due to the removal of woody vegetation. However the resources required to remediate all of these riparian zones simultaneously are unlikely to be available at one time. Consequently there is a need to identify priority areas, i.e. those areas where bank erosion is most likely to occur. To identify these areas, the λ parameter used to calculate BRI_{local} was incorporated into an existing bank erosion model (as described in Section 2.3 to calculate the BRI_{global}.

Range of BRI_{global} values

The abbreviations used in Table 6.3 are as follows: D, M, S and V stand for closed forest, open forest, woodland and open woodland respectively; FP and HS refer to floodplain and hillslope littoral zones; NRWV stands for no riparian woody vegetation and NRV stands for no riparian vegetation. The BRIglobal value for floodplain littoral zones are shown in Table 6.3. The BRI_{global} values shown in Figure 6.11 were calculated using Equation (2.20), which takes the basic form of 1-(normalized bank erosion term). So values close to zero indicate the scenario where bank erosion was most likely to occur.

Table 6.3 BRI_{global} values for each vegetation/landcover and stream order combination

BRI global	1st	2nd	3rd	3D	4th	4D	5th	5D	6th	6D
D FP	1.00	1.00	1.00	1.00	1.00	1.00	1.00	1.00	1.00	1.00
D HS	1.00	1.00	1.00	1.00	1.00	1.00	1.00	1.00	1.00	1.00
M FP	1.00	1.00	1.00	1.00	1.00	1.00	1.00	1.00	1.00	1.00
M HS	1.00	1.00	1.00	1.00	1.00	1.00	1.00	1.00	1.00	1.00
S FP	1.00	1.00	1.00	1.00	0.90	1.00	0.88	1.00	0.96	1.00
S HS	1.00	1.00	1.00	1.00	0.95	1.00	0.94	1.00	0.98	1.00
V FP	0.38	0.49	0.67	0.78	0.85	0.86	0.82	0.91	0.93	0.94
V HS	0.69	0.75	0.84	0.89	0.92	0.93	0.91	0.95	0.97	0.97
NRWV FP	0.17	0.33	0.56	0.71	0.82	0.81	0.79	0.88	0.92	0.91
NRWV HS	0.59	0.66	0.78	0.86	0.91	0.91	0.90	0.94	0.96	0.96
NRV FP	0.00	0.19	0.47	0.65	0.82	0.78	0.79	0.85	0.92	0.90
NRV HS	0.50	0.59	0.74	0.82	0.91	0.89	0.89	0.92	0.96	0.95

The BRI_{global} are strongly influenced by the unit stream power term *Power* in Equation (2.20), and values calculated for this term are shown in Figure 6.12.

The highest unit stream power occurred on 1st order streams, which is consistent with the peak in unit stream power close to the start of the channel network as described in Knighton (1999). So the lowest BRI_{global} value (*i.e.* the area where bank erosion is most likely to occur) was calculated for a 1st order stream located on a floodplain with no bank reinforcement whatsoever (*i.e* with bare soil forming the stream bank). and there is less potential for bank erosion on higher order streams owing to their lower unit stream

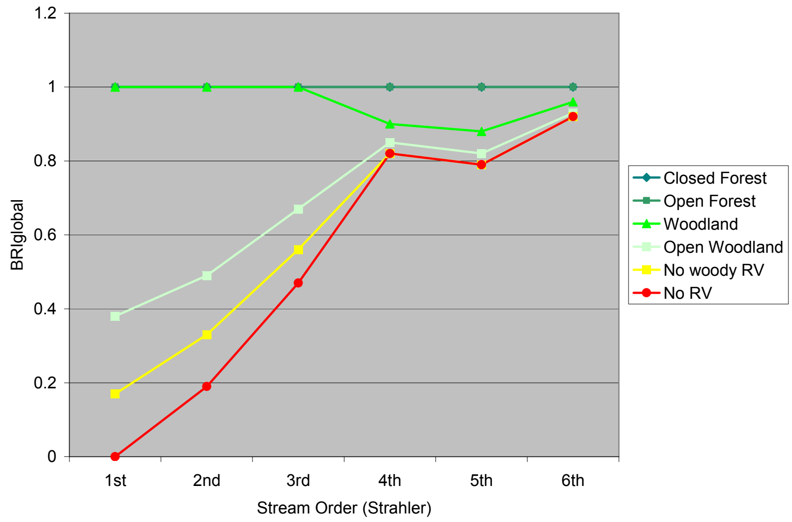

Figure 6.11 BRI_{global} values for each vegetation type and floodplain littoral zones with and without grass/stubble

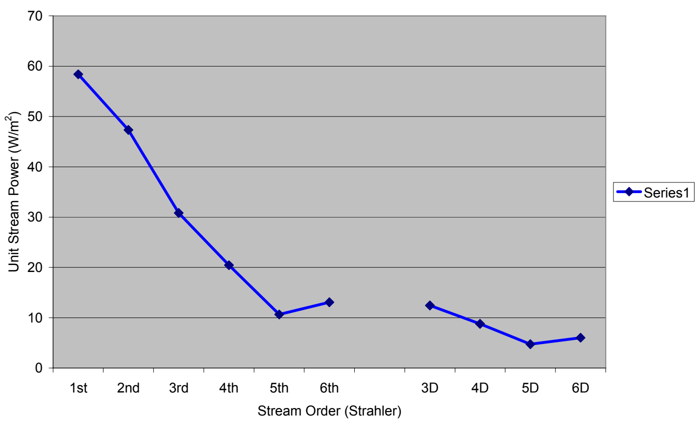

Figure 6.12 Unit stream power for each stream order

power.

A map of the BRI_{global} is presented in Figure 6.13. The map highlights in red a number of specific locations that are at highest risk of bank erosion, such as location A and the other red areas in the zoomed location. These red areas and other red areas within the study area are the locations most in need of riparian fencing and restoration to prevent further bank erosion. So the BRI_{local} quantifies how much bank reinforcement has changed since presettlement, whereas the $BRII_{global}$ identifies specific locations that are at greatest risk of bank erosion. Consequently the BRIlocal can be used for long term goal setting, whereas the BRIglobal provides specific information for the prioritisation of more immediate projects.

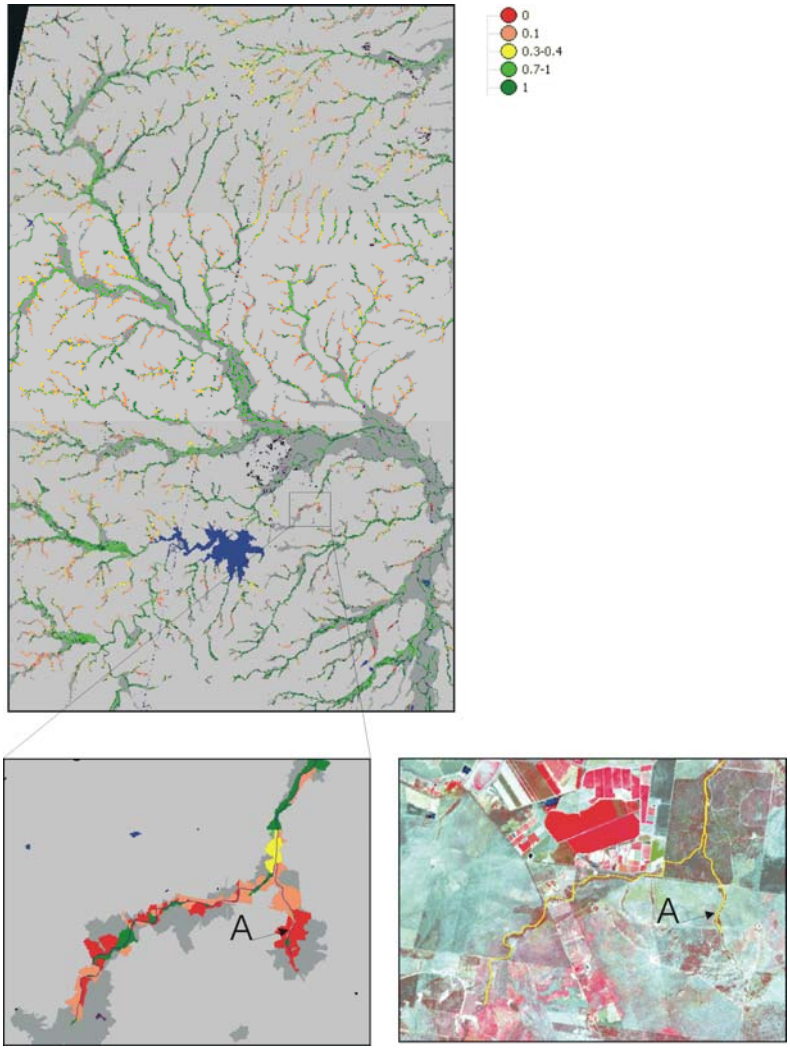

Figure 6.13 A map of BRI_{global} with a detailed example showing priority areas for bank stabilization

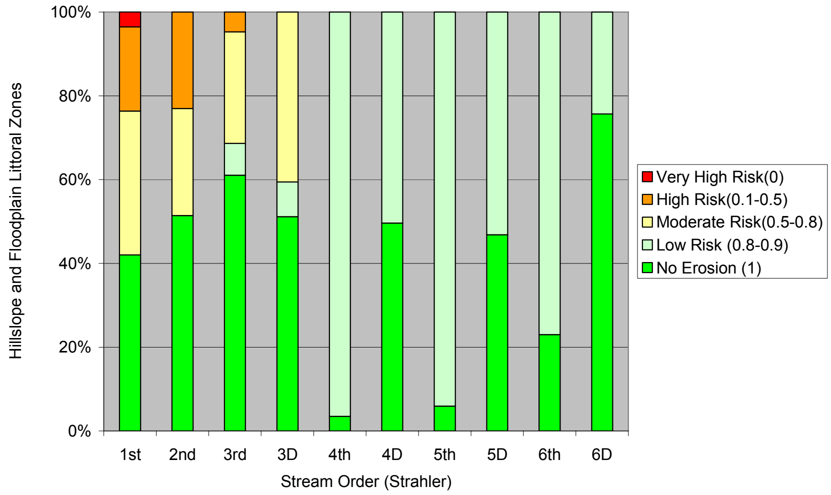

Figure 6.14BRI$_{global}$ values

It is interesting to note that the presence of any woody vegetation dramatically reduces the potential for bank erosion, emphasizing the importance of having woody vegetation of any structural class adjacent to lower order streams. Some care needs to taken in interpreting the results shown in Figure 6.11 because the index does not account for the destabilizing influences of cattle on stream banks (Belsky *et al*., 1999). So there may be littoral zones adjacent to high order streams that are at risk of bank erosion due to cattle activity which are not identified by the BRI$_{global}$. The *Floodplain Factor* term in Equation (2.20) was set to 0.5 based on the assumption that bank erosion is twice as likely to occur in alluvial soils than in bedrock constrained channels.

The BRI$_{global}$ index indicates that over 25% of 1st and 2nd order streams fall into the two highest risk categories, and 5% of 3rd order streams fall into the high risk category. These are the areas that would be of the high priority for remedial action, in particular the 4% of 1st order streams that fall into the very high risk category. Looking at these results on an area basis (Figure 6.15) shows that the highest risk category occurs in 314 hectares of 1st order stream littoral zones, and it is these areas that would be of the highest priority, in terms of reducing the amount of bank erosion.

Assumptions made in calculating the index

One of the assumptions made in calculating this index is that open forest is the climax vegetation for all streams 4th order or higher. This is based on the descriptions of the channel land units in Gunn *et al.* (1977). If there are sections of 4th – 6th order streams where the remnant native vegetation is woodland then this index will underestimate (BRI$_{local}$ = 0.8 (slight decrease) as opposed to BRI$_{local}$ = 1 (complete reinforcement)) the amount of reinforcement provided by the woodland. This scenario (woodland adjacent to higher order streams with a BRI of 0.8) occurs in a significant proportion of the riparian zone approximately 40% of all 4^{th} order streams and 70% of all 5^{th} order streams). These errors don't influence the BRI_{global} results because both woodland and open forest fall into the low risk or no erosion classes for the high order streams.

Index Reliability

At the most basic level the index can reliably identify areas with no woody riparian vegetation as distinct from those with woody vegetation (BRI_{local}=0 rather than BRI_{local} >0). This is useful as a 'first cut' tool for identifying areas of the stream network without any bank reinforcement due to woody vegetation. The reliability of the BRI_{local} for non-zero BRI_{local} values is reduced a little by uncertainty in the vegetation classification, and the assumptions about climax vegetation along high order streams. The vegetation classification has some limited confusion between open forest and woodland classes (these two classes are misclassified as each other 10% of the time) and between woodland and open woodland classes (these two classes are misclassified as each other 5% of the time). For littoral zones that are misclassified this will have a large impact on the BRI_{local} values calculated for low order streams where the vegetation structural classes have been misclassified, because open woodland has a BRI_{local} of 0.75 and woodland a BRI_{local} of 1. Similarly the BRI_{local} values calculated for higher order streams will be impacted by these classification errors. The overall influence of these classification errors will be a slight underestimation of the amount of stream bank reinforcement provided by the current vegetation.

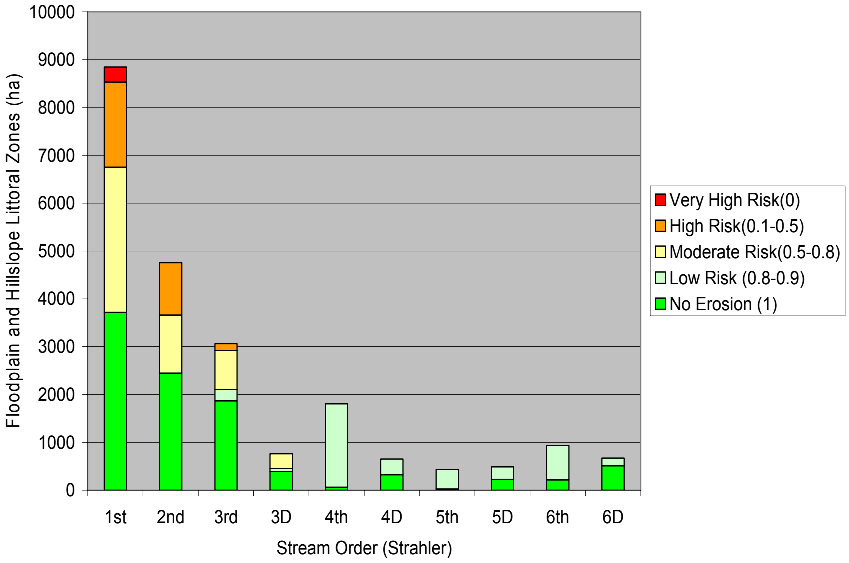

Figure 6.15. BRI_{global} values by hectare

The values of BRI_{global} are strongly influenced by mean stream power (Figure 6.12). The mean stream power is in turn calculated using extrapolated values of velocity for 1st and 2nd order streams. Direct measurements of velocity for these low order streams would be necessary to improve the reliability of this index. In other words, if the current estimates of velocity on low order streams are too high, the BRIglobal may be over-emphasizing the importance of managing these lower order streams at the expense of higher order streams, which may also be in urgent need of bank stabilization.

6.4 Denitrification Index

Introduction

The denitrification index was calculated for every stand of vegetation in the riparian zone that was located on the floodplain (*i.e.* the entire floodplain and floodplain littoral polygons). The range of DNI_{local} values is shown in Table 6.4. The lower DNI_{local} values for floodplain vegetation reflects the assumption that these areas of vegetation only denitrify during overbank events, whereas vegetation adjacent to the channel can denitrify during within-bank flow conditions.

The analysis of the DNI_{local} results is done for both areas adjacent to the channel and the floodplain, as shown in Figure 6.16, to reflect the fact that denitrification takes place in both places under different circumstances. The analysis of channel-adjacent areas is done in terms of stream order, these results are contained in Figure 6.17 and Figure 6.18. The analysis of floodplains is done independent of stream order and these results are contained in Figure 6.19.

The large red areas shown in Figure 6.16 represent the areas of the floodplain that have been cleared and converted to cropping (both irrigated and dryland) on the floodplains of the Nogoa and Comet rivers. These areas are of particular interest in the context of denitrification, because they are areas that would historically have supported woodland

Table 6.4 The range of DNI_{local} values for each vegetation type, stream order and the floodplain update

	FP	2nd	3rd	4th	5th	6th		3D	4D	5D	6D
Closed Forest	1.00	1.00	1.00	1.00	1.00	1.00		1.00	1.00	1.00	1.00
Open Forest	1.00	1.00	1.00	1.00	1.00	1.00		1.00	1.00	1.00	1.00
Woodland	1.00	1.00	1.00	0.93	0.93	0.96		1.00	1.00	1.00	1.00
Open Woodland	0.50	0.48	0.48	0.13	0.13	0.13		0.48	0.48	0.48	0.46
Grassland n Stubble	0.25	0.22	0.22	0.06	0.06	0.05		0.23	0.23	0.23	0.22
DN site -> N source	0.00	0.00	0.00	0.00	0.00	0.00		0.00	0.00	0.00	0.00

or possibly open forest (and thereby had a significant potential to remove nitrate from the system) but having been converted to cropping have gone from being a net sink of nitrate and nitrogen to being a source of nitrate.

Extremely high total nitrogen (TN) concentrations (median concentrations in excess of 5000 μg L^{-1}) have been recorded in cotton runoff on the Nogoa floodplain, and median concentration in the Nogoa river increases from 556 μg L^{-1} to 730 μg L^{-1} as it passes the Emerald Irrigation Area (Noble *et al*., 1997) indicating that nitrogen is entering the river system in this area. The fact that the TN concentrations are increasing would indicate that the nitrogen inputs in this area exceed the current denitrification capacity of the vegetation, further emphasising the importance of protecting the remaining vegetation. There has also been a large reduction in denitrification capacity on the floodplains of smaller rivers in the west of the study area, where these floodplains have been cleared for grazing (areas shown in yellow). The only areas where the potential for DN remains

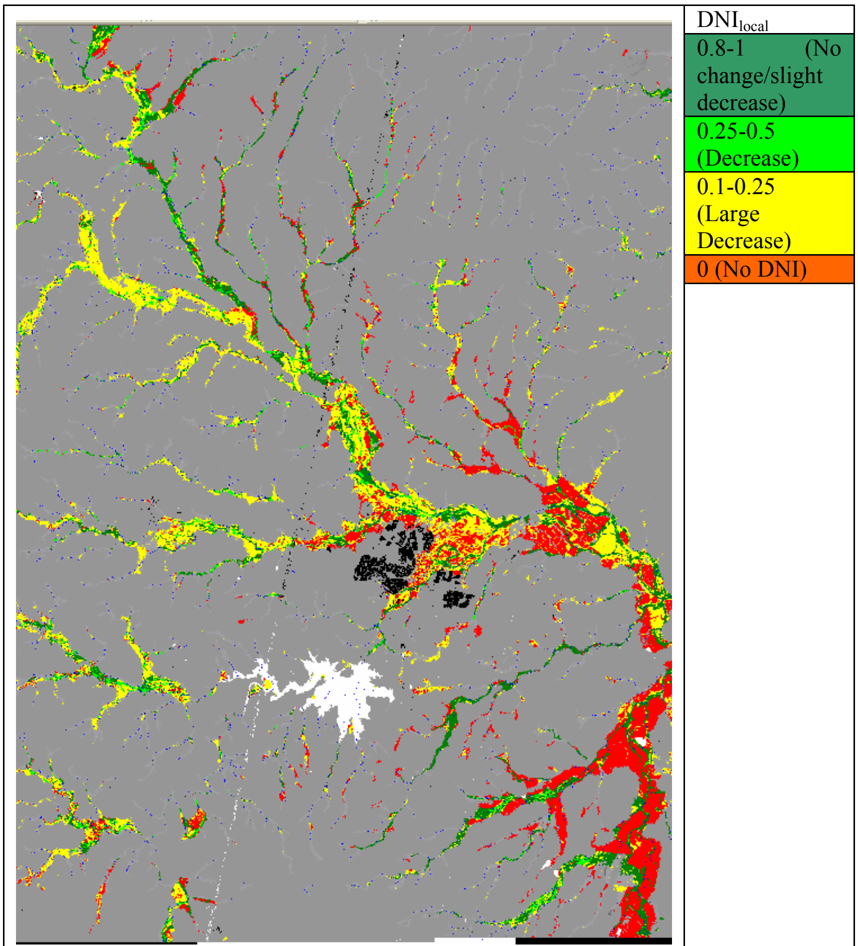

Figure 6.16 A map of the denitrification index (DNI_{local})

largely unchanged is the littoral zones of the main channels of the higher order streams.

The most striking feature in Figure 6.17 is the large decrease in denitrification along higher order streams. This is largely a function of the assumption that these streams supported open forest prior to European settlement. The light green 'decrease' class represents areas that have shifted 'down' a vegetation structural class. In other words prior to settlement these littoral zones would have contained woodland (low order streams) or open forest (high order streams) whereas they now contain open woodland (low order streams) or woodland (high order streams). This represents the decrease in water soluble carbon (WSC) associated with clearing and regrowth. The large decreases as shown in pale yellow represent the decrease in WSC associated with converting woody vegetation to pasture. The areas with no denitrification represent areas of bare soil or cropping immediately adjacent to the stream. Displaying these results on an areal basis gives Figure 6.18.

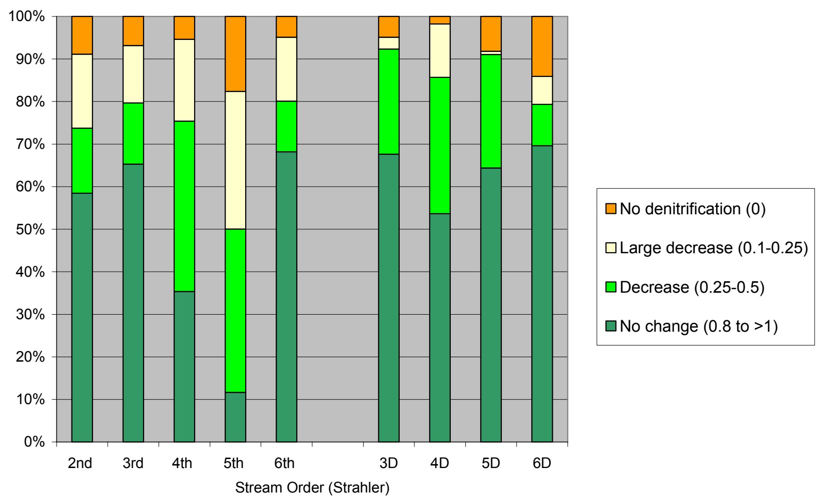

Figure 6.17 DNI values for the areas within 15 metres either side of the channel, sorted according to stream order.

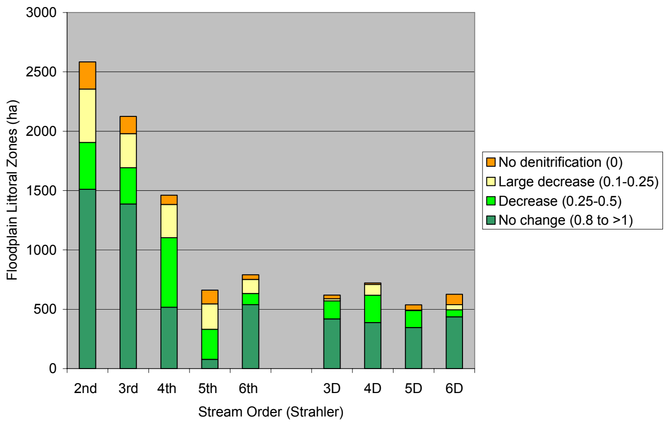

Figure 6.18 DNI$_{local}$ for each stream order

The greatest reduction in DNI$_{local}$ values has occurred on 2nd order streams, however there have been large reductions in the potential for denitrification for 3rd 4th and 5th order streams as well (592 ha, 866 ha and 467 ha respectively) 6th order streams have undergone a comparatively small reduction in DN potential of 213 ha, and there has been a moderate decrease in all D class channels. However all of these reductions are small in comparison to the reduction of DN potential that has occurred through the clearing of floodplain vegetation as shown in Figure 6.19, note that values are in square kilometres rather than hectares.

The potential for denitrification has been removed from one third of the floodplain, in many cases being replaced by cropping, in which case these areas have been converted from a net sink to a net source of nitrate. Nearly another third of the floodplain has seen a large decrease in the amount of WSC present in the soil, thereby reducing the potential for denitrification.

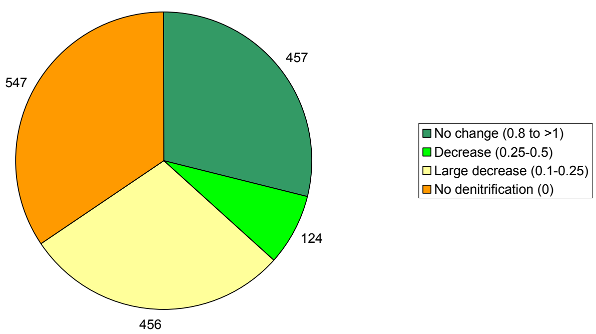

Figure 6.19 Change in denitrification for floodplains

Table 6.5 DNI_{global} values for the floodplain and littoral zones

	FP	2nd	3rd	4th	5th	6th		3D	4D	5D	6D
Closed Forest	0.66	1.00	1.00	0.80	0.61	0.23		0.96	0.77	0.58	0.22
Open Forest	0.54	0.93	0.92	0.74	0.57	0.22		0.88	0.71	0.54	0.21
Woodland LZ	0.18	0.26	0.26	0.21	0.16	0.06		0.25	0.20	0.15	0.05
Woodland FP	0.18	0.18	0.18	0.18	0.18	0.18		0.18	0.18	0.18	0.18
Open Woodland LZ	0.09	0.12	0.12	0.10	0.08	0.03		0.12	0.10	0.07	0.03
Open Woodland FP	0.09	0.09	0.09	0.09	0.09	0.09		0.09	0.09	0.09	0.09
Grassland n Stubble	0.05	0.06	0.06	0.05	0.03	0.01		0.06	0.05	0.03	0.01
DN site -> N source	0.00	0.00	0.00	0.00	0.00	0.00		0.00	0.00	0.00	0.00

To identify where these reductions in WSC have led to the largest decrease in DN potential, the DNI_{global} was calculated using the values presented in Table 6.5

The highest DNI_{global} values occur in stands of closed and open forest adjacent to mid-order (2^{nd}-3^{rd}) order streams (Figure 6.20). This is because these streams reach bank full flow conditions more frequently than 5^{th} and 6^{th} order streams, consequently there is a greater likelihood of water entering the WSC rich topsoil layers in these mid-order streams. Note that the colour coding of Table 6.5 is as follows, green represents stands of vegetation that have a high potential for denitrification and are therefore represented by a DNI_{global} value close to 1, yellow areas represent moderate DN potential, blue low DN potential, orange very low DN potential, and pink indicates areas with no DN

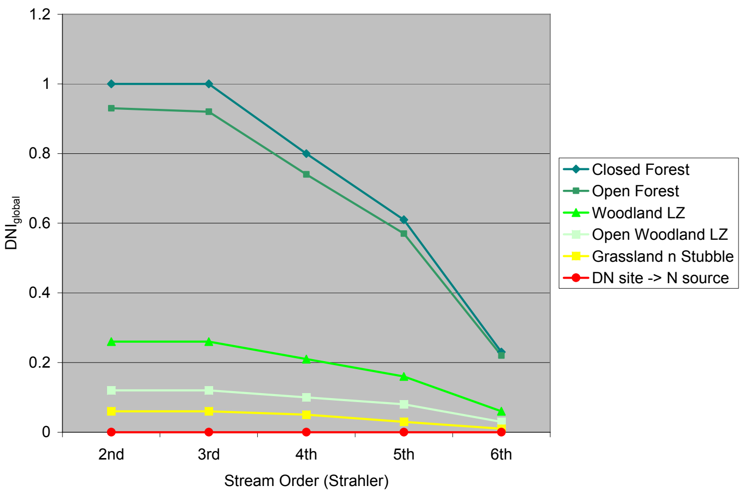

Figure 6.20 DNI_{global} values for floodplain littoral vegetation and land cover adjacent to each stream order

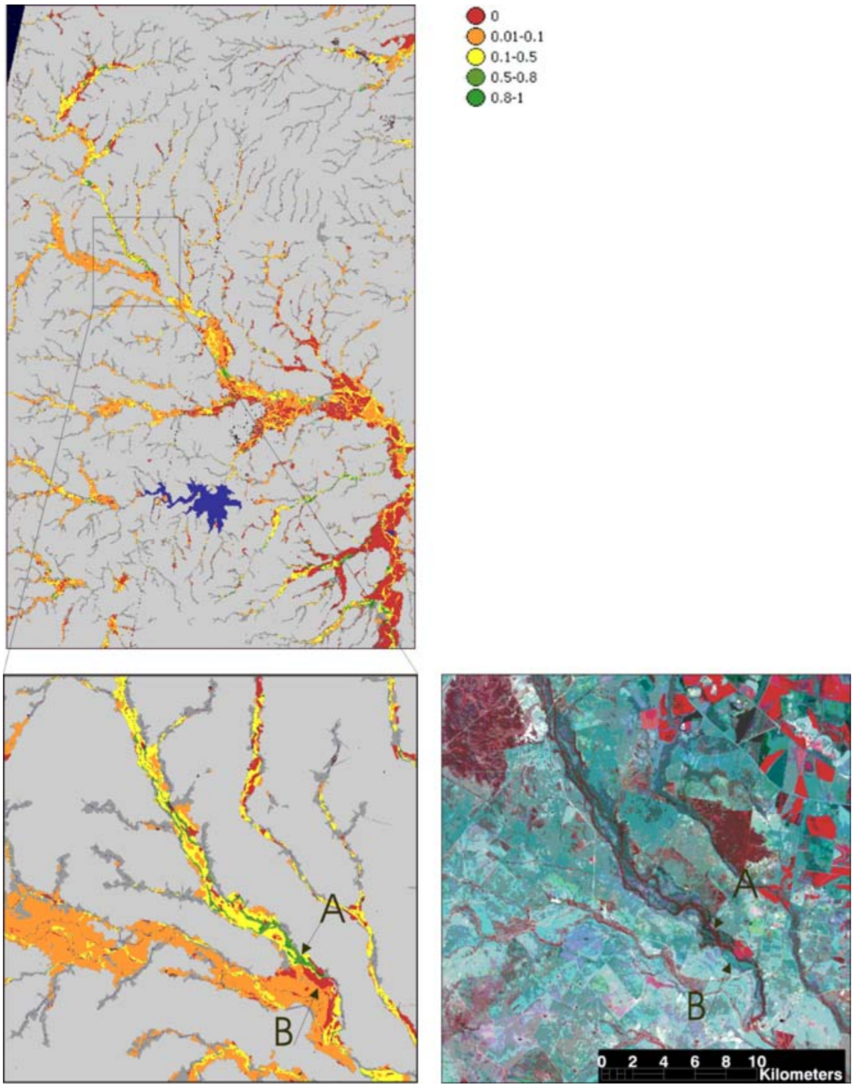

Figure 6.21 A map of DNI_{global} results with a zoomed area of interest

potential, these areas could now act as sources rather than sinks of nitrate.

An example of this is shown in the zoomed area of Figure 6.21, the riparian vegetation at location A generates a large amount of WSC into the soil profile and flow dynamics of the adjacent 3rd order stream mean that is high potential for denitrification at this location. However removal of littoral and floodplain vegetation and the introduction of cropping and bare soil areas into the riparian zone have removed the potential for denitrification from location B. To restore the denitrification potential to riparian zones within the study area, efforts should be focussed on areas such as location B where areas of zero DNI_{global} are adjacent to DNI_{global} values close to 1.

The DNI_{global} values shown in Figure 6.20 are strongly influenced by the calculation of bank full frequency and the $NDNE_x$ parameter in general. However the general trend of decreasing bank-full frequency with increasing catchment area is consistent with the theoretical relationship between these two parameters as described in Church (2002).

The areas with the greatest DN potential are present along approximately 25% of 2nd and 3rd order streams and over 40% of 3D order streams. The other important feature to notice is the presence of potential nitrogen sources adjacent to the higher order streams (both main channel and D class channels). Nitrogen entering the system at these points is unlikely to encounter another area with high denitrification potential before it arrives at the receiving waters.

These data are presented on an area basis in Figure 6.23. From a pollutant management point of view it would be important to protect the over one thousand hectares of high DN potential littoral zones adjacent to 2nd and 3rd (and 3D) order channels. It would also be important to target the areas adjacent to the 5th, 5D, 6th and 6D order channels (287 hectares in total) that are currently potential nitrate sources, and establish whether a. any nitrogen based fertilizer is being applied to these areas, and b. whether it is feasible to re-establish woody vegetation in these areas to restore their denitrification capacity.

The DNI_{global} results for both littoral zone and floodplains for the present day and pre-settlement are shown in Figure 6.24. Although the littoral zone only contains 13% of the WSC found in the floodplain both channel adjacent and floodplain denitrification are important during different parts of the hydrograph. The capacity to denitrify floodwaters is highly important, as it is during flood events that large amounts of nitrate are mobile in the stream network (Noble *et al.*, 1997). However denitrification during low flows is

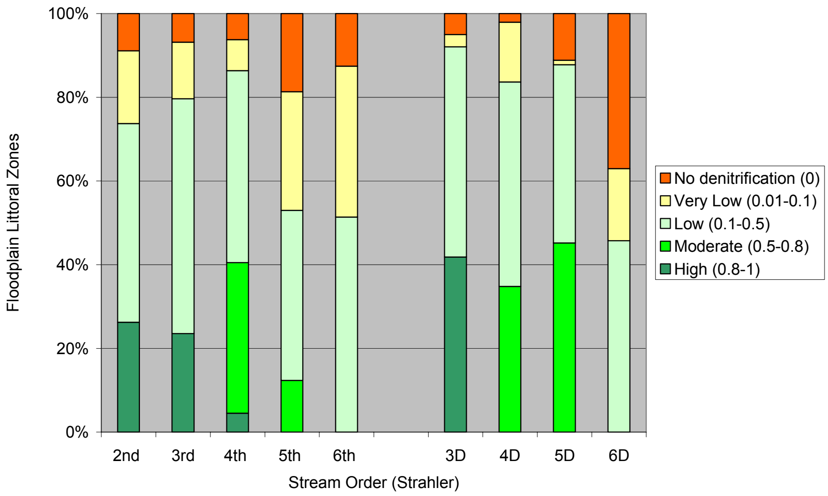

Figure 6.22 The distribution of DNI_{global} values for each stream order

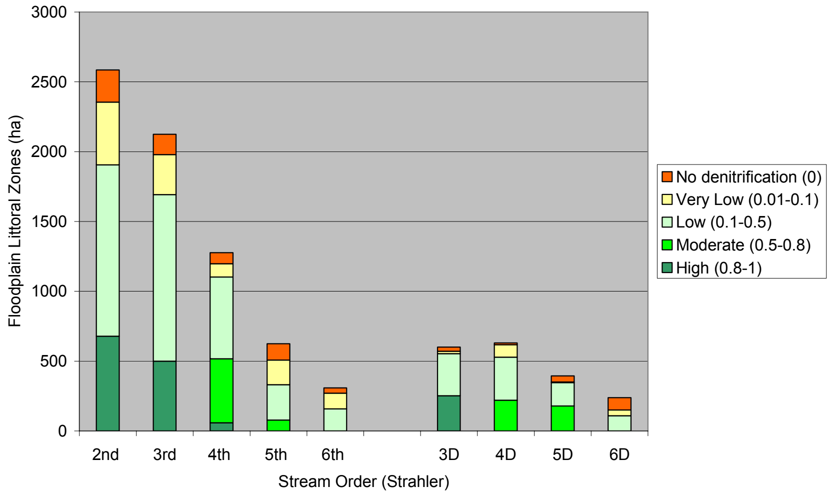

Figure 6.23 DNI_{global} values by hectare for littoral zones

also of high importance from an aquatic ecosystem point of view, because it will affect the chemistry of the isolated waterholes that support the aquatic ecosystem during periods of drought. The DNI_{global} values for floodplains and littoral zones for both the existing riparian vegetation and the pre-European vegetation are shown in Figure 6.24. The most striking feature of this figure is the large reduction of DNI_{global} on the floodplain, which reflects the impact that vegetation clearing and cropping has had on the denitrification potential of the floodplain.

It is possible to further quantify this change in denitrification potential by calculating the difference in terms of tonnes of WSC under each land use scenario, as shown in Figure 6.25. The total volume of WSC is based on a large number of assumptions, and would require additional fieldwork to establish its reliability, however the relative change in the amount of WSC carbon in the soil *i.e.* a reduction of approximately 50% as a result of conversion from woodland to buffel grass is consistent with the 50% reduction in labile carbon measured by Dalal *et al.* (2005) for a similar ecosystem in central Queensland. This has major implications for the amount of nitrate that can be removed from the system by riparian vegetation, which, particularly when coupled with increased nitrate and ammonium inputs from cropping and grazing that takes place on the floodplain, has major implications for the water quality both in-stream and in the receiving waters. This is consistent with water quality observations collected between 1993 and 1996 in the Lower Comet, Mid Nogoa, and Lower Nogoa, all of which had total nitrogen concentrations in excess of 750 μ L^{-1} (Noble *et al.* 1997), which is the upper environmental guideline identified by the Australian and New Zealand Environment and Conservation Council (ANZECC 1992).

Future studies to accurately quantify the amount of nitrate removed by stand of vegetation adjacent to different stream orders could be coupled with the approach described here, and, in combination with estimates of fertilizer inputs, could be used to develop a 'whole-of-catchment' nitrogen budget. The other interesting feature to note is that while closed forest and open forest (moderate and high classes) only make up a very small amount of the riparian vegetation they contain a large proportion of the WSC.

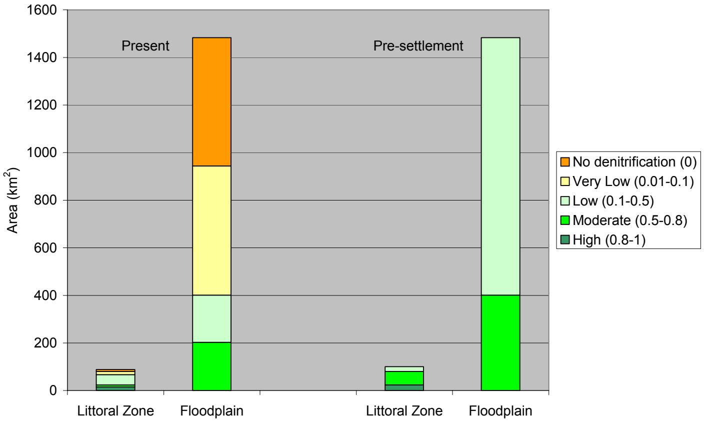

Figure 6.24 Change in DNI_{global} between pre-European conditions and present conditions.

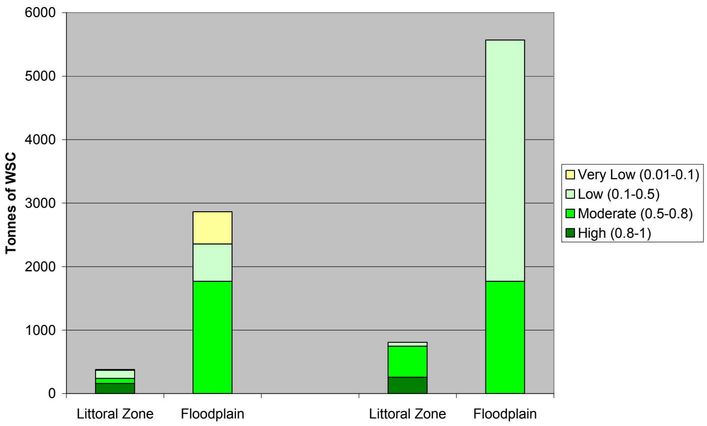

Figure 6.25 Change in the amount of WSC in riparian soils between pre-European conditions and present conditions.

Assumptions made in calculating the index

The assumptions made in extrapolating the parameters required to calculate this index are described in Sections 2.4 and 4.4.4. The calculation of this index is based on the assumption that there is an exchange of hyporheic ground water between the channel and adjacent banks, and that this exchange happens at a consistent rate throughout the catchment. This assumption is unlikely to be true for the whole catchment, but is necessary because of a lack of data about bank permeability and rates of exchange.

There is also an assumption that all streams of the Strahler order have the same flow characteristics. This is also likely to be untrue, but is necessary due to a lack of data about the flow characteristics each stream link[27].

Index reliability

At its most basic level the index is useful for identifying the two main areas where denitrification occurs:

1. The stands of vegetation adjacent to the channel (particularly high order channels on floodplains), and;
2. All vegetation located on floodplains.

Beyond this level the index needs to be interpreted with some caution. The capacity of the index to accurately discriminate between the importance of littoral and floodplain denitrification is limited by a lack of information about the spatial extent and duration of overbank events. The areas identified by the MrVBF algorithm may represent areas that were subject to flooding under different climatic conditions than those encountered at present. If this is the case then the DNI_{global} may be being calculated for areas that rarely experience the conditions required for denitrification to occur.

The fact that stage height characteristics are calculated uniformly for each stream order, and the use of literature values to identify the relative amounts of organic carbon, limit the usefulness of comparing the DNI_{global} values closed forest on a 5th order stream with an open forest on a 4th order stream, but the index is reliable in the sense that both classes have a relatively high DNI value.

The index is sensitive to channel geometry, so the assumptions and statistics described in Section 0 impact significantly on the reliability of this index. A more accurate map of channel geometry would improve the reliability of this index, particularly the importance of stream order amongst high order streams.

6.5 Stream Shading Index

Introduction

The stream shading index is calculated for littoral stands of vegetation on high order streams (4^{th} to 6^{th}) that are located on floodplains because these are the areas where riparian vegetation is important in terms of aquatic ecology. The fact that all of the streams in the study area have highly variable flows, and even the largest streams cease to flow at some point means that many aquatic species rely on a series of waterholes to survive during periods of drought (Puckridge *et al*., 1998). These waterholes typically form on high order (4^{th}, 5^{th} or 6^{th}) streams and are generally surrounded by floodplains. Stream shading is of less importance for low order streams in the study area because these streams generally only flow during rainfall events and support little, if any aquatic life. Consequently the stream shade index has only been calculated for 4^{th}, 5^{th} and 6^{th} order streams. The LWDI is calculated for all streams that are likely to support aquatic life at the height of the wet season, so the two indices can be viewed in combination to identify all the stands of riparian vegetation that perform some kind of aquatic ecological function.

The stream shade index was calculated to identify the importance of a stand of vegetation in providing shade to the stream network. It was NOT calculated to identify the amount of sunlight and/or shade received by the stream (or waterhole). The SSI_{local} values were calculated by entering the canopy and channel geometry values described in Sections 4.3 and 0 into Equation (2.52). These values are the same because the SSI_{local} ignores the influence of channel geometry and stream orientation on stream shade, because it compares the amount of shade provided by the existing riparian vegetation at a given location with the amount of shade that would have been provided prior to European settlement. So SSI_{local} simply measures the change in PFC between the pre-European and the current vegetation. Assuming that all higher order channels supported open forest prior to European settlement gives Table 6.6.

Table 6.6 SSI_{local} values for each vegetation type and each stream order

Vegetation Structure	4th	5th	6th
Closed Forest	1.6	1.6	1.6
Open Forest	1	1	1
Woodland	0.5	0.5	0.5
Open Woodland	0.3	0.3	0.3
No woody vegetation	0.0	0.0	0.0

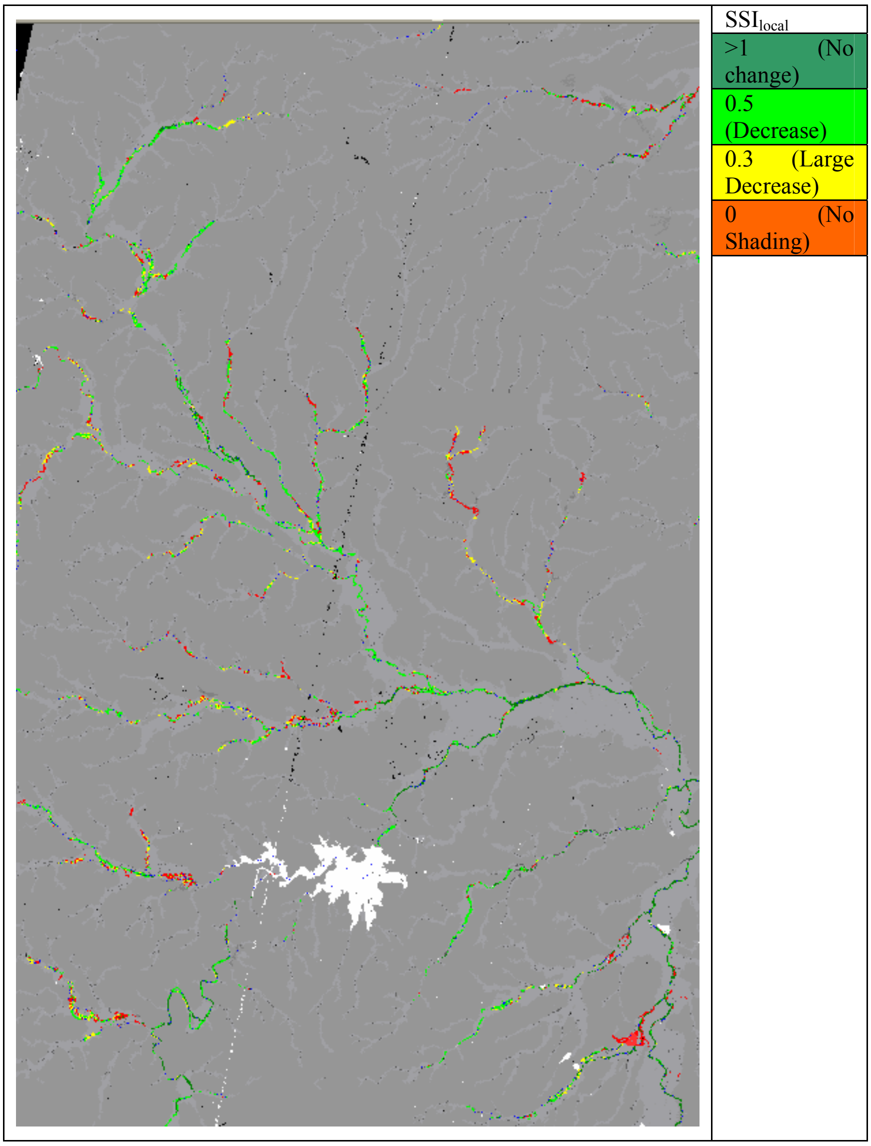

Figure 6.26 A map of the stream shading index (SSI_{local}).

The red areas indicate stream reaches where there is no woody vegetation adjacent to the channel to provide shade to the channel, yellow a areas indicate stream reaches where the changes in riparian vegetation have lead to a large decrease in the amount of shade provided by woody vegetation (consistent with closed forest or open forest being replaced by open woodland). Areas shown in lime green represent areas where woodland has replaced forest (either open or closed) resulting in an increase in the amount of sunlight reaching the channel dark green regions indicate areas where riparian vegetation is providing the same amount of shade as prior to settlement (this does not mean that the stream is fully shaded at these points). The results shown in Figure 6.26 are summarised according to stream order in Figure 6.28.

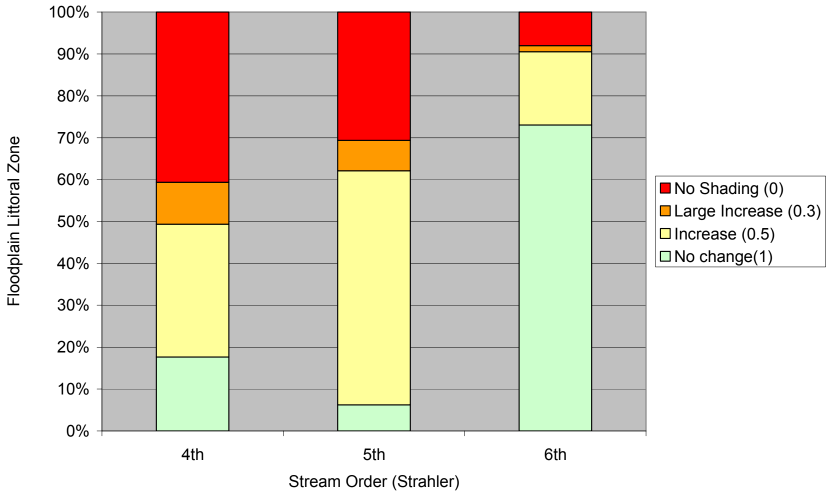

Figure 6.28 SSI_{local} values for each to stream order

The most striking feature about Figure 6.28 is the large proportion of 4th and 5th order streams without any shading (40% and 30% respectively) any waterholes that formed in these stream reaches would be subject to higher amounts of solar radiation, altering the thermal and trophic conditions encountered in these waterholes. Furthermore, the capacity of the riparian vegetation to provide shade has been reduced along over 80% of 4th order streams and over 90% of 5th order streams, further altering the energy budget of these streams at low or zero flow conditions. The 6th order streams are in better condition with over 70% experiencing no change in the amount of shade provided by the littoral

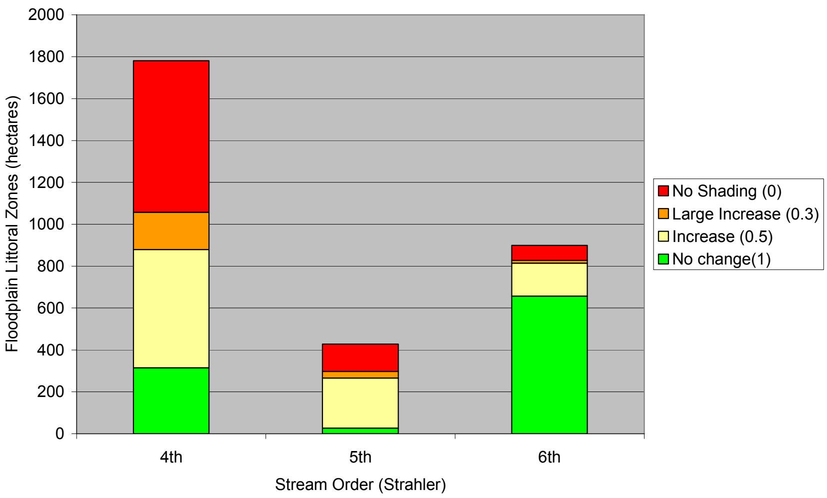

Figure 6.27 SSI_{local} values on a hectare basis

vegetation. Displaying these results on an area basis gives Figure 6.27, and in this context the extent of the impact on 4th order streams becomes particularly striking, with nearly 800 hectares providing no shade and increased solar radiation inputs being experienced through 1500 hectares of littoral vegetation. The impact on 5th order streams is also clear with only 27 hectares experiencing no change, and all other sections experiencing some increase in the amount of solar radiation reaching the water surface. To improve the quality of the aquatic habitat in the study area it would be necessary to restore the riparian vegetation adjacent to these higher order streams, but there is a need to identify the highest priority areas, because the cost of restoring it all simultaneously is likely to be prohibitive. To identify where rehabilitation will be most effective in reducing the amount of sunlight reaching the stream surface, the SSI_{global} was calculated.

SSI_{global}

The stands of closed forest adjacent to both 4th and 6th order streams are highly important in reducing the amount of sun reaching the streams surface. A stand of closed forest adjacent to a 4th order stream blocks more of the suns radiation (31%) than one adjacent to a 6th order stream (16%), however waterholes are more likely to form along 6th order streams, which is why the two have similar SSI_{global} values (Figure 6.29). The 5th order streams have similar channel geometry to the 6th order streams, but the lower probability of waterhole formation gives them a lower SSI_{global} value.

The SSI_{global} values on an area basis are shown in Figure 6.31. The high importance areas

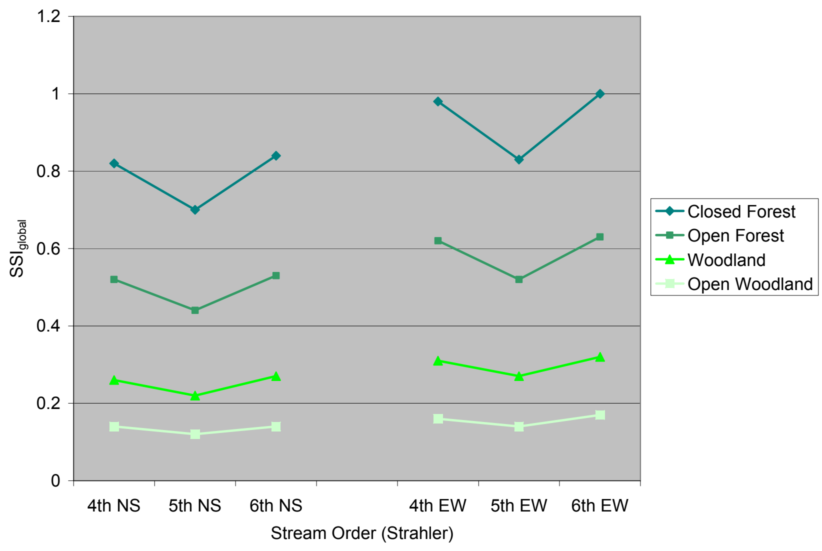

Figure 6.29 Range of SSI_{global} values for each stream order and stream orientation for floodplain littoral vegetation on higher order streams

represent stands of closed forest and it is these areas that would be the highest priority for conservation, particularly if they are adjacent to an east-west oriented section of the stream channel. In terms of restoration, efforts should initially be focussed on the areas along 6th order streams where waterholes are most likely to form, then on 4th order streams where the vegetation will have a large impact on the amount of sunlight reaching the channel, and also perform the other riparian functions described in this thesis.

An example of this is shown in Figure 6.30. Location A in the zoomed area in this figure shows a cleared section of the littoral zone on the floodplain of the Comet river (one of

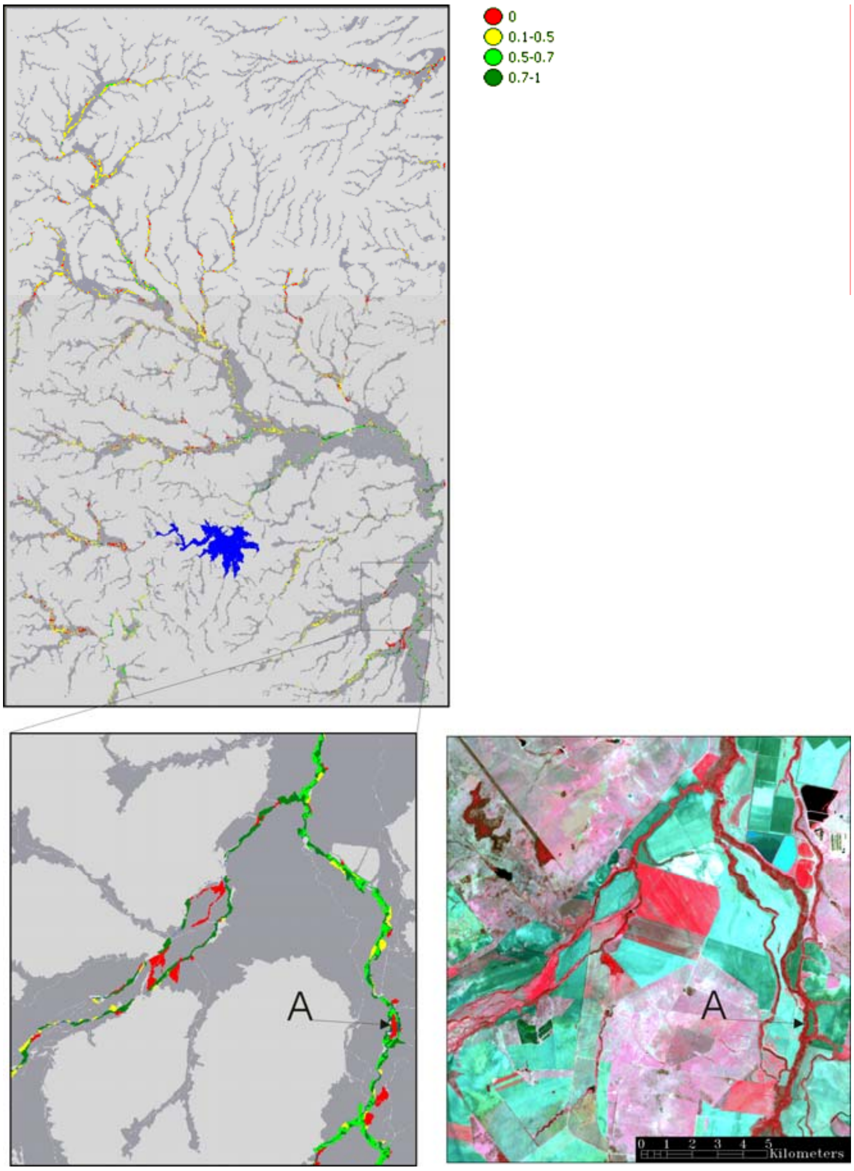

Figure 6.30 A map of SSIglobal with detailed area showing high priority area for restoration (A)

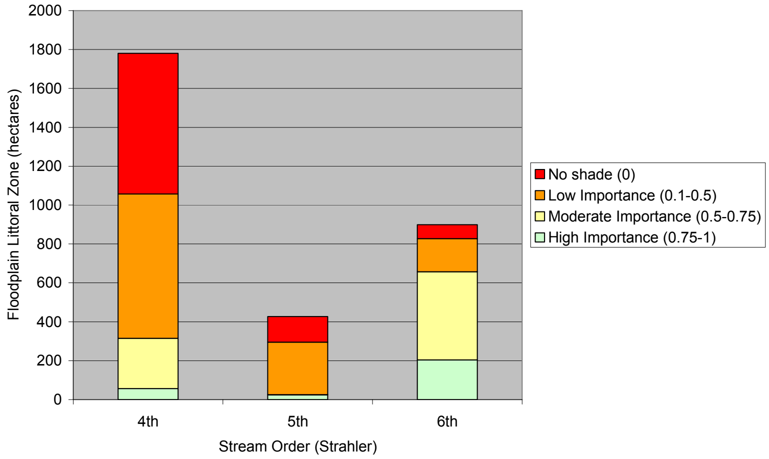

Figure 6.31 SSI_{global} values on a hectare basis

the two 6th order streams in the study area). To restore stream shading (and LWD production) to this portion of the Comet river it would be necessary to restore the littoral vegetation at location A. This could be done either via fencing and natural regeneration or via tree planting.

The assumptions made in extrapolating the parameters used to calculate this index are discussed in detail in Sections 4.3 and 0. The index assumes that the waterhole forms in the centre of the channel, whereas in a fluvial environment, waterholes are likely to form along the thalweg of the channel. However, identifying the thalweg position for each channel, and calculating the SSI for the thalweg along each channel is beyond the scope of this thesis.

At its most basic level, this index is reliable insofar as it identifies areas of the stream network where there is no woody vegetation to provide shade to the channel, and it identifies riparian zones adjacent to high order streams where stream shade is important for the aquatic ecosystems supported by higher order streams. The global version of the index is sensitive to three factors, percentage foliage cover (PFC), channel geometry, and the probability of a waterhole parameter *Pwh*. PFC is strongly linked to vegetation structure, and contributes directly to the reflectance properties of vegetation (Verstraete *et al*., 1996). Therefore its prediction using a vegetation structural map is reliable, except where, class confusion between open woodland and woodland leads to some uncertainty between those two classes. The sensitivity of SSI_{global} to channel geometry means that variability in channel geometry can reduce the reliability of this index. The variability in channel geometry described Section 0.The *Pwh* parameter has a large influence on the SSI_{global} values. The *Pwh* parameter increases with increasing stream order, which is intuitive. However additional fieldwork conducted at the end of a drought or dry season would provide a valuable adjunct to the existing gauging station analysis, which may be under or over-estimating the *Pwh* at any given stream order.

6.6 Large Woody Debris Index

Introduction

The $LWDI_{local}$ and $LWDI_{global}$ are calculated for all higher order channels, both main channels and D class channels. This reflects the maximum extent of the aquatic ecosystem in the study area, and represents the multiple aquatic ecosystem functions provided by in-stream LWD *i.e.* velocity refuge during high flow events as well as feeding and breeding sites for the 26 freshwater fish species encountered in the study area.

The $LWDI_{local}$ is calculated using the LWV parameter, which is the volume of standing timber on the stream bank that can contribute to LWD (details in Section 2.6). The volume of standing timber on the banks at present is compared with the amount of standing timber that would have been present on the banks prior to European settlement. As with the previous indices the reference vegetation type for 3rd order and all D class channels is woodland, and open forest for the main channels of the high order streams

Table 6.7 $LWDI_{local}$ values for high order streams

	3rd	4th	5th	6th		3D	4D	5D	6D
Closed Forest	1.63	0.93	0.93	0.93		1.63	1.63	1.63	1.63
Open Forest	1.76	1.00	1.00	1.00		1.76	1.76	1.76	1.76
Woodland	1.00	0.57	0.57	0.57		1.00	1.00	1.00	1.00
Open Woodland	0.52	0.29	0.29	0.29		0.52	0.52	0.52	0.52
NWRV	0.00	0.00	0.00	0.00		0.00	0.00	0.00	0.00

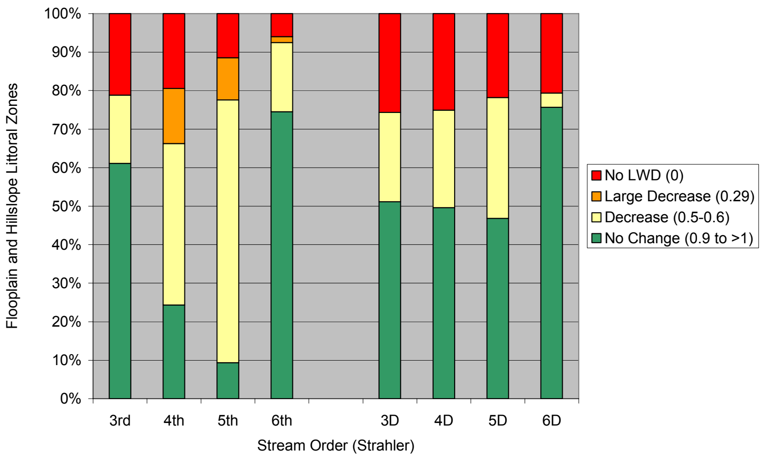

Figure 6.32 $LWDI_{local}$ values for each stream order

(4^{th}-6^{th}) Areas that support vegetation types that contain more standing timber than the reference for that stream order have an index value greater than one, these areas are treated as 'no change' areas, and are analysed as having a $LWDI_{local}$ value of 1

One of the most striking features of Figure 6.32 is that all but 6^{th} order stream have 20% of their length without any LWD or with a large decrease in potential for LWD recruitment. There is a dramatic decrease in the potential for LWD recruitment on the main channel of both 4^{th} and 5^{th} order streams, with over 90% of 5^{th} order stream littoral zones undergoing some reduction in their LWD recruitment capacity.

The reduction of LWD recruitment in over 50% of 3^{rd}, 4^{th} and 5^{th} order D class channels

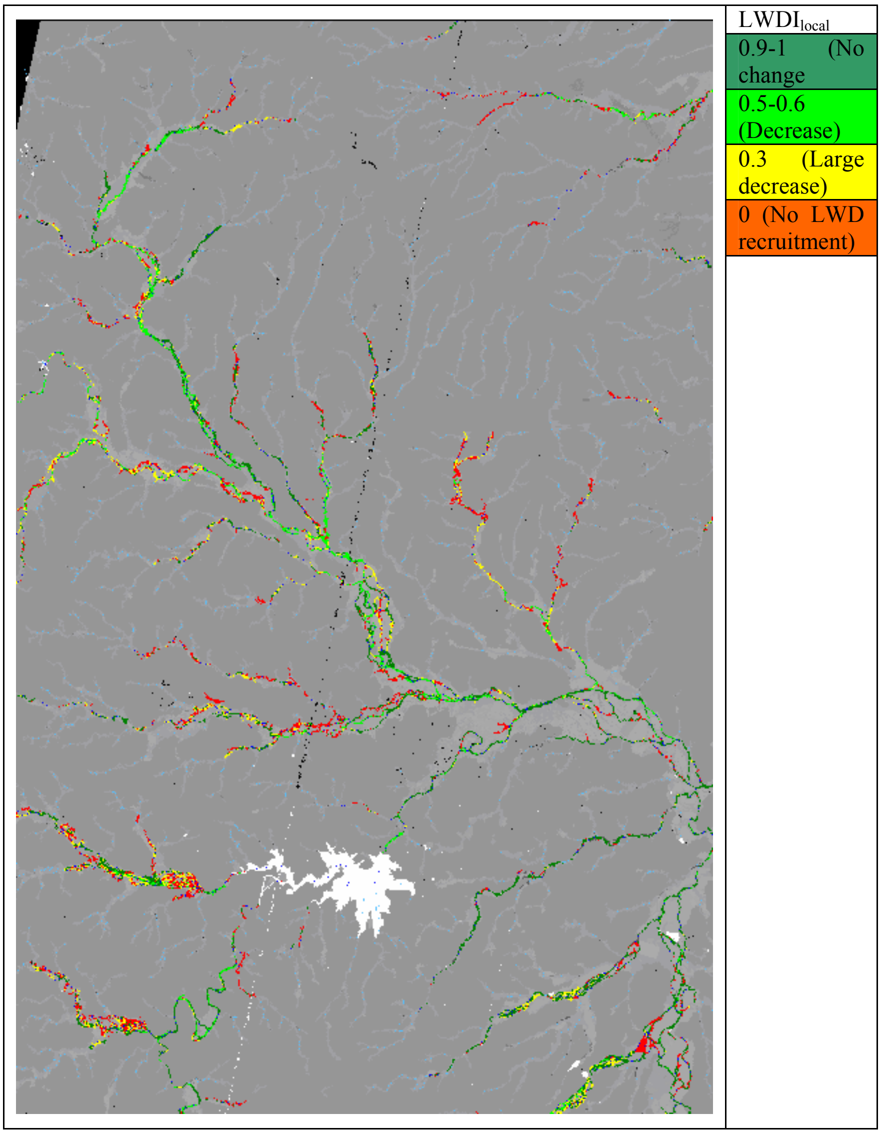

Figure 6.33 A map of $LWDI_{local}$

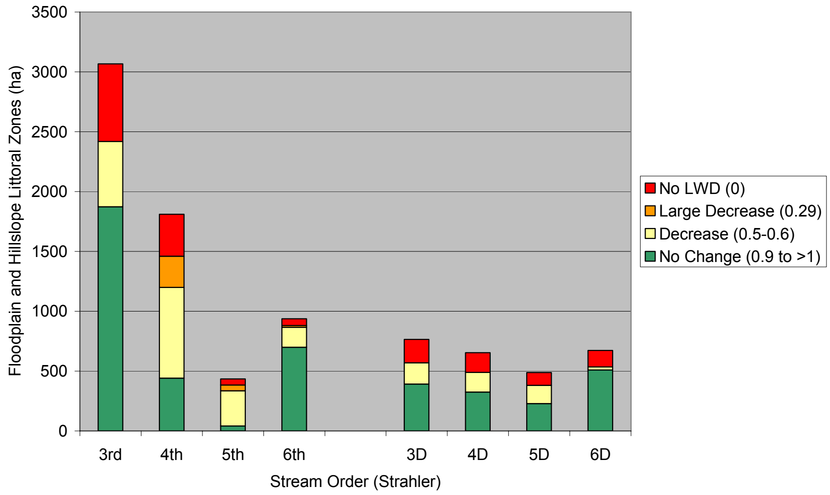

Figure 6.34 $LWDI_{local}$ values per hectare of the littoral zone

also has important implications because many of the freshwater species that live in the Comet and Nogoa river systems take refuge in these backwater channels during high stage events, and may live out their larval stages in these channels (Erskine *et al*., 2005). Consequently, the 50% reduction of the volume of LWD in these channels, both now and into the future, constitutes a serious loss of habitat for these species.

The red areas in Figure 6.33 indicate regions that lack woody riparian vegetation and are therefore unable to supply any LWD to the channel. Areas of lime green and yellow indicate that changes in the vegetation structural class encountered in the riparian zone have lead to a decrease or a large decrease in LWD recruitment respectively. Areas where the potential for LWD recruitment is unchanged are shown in dark green.

Presenting these results on an area basis gives Figure 6.34. The main channels of the 3rd and 4th order streams have undergone the greatest decrease in LWD potential (over 1500 hectares, and nearly 1000 hectares respectively). It is interesting to note that although the D class channels make up a relatively small proportion of the channel network the 3rd, 4th and 5th order D class channels have reduced LWD recruitment capacity for 196 ha, 163 ha and 106 ha respectively.

$LWDI_{global}$

The $LWDI_{global}$ values calculated using Equation (2.56) are presented in Table 6.8. The high values shown for the D class channels reflect the large volume of standing timber on the bank, and the relatively small channel. Mature trees falling into these channels would create sufficient LWD to create a very high blockage ratio. The lower $LWDI_{global}$ values (Figure 6.36) calculated for higher order streams reflect the relationship between channel cross section area at bank full stage, which is large relative to the amount of LWD generated by the littoral vegetation.

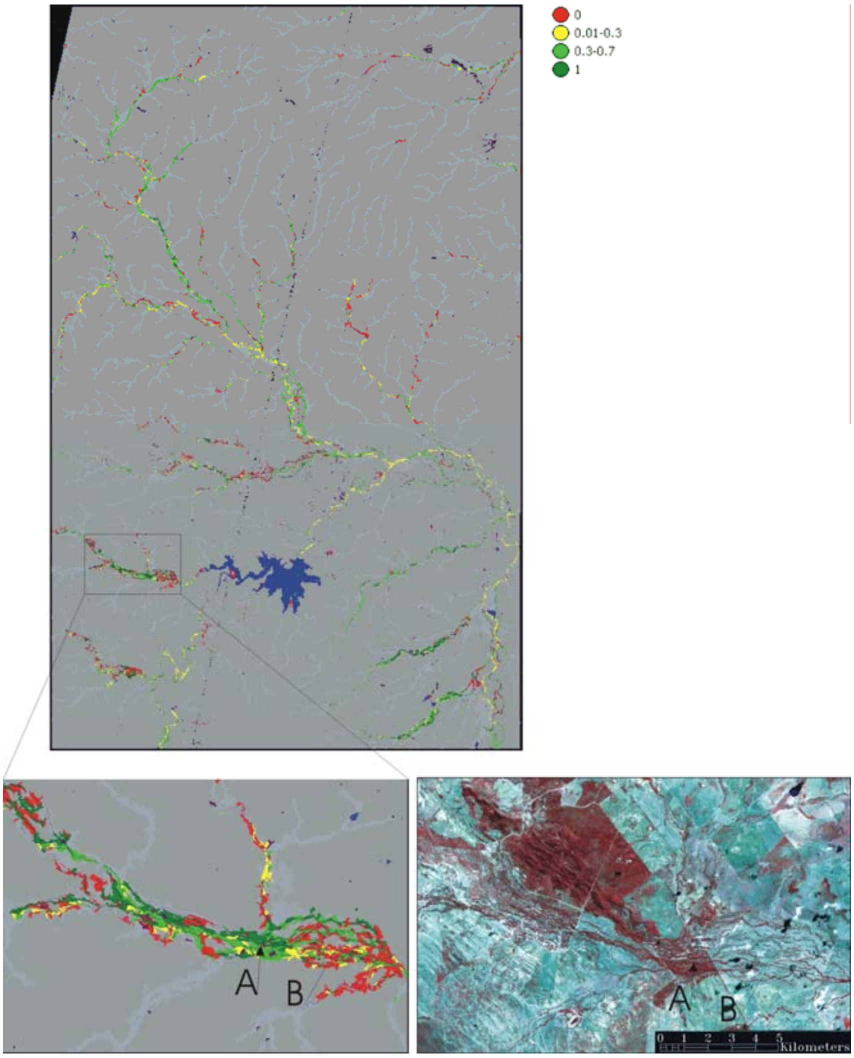

Figure 6.35 A map of $LWDI_{global}$ with detail showing clearing of floodplain vegetation

The distribution of the $LWDI_{global}$ values throughout the study area is shown in Figure 6.35. The zoomed area shows an areas where littoral vegetation has been removed (B) in comparison to a neighbouring property where it has not (A). As expected the removal of littoral vegeation has resulted in a decrease in the potential for LWD recruitment, and this is reflected by the $LWDI_{global}$ values.

The $LWDI_{global}$ values for each stream order is shown in Figure 6.36. These values are determined by the relationship between channel cross-sectional area and the projected area of LWD (the blockage ratio *sensu* Abernethy and Rutherfurd (1998)). The low values shown for 5th and 6th order channels reflect the large cross-sectional areas encountered in these channels. It is worth noting that whilst the $LWDI_{global}$ in these large streams is relatively low, as the floods recede and the river levels fall the LWD in the main channel become increasingly important. This phenomenon is not reflected in the current $LWDI_{global}$ values.

Table 6.8 Range of $LWDI_{global}$ index values for each stream order

	3rd	4th	5th	6th		3D	4D	5D	6D
Closed Forest	0.36	0.27	0.12	0.09		1.00	1.00	1.00	1.00
Open Forest	0.38	0.29	0.13	0.10		1.00	1.00	1.00	1.00
Woodland	0.22	0.16	0.07	0.06		1.00	1.00	0.66	0.52
Open Woodland	0.11	0.08	0.04	0.03		1.00	0.76	0.34	0.27
NWRV	0.00	0.00	0.00	0.00		0.00	0.00	0.00	0.00

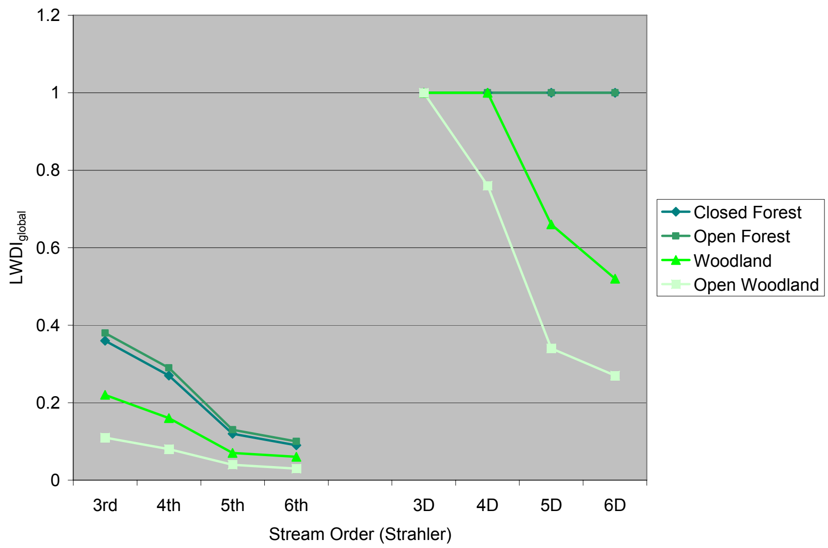

Figure 6.36 LWDIglobal value for littoral zones on high order streams

The littoral vegetation on over 80% of high order streams has the potential to generate a small amount of LWD relative to the cross-sectional areas of these channels. The stands of closed and open forest on 3rd and 4th order streams can generate a moderate amount of LWD, and as such it would be important to protect these areas to maintain the aquatic habitat values of these channels. It is in the D class channels that littoral vegetation has the biggest impact in terms of LWD recruitment potential, and this is strongly influenced by the smaller channel geometry of these D class channels. It is important to note that whilst woody vegetation can generate a large amount of LWD to these channels the removal of woody vegetation from over 20% of the littoral zones of all D class channels will seriously impact on the aquatic habitat values of these channels.

The $LWDI_{global}$ values expressed on a per hectare basis are shown in Figure 6.38. The sections of the main channel on 3rd and 4th order streams (650 ha and 350 ha respectively) that lack any woody vegetation would be of the highest priority, because restoring vegetation here not only improves the long-term potential for LWD recruitment, but also restores stream shade and mitigates bank erosion.

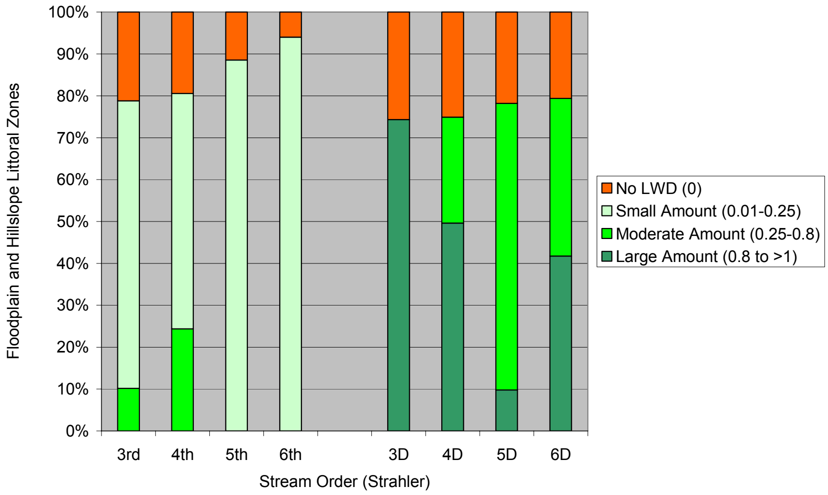

Figure 6.37 $LWDI_{global}$ values for each stream order

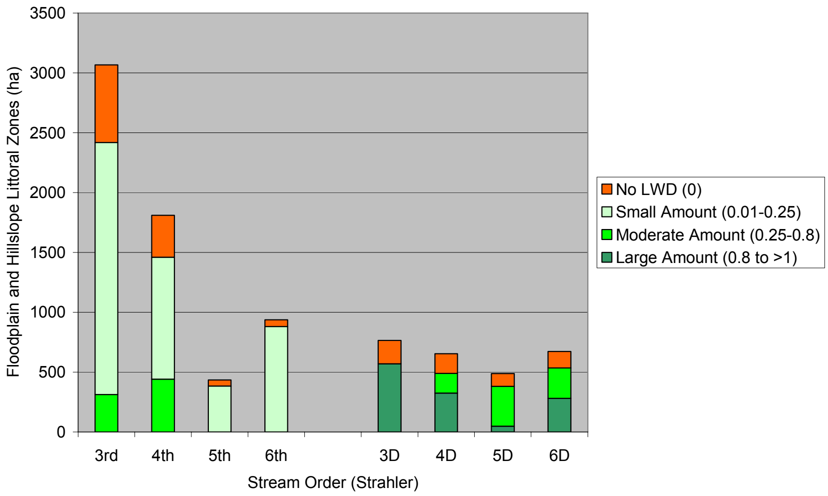

Figure 6.38 $LWDI_{global}$ values per hectare of littoral zone

LWD placement would be an option for the 5th or 6th order channels or limited locations within the D class channels, but the sites for LWD placement would need to be selected with the overall connectivity of the aquatic ecosystem in mind.

Index reliability

This index is certainly reliable at the basic level of discriminating those areas that are capable of recruiting aquatic LWD from those that are not. Local variations in channel geometry, and the fact the LWD recruitment is an episodic rather than continual event means that this index may not accurately predict the volume of LWD or the blockage ratio of LWD to channel cross sectional area at any given point. This is why the

$LWDI_{global}$ results have been aggregated into the classes shown in Figure 6.37 and Figure 6.38. This aggregation encapsulates any errors in LWD volume that may be due to classification errors in the remote sensing data, and provides a more realistic representation of the accuracy of the index (*i.e.* a D class channel with either closed or open forest next to it will contain a high amount of LWD rather than a 4th order channel with closed forest adjacent to it will have a blockage ratio of exactly 0.4).

6.7 Chapter Summary.

The results of the 5 RFIs developed in Chapter 2 are presented and analysed in terms of stream order, and position within the landscape. The results of each index are summarised briefly below.

The STI identified that 1600 hectares of littoral zones located on hillslopes adjacent to low order streams are either subject to heavy grazing or contain bare soil, and therefore trap much less sediment, or in the case of bare soil, actively contribute sediment to the stream network.

The BRI_{local} identified that over 5000 hectares of littoral zones adjacent to the stream network contained no bank reinforcement whatsoever, and further 3500 hectares was reinforced by grass only, and only 47% of the stream network had experienced no change in the amount of bank reinforcement. The BRI_{global} identified the areas at highest risk of bank erosion, *i.e.* areas with high unit stream power and no bank reinforcement. The areas at highest risk where bare soil areas located on the floodplains of 1st order streams, which make up a relatively minor 314 hectares of the catchment area.

The DNI_{local} was calculated for all floodplain littoral zones located on 2nd order or higher streams. The DNI (both local and global) were also used calculated for the entire floodplain. The DNI_{local} identified that the capacity for denitrification had been removed from 7% of littoral zones and 36% of the floodplain, it also identified that there had been a further reduction in the denitrification capacity of the 37% of littoral zones and 36% of the floodplain. The DNI_{global} identified closed forest and open forest on the floodplain and adjacent to 2nd, 3rd and 4th order streams as having the greatest potential for denitrification, these vegetation types make up less than 20% of the riparian vegetation but contain over 60% of the WSC available for denitrification. Estimates based on the DNI_{global} calculations indicate that the denitrification capacity of riparian zones in the study area has nearly halved as a result of land clearing and the practice of cropping on the floodplain. This, in combination with the practice of applying nitrate enriched fertilizer to the floodplain cropping areas has serious implications for in-stream nitrogen loads and concentrations.

The SSI_{local} indicated that 40% of 4th order streams and 30% of 5th order streams are not receiving any shade from riparian vegetation. Furthermore only 17% and 7% of these stream orders (respectively) were being shaded to the same extent that they would have been prior to European settlement. 6^{th} order streams were in much better condition with over 70% receiving the same amount of shade as pre-settlement, and only 7% receiving no shade from riparian vegetation. The SSI_{global} showed some interesting results, because riparian vegetation has the biggest impact on the amount of sunlight reaching the stream surface on 4^{th} order streams, but waterholes are more likely to form along 6^{th} order streams, so riparian vegetation adjacent to both streams orders were weighted evenly. The SSI_{global} identified 72 hectares of littoral zone adjacent to 6^{th} order streams as the highest priority area in terms of restoring stream shade. However restoring the vegetation in the 724 hectares adjacent to 4^{th} order streams may also enhance a range of other riparian functions such as denitrification too.

The $LWDI_{local}$ indicated that the potential for LWD recruitment has been removed from 20% of 3^{rd} and 4^{th} order streams, 12% of 5^{th} order streams and 7% of 6^{th} order stream, and from over 20% of all D class channels. The capacity for LWD recruitment was also reduced for an additional 30% of littoral zones. The $LWDI_{global}$ identifies littoral zones adjacent to D class channels of being of high importance, reflecting the fact that LWD falling into these relatively small channels will have a larger impact on the blockage ratio (relationship between area of LWD projected into the flow and the channel cross sectional area) than an equivalent piece of LWD falling into a large channel. With the exception of 6^{th} D order streams, LWD recruitment has decreased in over 50% of D class channels, and this has significant implications for the quality and connectivity of aquatic habitat in these channels and on the floodplains of these higher order streams.

All of the indices were reliable at the basic level of discriminating areas that were performing a specific riparian function from those that are not. The RFI_{local} provide a good indication as to the change between the functions performed by riparian vegetation prior to European settlement and those being performed at present. The RFI_{global} values are important insofar as they place the riparian vegetation functions in a catchment context, however the level of importance applied to different areas is sensitive to accuracy of some parameters. The results presented in this chapter show how the RFIs developed in Chapter 2 can be used to:

1. Quantify the change in five important riparian functions between pre-settlement and the present day, and;
2. Identify the specific locations within the catchments where each function is of greatest importance.

This represents previously unavailable information, and will assist catchment managers in i) setting realistic goals in terms of catchment restoration, and ii) identifying priority areas within the catchment to restore specific riparian functions The reliability and sensitivity of these indices, as well as potential areas for future work are discussed in Chapter 7.

Chapter 7 Index Reliability and Applications

7.1 Introduction

This chapter is structured in the following way. The first section discusses how the RFI approach developed in this thesis fits in to the broader framework of riparian zone research and describes the key science questions that were addressed in this thesis. The second section discusses the application and limitations of the local and global forms of each RFI and identifies avenues for further research. The third section discusses the potential for using the indices in combination, and discusses the reasons for not using a 'composite index'. The final section describes the potential for using these indices to inform catchment management decisions, and discusses the reliability of using the riparian function indices for this purpose.

7.2 Overall Approach

The RFI approach described in this thesis sits at the intersection between two existing areas of riparian zone research, riparian zone modelling and riparian zone monitoring. The suite of RFI_{local} indices developed in this thesis represent the monitoring approach, insofar as a baseline (pre-settlement vegetation) is compared with the current riparian vegetation. The RFI_{global} indices on the other hand place the present day riparian functions into a catchment context based on a indices of each riparian function.

The concept of riparian zone monitoring based on field surveys has been explored in numerous previous studies including the Index of Stream Condition (Ladson *et al*., 1996), the State of the Rivers (Anderson, 1993), and Tropical Rapid Assessment of Riparian Condition (Jansen *et al*., 2004). These approaches are well suited to describing riparian conditions in detail at a small scale, but typically rely on assumptions, such as the assumption of stream reach uniformity used in the State of the Rivers, to infer conditions elsewhere within the channel network. These approaches also typically combine a series of 'indicators' into a composite condition index to describe the condition of the riparian zone. Whilst such indices provide a useful description of the overall condition of riparian zones at the sites surveyed, they do not necessarily provide information at the spatial scale that is required by catchment managers to support their decision making processes.

The RFI approach described here is not intended to replace field based surveys. Indeed, many of the parameters/indicators collected during field surveys are essential to support and validate the parameters used in the stream order and vegetation classifications used to calculate the RFIs. Field survey information is also essential to provide validation of the RFI_{global} models too. The RFI approach is designed to complement and enhance existing field survey programs, and in conjunction with these field programs, the RFI approach aims to provide catchment managers with the information they need to identify and prioritize appropriate riparian management options.

While catchment scale riparian zone management forms the conceptual framework for this thesis, there are a number of key science questions that had to be addressed in order to inform the process of riparian zone prioritization. These questions were:

1. Where is hillslope generated sediment most likely to enter the channel network?
2. Where is stream bank erosion most likely to occur?
3. Where is denitrification occurring in the catchment (both in terms of location and relative amount)?
4. Where is woody riparian vegetation maintaining channel stability and improving the aquatic environment by providing LWD to the channel
5. How much shade is the riparian vegetation providing to the stream (particularly in the context of an ephemeral stream network that relies on waterholes to support the aquatic ecosystem during the dry season)?
6. How much has the sediment trapping, bank stabilizing, denitrifying, stream shading and LWD producing capacity of the riparian vegetation changed between pre-settlement and the current day?

These questions were addressed by developing indices of each process that could be run using inputs generated from either classification of remote sensing data or terrain analysis. Questions 1 and 2 have been addressed by regional scale sediment transport models such as SEDNET (Prosser *et al*., 2001), however the use of a vegetation classification (generated using data with a 15 metre spatial resolution) to represent the impact of vegetation structural class on bank reinforcement and the application of the MrVBF algorithm to a digital elevation model (DEM) that contains greater detail within depositional areas of the landscape, mean that the STI and BRI_{global} provide far more detailed spatial and process information than that provided by GIS based models.

Addressing question 3 presented the greatest challenge, and to the authors knowledge no-one else has modelled catchment scale denitrification in semi-arid catchments using a map of water soluble carbon (WSC) (calculated as function of vegetation structure/land cover) the flow characteristics of channel network (estimated from long term gauging station records), and the distribution of alluvial soils (calculated using the MrVBF algorithm).

Addressing question 4 entailed combining a pre-existing LWD recruitment model with field data, and combining that with the proportion of the channel network that is likely to support aquatic life during the wet season.

Question 5 required the development of a model that estimates the amount of sun blocked from the stream channel by a stand of riparian vegetation that accounts for canopy geometry, channel geometry and stream orientation.

Question 6 was addressed by running all models using pre-settlement vegetation and comparing the results with the existing vegetation.

The RFI approach developed in this thesis is similar to that described in Quinn *et al.* (2001). Quinn *et al.* (2001) used a categorization of different stream and valley types to identify where different riparian functions dominate in a temperate catchment in New Zealand. The fundamental difference between the RFI approach and that described in Quinn *et al.* (2001) is that, rather than using broad reach or valley descriptions, the RFI approach uses high spatial resolution data to model and describe the riparian vegetation function at every point within the study area. Furthermore the RFI approach uses this detailed spatial data to quantify each riparian function using the indices developed in Chapter 2 rather than using a subjective condition score for each stream reach.

7.3 Individual Riparian Function Indices

7.3.1. Sediment Trapping Index

The STI describes the sediment trapping capacity of the existing ground cover in the riparian zone with that of a reference riparian zone that maintains high ground cover in the absence of grazing. Calculation of the sediment trapping capacity of riparian zones requires three things: first the identification of small features such as riparian buffer strips and grassed waterways; second the capacity to quantify ground cover dynamics over time, particularly in areas where grazing pressure can rapidly change ground cover levels; and third the ability to identify hillslopes that are immediately adjacent to the channel network. To capture these three phenomena the STI combines the high spatial resolution of ASTER data to capture narrow riparian features such as grassed waterways with the temporal resolution of MODIS data to describe the temporal dynamics in ground cover. Terrain analysis in the form of the MrVBF algorithm (Gallant and Dowling, 2003) was applied to 90 metre SRTM data to identify streams that do not have extensive floodplains or alluvial soils and are consequently closely coupled to the adjacent hillslope.

The combination of three different sources of spatial data to describe the three key aspects of sediment trapping provides a tool for identifying areas within the catchment that are a high sediment transport risk, *i.e.* areas of bare soil or heavy grazing on hillslopes immediately adjacent to stream channels. These are the areas that are most likely to export sediment to the stream network during an erosion/rainfall/storm event. The capacity to identify where these areas are located in the context of a large catchment constitutes a significant contribution to our understanding of where and how riparian zones operate in different parts of the catchment. Furthermore, it provides previously unavailable data to catchment managers that will assist them in optimizing riparian zone management to meet end-of-valley targets in reducing pollutant and sediment loads.

The simple analysis applied to the MODIS derived grazing pressure index (GPI) (a histogram threshold was applied to the GPI to separate grazing areas into light grazing and heavy grazing) reflects the absence of stocking rate data. Consequently the STI provides a temporally invariant estimate of sediment trapping, because although multi-temporal MODIS data were used to estimate grazing pressure, the index values assigned to each grazing pressure were based on field data, which represents the sediment trapping capacity of riparian zones at the end of the dry season.

In future studies, a GIS containing information about stocking rate data over time would allow a more sophisticated analysis of the MODIS data, enabling more accurate estimates of ground cover at any given time. This in turn would provide information about the change in sediment trapping capacity of riparian zones over time.

The use of the MrVBF algorithm to identify areas where slopes exceeded 2% and were therefore likely to be closely coupled to the channels represents an improvement on the buffer analysis technique that is frequently applied to non-point source pollution studies of riparian zones. By separating riparian zones into broad hill slope and floodplain classes enables identification of riparian zones where ground cover levels are likely to have the greatest impact on the sediment transport capacity.

The STI is likely to be very useful in the Fitzroy basin, because hillslope generated sediment contributes approximately 60% of the 2900 kt y-1 of suspended sediment exported from the Fitzroy basin (values based on SedNet model outputs described in (McKergow *et al*., 2005)). In a study of the impact of grazing on sediment and nutrient exports carried out in the neighbouring Burdekin catchment O'Reagain *et al.* (2005) states that

"*Watercourses draining hillier grano-diorite landscapes with lower cover had markedly higher sediment and nutrient loads compared to those draining flatter sedimentary landscapes.*"

Clearly catchment managers in basins such as the Fitzroy and Burdekin that have significant hillslope erosion problems need to be able to identify where in the catchment hillslope erosion is an active/dominant/significant process. In particular identifying areas that are being consistently overgrazed and areas where there is inadequate buffering of cropping areas enables catchment managers to identify specific areas for remedial action.

One factor that limits the accuracy of the STI calculations is the lack of information about the distribution of riparian fences. The STI values could be calculated more reliably if information about the presence or absence of riparian fences were available. Ground cover data collected for fenced and unfenced RZs during the fieldwork suggest that fenced RZs have considerably higher cover levels (for a brief description of this data see Appendix X) than unfenced riparian zones. Spatial information about the distribution of riparian fences could be used to improve the accuracy of the riparian ground cover predictions, and thereby improve the accuracy of the STI.

Future research into the STI can take a number of directions. These include:

1. Improved index accuracy;
2. Index calculation using other remote sensing platforms; and,
3. Integrating the index with catchment scale sediment transport models.

Improving the accuracy of the STI could be achieved in a number of ways. First, a series of ASTER scenes collected for the same location during different seasons could be used to discriminate permanent buffer strips from stubble, based on the logic that an area that contained a stubble signature in all scenes was likely to be a permanent buffer strip rather than a field with stubble in it[28]. Second, GIS data of riparian fence locations would also improve the accuracy of STI calculations, however the logistics of collecting such a GIS are considerable. Third, the STI could be calculated from other remote sensing platforms. The higher spatial resolution of sensors such as SPOT, and more specifically IKONOS and QuickBird would enable the calculation of STI for riparian buffer strips that are narrower than 15 metres. Finally, the STI could be incorporated into existing sediment transport models in one of two ways, i) STI values could be used to improve estimates of sediment delivery ratio in sediment transport models such as SEDNET (Prosser *et al*., 2001), and ii) the approach used to calculate the STI could be used to generate dynamic estimates of ground cover and sediment trapping capacity once the relationship between MODIS time series and ground cover dynamics was established and the dynamic STI values could be used as input into event based models such as the Agricultural Nonpoint Source Pollution model (AGNPS) (Young *et al*., 1987).

At present the STI describes the sediment trapping capacity of the current riparian zone relative to a reference riparian zone that contains high ground cover levels. To calculate the amount of sediment trapped in each riparian zone (*i.e.* the sort of data required by some sediment transport models) the Manning's *n* values for each riparian zone would need to be combined with information about the slope and width of each riparian zone to estimate their sediment trapping capacity.

In the broader Australian and global context, hillslope generated sediment that enters the channel network is a problem in many catchments, and consequently the STI has potential applications elsewhere. In applying the STI to other areas a series of questions need to be considered: how much field work will be required; which sensor has the appropriate spatial resolution for the buffer strips in the area of interest; and is data available at the scale, and for the time frame of interest. Fieldwork is essential to

[28] The success of this approach would be dependent on the timing of the scene acquisitions.

establish the link between land use and ground cover levels, particularly if ground cover levels beneath tree canopies will be inferred from the adjacent paddock/field. Consequently fieldwork to establish this link would need to be carried out for the region the STI was to be calculated in. Ideally this fieldwork would be carried out during the same season (preferably same time) as the image was acquired. It is also important to ensure that the Manning's *n* values calculated by the fieldwork are based on Manning's *n* values collected for similar cover types.

7.3.2. Bank Reinforcement Indices

BRI_{local}

The BRI_{local} was developed to identify areas that had undergone a decrease in the amount of bank reinforcement provided by woody vegetation, and are therefore more prone to bank erosion than they would have been prior to European settlement. The relatively high spatial resolution of ASTER data (15 metre pixel) enables the identification of narrow strips of remnant riparian vegetation that continue to provide bank reinforcement, and also identifies areas where grazing or cropping practices have resulted in bare soil immediately adjacent to the channel. By combining existing models of bank reinforcement (Abernethy and Rutherfurd, 2001, Simon and Collison, 2002) with vegetation structural classes that can be identified using remote sensing data the BRI_{local} provides capacity to estimate the amount of bank reinforcement as a function of vegetation class and stream order anywhere within the study area. This represents a contribution to our understanding of, and our capacity to, quantify how riparian vegetation acts to reduce bank erosion at different locations throughout large catchments.

One of the main advantages of the BRI_{local} is that it identifies stream banks throughout the catchment that have no bank reinforcement provided by woody riparian vegetation. This information was provides a valuable tool for identifying areas throughout the catchment that are likely to have unstable banks, and could potentially deliver large amounts of sediment to the stream via bank collapses, and mass failure. These areas are of particular interest in the Fitzroy basin where 35% of the 2900 kt of suspended sediment load that is exported from the catchment into the Great Barrier Reef Marine Park each year is generated by bank erosion (values based on SedNet modelling results described in (McKergow *et al*., 2005)). The BRI_{local} also has the capacity to identify areas where woody riparian vegetation is providing the maximum amount of bank reinforcement (BRI_{local} = 1), and it is these areas that should be conserved to prevent further destabilisation of stream banks. Another advantage of the BRI_{local} is that it can be calculated with relatively few data sources compared to other bank stability models (Simon and Collison, 2002). This is because it focuses solely on the influence of vegetation (rather than soil and hydrology) on bank stability.

A limitation to the accuracy of the BRI_{local} is that assumptions made about pre-settlement riparian vegetation for higher order stream orders are difficult/impossible to validate (particularly in a spatially explicit sense). In index value terms this means that high order stream reaches with woodland adjacent to them (BRI_{local} = 0.7), may have had woodland in their littoral zones prior to European settlement in which case the BRI_{local} value should be 1 rather than 0.7. Consequently the BRI_{local} values of 0.7 for higher order streams should be treated with caution as they may not be a true representation of the change in the amount of bank reinforcement. This limitation does not dramatically reduce the usefulness of the BRI_{local} because the index can still be reliably used to identify a. areas of bare soil adjacent to the channel (BRI_{local} = 0) b. areas where the removal of woody vegetation has lead to a large reduction in the amount of bank reinforcement (BRI_{local} =0.1) and areas where the conversion of woodland into open woodland has lead to reduction in the amount of bank reinforcement (BRI_{local} = 0.3-0.4).

To the authors knowledge the only other spatially distributed model of stream bank stability is described in Wilkinson *et al*. (2005), and the BRI_{local} approach represents a significant improvement both in terms of the spatial resolution with which riparian vegetation is represented (15 metres as opposed to 250 metres) and in terms of the detail in which vegetation structure influences bank stability. Wilkinson *et al*. (2005) uses a simple proportion of riparian vegetation whereas the BRI_{local} calculates stability as a function of both vegetation structure and stream order.

There are a number of avenues for further research into the BRI_{local}. These include: the integration of the BRI_{local} into catchment scale sediment transport models, and additional fieldwork to examine the assumptions that were made in calculating the BRI_{local}. The BRI_{local}, and the parameters used to calculate the BRI_{local} could be incorporated into a catchment scale sediment transport model such as SEDNET (Prosser *et al*., 2001). Prior to inclusion in a broader sediment transport model it would be prudent to undertake more fieldwork to examine the assumptions relating to climax vegetation adjacent to high order streams and, if possible, the root distribution of riparian species in the study area. Assumptions about climax vegetation would also need to be re-assessed in applying the BRI_{local} to other areas. In areas where water availability is not limiting climax riparian vegetation may not differ throughout the channel network, and in areas where water availability is even more limiting, then differences in climax vegetation with stream order may be more pronounced than those observed in the study area.

BRI_{global}

The BRI_{global} values were determined by the bank erosion term in Equation (2.20) which estimates the likelihood of bank erosion using

$$BE = \left(Power \times \left(1-\lambda_n\right) \times FloodplainFactor\right). \tag{5.6}$$

Where *BE* is the likelihood of bank erosion occurring, *Power* is the unit stream power, λ_n is the number of trees per hectare normalised against the number of trees per hectare that would have existed at that location prior to European settlement and

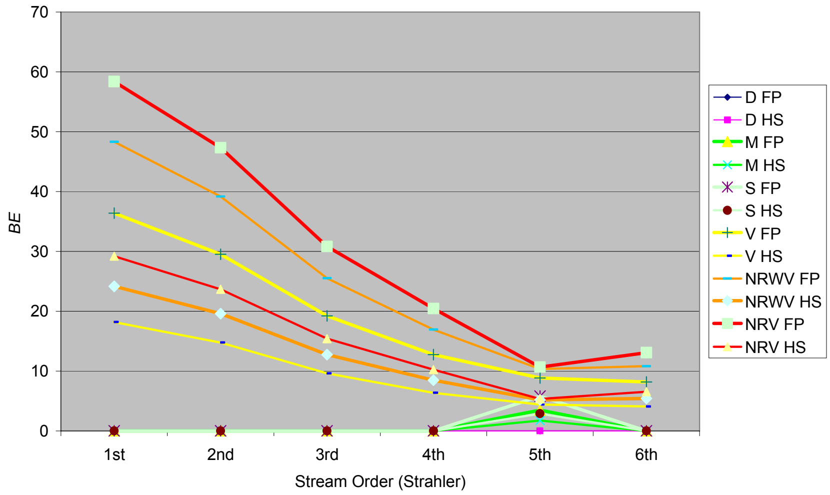

Figure 7.1 Sensitivity analysis of the bank erosion term in BRI_{global}

FloodplainFactor is a variable used to reflect the increased likelihood of bank erosion in alluvial soils as opposed to hill slope or bedrock constrained channels (these are the same terms as used in the original model described in Wilkinson *et al*. (2005)). A sensitivity analysis of these parameters is shown in Figure 7.1.

Note that the colour coding indicates the same vegetation/land cover class located on the floodplain or on hillslope constrained channels. The *BE* term is most sensitive to the λ_n parameter, which can alter the *BE* term from maximum to zero for any given stream order. The fact that λ could be reliably predicted using a vegetation classification (Section 4.3.4) and the vegetation classification itself had a high degree of accuracy (94%, Section 5.2.2) mean that this parameter can be reliably predicted for the study area. The *BE* term is also sensitive to the *FloodplainFactor* term. Originally calculated as a function of floodplain width, the *FloodplainFactor* is set to 1 for channels located on floodplains and zero for bedrock constrained channels (Wilkinson pers comm. 2005). The low order streams in the study area were typically constrained on either side by hillslopes, but did not necessarily flow through bedrock constrained gorges. Based on observations made during the fieldwork, bank erosion was occurring along low order hillslope constrained channels, although not as frequently as on channels located on floodplains. The hillslope constrained channels represent small, relatively high slope channels with relatively large unit stream power that have the capacity to erode the colluvial soils that make up the stream bank, particularly in areas where land clearing or vegetation removal has reduced the capacity of the woody riparian vegetation to stabilize the banks. To reflect this scenario the *FloodplainFactor* was set to 0.5 rather than 0. This value is arbitrary, and it would be important to revise this figure based on field surveys carried out on a large number of hillslope constrained and floodplain channels prior to including these model results into a sediment transport model. The *BE* term is determined by the *Power* term, because without stream power bank erosion will not occur. Interestingly the variations in *Power* term between stream orders have a smaller influence on *BE* than the λ_n or *FloodplainFactor* terms have within each stream order. *Power* term was calculated for each stream order (as seen previously in Figure 6.12) and the absence of flow velocity measurements for 1st and 2nd order streams makes estimates of the *Power* parameter for these stream order unreliable. The distribution and values calculated for the *Power* term are consistent with expected trends and values described in other studies (Knighton, 1999; Reinfelds *et al*., 2004). Even if we assume that the velocity of the lower order streams is identical to the third order stream (rather than using extrapolated values) the slope values used for the 1st and 2nd order streams mean that they still have higher unit stream power. So while the BRI_{global} in its current form may tend to overemphasize the erosion risk on first order streams relative to 2nd and 3rd order streams, the sensitivity of the *Power* term to slope and channel geometry means that unit stream power will be higher for lower order than higher order streams, irrespective of what flow velocity values are used.

One limitation of the BRI_{global} is that it uses unit stream power to describe the erosive force of the stream, but does not condsider other forms of bank erosion that are not dependent on unit stream power. For instance, in areas that are subject to extensive cattle grazing, such as those encountered in much of the study area, banks can be denuded, damaged or destabilized by cattle (Belsky *et al*., 1999). Consequently, the current form of the BRI_{global} may underestimate the amount of bank erosion because it does not consider these processes. In the future the BRI_{global} could be modified to include the influence of cattle in areas subject to grazing. This would ideally be done using estimates of grazing pressure calculated from MODIS data as discussed in Section 5.2.3 in combination with field surveys to ensure that the remote sensing estimates of grazing pressure could be reliably used to estimate cattle impacts on stream banks. Identifying areas where grazing pressure is high in riparian zones is also important for the BRI_{global} in the longer term as well. This is because heavy grazing in riparian zones prevents recruitment of new riparian trees from existing seedbanks. So while the existing riparian forest may have a contiguous canopy and appear intact from the satellite image, the absence of saplings and smaller trees may result in unstable banks in the longer term via the long term loss of bank reinforcement (Jansen and Robertson, 2001).

7.3.3. Denitrification Indices

DNI_{local}

Characterizing the spatial distribution and amount of denitrification requires two things, the spatial distribution of water soluble carbon in the soil profile, and the frequency with which conditions are suitable for that water soluble carbon (WSC) to be used as an electron donor in the process of denitrification. The vegetation classification used to estimate the distribution of WSC was generated from ASTER data. The 15 metre pixel size of ASTER enabled identification of narrow stands of littoral vegetation that generate higher amounts of WSC than the surrounding floodplain vegetation. The frequency with which conditions were suitable for denitrification was calculated by analysing the stage height records for stream gauging stations throughout the study area and calculating stage height characteristics for each Strahler stream order. To the authors knowledge this is the first study to use stage height records to calculate the likelihood of conditions being suitable for denitrification. Furthermore, the combination of these two data sources with floodplain extent data calculated using MrVBF provides a relatively simple model to estimate where denitrification is likely to be occurring in a large semi-arid catchment. In addition, the DNI_{local} provides an estimate as to the change in denitrification potential between pre-settlement vegetation and the riparian vegetation encountered at present. In so doing, the DNI_{local} provides new spatial assessment concerning the role of riparian vegetation in reducing in-stream nitrogen loads at a catchment scale in semi-arid areas.

One of the important features of the DNI_{local} is its use of stage height characteristics to incorporate the temporal behaviour of the stream into the index. This makes the DNI_{local} sensitive to changes in stage height (flow) duration that might be expected to occur under a land use change scenario, or as a result of river regulation. Stream regulation that reduced the frequency and duration of bankfull or overbank events would dramatically reduce the capacity for denitrification. The capacity to estimate the change in denitrification potential for different flow regimes as well as land-use management strategies is useful.

Another advantage of the DNI_{local} is that it describes the denitrification processes that occur both adjacent to the channel during within-bank flows, and the floodplain processes. It also describes the relative importance of both locations (although the estimates of relative importance are sensitive to the accuracy of the overbank frequency and duration data). This capacity to describe in-channel and floodplain processes is particularly important for a system like the Fitzroy, where nitrogen loads and concentrations during both low flow and flood events have large impacts on the in-stream and estuarine ecology. Consequently the capacity to identify areas where denitrification is occurring within the system is essential, so that these areas can be protected or restored.

The use of a floodplain and alluvial soils map generated from MrVBF is a significant improvement on the fixed buffer width approach used in other denitrification models (Basnyat *et al*., 1999) or the stream channel surface area approach used by Bartkow and Udy (2004). This is because the depositional areas identified by MrVBF are likely to be closely coupled to the local phreatic and hyporheic groundwater systems, so that WSC, either at depth, or in the topsoil, is likely to encounter conditions suitable for denitrification at some point in time (even if it is only during an infrequent major flood event). Also, by definition, areas with high MrVBF values have low topographic slope, and therefore high stage events that occur in these areas are likely to persist for long enough for denitrification to start, and, in many cases, run to completion.

One of the limitations of the DNI_{local} is its sensitivity to estimates of channel dimensions, and the assumptions relating the stage height duration for a specific Strahler stream order. The use of Strahler stream order, rather than upstream contributing area[29] reduces the sensitivity of this index to changes in channel geometry that may occur within any give stream order, consequently estimates of the amount of denitrification may be locally inaccurate in areas where channel geometry and/or stage height characteristics (particularly bank full frequency) differ significantly from the average values used for each stream order. The DNI_{local} is also sensitive to the amount of denitrification potential (calculated using fine roots to estimate the amount of WSC, and in turn the amount of denitrification) ascribed to each vegetation type. At present these values are based on literature values, however additional fieldwork within the study area would be able to reduce uncertainties in the amount of denitrification potential ascribed to each vegetation structural type. These limitations and the future research required to address them is discussed in detail below in terms of the DNI_{global} model

Another limitation to the DNI_{local} is the assumption of simple channel geometry. A single U shaped channel is used to calculate the DNI (both local and global) and this may underestimate the amount of WSC available for denitrification during low stage events because it doesn't include the areas of organic rich soil associated with trees, particularly *Calistemon viminalis* or *Melaleuca* sp. growing on 'in-channel' features such as benches, bars and islands. This limitation will tend to underestimate the amount of denitrification that occurs in the littoral zones of the higher (5^{th} and 6^{th}) order streams where such features occur.

There are a number of considerations that need to be made in applying DNI_{local} to other areas, particularly areas with different climatic/hydrological regimes. The approach could be applied to other semi-arid areas with ephemeral stream networks, and vegetation distribution that was water limited without major modification. However fieldwork to establish channel dimensions, and a stage height duration to stream order relationship would need to be established for the area. The approach would need significant modification and additional data if it were to be applied to areas that did not meet these criteria (semi-arid, ephemeral stream network). This is because the

---

[29] Which was necessary because the lack of terrain information on the floodplain necessitated manual digitization of the channel network, thereby removing the link between each stream link and upstream catchment area. It is possible to manually re-establish the link between stream links and catchment area, but this is very time consuming, and can be unreliable for areas where the channel anabranches.

mechanisms for, and location of, denitrification are different in temperate, humid environments with permanent stream flow (Quinn *et al*., 2001). It is likely that a groundwater flow model would be required for these areas, to identify areas where shallow groundwater is likely to intercept (rather than bypass) the riparian root zone, one such model is described in Gold *et al*., (2001).

DNI_{global}

Calculation of the DNI_{global} entailed identifying which vegetation and stream order combination would result in the highest amount of denitrification during a wet year[30]. The scenario for the maximum amount of denitrification identified in this analysis was closed forest located on the floodplain of a 2nd order or 3rd order stream. This scenario was identified because the frequency with which these lower order streams reach bank-full or over bank stage heights means that nitrate enriched water in these 2nd and 3rd order streams is more likely to interact with the WSC rich layers of topsoil. For higher order streams that have deeper channels and do not reach bank full stage as frequently the nitrate enriched stream water is less likely to interact with the WSC in the topsoil. A sensitivity analysis of the DNI_{global} is shown in Figure 7.2.

The model is sensitive to the amount of WSC assigned to each vegetation structural class for any given stream order, but is most sensitive to the stage height characteristics and in particular estimates of bank full frequency for each stream order. This is consistent with the observations contained in Takatert *et al*. (1999) which notes in relation to denitrification occuring in floodplain soils that "*The hydrological variations are much more important than those concerning substrate and type of vegetation*".

The stage height characteristics were calculated directly from gauging station records that date back up to 60 years and represent at reasonably accurate characterisation of stage heights at those gauging stations. There are insufficient gauging stations within the study area to assess whether gauging station records recorded at one location can be reliably used to characterise all channels with the same Strahler stream order, and this is likely to represent the greatest limitation to the accuracy of the DNI_{global} model. This limitation is of particular concern in relation to the typical location of gauging stations in catchments. Gauging stations are typically located on bedrock constrained reaches or at constrictions within the catchment to enable calculation of total stream discharge. Areas upstream or downstream of the gauging station (but still of the same Strahler stream order) may anastomose and/or be surrounded by extensive floodplains, and flow is likely to reach bank full stage or go overbank in these settings (Western *et al*., 1997; Jansen and Nanson, 2004). Consequently the current DNI_{global} model may be underestimating the

---

[30] The term 'wet year' used here refers to a year in 3 major rainfall events occur, one at the beginning of the wet season, one at the end of the wet season, and a major rainfall event during the dry season.

amount of denitrification occuring on any given stream order, particularly for stream reaches that contain extensive anastomosis.

A further limitation is that the WSC estimates for each vegetation class are literature rather than field work based. The values identified from the literature represent the vegetation and climatic conditions encountered in the catchment. However they may be locally inaccurate given the hydrological conditions encountered on the floodplain and in littoral zones. The literature values are for non – riparian tree species in the study area , and riparian tree species may differ in rooting habit to those species described in the literature. The values for WSC used in this study reflect expected trends insofar as areas with high aboveground biomass support high amounts of WSC and decreases in the amount of above ground biomass correspond with decreasing amounts of WSC. Furthermore WSC declines exponentially with increasing soil depth, which is consistent with the description of WSC dynamics for vegetation in the study area as described in Dalal *et al*. (2005). However to calculate the amount of denitrification with any degree of certainty it would be necessary to measure the distribution of WSC with depth for the different structural classes encountered in littoral zones and on the floodplain within the study area, and ideally carry out a series of these measurements at different times during the year *i.e* start of the wet season, end of the wet season, middle of the dry season. In addition to this, surveys of denitrifying enzyme activity (DEA) would be carried out to establish whether the WSC is being consumed by denitrifying bacteria, or via other processes. Remote sensing may prove a useful tool in quantifying the fine root and WSC dynamics on the floodplains based on the following proposal.

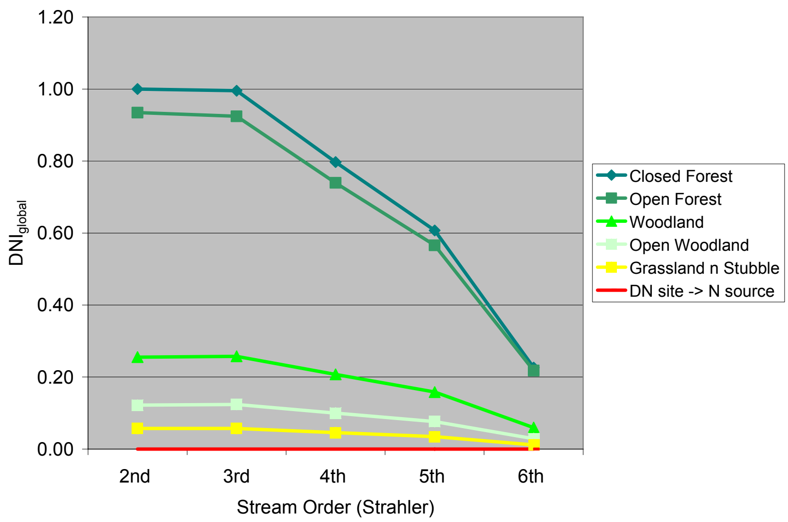

Figure 7.2 Range of DNI_{global} values for every stream order and vegetation type combination

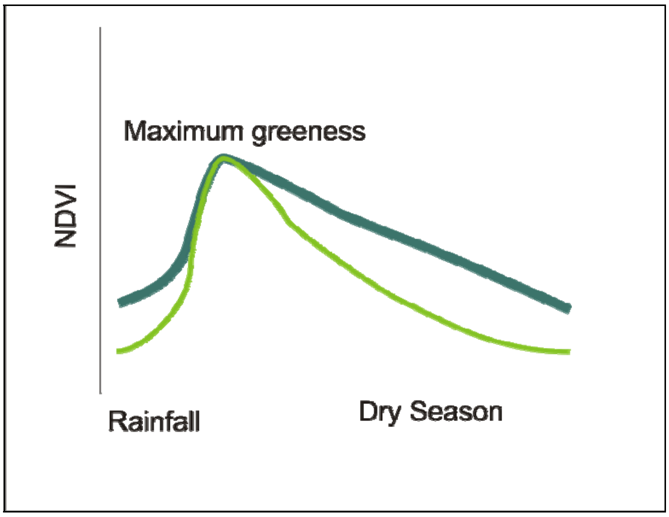

Figure 7.3 The difference in NDVI over time between woody vegetation accessing plant available water in the topsoil (light green) and those accessing groundwater (dark green)

Theoretically, if woody vegetation is located on a large floodplain, and has access to groundwater or water that is deeper in the soil profile, then it will tend to maintain a relatively high leaf area throughout the year, while other vegetation in the landscape dries out as the dry season progresses. Under these circumstances the Nomalized Difference Vegetation Index (NDVI) time series of floodplain vegetation will tend to vary less over time than woody vegetation elsewhere within the landscape (Goodrich *et al*., 2000) as shown in Figure 7.3.

This phenomenon has been observed and described using multi-temporal NDVI data in Glenn and Nagler (2005). To identify whether the MODIS NDVI data could be used to estimate groundwater/deep soil water behaviour in floodplains within the study area the following steps were taken:

1. Stands of woody vegetation located on the floodplain (definition of floodplain vegetation is contained in Section 5.3.3) that were larger than a MODIS pixel (250m x 250m) were identified from the vegetation/land cover classification;

2. A mask was generated using the areas identified in step one and this mask was used to identify the NDVI timeseries of woody vegetation located on the floodplain, and;

3. A Minimum Noise Fraction (MNF) analysis (Green *et al*., 1988) was performed on the masked data to identify areas of low variability.

The MNF transform performs two principal components analysis (PCA) transforms on the data, the first transform decorrelates, removes noise and re-scales the data, and the second transform performs a traditional PCA analysis of the data. The second MNF

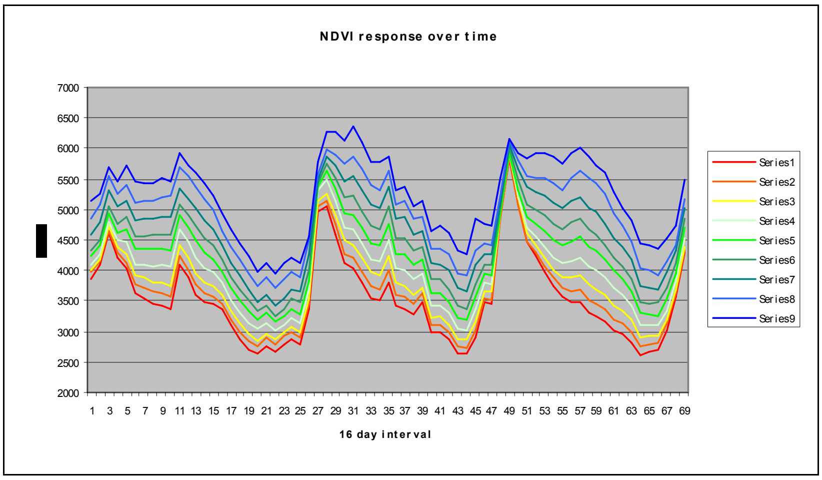

Figure 7.4 NDVI time series for floodplain woody vegetation

band appeared to be closely related to the variation in the amount of NDVI. Areas of the landscape where NDVI did not vary much over time (such as areas of native vegetation) had very low values in the second MNF band, whereas areas that varied a lot over time (such as areas subject to cropping or grazing) had high values in the second MNF band.

A series of masks were generated by thresholding this MNF band, and the masks were applied to the original MODIS data to generate an average time series for each masked area. These average time series are shown in Figure 7.4. In Figure 7.4 Series 1 (red) corresponds with riparian zones adjacent to low order streams, the woody vegetation in these areas may consist of open woodland, and therefore be dominated by a 'grass' rather

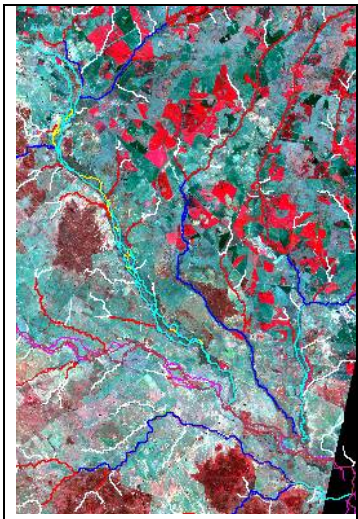

Figure 7.5 ASTER imagery showing channel network

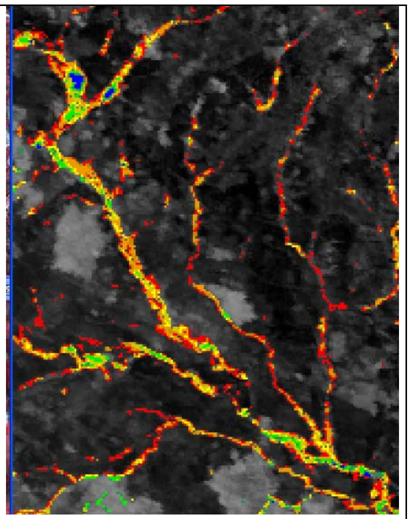

Figure 7.6 Groundwater signal calculated from NDVI timeseries.

than 'woody vegetation' signal, hence the similarity to the time series seen for grazing areas previously in Figure 5.12 and Series 9 (blue) corresponds with riparian vegetation that has more persistent access to moisture deeper in the soil profile or groundwater. (colours of series **Figure 7.4** in above correspond to colours of pixels in Figure 7.6) It is also interesting to note that the two blue series Series 8 and 9 correspond with stands of closed or open forest.

Stands of vegetation that access water deeper in the soil profile (irrespective of whether it is rainwater infiltrating deeper into the soil or regional groundwater) will have fine roots in the capillary fringe, and the turnover of these fine roots and the exudates produced by these roots will generate WSC deeper within the soil profile thereby replenishing stores of WSC for future denitrification events(Kätterer *et al*., 1995).

This preliminary analysis of MODIS NDVI timeseries could be used to identify the location and timing of field measurements of WSC and fine root distribution, and, in conjunction with these measurements, could be used to improve our understanding of groundwater and fine root dynamics on large floodplains. This would in turn lead to an improvement in the accuracy of the DNI_{global} model.

Another way in which remote sensing could be used to improve the DNI_{global} model would be the acquisition of more accurate DEM using laser induced direction and ranging (LIDAR). Such a DEM would provide valuable data about channel geometry and planform morphology, and could be coupled with a hydraulic model to calculate inundation duration and frequency for different parts of the floodplain. An alternative, and considerably cheaper means of improving the reliability of the DNI_{global} model would be to improve the characterisation of channel dimensions for each of the sub-classes of each Strahler stream order (seen previously in Figure 5.15). This could be done by collecting additional channel cross section information, with numerous cross sections collected throughout the catchment, from small streams to large rivers. The emphasis in this data collection exercise would be on large rivers, and their adjacent floodplains, particularly those with anastomosing channels (and their associated B, C and D class channels). This data could analysed using the techniques described in Western *et al.* (1997) to identify more reliable relationships between the channel dimensions of each Strahler sub-class and catchment characteristics, such as area, rainfall/runoff coefficient and hypsometric value. These improved estimates of channel geometry would improve the reliability of the bank full frequency predictions and thereby increase the reliability of the DNI_{global} model.

The reliability of the DNI_{global} could be further improved by carrying out fieldwork within the study area to quantify the link between vegetation structure and denitrification potential. Ideally the fieldwork would measure the denitrification potential (rather than fine root or WSC surrogates) for each vegetation type found adjacent to the channel, and each vegetation type found on the floodplain. With this information, in combination with either a LIDAR based DEM or improved estimates of channel dimension and characteristics it would become possible to estimate the amount of denitrification performed by any particular stand of riparian vegetation on a kg ha^{-1} $year^{-1}$ basis. This data could then either: a. be used to calculate nitrogen budgets at a whole-of catchment scale or b. used as input into existing pollutant transport models such as SEDNET (Prosser *et al*., 2001).

A more empirical evaluation of the DNI_{global} model could be made by examining the statistical relationship between the nitrogen loads and concentrations at various locations in the river system and nitrogen sources and cumulative DNI values upstream of that point. This could be done using a modified version of the approach described in Basnyat *et al*. (1999).

Even though the DNI_{global} model has some limitations as detailed above, it does reveal some interesting patterns in terms of denitrification within the catchment. As discussed in Chapter 4 denitrification was considered to start (DN_{start}) at a given bank height (soil depth) range in the stream bank when flow had exceeded that height for more than 48 hours (Sigunga *et al*., 2002) and denitrification was considered to be complete ($DN_{complete}$) when the flow had exceed that height for more than 8 days (Powlson *et al*., 1988). The DNI_{global} model was calculated using $DN_{complete}$ parameter. However a comparison of the DNI_{start} and $DNI_{complete}$ statistics identifies some interesting trends. Based on the analysis of the stage height records it is interesting to note that while the number of DN_{start} events is much higher for lower order streams, the number of $DN_{complete}$ events (see Section 2.4 for the definition of these two terms) is more comparable between lower and higher stream orders (see Figure 7.7).

The reason for this is the lower order streams are more dominated by event flow or ‘flashy’, consequently flow might reach a certain stage height for 48 hours (long enough for denitrification to start), but may not remain at that stage height for 8 days (long enough for all available WSC to be consumed). Whereas for higher order streams that have a larger base flow component and that may receive a series of flood pulses from different sub-catchments, the stage height varies more slowly so that if conditions at a certain stage height are suitable for denitrification to occur, it is more likely that the water will remain at that point in the stream bank long enough for all the WSC to be consumed.

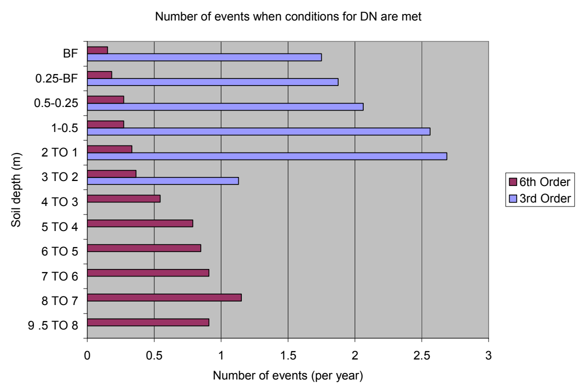

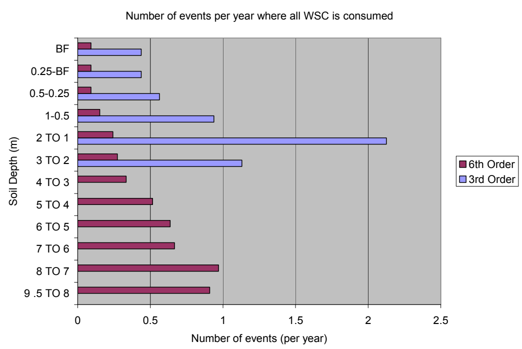

Figure 7.7 The number of DN_{start} and $DN_{complete}$ events for 3rd order and 6th order streams

When denitrification begins but does not run to completion due to falling soil moisture levels, the denitrifying bacteria produce nitrous oxide (N_2O) rather than nitrogen gas (N_2) (Dalal *et al*., 2003). Nitrous oxide is an important greenhouse gas, and calculating the amount of nitrous oxide emissions of from agricultural lands remains problematic (Dalal *et al*., 2003). Once additional field measurement have been made to improve the reliability of the DNI_{global} model, then results such as those shown in Figure 7.7 could be used to provide previously unavailable information about the spatial distribution, timing, and amount of nitrous oxide emissions from floodplains and riparian zones.

7.3.4. Large Woody Debris Indices

$LWDI_{local}$

The capacity of woody riparian vegetation to produce LWD is important for both the terrestrial and aquatic ecosystems, as well as river and floodplain geomorphology Information about the spatial distribution of vegetation capable of producing LWD can be used to identify stream reaches where the removal of woody vegetation has led to a decrease in the amount of LWD inputs, thereby reducing the quality of the aquatic environment, increasing terrestrial habitat fragmentation and altering the hydraulics, both in stream and overbank. Furthermore, the capacity to identify areas in need of protection, riparian planting and candidate sites for LWD placement means that the limited resources available for riparian and LWD management can be used with a high degree of efficiency.

The use of high spatial resolution (15 metre pixel) ASTER imagery was essential to capture the narrow strips of fringing littoral forest along the larger channels that generate large amounts of LWD relative to other vegetation throughout the catchment. The ability to identify stands of vegetation capable of generating LWD that were located on floodplains (as identified by MrVBF) was also important because it is in these areas where water is likely to remain in the channel network long enough for aquatic species to complete their life cycle, whereas low order, bedrock or hillslope constrained channels typically only flow during and immediately after rainfall events. By combining these two layers with a simple LWD recruitment model the $LWDI_{local}$ provides an estimate of how much the capacity for LWD production has changed between pre-settlement and the present day.

The main limitation of both $LWDI_{local}$ and $LWDI_{global}$ (discussed in greater detail below) is that they predict recruitment loads (the amount of LWD that is likely to be generated at a stand of riparian vegetation), rather than predicting actual loads (the amount of LWD that would be found in the channel adjacent to that stand of vegetation). This reflects the fact that the LWD generation occurs via a number of mechanisms such as windthrow (Abernethy and Rutherfurd, 1998), limb mortality or channel undercutting (Fetherston *et al*., 1995). These processes are all episodic in nature, and may vary in dominance in different parts of the catchment. The episodic nature of LWD generation combined with the potential for transport of LWD during large flow events makes it difficult to accurately predict the in-stream volume of LWD at any given location. The other limitation to the LWDIs is that they both rely on the assumption that the relationship between standing timber and LWD observed by Marsh *et al.* (2001), applies to vegetation found in the study area. The data that Marsh *et al.* (2001) refer to are for the same genus of tree, and include data collected in a similar climatic region, but additional research would be required to establish whether the relationships described in Marsh *et al.* (2001) apply directly to the study area.

The distribution of LWD in relation to stream order observed in this study differs from that observed by Diez *et al.* (2001), in Spain and by Gurnell *et al*. (2002) in Pacific Northwest forests. The key difference being that the amount of predicted LWD recruitment tends to increase downstream rather than decrease. This reflects a fundamental difference in the land use practices and climatic conditions between this study area and the other study areas. In this study area riparian vegetation along some 1st and 2nd order streams was cleared for grazing. In contrast the 1st and 2nd order streams in Pacific Northwest and the Iberian peninsula are often surrounded by high relief watersheds and remain partially or fully forested headwater streams. The distribution of riparian vegetation within the study area is strongly controlled by water availability, so that even pre-clearing many of the 1st, 2nd and 3rd order streams would only have supported woodland, whereas open forest would have been present in the littoral zones of 4th, 5th and 6th order streams with small pockets of closed forest found along 5th and 6th order streams. The higher order streams within the study area have significant portions of remnant vegetation along the banks, and it is these portions of vegetation, particularly the open forest and closed forest that are predicted to be producing the large amounts of LWD.

The information generated by the $LWDI_{local}$ approach can be used to support decisions concerning the spatial prioritisation of riparian conservation and rehabilitation projects. Areas along high order streams where closed forest and open forest are providing large amounts of LWD to the stream would be of high priority for conservation as part of a management strategy aimed at maintaining LWD loads within streams. The $LWDI_{local}$ also identifies areas where no woody riparian vegetation is adjacent to the channel. Such areas could be visited and assessed as possible locations for LWD replacement depending on the local conditions.

Previous attempts to describe the spatial distribution of LWD have included the use of airborne remote sensing to identify pieces of LWD within a channel network (Marcus *et al*., 2003). The success of this approach is hampered by the similarity in colour (and therefore reflectance) between LWD and other objects in the stream network. Another approach is the mechanistic model, such as the Riparian Aquatic Interaction Simulator (RAIS) described in Welty *et al.* (2002). Such models seem useful for the areas in which they are developed, but can require a wide range of input data that can be difficult to obtain for large areas. One of the advantages of the $LWDI_{local}$ approach is that, with a limited amount of field work, and some inexpensive satellite imagery, it is possible to estimate the amount of LWD being generated by riparian vegetation anywhere within large (>100 000 ha) catchments.

There are a number of avenues for future research into the LWDI. One of the key areas of future research would be to assess how well the model described in Marsh *et al.* (2001) applies to the study area. This could be done as part of a broader field campaign aimed at assessing whether in-stream LWD volumes are correlated to the $LWDI_{local}$ of the adjacent stream banks or some function of $LWDI_{local}$ values upstream..

The $LWDI_{local}$ could be applied to other areas, but fieldwork would need to be carried out to establish the relationship between vegetation structure and standing timber volumes. Additional fieldwork would also need to be carried out to establish the relationship between standing timber volumes and LWD loads for areas where *Eucalyptus* was not the dominant riparian species. Care would need to be taken in interpreting the LWDIs particularly in environments where the streams capacity to transport LWD is high, and in areas where the wood is less dense, and therefore likely to be more buoyant, and therefore more easily transportable.

$LWDI_{global}$

The $LWDI_{global}$ places the predicted amount of LWD recruitment into a catchment scale context by looking at the relationship between the volume of LWD produced and the volume of the channel into which that piece of LWD would fall. This is done by dividing the area that the LWD projects into the flow (assuming random orientation) by the channel cross-sectional area. This is equivalent to the blockage ratio B described in Abernethy and Rutherfurd (1998). This is a particularly useful measure of the ecological and hydraulic functions of LWD because it simultaneously describes the influence of LWD on in-channel hydraulics (Abernethy and Rutherfurd, 1998) and the influence of LWD in providing visual protection from predators and velocity refuges (Crook and Robertson, 1999). The blockage ratio values used to describe $LWDI_{global}$ are shown in Figure 7.8.

The values shown in Figure 7.8 represent the blockage ratios generated by LWD under bank-full flow conditions assuming a simple U shaped channel. The $LWDI_{global}$ are most sensitive to channel cross sectional area, and less sensitive to vegetation structural classes. The channel dimension parameters bank height and channel width were reliably predicted as a function of Strahler stream order (see section 0 for details) and the $wood_A$ parameter used to calculate LWD recruitment can be reliably predicted using a map of vegetation structural classes (see section 4.3.5 for details).

This means that the values shown in Figure 7.8 are likely to be reliable at the stream

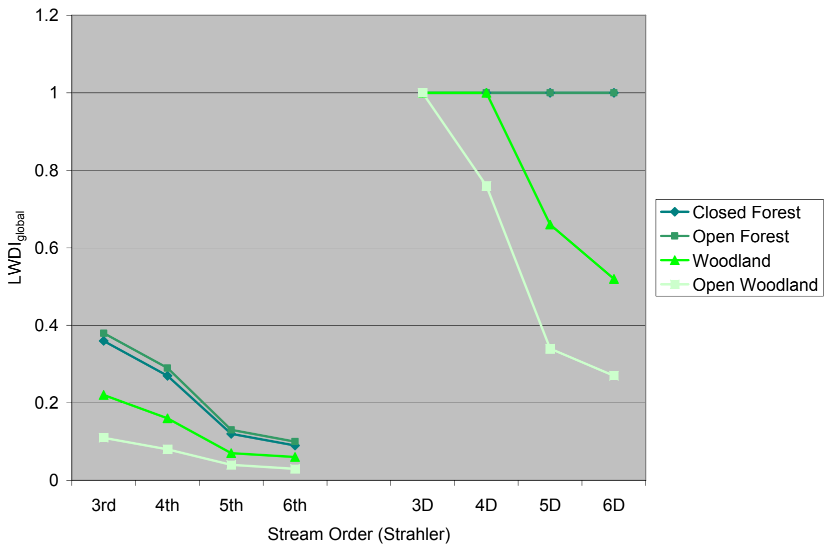

Figure 7.8 Range of $LWDI_{global}$ values

reach scale, provided the LWD is not being transported. There will of course be local variations in the blockage ratio due to both the episodic nature of LWD recruitment, the possibility of LWD transport and the variability in channel geometry for any given stream order. The absolute values of the blockage ratio (Figure 7.8) are sensitive to the U shaped channel assumption. If the channels are assumed to be V rather than U shaped then the blockage ratios all increase. However the relative importance of any given vegetation class and stream order combination remains unchanged. The high blockage ratios encountered on D class channels (Figure 7.8) represent a scenario whereby the volume of LWD recruited may be larger than the channel. In this case the channel may either be partly or fully blocked, or the tree may simply bridge the channel and provide some blockage in the form of tree limbs. Given the low unit stream power calculated for these D class channels the presence of a large piece of LWD may have significant impacts on the floodplain geomorphology, potentially leading to new channelization to enable flow to bypass the blockage caused by the LWD. This is consistent with the theoretical influence of LWD on floodplains as described in Brooks *et al* (2003).

One of the major limitations of the $LWDI_{global}$ model as shown in Figure 7.8 is that it only shows the blockage ratio at a single time, in this instance when the flow is bank-full. This underemphasises the importance of LWD in higher order streams. Blockage ratios in these streams are likely to rise rapidly as channel network starts to dry up and are likely to provide valuable habitat as the dry season progresses. This effect is enhanced by the tendency for LWD to accumulate at the base of the channel. The temporal nature of the blockage ratio is approximated in Figure 7.9. So, while the LWD in a 4D order stream may provide valuable instream habitat during high stage events, LWD becomes increasingly important in higher order streams as the dry season progresses (Note that the sudden drop in blockage ratio represents the point at which the channel dries out and the LWD therefore ceases to provide any aquatic habitat due to the lack of water).

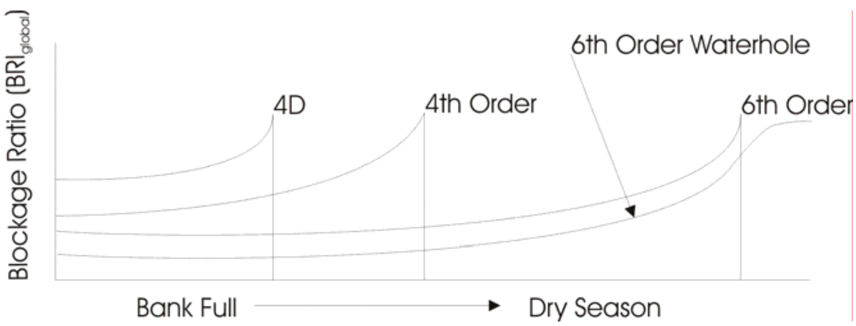

Figure 7.9 Theoretical change in BRI_{global} over time.

To account for this temporal dynamic it is important to consider both the LWDI and SSI (described in greater detail in the following section) simultaneously, because the SSI is calculated for those areas of the channel network that are likely to support waterholes. Consequently the stands of woody vegetation capable of providing shade to waterholes are also those likely to produce LWD to the waterholes. So in some senses the areas identified by the LWDI represent the maximum extent of the aquatic habitat during the wet season habitat, and the shading and LWD recruitment capacity of the littoral vegetation in this area are essential during the wet season. The SSI also identifies stands of littoral vegetation that provide shade and LWD to the limited proportion of the stream network that supports the aquatic ecosystem during the dry season.

7.3.5. Stream Shade Index

SSI_{local}

One of the main advantages of the SSI_{local} is that provides an estimate of how the amount of stream shade provided by a stand of riparian vegetation has changed since European settlement. Furthermore it can do so without the complex data requirements and computational intensity of the Chen model (Chen *et al*., 1998a; Chen *et al*., 1998b). This means that a broad description of the stream shading function of riparian vegetation can be quickly and easily calculated for large areas using inexpensive satellite imagery and some simple terrain analysis.

Another advantage of the SSI is that it enables rapid identification of high order stream reaches (that are likely to support aquatic life in the study area) that are devoid of any riparian vegetation. These areas would be a high priority in terms of regeneration to restore the stream shading to pre-European levels. This is of importance in the Fitzroy basin where the amount of sunlight reaching the water surface can rapidly alter the temperature and chemistry of isolated waterholes that support the aquatic ecosystem during the dry season, potentially resulting in fishkill events (Puckridge *et al*., 1998; Erskine *et al*., 2005).

The SSI_{local} provides a robust estimate of how much the stream shading has changed as a result of changes to the vegetation, because it is calculated using a local reference, and therefore is insensitive to channel geometry. The SSI_{local} assumes that the channel geometry hasn't changed between pre-settlement and the current day. This assumption may be violated in areas where channel geometry has been altered via cattle activity, channel incision or channel infilling. In such areas the SSI_{local} will still provide an indication as to how the stream shading capacity of the riparian vegetation has changed, but may under or over estimate the magnitude of this change. Bearing this limitation in mind, the SSI_{local} assumes that any change in the amount of sunlight reaching the streams surface is solely due to changes in the riparian canopy architecture and projected foliage cover (PFC). Both the canopy architecture parameters and the PFC parameter were reliably predicted using the vegetation classification (see Section 4.3.1 for details).

Consequently the SSI_{local} values are likely to be fairly accurate in terms of estimating the change in the amount of shade provided by riparian vegetation.

One limitation to this accuracy is the assumption (as previously discussed) about the distribution of pre-settlement littoral vegetation. If there were areas of littoral zone on 4th 5th or 6th order stream that contained woodland (rather than open or closed forest) prior to settlement, then the SSI_{local} will indicate a reduction in the amount of stream shade (SSI_{local} = 0.5) when there has not actually been a reduction.

Another limitation of the SSI (both local and global) is that it describes the importance of a stand of vegetation in providing shade to the adjacent channel, however it doesn't calculate the amount of sunlight arriving at the stream surface (which is a function of the amount of shade provided by both banks and their littoral vegetation). This reflects the fact that the SSI_{local} and SSI_{global} were developed as tools for prioritizing riparian vegetation based on the amount of stream shade each stand of vegetation provides, and identifying areas where vegetation is likely to assist in providing stream shade.

SSI_{global}

The SSI_{global} is useful because it can quantify the relative importance of channel-adjacent vegetation in providing shade to the stream[31]. This is particularly useful because it identifies areas where planting riparian vegetation is likely to have a significant impact on the amount of sunlight reaching the stream, and also identifies areas where planting

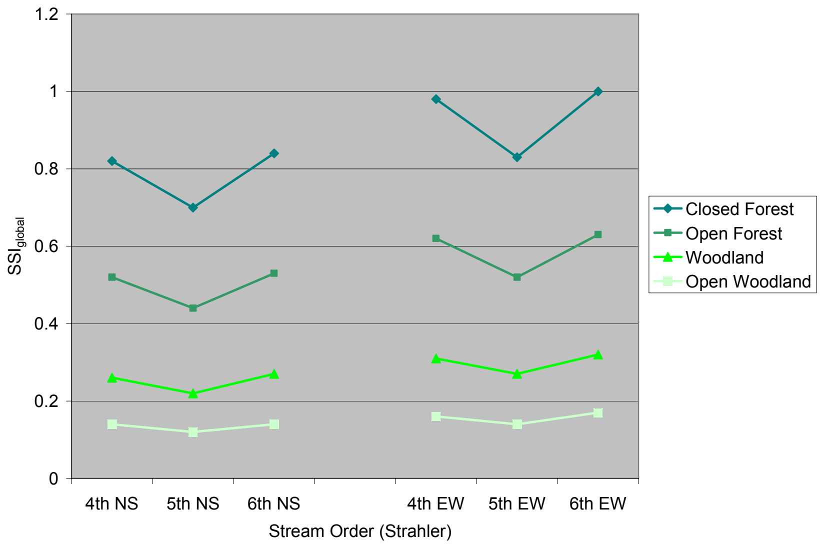

Figure 7.10 Sensitivity analysis of SSI_{global}

the same riparian vegetation would have considerably less impact.

Please note that the NS and EW terms in Figure 7.10 refer to the channel orientation (north-south, or east-west respectively). The SSI_{global} is most sensitive to the canopy geometry parameters, and in particular the PFC. The PFC is reliably predicted by the vegetation classification, and the vegetation classification has a classification accuracy of 96%, so the PFC parameter is likely to be fairly reliable throughout the study area. As a consequence of this the SSI_{global} is likely to be reasonably reliable, although it is sensitive to a number of other parameters. The SSI_{global} is sensitive to both channel orientation and channel geometry. The channel network was manually digitized to match the channel network observed in the satellite imagery, so the channel orientation is fairly accurate, although the conversion of the channel network from vector to grid does generate some small errors. The SSI_{global} is sensitive to the accuracy with which the channel geometry is estimated as shown in Figure 7.10. Accurate channel geometry estimates are required to improve the reliability of the SSI_{global}, particularly in calculating non-zero values. The accuracy with which channel geometry is estimated impacts on the reliability of the SSI_{global} in two ways. It influences the identification of the stream order upon which the riparian vegetation has the largest influence. It also influences the maximum value of the θ_{RV} against which all other θ_{RV} values are normalized. If the research into the relationship between catchment characteristics and channel dimensions, discussed previously in terms of DNI_{global}, were carried out, then the outputs could be used to address this particular limitation. The SSI_{global} is also sensitive to the probability of waterhole (*Pwh*) parameter (without which the SSI_{global} values for 6^{th} order streams would be lower than that of 5^{th} order streams, based solely on channel geometry). The *Pwh* parameter is calculated from long term gauging station records, and the values calculated from these records fit with expectations, *i.e.* larger rivers have a bigger base flow component and therefore flow for longer and are therefore more likely to support waterholes (Puckridge *et al*., 1998).

Another limitation of the SSI_{global} is that it doesn't account for the location of the waterhole relative to the centre of the channel (*i.e.* it assumes that all waterholes are at the centre of the channel). This is likely to lead to an underestimate in the maximum θ_{RV} value (*i.e.* a tree that overhangs a waterhole is likely to have a large shading influence than a tree on the top of a bank with a waterhole in the centre of the channel. In reality there are a wide range of vegetation and channel geometry scenarios, combined with a range of waterhole location scenarios, which limits the capacity of the index to infer the exact amount of shade provided by any specific stand of vegetation. The simplified channel geometry and central waterhole assumptions are necessary because remote sensing and terrain analysis are unable to resolve which of the many canopy geometry,

[31] These figures should be interpreted with some caution because they are sensitive to the accuracy of the channel dimensions for each stream order.

channel geometry, and waterhole location scenarios should be used at each location along high order streams. However it is important to keep those assumptions in mind when interpreting the index.

There are a number of avenues for further research into the SSI_{global}. The most important of which is providing reliable channel geometry measurements, because without these the index is relatively unreliable. Fieldwork could also be carried out to establish the reliability of the θ_{RV} value, based on a series of predicted vs observed θ_{RV} values for various points throughout the catchment adjacent to different stream orders.

The parameters used to calculate the SSI_{global} could also be used to parameterize a stream shade model that could be used to estimate stream temperatures, which can in turn be linked to temperature sensitivities of native species to identify the influence of maintaining and/or increasing stream shade on the mortality rates of aquatic biota, based on the approach described in Rutherford *et al.* (1997).

The SSI_{global} could be refined further by combining it with a map of waterholes for the study area. A map of waterhole locations could be collected at the end of a drought period using light plane or helicopter. This would then be combined with the SSI_{global} to highlight specific stands of vegetation that were capable of providing shade and producing large amounts of LWD and were immediately adjacent to waterholes. There is an interesting feedback between waterholes and vegetation structure. Permanent waterholes indicate a permanent supply of water. In semi-arid climates, where water is a limiting factor for plant growth, a permanent water supply is likely to support the highest canopy cover anywhere within the landscape based on the concepts of eco-hydrology (Caylor *et al.*, 2005). Therefore it is possible that stands of closed forest immediately adjacent to the channel are indicative of permanent waterholes (or areas with water supply significantly greater than elsewhere within the catchment). It would be interesting to examine this relationship by combining the waterhole map with the vegetation structural map, particularly in light of the areas predicted to have groundwater in the root zone throughout the year as identified using the preliminary MODIS NDVI analysis described in the DNI_{global} section of the discussion.

In applying the SSI_{global} to other areas it would be necessary first of all to carry out fieldwork to establish all of the parameters required to calculate the SSI_{global} (with particular attention to channel geometry). It would also be necessary to review assumptions about solar azimuth angle also. For the purposes of this study the solar azimuth angle is considered to be 90 (*i.e.* the sun tracks from due east to due west and is directly overhead at noon) which is reasonable for mid summer at the study area (which is located on the Tropic of Capricorn). In applying this approach to areas further away from the equator a different solar azimuth would be required, and this will impact on the magnitude of the θ_{RV} parameter for vegetation of a fixed geometry (the further from the equator the larger the θ_{RV} for any given stand of riparian vegetation.

The SSI_{global} would also be unreliable in areas with more extreme terrain (the study area is relatively flat, particularly the floodplains where the SSI_{global} is calculated). In areas where terrain provides significant amounts of shade to the stream, the SSI_{global} is likely to overestimate the importance of riparian vegetation in providing shade.

7.4 Use of RFIs for catchment management purposes

One of the potential applications for the riparian function indices (RFIs) is as decision support tools for catchment managers who are required to make decisions about allocating limited resources to achieve various objectives such as reducing in-stream sediment loads, maintaining water quality and protecting the aquatic ecosystems. The RFIs will provide useful information to catchment managers faced with such decisions and could be used in a number of ways. An index could be used to focus on a specific process within the catchment, indices can be assessed in functional groups, or all indices can be considered collectively as part of an integrated catchment management plan.

7.4.1. Using Individual Indices

The use of individual indices to address specific problems is relatively self explanatory. An index such as the STI could be used to identify areas in the catchment where there are areas of bare soil immediately adjacent to the channel. Such areas would be a high priority in a catchment, such as the Nogoa and Comet, where hillslope sediment is one of the major contributors to in-stream sediment loads. The catchment manager would then be able to identify where installing additional riparian buffer strips or reducing grazing pressure would have the greatest impact in reducing the amount of hillslope-generated sediment reaching the stream. The indices are more informative when used in combination to focus on a catchment scale process, such as sediment transport and in-stream sediment loads, pollutant loads, and aquatic ecosystem values.

7.4.2. Functional Index Groups

Three scenarios are described below that detail how a series of RFIs can be combined to address catchment scale processes. The capacity to combine these indices to focus on catchment scale processes represents an important new development in integrated riparian management at the 'whole-of-catchment' scale. It enables the allocation of resources to multiple locations in the catchment, in such a way that those resources are allocated to areas where they are likely to have the greatest effect in reducing undesirable impacts, or protecting desirable riparian functions.

Sediment Load Reduction Scenario

For catchments where in-stream sediment loads and sediment exports are a major concern, the STI, and BRI indices could be analysed simultaneously to identify a range of riparian zone management options that would be used in conjunction to reduce the amount of in-stream sediment, and reduce the amount of sediment exiting the catchment. The STI would be used to identify hillslope areas that were contributing sediment to the stream, and identify areas where the installation of riparian buffer strips, reduced grazing pressure, or riparian fencing would be most effective in reducing the amount of hillslope-generated sediment entering the stream. The BRI would be used to identify areas where stream bank erosion could be mitigated by the planting of woody riparian vegetation, or the installation of riparian fences to allow woody vegetation to regenerate. The cost, feasibility and likelihood of land-holder adoption would have to be assessed by the catchment manager, or catchment management agency. However these two indices in combination could certainly be used to identify areas throughout the catchment that are potential sediment sources. In a survey of landholder sentiment towards riparian zone management in the Fitzroy basin Fielding *et al.* (2005) established that approximately half the landholders surveyed have strong intentions to actively manage their riparian zones via riparian fencing, altered stocking rates or installation of off-stream watering points, and half had weak or no intentions to do so. Clearly, the capacity to convince the weak intenders that the riparian zones on their properties are directly impacting on the in-stream water quality and the water quality of the Fitzroy estuary and Great Barrier Reef Marine Park is highly important. The indices developed in this thesis will be able to assist in this process.

Pollutant Load Reduction Scenario

For catchment areas where in-stream pollutants were a major problem, and maintaining water quality was a high priority then the STI, BRI and DNI indices could be used in conjunction to: 1. Identify areas that were non-point-source pollution was entering the stream network using the STI as described above; and 2. Identify floodplain and channel adjacent areas that needed to be protected because they were providing sites for denitrification in the system. The timeframe for regenerating the denitrification potential for a specific site based on native vegetation regeneration is unclear. Consequently this is approach is not developed further here.

Aquatic Habitat Protection Scenario

For a catchment where maintaining the aquatic ecosystem was a high priority then the LWDI or SSI would be used to identify areas of riparian vegetation adjacent to high order streams, providing a range of important functions for the aquatic ecosystem. These areas would be a high priority for a protection because the functions provided by these stands of vegetation take a long time (decadal timescale) to establish. So, for a catchment manager concerned solely with maintaining terrestrial and aquatic biodiversity and protecting the aquatic ecosystem, the highest priority would be protecting high SSI and LWDI value stands of riparian vegetation adjacent to high order streams. This is because protecting these areas is a more efficient use of resources than trying to regenerate/replant riparian vegetation to perform those functions after the riparian vegetation has been removed.

7.4.3. Combining All Indices for an Integrated Riparian Management Strategy

As discussed above, combining a series of the RFIs to focus on particular processes, provides a useful tool to catchment managers concerned with a specific problem in the catchment. However the RFIs are most useful when considered collectively. This is because there is little point in maintaining levels of riparian shade and aquatic large woody debris production if the water flowing through the high order streams is excessively turbid, has a high nitrogen concentration, and the waterholes are filled up with coarse sediment. Consequently riparian zones need to be managed in an integrated fashion at a catchment scale, and the RFIs provide the tools to do so. The following riparian management strategy has been formulated using all of the RFIs. The management strategy consists of a series of phases, based on the timescales at which the riparian functions operate, and the timescales at which they can be restored.

Phase 1: Low order streams adjacent to hillslopes management

Identify areas of bare soil and heavy grazing adjacent to low order streams using the STI. These are the priority areas for installation of riparian buffers and/or riparian fencing[32]. Grassed riparian buffer strips and grassed waterways are relatively quick to establish, and it is important to reduce the amount of hillslope-generated sediment and sediment sorbed pollutants entering the stream network to reduce turbidity and increase water quality downstream. Use the BRI_{global} to identify banks that are reinforced with woody vegetation (for protection) and areas without any reinforcement by woody vegetation (for riparian fencing and planting, particularly along 2nd and 3rd order streams, where riparian grasses alone are insufficient to reinforce the banks).

Phase 2: Floodplain management

Prioritize areas for protection based on the DNI_{global} and BRI_{global}. Priority areas for restoration could be identified based on zero index values for both DNI and BRI. Restoring DNI and BRI values adjacent to the channel is likely to involve some form of bush re-establishment or regeneration. The results described in Hancock *et al.* (1996) would suggest that areas of zero index value, adjacent to areas with non-zero values would be the optimal place to start. This is because it is easier to regenerate bush if there is remnant bushland adjacent to it, rather than starting in the middle of an empty paddock.

Away from the channels, riparian vegetation management would be based on the DNI. Areas with non-zero values would be a priority for conservation/protection (although not

---

[32] The cost of fencing off all 1st order streams subject to grazing may be unrealistic, in which case impressing to graziers the importance of maintaining ground cover levels in these areas becomes a priority.

as high a priority as those identified using the composite DNI/BRI scores described above). Suggesting management scenarios for areas of the floodplain that have been cleared of all woody vegetation is beyond the scope of this thesis. However the author would suggest that maintaining cover levels within these areas is of particular importance given their potential to erode during flood events.

Phase 3: High order stream management

Once phases one and two have been implemented, areas adjacent to high order channels that perform multiple functions would be identified and protected. Areas for protection/conservation would be selected based on composite scores of the following indices LWDI, BRI, DNI, and SSI. Alternatively, areas could be selected based on a specific index, if a specific process was of concern for these higher order streams. The composite score could also be based on a weighted mean depending on the relative importance of the processes within the catchment in question. Although they are identified relatively late in the riparian management strategy, stands of mature vegetation, adjacent to high order channels (which have high LWDI, BRI, DNI and SSI values) are the highest priority in terms of protection and conservation. Not only because they provide a wide range of riparian functions, but also because they are generally limited in extent, they are difficult to re-establish once removed, and can take many decades to reach maturity to provide the full range of riparian functions.

Areas for restoration could be identified as described above by identifying zero index values adjacent to stands of riparian vegetation with non-zero values for a range of indices. An alternative method of prioritizing restoration would be to identify waterhole locations throughout the network of high order streams, and base stream restoration works around those waterhole locations.

Phase 4: Monitor

Biannual updates to assess changes in the RFIs would provide useful feedback for catchment managers, and would allow identification of ongoing problem areas. Ongoing monitoring of in-stream indicators, such as sediment loads, pollutant concentrations and waterhole temperature ranges would provide valuable feedback to the catchment managers and scientists to compare the changes made to the system with the changes observed in the system. It is important to note that due to the time frames at which sediment transport and other catchment scale processes operate, it may be possible to implement the four phases of the riparian management plan, and only observe minor changes to sediment loads in the immediate future, with more significant changes place over longer periods. Consequently the monitoring phase may need to continue for many years to detect any long term reductions in sediment output that result from the integrated riparian management strategy.

Chapter 8 Conclusions

Land use changes within the Nogoa and Comet catchments have lead to the removal and alteration of riparian vegetation at various locations throughout both catchments. The approach developed in this thesis enables the quantification of how these changes have impacted on the capacity of riparian vegetation to perform a range of important functions. The combination of field data and historical gauging station data with recent developments in image processing and terrain analysis provides new insight into the important spatial and temporal dynamics of the following riparian zone functions: sediment trapping; bank stabilization; denitrification; stream shading and large woody debris production. This capacity to quantify riparian vegetation functions, and understand how human activities can improve or reduce these functions provides new information to catchment managers who are faced with making decisions about allocating resources across large catchments to meet end-of-valley targets in terms of reduced sediment and pollutant loads (Table 8.1 and Table 8.2). In addition to this the RFI_{global} algorithms can potentially be adapted to improve existing long-term or event based models of sediment/pollutant transport or stream ecology.

Table 8.1 Priority areas for protection (hectares of littoral zone)

Process	**1st order**	**2nd order**	**3rd order**	**4th order**	**5th order**	**6th order**
Sediment trapping (STI=1)	5215	2303	1283	483	86	356
Bank stabilisation (BRI_{local}=1)	3715	2430	1853	452	391	686
Denitrification (DNI_{local}=1)	N/A	1500	1312	509	115	590
Stream Shade (SSI_{local}=1)	N/A	N/A	N/A	310	42	651
LWD production ($LWDI_{local}$=1)	N/A	N/A	1853	452	97	705

Table 8.2 Priority areas for restoration (hectares of littoral zone)

Process	**1st order**	**2nd order**	**3rd order**	**4th order**	**5th order**	**6th order**
Sediment trapping (STI=0)	1097	502	156	<1	<1	<1
Bank stabilisation (BRI_{global}=0)	917	427	631	347	50	56
Denitrification (DNI_{global}=0)	N/A	223	130	97	110	<1
Stream Shade (SSI_{global}=0)	N/A	N/A	N/A	780	110	201
LWD production ($LWDI_{global}$=0)	N/A	N/A	631	780	110	201

Table 8.1 summarises results presented in previous chapters and demonstrates how the RFI approach can be used to identify priority areas for protection to conserve the remaining riparian vegetation that is currently performing a range of functions. Table 8.2 demonstrates how the RFI approach can be used to identify priority areas for restoration, and how restoration in different parts of the catchment is required to restore specific functions. Maps of each RFI and the rationale for not calculating some indices for certain stream orders are contained in Chapter 6.

Sediment Trapping Index

Grazing and cropping practices have lead to a decrease in the sediment trapping capacity of many littoral zones within the study area. This is of greatest concern in areas where hillslopes drain directly into the stream channel. The 1500 hectares of riparian zone that contained bare soil and heavy grazing, as highlighted by the STI, are areas that would need to be targeted to reduce the 1750 kt y^{-1} of hillslope generated suspended sediment exported from the Fitzroy catchment (value based on SEDNET model results described in McKergow *et al.* (2005). The areas of highest priority would be those that are not upstream of Fairbairn reservoir. Future development of the STI could follow a number of avenues including:

1. Fieldwork to establish whether remotely sensed estimates of grazing pressure can reliably predict ground cover levels beneath tree canopies;
2. Further analysis of the MODIS MOD13Q1 product to quantify the temporal dynamics of the sediment trapping capacity of riparian zones, with a particular emphasis on using NDVI timeseries to estimate stocking rate, and thereby estimate ground cover levels (both green and senescent) at different times of the year;
3. Using the STI in combination with information about riparian zone slope and width to calculate the sediment delivery ratios for different particle size classes to estimate the capacity of riparian zones to trap pollutants such as phosphorous that are sorbed to small particles;
4. Linking the STI with an event-based sediment transport model to quantify the impact that various ground cover management strategies would have on reducing end-of-valley sediment loads.

Bank Reinforcement Index

The removal of woody vegetation from riparian zones in the Nogoa and Comet catchments has lead to a dramatic increase in the risk of bank erosion. The combination of the bank reinforcement processes described in Abernethy and Rutherfurd (1998) with a parameter that can be linked to a vegetation classification (the number of trees per hectare) is an improvement in our ability to predict the amount of bank reinforcement at any point in the catchment. In combination with estimates of unit stream power and a detailed description of the channel network this enables more detailed predictions about where bank erosion is likely to occur. This ability not only allows improved estimates of bank erosion in sediment transport models, it also enables targeted strategies to reduce the potential for bank erosion in the highest risk areas. The BRI_{global} is currently limited by the reliability of the unit stream power values assigned to each stream order. To address this limitation and to further develop the BRI (both local and global) future research should focus on the following:

1. Comparing BRI_{global} values with observations of bank erosion to assess whether bank erosion is occurring in the high risk areas predicted by BRI_{global};
2. Improving the reliability of the stream power estimates applied to each link in the channel network. This would ideally be based on the catchment area and slope for each stream link rather than the current Strahler stream order based estimates;
3. Examining the relationship between channel geometry and the Strahler stream order sub-classes (A, B, C and D), this would also potentially improve the reliability of the DNI_{global} calculations.;
4. Inclusion of the BRI_{global} results into long term sediment transport models; and
5. Improved estimates of the spatial location of bank erosion through the inclusion of bank material information and channel planform morphology.

The Denitrification Index

The DNI_{global} describes the relative importance of channel-adjacent areas, and floodplains in terms of denitrification, and provides an estimate of how much denitrification is likely to take place at each location. Soils beneath stands of closed forest and open forest located in floodplain littoral zones on 2nd and 3rd order streams were identified as the places where denitrification was most likely to take place, based on the coincidence of high concentrations of water soluble carbon (WSC) in the topsoil and high frequency of bank full events. Denitrification was less likely to occur in progressively higher stream orders due to the fact that flow reaches bank full capacity less frequently for the larger streams. The results of the DNI_{local} indicate that land clearing and the presence of cropping on the floodplain has resulted in a substantial decrease in the denitrification potential of riparian zones throughout the study area. This has potentially resulted in a switch in the between nitrogen sink to nitrogen source in floodplain soils that are subject to the application of nitrogen fertilizer. This is of particular concern on high order streams because nitrate that enters these high order streams is more likely to be delivered to the estuary, and, according to the DNI_{global} model is less likely to encounter conditions suitable for denitrification before it arrives at the estuary.

The major limitation of the DNI_{global} is its sensitivity to uncertainty in the prediction of channel dimensions and thereby estimates of bank-full and overbank flow frequencies, and an absence of WSC measurements from riparian soils within the study area. Despite the limitations of the DNI_{global}, the following catchment management actions would be prudent to reduce the amount of nitrogen reaching the estuary. First, cease removal of riparian (both floodplain and littoral) vegetation from the floodplains of all higher order stream with a particular emphasis on 2nd and third order streams, and an additional emphasis on the two forest structural classes. Second, where possible, exclude cattle from the stream channel to reduce the amount of nitrogen rich animal waste being generated directly into the channel network. Third, review the amount of nitrate being applied to flooplain soils by farmers engaged in broadacre and irrigated cropping to assess whether lower application rates are feasible, and encourage farmers who are applying nitrate or nitrogen rich fertilizers to restore and maintain the woody riparian vegetation on their property.

To address the limitations of the existing DNI_{global} model and further develop a catchment scale model for denitrification the following avenues of research will be pursued:

1. Measurement of WSC and denitrification enzyme activity for each vegetation type and stream order combination within the study area;
2. Based on the results of these measurements a catchment scale model of denitrification would be developed which could be coupled with estimates of nitrogen inputs from various land uses to develop a catchment scale nitrogen budget; and
3. Investigation of the MODIS MOD13Q1 product to assess whether NDVI timeseries can be used to describe the dynamics of WSC at depth on large floodplains.

The Large Woody Debris Index

The $LWDI_{local}$ results indicate that removal of woody vegetation from the riparian zone has lead to a significant decrease in the quality of the aquatic habitat during the wet season, with fewer velocity refuges during flood events, increased habitat fragmentation and fewer breeding sites for the 26 species of native fish that live in the study area. Fencing and regeneration of woody vegetation along stream and river banks would ensure the long term potential for LWD recruitment, whilst simultaneously improving the bank stability and denitrification potential of these littoral zones. This is particularly important for 3rd and 4th order streams which have experienced the greatest reduction in the amount of stream bank vegetation. The $LWDI_{global}$ should be considered in conjunction with the SSI, because they describe the importance of woody riparian vegetation to aquatic ecology from a ‘wet season’ and ‘dry season’ perspective respectively. One of the advantages of the $LWDI_{global}$ is that it provides the capacity to identify stands of vegetation that are likely to produce large amounts of LWD, and thereby, enables more targeted vegetation management strategies for high order streams.

The main disadvantage of the LWDI is that the index predicts the potential for recruitment, rather than actual LWD volumes. Future research in the LWDI can take a number of directions including:

1. Field work to identify whether LWD recruitment is a useful predictor of local in-stream LWD volumes, or whether a transport term needs to be included to estimate LWD distribution; and

2. Integrate the $LWDI_{global}$ model over time to encapsulate the behaviour of the blockage ratio at different stage heights;

The Stream Shading Index

The SSI_{global} model indicates that while riparian vegetation provides the most shade to 4th order channels (based on channel and canopy geometry) and provides progressively less shade to higher order streams on account of deeper channels lessening the influence of riparian vegetation in providing stream shade. However the shading function is particularly important along 6th order streams because it is on these streams that waterholes are most likely to form. The inclusion of a channel orientation term in the SSI_{global} provides additional insight into the relative importance of each stand of riparian vegetation in providing shade to the channel.

Future research into the SSI could include the following:

1. Coupling the SSI_{global} with models of in-stream water temperature;

2. The inclusion of a solar azimuth term to allow the SSI_{global} model to be applied to other geographic locations;

3. Fieldwork along the base of higher order streams to assess the reliability of the SSI in terms of amount of shade provided by riparian vegetation; and

4. Assess whether a thalweg location model improves the reliability of stream shade estimates.

Applying the RFI approach to other areas

The RFI approach could be readily applied to other areas that are subject to similar climate and land use practices, however the models that underly each RFI_{global} would need to be modified prior to application in other climatic areas. The use of multi-temporal data to estimate grazing pressure could be applied to other climatic areas, however the relationship between NDVI timeseries and grazing pressure would need to be re-examined. Furthermore it would be necessary to use a higher spatial resolution sensor to identify the narrow riparian buffer strips that are used for runoff control in more temperate climates with lower rainfall intensities. The BRI could be applied to more temperate riparian zones, however maximum rooting depth (as constrained by the height of the water table) would need to be incorporated into the BRI_{global} to account for influence of rooting depth on bank stability. The DNI_{global} model has been developed specifically for a semi-arid setting, and would need to be modified significantly prior to application in a temperate or wet tropical catchment. The use of stage height records to calculate the frequency of denitrification events at different locations throughout the catchment could certainly form the basis for a component of such a model, however the distribution of WSC and the role of shallow groundwater generated in hillslope soils in temperate catchments would need to be considered. The $LWDI_{global}$ model would need to be revised in the context of LWD generation mechanisms and the potential for LWD transport, particularly in areas with higher stream power or more buoyant wood. The SSI_{global} would need to be modified to include terrain and solar azimuth terms particularly if it were applied to areas outside the tropics or in areas with more pronounced terrain closer to the stream channel.

Catchment managers using the information provided by an analysis of the RFI results may choose to use individual indices to identify specific problem areas, or combine the index results for an integrated riparian zone management plan. Such a plan could apply a series of weights to individual indices, with the weights determined by community or the decision-makers values. This weighted approach would have advantages over current ‘whole-of-river’ indexes insofar as each of the five riparian zone functions is explicitly represented, and the component indices can be used to identify suitable management actions for priority areas.

Reference List

Abdelouas, A., Deng, L., Nuttall, E., Lutze, W., Fritz, B. and Crovisier, J.L. (1999) 'In Situ Biological Denitrification of Groundwater.' *Comptes Rendus De Lacademie Des Sciences Series Iia Earth and Planetary Science* 328, 161-166.

Abe, T. and Nakamura, F. (1996) 'Pool and cover formation by coarse woody debris in a small low-gradient stream in northern Hokkaido.' *Journal of the Japanese Forestry Society* 78, 36-42.

Abernethy, B. and Rutherfurd, I.D. (1998) 'Where along a river's length will vegetation most effectively stabilise stream banks?' *Geomorphology* 23, 55-75.

Abernethy, B. and Rutherfurd, I.D. (2001) 'The distribution and strength of riparian tree roots in relation to riverbank reinforcement.' *Hydrological Processes* 15, 63-79.

Abrams, M., Hook, S. and Ramachandran, B. (2002) ASTER Users Handbook (Version 2). California USA. Jet Propulsion Laboratory.

Agrawal, G.D., Lunkad, S.K. and Malkhed, T. (1999) 'Diffuse Agricultural Nitrate Pollution of Groundwaters in India.' *Water Science and Technology* 39, 67-75.

Anderson, G. P., Berk, A., Acharya, P. K., Matthew, M. W., Bernstein, L. S., Chetwynd, J. H. , Dothe, H. S., Adler-Golden, M. A., Ratkowski, J., Felde, G. W., A. Gardner, J. A., Hoke, M. L., Richtsmeier, S. C., Pukall, B., Mello J., and Jeong, L. S.'MODTRAN4: Radiative Transfer Modeling for Remote Sensing, In Algorithms for Multispectral, Hyperspectral, and Ultraspectral Imagery.' in Proceedings of SPIE Sylvia, V.I., Chen, S. and . Descour, M.R., (Eds.) 4049, edn. 176-183p. (2000)

Anderson, J.R. (1993) Report 2. Implementation Manual. Brisbane, Queensland: Queensland Department of Primary Industries.

Archer, E.R.M. (2004) 'Beyond the "Climate Versus Grazing" Impasse: Using Remote Sensing to Investigate the Effects of Grazing System Choice on Vegetation Cover in the Eastern Karoo.' *Journal of Arid Environments* 57, 381-408 .

Armstrong, J.D., Kemp, P.S., Kennedy, G.J.A., Ladle, M. and Milner, N.J. (2003) 'Habitat Requirements of Atlantic Salmon and Brown Trout in Rivers and Streams.' *Fisheries Research* 62, 143-170.

Aspinall, R.J. (2002) 'Use of logistic regression for validation of maps of the spatial distribution of vegetation species derived from high spatial resolution hyperspectral remotely sensed data.' *Ecological Modelling* 157, 301-312.

Bartkow, M.E. and Udy, J.W. (2004) 'Quantifying Potential Nitrogen Removal by Denitrification in Stream Sediments at a Regional Scale.' *Marine and Freshwater Research* 55, 309-315.

Basnyat, P., Teeter, L.D., Flynn, K.M. and Lockaby, B.G. (1999) 'Relationships between landscape characteristics and nonpoint pollution inputs to coastal estuaries.' *Environmental Management* 23, 539-549.

Basnyat, P., Teeter, L., Lockaby, B.G. and Flynn, K.M. (2000) 'Land Use Characteristics and Water Quality: A Methodology for Valuing of Forested Buffers.' *Environmental Management* 026, 153-161.

Belsky, A.J., Matzke, A. and Uselman, S. (1999) 'Survey of livestock influences on stream and riparian ecosystems in the western United States.' *Journal of Soil & Water Conservation* 54, 419-431.

Blair, N. and Crocker, G.J. (2000) 'Crop Rotation Effects on Soil Carbon and Physical Fertility of Two Australian Soils.' *Australian Journal of Soil Research* 38, 71-84.

Bolstad, P. (2003) *GIS Fundamentals: A first text on geographic information systems*, White Bear Lake, Minnesota: Eider Press.

Brodie, J.E. and Mitchell, A.W. (2005) 'Nutrients in Australian tropical rivers: changes with agricultural development and implications for receiving environments.' *Marine and Freshwater Research* 56 (3),:279-302.

Brooks, A.P., Brierley, G.J. and Millar, R.G. (2003) 'The long-term control of vegetation and woody debris on channel and flood-plain evolution: insights from a paired catchment study in southeastern Australia.' *Geomorphology* 51, 7-29.

Bryant, R.G. and Gilvear, D.J. (1999) 'Quantifying geomorphic and riparian land cover changes either side of a large flood event using airborne remote sensing.' *Geomorpholgy* 29 , 307-321.

Bunn, S.E., Davies, P.M. and Mosisch, T.D. (1999) 'Ecosystem measures of river health and their response to riparian and catchment degradation .' *Freshwater Biology* 41, 333-345.

Burt, T.P., Matchett, L.S., Goulding, K.W.T., Webster, C.P. and Haycock, N.E. (1999) 'Denitrification in riparian buffer zones: the role of floodplain hydrology.' *Hydrological Processes* 13, 1451-1463.

Caraco, N.F. and Cole, J.J. (2001) 'Human influence on nitrogen export: a comparison of mesic and xeric catchments.' *Marine and Freshwater Research* 52, 119-125.

Carnahan, J.A. (1989) Australia's vegetation in the 1780s. Canberra: Australian Surveying and Land Information Group.

Carroll, C., Merton, L., Burger, P., Bell, K., Sallaway, M.M. and Yule, D.F. (2000) 'Impact of vegetative cover and slope on runoff, erosion, and water quality for field plots on a range of soil and spoil materials on central Queensland coal mines.' *Australian Journal of Soil Research* 38, 313-328.

Caylor, K.K., Manfreda, S. and Rodriguez-Iturbe, I. (2005) 'On the Coupled Geomorphological and Ecohydrological Organization of River Basins.' *Advances in Water Resources* 28, 69-86.

Chen, D., Carsel, R.F., McCutcheon, S.C. and Nutter, W.L. (1998a) 'Stream temperature simulation of forested riparian areas: I. Watershed-scale model development.' *Journal of Environmental Engineering* 124, 304-315.

Chen, D., McCutcheon, S.C., Norton, D.J. and Nutter, W.L. (1998b) 'Stream temperature simulation of forested riparian areas: II Model application.' *Journal of Environmental Engineering* 124, 316-328.

Chen, D.J.Z. and MacQuarrie, K.T.B. (2004) 'Numerical Simulation of Organic Carbon, Nitrate, and Nitrogen Isotope Behavior During Denitrification in a Riparian Zone.' *Journal of Hydrology* 293, 235-254.

Church, M. (2002) Geomorphic thresholds in riverine landscapes. *Freshwater Biology* 47, 541-557.

Cirmo, C.P. and McDonnell, J.J. (1997) 'Linking the hydrologic and biogeochemical controls of nitrogen transport in near-stream zones of temperate-forested catchments: a review.' *Journal of Hydrology* 199, 88-120.

Congalton, R.G., Birch, K., Jones, R. and Schriever, J. (2002) 'Evaluating remotely sensed techniques for mapping riparian vegetation.' *Computers and Electronics in Agriculture* 37, 113-126.

Connolly, R.D., Freebairn, D.M. and Bridge, B.J. (1997) 'Change in Infiltration Characteristics Associated With Cultivation History of Soils in South-Eastern Queensland.' *Australian Journal of Soil Research* 35, 1341-1358.

Cosandey, A.-C., Guenat, C., Bouzelboudjen, M., Maître, V. and Bovier, R. (2003) 'The modelling of soil-process functional units based on three-dimensional soil horizon cartography, with an example of denitrification in a riparian zone.' *Geoderma* 112, 111-129.

Crook, D.A. and Robertson, A.I. (1999) 'Relationships between riverine fish and woody debris: implications for lowland rivers.' *Marine and Freshwater Research* 50, 941-953.

Dalal, R.C. and Chan, K.Y. (2001) 'Soil organic matter in rainfed cropping systems of the Australian cereal belt.' *Australian Journal of Soil Research* 39, 435-464.

Dalal, R.C., Wang, W., Robertson, G.P. and Parton, W.J. (2003) 'Nitrous oxide emission from Australian agricultural lands and mitigation options: a review.' *Australian Journal of Soil Research* 41 (2),:165-195.

Deletic, A. (2001) 'Modelling of water and sediment transport over grassed areas.' *Journal of Hydrology* 248 , 168-182.

Diez, J.R., Elosegi, A. and Pozo, J. (2001) 'Woody Debris in North Iberian Streams: Influence of Geomorphology, Vegetation, and Management.' *Environmental Management* 28, 0687-0698.

Dudley, S.J., Fischenich, J.C. and Abt, S.R. (1998) 'Effect of woody debris entrapment on flow resistance.' *Journal of the American Water Resources Association* 34, 1189-1197.

Erskine, W.D., Saynor, M.J., Erskine, L., Evans, K.G. and Moliere, D.M. (2005) 'A preliminary typology of Australian tropical rivers and implications for fish community ecology.' *Marine and Freshwater Research* 56, 253-267.

Evrendilek, F., Celik, I. and Kilic, S. (2004) 'Changes in Soil Organic Carbon and Other Physical Soil Properties Along Adjacent Mediterranean Forest, Grassland, and Cropland Ecosystems in Turkey.' *Journal of Arid Environments* 59, 743-752.

Fetherston, K.L., Naiman, R.J. and Bilby, R.E. (1995) 'Large woody debris, physical process, and riparian forest development in montane river networks of the Pacific Northwest.' *Geomorphology* 13, 133-144.

Fielding, K.S., Terry, D.J., Masser, B.M., Bordia, P. and Hogg, M.A. (2005) 'Explaining landholders' decisions about riparian zone management: The role of behavioural, normative, and control beliefs.' *Journal of Environmental Management* 77 (1),:12-21.

Flite III, O.P., Shannon, R.D., Schnabel, R.R. and Parizek, R.R. (2001) 'Nitrate removal in a riparian wetland of the Appalachian Valley and Ridge Physiographic Province.' *Journal of Environmental Quality* 30, 254-261.

Francis, C. and Sheldon, F. (2002) 'River Red Gum (Eucalyptus Camaldulensis Dehnh.) Organic Matter as a Carbon Source in the Lower Darling River, Australia.' *Hydrobiologia* 481, 113-124.

Gallant, J.C. and Dowling, T.I. (2003) 'A Multiresolution Index of Valley Bottom Flatness for Mapping Depositional Areas.' *Water Resources Research* 39, p-ESG413

Gerhard, M. and Reich, M. (2000) 'Restoration of streams with large wood: effects of accumulated and built in wood on channel morphology, habitat diversity and aquatic fauna.' *International review of hydrobiology* 85, 123-137 .

Glenn, E.P. and Nagler, P.L. (2005) 'Comparative ecophysiology of Tamarix ramosissima and native trees in western U.S. riparian zones.' *Journal of Arid Environments* 61 (3),:419-446.

Gold, A.J., Groffman, P.M., Addy, K., Kellog, D.Q., Stolt, M. and Rosenblatt, A.E. (2001) 'Landscape attributes as controls on ground water nitrate removal capacity of riparian zones.' *Journal of the American Water Resources Association* 37, 1457-1464.

Goodrich, D.C., Scott, R., Qi, J., Goff, B., Unkrich, C.L., Moran, M.S., Williams, D., Schaeffer, S., Snyder, K., MacNish, R., Maddock, T., Pool, D., Chehbouni, A., Cooper, D.I., Eichinger, W.E., Shuttleworth, W.J., Kerr, Y., Marsett, R. and Ni, W. (2000) 'Seasonal estimates of riparian evapotranspiration using remote and in situ measurements .' *Agricultural & Forest Meteorology* 105, 281-309.

Grayston, S.J., Vaughan, D. and Jones, D. (1997) 'Rhizosphere Carbon Flow in Trees, in Comparison With Annual Plants: the Importance of Root Exudation and Its Impact on Microbial Activity and Nutrient Availability.' *Applied Soil Ecology* 5, 29-56.

Green, A.A., Berman, M., Switzer, P. and Craig, M.D. (1988) 'A transformation for ordering multispectral data in terms of image quality with implications for noise removal.' *IEEE Transactions on Geosciences and Remote Sensing* 26, 65-74.

Gunn, R.H., Galloway, R.W., Pedley, L. and Fitzpatrick, E.A. (1967) *Land Units of the Nogoa and Comet region* Melbourne: CSIRO Publishing.

Gunn, R.H. and Nix, H.A. (1977) *Land Units of the Fitzroy Region, Queensland*, Melbourne: CSIRO Publishing.

Gurnell, A.M., PiéGay, H., Swanson, F.J. and Gregory, S.V. (2002) 'Large Wood and Fluvial Processes.' *Freshwater Biology* 47, 601-619.

Gutiérez, M., Johnson, E. and Mickus, K. (2004) 'Watershed Assessment Along a Segment of the Rio Conchos in Northern Mexico Using Satellite Images.' *Journal of Arid Environments* 56, 395-412.

Hairsine, P.B. and Rose, C.W. (1992a) 'Modeling Water Erosion Due to Overland Flow Using Physical Principles 1. Sheet Flow.' *Water Resources Research* 28, 237-243.

Hairsine, P.B. and Rose, C.W. (1992b) 'Modeling water erosion due to overland flow using physical principles 2. Rill flow.' *Water Resources Research* 245-250.

Hancock, C.N., Ladd, P.G. and Froend, R.H. (1996) 'Biodiversity and management of riparian vegetation in Western Australia.' *Forest Ecology and Management* 85, 239-250.

Harvey, A.M. (1969) 'Channel capacity and adjustment of streams to hydrologic regime.' *Journal of Hydrology* 8, 82-98.

Henderson, C. (2000) Brisbane, QLD: Queensland Department of Natural Resources.

Hill, A.R., Devito, K.J., Campagnolo, S. and Sanmugadas, K. (2000) 'Subsurface Denitrification in a Forest Riparian Zone: Interactions Between Hydrology and Supplies of Nitrate and Organic Carbon.' *Biogeochemistry* 51, 193-223.

Hill, A.R., Vidon, P.G.F. and Langat, J. (2004) 'Denitrification potential in relation to lithology in five headwater riparian zones.' *Journal of Environmental Quality* 33, 911-919.

Hill, M.J., Vickery, P.J., Furnival, P.E. and Donald, G.E. (1999) Pasture Land Cover in Eastern Australia from NOAA-AVHRR NDVI and Classified Landsat TM. *Remote Sensing of Environment* 67, 32-50.

Holt, J.A. (1997) 'Grazing Pressure and Soil Carbon, Microbial Biomass and Enzyme Activities in Semi-Arid Northeastern Australia.' *Applied Soil Ecology* 5, 143-149.

Horton, J.L. and Clark, J.L. (2001) 'Water table decline alters growth and survival of Salix gooddingii and Tamarix chinensis seedlings.' *Forest Ecology and Management* 140 (2-3),:239-247.

Huete, A.R., Liu, H.Q., Batchily, K. and Leeuwen, v.W. (1997) 'A comparison of vegetation indices over a global set of TM images for EOS-MODIS.' *Remote Sensing of Environment* 59, 440-451.

Hutchings, P., Haynes, D., Goudkamp, K. and McCook, L. (2005) 'Catchment to Reef: Water quality issues in the Great Barrier Reef Region—An overview of papers.' *Marine Pollution Bulletin* 51 (1-4),:3-8.

Ibbitt, R.P. (1997) 'Evaluation of optimal channel network and river basin heterogeneity concepts using measured flow and channel properties.' *Journal of Hydrology* 196, 119-138.

Jansen, A., Robertson, A., Thompson, L. and Wilson, A. (2004) Development of a method for rapid appraisal of riparian condition. Land and Water Australia, Canberra.

Jansen, A. and Robertson, A.I. (2001) 'Riparian bird communities in relation to land management practices in floodplain woodlands of south-eastern Australia.' *Biological Conservation* 100, 173-185.

Jansen, J.D. and Nanson, G.C. (2004) 'Anabranching and maximum flow efficiency in Magela Creek, Northern Australia.' *Water Resources Research* 40, 1-12.

Johnson, A.K.L., Ebert, S.P. and Murray, A.E. (1999) 'Distribution of coastal freshwater wetlands and riparian forests in the Herbert River catchment and implications for management of catchments adjacent to the Great Barrier Reef Marine Park.' *Environmental Conservation* 26, 229-235.

Jupp, D.L.B. and Lovell, J. Jupp, D.L.B. and Lovell, J., (Eds.) (2000) CSIRO Earth Observation Centre, Canberra: CSIRO.

Karssies, L. and Prosser, I. (1999) 'Sediment Storage Capacity of a Grass Buffer Strip.' in Second Australian Stream Management Conference. 8th-11th February Adelaide, South Australia.

Kätterer, T., Fabião, A., Madeira, M., Ribeiro, C. and Steen, E. (1995) 'Fine-Root Dynamics, Soil Moisture and Soil Carbon Content in a Eucalyptus Globulus Plantation Under Different Irrigation and Fertilisation Regimes.' *Forest Ecology and Management* 74, 1-12.

Kellndorfer, J., Walker, W., Pierce, L., Dobson, C., Fites, J.A., Hunsaker, C., Vona, J. and Clutter, M. (2004) 'Vegetation Height Estimation From Shuttle Radar Topography Mission and National Elevation Datasets.' *Remote Sensing of Environment* 93, 339-358.

Knighton, A.D. (1999) 'Downstream variation in stream power.' *Geomorphology* 29, 293-306.

Knighton, A.D. and Nanson, G.C. (2000) 'Waterhole form and process in the anastomosing channel system of Cooper Creek, Australia.' *Geomorphology* 35, 101-117.

Knighton, D. (1998) *Fluvial Forms and Processes: A New Perspective*, London, Great Britian: Hodder Headline Group.

Knighton, D.A. and Nanson, G.C. (2002) 'Inbank and overbank velocity conditions in an arid zone anastomosing river.' *Hydrological Processes* 16, 1771-1791.

Kruse, F.A., Lefkoff, A.B., Boardman, J.B., Heidebrecht, K.B., Shapiro, A.T., Barloon, P.J. and Goetz, A.F.H. (1993) 'The Spectral Image Processing System (SIPS) - Interactive Visualization and Analysis of Imaging spectrometer Data.' *Remote Sensing of Environment* 44, 145-163.

Ladson, A., Doolan, J., White, L., Metzeling, L. and Robinson, D. (1996) Index of Stream Condition as a Tool to Aid Management of Rivers. Melbourne: Department of Conservation and Natural Resources.

Lawrence, R.L.R.W.J. (1998) Comparisons among vegetation indices and bandwise regression in a highly disturbed, hetergenous landscape: Mount St Helens, Washington. *Remote Sensing of Environment* 64, 91-102.

Lillesand, T.M., Keifer, R.W. and Chipman, J.W. (2004) *Remote Sensing and Image Interpretation (5th Edition)*, New York: John Wiley and Sons.

Liu, C.P. and Sheu, B.H. (2003) 'Dissolved Organic Carbon in Precipitation, Throughfall, Stemflow, Soil Solution, and Stream Water at the Guandaushi Subtropical Forest in Taiwan.' *Forest Ecology and Management* 172, 315-325.

Loch, R.J., Espigares, T., Costantini, A., Garthe, R. and Bubb, K. (1999) 'Vegetative filter strips to control sediment movement in forest plantations: validation of a simple model using field data.' *Australian Journal of Soil Research* 37, 929-946.

Lopes, A., Nezry, E., Touzi, R. and Laur, H. (1993) 'Structure detection and statistical adaptive speckle filtering in SAR images.' *International Journal of Remote Sensing* 14, 1735-1758.

Luo, J., Tillman, R.W., White, R.E. and Ball, P.R. (1998) 'Variation in denitrification activity with soil depth under pasture.' *Soil Biology & Biochemistry* 30, 897-903.

Marcus, W.A., Legleiter, C.J., Aspinall, R.J., Boardman, J.W. and Crabtree, R.L. (2003) 'High spatial resolution hyperspectral mapping of in-stream habitats, depths, and woody debris in mountain streams.' *Geomorphology* 55, 363-380 .

Marsh, N., Rutherfurd, I., and Jerie, K.'Predicting pre-disturbance loading and distribution of large woody debris.' in Proceedings of the Third Australian Stream Management Conference Rutherfurd, I., Sheldon, F., Brierley, G. and Kenyon, C., (Eds.) edn. 391-395p. Brisbane: CSIRO Publications. (2001)

Martin, M.E., Newman, S.D., Aber, J.D. and Congalton, R.G. (1998) 'Determining forest species composition using high spectral resolution remote sensing data.' *Remote Sensing of Environment* 65, 249-254.

Martz, L.W. and Garbrecht, J. (1992) Numerical definition of drainage network and subcatchment areas from digital elevation models. *Computers and Geosciences* 8, 747-761.

McDonald, R.C., Isbell, R.F., Speight, J.G., Walker, J. and Hopkins, M.S. (1990) *Australian Soil and Land Survey*, Melbourne: Inkata Press.

McKenney, R., Jacobson, R.B. and Wertheimer, R.C. (1995) 'Woody vegetation and channel morphogenesis in low-gradient, gravel-bed streams in the Ozark Plateaus, Missouri and Arkansas.' *Geomorphology* 13, 175-198.

McKergow, L., Prosser, I., and Heiner, D.'Preliminary results on the effectiveness of riparian buffers in Far North Queensland.' in 2nd Australian Stream Management Conference edn.

McKergow, L.A., Prosser, I.P., Hughes, A.O. and Brodie, J. (2005) 'Sources of sediment to the Great Barrier Reef World Heritage Area.' *Marine Pollution Bulletin* 51 (1-4),:200-211.

McKergow, L.A., Weaver, D.M., Prosser, I.P., Grayson, R.B. and Reed, A.E.G. (2003) 'Before and after riparian management: sediment and nutrient exports from a small agricultural catchment, Western Australia.' *Journal of Hydrology* 270, 253-272.

Merritt, D.M. and Wohl, E.E. (2003) 'Downstream hydraulic geometry and channel adjustment during a flood along an ephemeral, arid-region drainage.' *Geomorphology* 52, 165-180.

Montgomery, D.R. and Piégay, H. (2003) 'Wood in rivers: interactions with channel morphology and processes.' *Geomorphology* 51, 1-5.

Muller, E. (1997) 'Mapping riparian vegetation along rivers: old concepts and new methods.' *Aquatic Botany* 58, 411-437.

Muñoz-Carpena, R., Parsons, J.E. and Gilliam, J.W. (1999) 'Modeling hydrology and sediment transport in vegetative filter strips.' *Journal of Hydrology* 214, 111-129.

Noble, R.M., Duivenvoorden, L.J., Rummenie, S.K. , Long, P.E. and Fabbro, L.D. (1997) Brisbane, QLD: Queensland Department of Natural Resources and Mines.

Northup, B.K., Brown, J.R. and Holt, J.A. (1999) 'Grazing impacts on the spatial distribution of soil microbial biomass around tussock grasses in a tropical grassland.' *Applied Soil Ecology* 13, 259-270.

O'brien, N.D., Attiwill, P.M. and Weston, C.J. (2003) 'Stability of Soil Organic Matter in Eucalyptus Regnans Forests and Pinus Radiata Plantations in South Eastern Australia.' *Forest Ecology and Management* 185, 249-261.

O'Reagain, P.J., Brodie, J., Fraser, G., Bushell, J.J., Holloway, C.H., Faithful, J.W. and Haynes, D. (2005) 'Nutrient loss and water quality under extensive grazing in the upper Burdekin river catchment, North Queensland.' *Marine Pollution Bulletin* 51 (1-4),:37-50.

Palis, R.G., Ghandiri, H., Rose, C.W. and Saffigna, P.G. (1997) 'Soil erosion and nutrient loss. III. Changes in the enrichment ratio of total nitrogen and organic carbon under rainfall detachment and entrainment.' *Australian Journal of Soil Research* 35, 891-906.

Pickup, G. (1994) Modelling patterns of defoliation by grazing animals in rangelands. *Journal of Applied Ecology* 31, 231-246.

Pickup, G. and Bastin, G.N. (1997) Spatial distribution of cattle in arid rangelands as detected by patterns of change in vegetation cover. *Journal of Applied Ecology* 34, 657-667.

Pickup, G., Bastin, G.N. and Chewings, V.H. (1998) Identifying trends in rangeland degradation in non-equilibrium rangelands. *Journal of Applied Ecology* 35, 365-377.

Piégay, H. and Gurnell, A.M. (1997) 'Large woody debris and river geomorphological pattern: examples from S.E. France and S. England.' *Geomorphology* 19, 99-116.

Poole, G.C. and Berman, C.H. (2001) 'An Ecological Perspective on In-Stream Temperature: Natural Heat Dynamics and Mechanisms of Human-Caused Thermal Degradation.' *Environmental Management* 27, 787-802.

Powlson, D.S., Saffigna, P.G. and Kragt-Cottaar, M. (1988) 'Denitrification at sub-optimal temperatures in soils from different climatic zones.' *Soil Biology and Biochemistry* 20, 719-723.

Prosser, I., Rustomji, P., Young, B., Moran, C. and Hughes, A. Prosser, I., Rustomji, P., Young, B., Moran, C. and Hughes, A., (Eds.) (2001) Constructing River Basin Sediment Budgets for the National Land and Water Resources Audit. Canberra: CSIRO Publishing.

Prosser, I.P., Dietrich, W.E. and Stevenson, J. (1995) 'Flow resistance and sediment transport by concentrated overland flow in a grassland valley.' *Geomorphology* 13, 71-86.

Prosser, I.P., Rutherfurd, I.D., Olley, J.M., Young, W.J., Wallbrink, P.J. and Moran, C.J. (2001) 'Large-scale patterns of erosion and sediment transport in river networks, with examples from Australia.' *Marine and Freshwater Research* 52, 81-99.

Puckridge, J.T., Sheldon, F., Walker, K.F. and Boulton, A.J. (1998) 'Flow variability and the ecology of large rivers.' *Marine and Freshwater Research* 49, 55-72.

Pusey, B.J. and Arthington, A.H. (2003) 'Importance of the Riparian Zone to the Conservation and Management of Freshwater Fish: a Review.' *Marine and Freshwater Research* 54, 1-16.

Elevation Model of the Nogoa Catchment. Queensland Department of Natural Resources Mines and Energy Digital File: Queensland Department of Natural Resources Mines and Energy. (2001)

Quinn, J.M., Brown, P.M., Boyce, W., Mackay, S., Taylor, A. and Fenton, T. (2001) 'Riparian Zone Classification for Management of Stream Water Quality and Ecosystem Health.' *Journal of the American Water Resources Association* 37, 1509-1515.

Read, M.G., and Barmuta, L.A.(1999) 'Comparisons of benthic communities adjacent to riparian native eucalypt and introduced willow vegetation' *Freshwater Biology* 42 Page 359-374 1999

Reinfelds, I., Cohen, T., Batten, P. and Brierley, G. (2004) 'Assessment of Downstream Trends in Channel Gradient, Total and Specific Stream Power: a Gis Approach.' *Geomorphology* 60, 403-416.

Robertson, A.I., Bunn, S.E. and Boon, P.I.W.K.F. (1999) 'Sources,sinks and transformations of organic carbon in Australian floodplain rivers.' *Marine & Freshwater Research.* 50, 813-829.

Rose, C.W., Hogarth, W.L., Ghadiri, H., Parlange, J.-Y. and Okom, A. (2002) 'Overland flow to and through a segment of uniform resistance.' *Journal of Hydrology* 255, 134-150.

Roth, G., La Barbera, P. and Greco, M. (1996) 'On the description of the basin effective drainage structure.' *Journal of Hydrology* 187, 119-135.

Rovira, P. and Vallejo, V.R. (2002) 'Labile and Recalcitrant Pools of Carbon and Nitrogen in Organic Matter Decomposing at Different Depths in Soil: an Acid Hydrolysis Approach.' *Geoderma* 107, 109-141.

Running, S.W., Loveland, T.R., Pierce, L.L., Nemani, R.R. and Hunt ER. (1995) 'A remote sensing based vegetation classification logic for global land cover analysis.' *Remote Sensing of Environment* 51, 39-48.

Rustomji, P. and Prosser, I. (2001) 'Spatial patterns of sediment delivery to valley floors: sensitivity to sediment transport capacity and hillslope hydrology relations.' *Hydrological Processes* 15, 1003-1018.

Rutherford, J.C., Blackett, S., Blackett, C., Saito, L. and Davies-Colley, R.J. (1997) 'Predicting the effects of shade on water temperature in small streams.' *New Zealand Journal of Marine and Freshwater Research* 31, 707-721.

Schade, J.D., Marti, E., Welter, J.R., Fisher, S.G. and Grimm, N.B. (2002) 'Sources of Nitrogen to the Riparian Zone of a Desert Stream: Implications for Riparian Vegetation and Nitrogen Retention.' *Ecosystems* 5, 0068-0079.

Serena, M., Thomas, J.L., Williams, G.A. and Officer, R.C.E. (1998) 'Use of Stream and River Habitats by the Platypus, Ornithorhynchus Anatinus, in an Urban Fringe Environment.' *Australian Journal of Zoology* 46, 267-282.

Sigunga, D.O., Janssen, B.H. and Oenema, O. (2002) 'Denitrification risks in relation to fertilizer nitrogen losses from vertisols and phaoezems.' *Communications in Soil Science and Plant Analysis* 33, 561-578.

Simon, A. and Collison, A.J.C. (2002) 'Quantifying the mechanical and hydrologic effects of riparian vegetation on streambank stability.' *Earth Surface Processes and Landforms* 27, 527-546.

Specht, R.L. (1970) *The Australian Environment*, Melbourne: CSIRO and University of Melbourne Press .

Sponseller, R.A., Benfield, E.F. and Valett, H.M. (2001) 'Relationships between land use, spatial scale and stream macroinvertebrate communities.' *Freshwater Biology* 46, 1409-1424.

Story, R., Galloway, R.W., Gunn, R.H. and Fitzpatrick, E.A. (1967) *Lands of the Isaac-Comet Area*, Melbourne: CSIRO Publishing.

Strahler, A.N. (1964) Handbook of Applied Hydrology. In: Anonymous *Quantitative geomorphology of drainage basins and channel networks*, pp. 4-39 to 4-76. New York: McGraw-Hill]

Takatert, N., Sánchez-pérez, J.M. and Trémoliéres, M. (1999) 'Spatial and temporal variations of nutrient concentration in the groundwater of a floodplain: effect of hydrology, vegetation and substrate.' *Hydrological Processes* 13 , 1511-1526

Tarboton, D.G. (1997) 'A new method for the determination of flow directions and upslope areas in grid digital elevation models.' *Geomorphology* 33, 309-319.

Tooth, S. and Nanson, G.C. (2000) 'The role of vegetation in the formation of anabranching channels in an ephemeral river, Northern plains, arid central Australia .' *Hydrological Processes* 14, 3099-3117.

Van Zyl, J.J. (2001) 'The Shuttle R0adar Topography Mission (Srtm): a Breakthrough in Remote Sensing of Topography.' *Acta Astronautica* 48, 559-565.

Verry, E.S., Dolloff, C.A. and Manning, M.E. (2004) Riparian ecotone: a functional definition and delineation for resource assessment. *Water, Air and Soil Pollution* 4, 67-94.

Verstraete, M.M., Pinty, B. and Myneni, R.B. (1996) 'Potential and Limitations of Information Extraction on the Terrestrial Biosphere from Satellite Remote Sensing.' *Remote Sensing of Environment* 58, 201-214.

Vogt, J.V., Colombo, R. and Bertolo, F. (2003) 'Deriving drainage networks and catchment boundaries: a new methodology combining digital elevation data and environmental characteristics.' *Geomorphology* 53, 281-298.

Vought, L.B.M., Pinay, G., Fuglsang, A. and Ruffinoni, C. (1995) 'Structure and function of buffer strips from a water quality perspective in agricultural landscapes.' *Landscape and Urban Planning* 31, 323-331.

Walker, J., Jupp, D.L.B., Penridge, L.K. and Tian, G. (1986) 'Interpretation of vegetation structure in Landsat MSS imagery: A case study in distributed semi-arid Eucalupt woodlands. Part 1. Field Data Analysis.' *Journal of Environmental Management* 23, 19-33.

Wallerstein, N.P., Alonso, C.V., Bennett, S.J. and Thorne, C.R. (2001) 'Distorted Froude-scaled flume analysis of large woody debris.' *Earth Surface Processes and Landforms* 26, 1265-1283.

Welty, J.J., Beechie, T., Sullivan, K., Hyink, D.M., Bilby, R.E., Andrus, C. and Pess, G. (2002) 'Riparian Aquatic Interaction Simulator (RAIS): a Model of Riparian Forest Dynamics for the Generation of Large Woody Debris and Shade.' *Forest Ecology and Management* 162, 299-318.

Western, A.W., Finlayson, B.L., McMahon, T.A. and O'Neill, I.C. (1997) 'A method for characterising longitudinal irregularity in river channels.' *Geomorphology* 21, 39-51.

Wilcock, R.J., Scarsbrook, M.R., Costley, K.J. and Nagels, J.W. (2002) 'Controlled release experiments to determine the effects of shade and plants on nutrient retention in a lowland stream.' *Hydrobiologia* 485, 153-162.

Wilkinson, S., Henderson, A. and Chen, Y. (2005) ‘Sednet Users Guide’. Canberra, Australia: CSIRO Land and Water.

Wright, A., Marcus, W.A. and Aspinall, R. (2000) 'Evaluation of multispectral, fine scale digital imagery as a tool for mapping stream morphology.' *Geomorphology* 33, 107-120.

Young, R.A., Onstad, C.A., Bosch, D.D. and Anderson, W.P. (1987) AGNPS, Agricultural Nonpoint Source Pollution. A Watershed Analysis Tool. Washington DC.: US Department of Agriculture.

Appendices

Appendix 1: Additional RFIs

The Pollutant Trapping Index

The pollutant trapping index (PTI) refers to the capacity for riparian zones to trap pollutants carried in shallow overland flow from the adjacent hillslope. The PTI describes one of the important functions served by riparian zones in maintaining water quality for both consumptive and ecological purposes. The pollutant trapping index is described by

$$PTI = 1 - \frac{Mannings' n(current) \;\; N(current)}{Mannings' n(noRZV) \;\; N(noRZV)} \tag{5.7}$$

where, Manning's n(current) is the sediment trapping capacity of the current riparian zone, N(current) is the current concentration of sediment adsorbed nutrients per unit mass of sediment leaving the riparian zone (enrichment ratio), Manning's n(noRZV) is the sediment trapping capacity of the riparian zone without any vegetation, and N(noRZV) is the concentration of sediment adsorbed nutrients per unit mass of sediment that would leave the riparian zone if there was no riparian vegetation. This index follows the approach developed by Hairsine and Rose (1992) with modification based on Palis *et al*. (1990) for sediment-bound nutrient transport. This index could be used to calculate pollutant loads for a range of different pollutants provided that specific enrichment ratio data was available for that pollutant on that soil type. Such information would be of particular interest for areas where the OFI is less than 1.

The Overland Flow Interception Index

Overland flow entering a riparian zone from an adjacent hillslope can be stored in riparian soil. The volume of overland flow that can be stored in the riparian zone is determined by the available soil water storage, which in turn is determined by the width of the riparian zone and the depth and porosity of the riparian soils (Herron and Hairsine, 1998). By reducing the amount of overland flow entering a stream channel riparian soil storage also reduces the amount of flow-transported sediment reaching the stream channel.

This index uses the model of Herron and Hairsine (1998) which defines the riparian ratio Ψ as the ratio of riparian zone width to hill-slope length (expressed as a proportion of the total hill-slope length) required to capture the runoff generated by a 1 in 5 year rainfall event of 30 minutes duration, under soil storage limiting conditions. The model of Herron and Hairsine (1998) has been modified slightly to enable calculation using spatial data. The new model uses hillslope and riparian areas rather than lengths. On this basis the Ψ5 year is defined as

$$\Psi_{5year} = \left[1 + \left(\frac{(pD - PT)}{T(P - I_c)} \right) \right]^{-1} \tag{5.8}$$

where: p is the available porosity; D is the depth to the water table or an impermeable layer; and pD is the product of p and D, P is the precipitation rate of a 1 in 5 year storm event (mm/hr); T is the duration of the rainfall event for a 1 in 5 year storm event (hr) and Ic is the infiltration rate of the hillslope (mm/hr) for a particular land use and soil type. The spatial data inputs for this model are described in section 3 of this paper.

This index is used as a reference point for comparison with current riparian ratio Ψcurrent values as measured using remote sensing and a DEM. The current riparian ratio is given by

$$\Psi_{current} = \left[\frac{A_{RZ}}{A_{RZ} + A_{CZ}} \right] \tag{5.9}$$

where ARZ is the area of the riparian zone, and ACZ is the area of the contributing hillslope. Consequently a new Overland Flow Index (OFI) is defined as

$$OFI = \left(\frac{\Psi_{current}}{\Psi_{5year}} \right) \tag{5.10}$$

The OFI describes the current riparian zone as a proportion of a hypothetical riparian zone that would trap all the runoff generated by a 1 in 5 year storm event. Where the area of the current riparian zone exceeds the amount required to trap all of the runoff, the index will have a value greater than 1; where there is no riparian zone (identifiable via riparian vegetation) the index will approach 0.

Flood Resistance Index

The flood resistance index is important because it allows a quantification of the flood attenuation caused by riparian that can alter local and downstream flood heights, with obvious implication for human infrastructure. The flood attenuation index is based on the relationships between flood attenuation and woody and non-woody riparian vegetation described in Darby (1999) For the purposes of this index, riparian vegetation refers to all vegetation inundated by a 1 in 25 year flood. This flood return period has been chosen primarily because the rainfall records throughout Australia are only long enough to generate the magnitude of a 1 in 25 year rainfall event (that drives the 1 in 25 year flood) with any statistical rigour (Pickup and Marks, 2001), this flood return period was also chosen because it is the large magnitude events that have the largest impact in terms of transporting sediment to the near shore reefs (Mitchell *et al.,* 1997). The formula described in Equation 10 is based on a simplification of the model described in (Darby, 1999) The key simplifications include the removal of a hydraulic model and the omission of any bed material (of the regular channel) parameters. The result is an index that describes the drag imparted by riparian woody and non-woody vegetation based on their respective drag coefficients and the proportional channel width taken up by each vegetation type,

$$FAI = \left[\frac{(W_{WV} \times C_1) + (W_G \times C_2)}{W_{WA}} \right] \tag{5.11}$$

where W_{WV} is the width of woody vegetation (perpendicular to the channel), W_G is the width of grass (or other non woody vegetation) perpendicular to the channel, C_1 and C_2 are coefficients describing the roughness or resistance to flow of the respective vegetation types and, W_{WA} is the width of the wetted perimeter during a 1 in 25 year flood event. This index will scale between 0 and 1, where 0 values represent no riparian vegetation within the wetted perimeter, and 1 would represent woody vegetation and grasses covering the entire wetted perimeter.

Appendix 2 Relationship between LWD and ω

Equations 2 through to 12 in Abernethy and Rutherfurd (1998) can be used to calculate the change in ω for a stream of known bankfull discharge Q and known channel geometry for channels with and without LWD. For the purposes of this thesis, the Equations 2 through to 12 presented in Abernethy and Rutherfurd (1998) are used to calculate the change in ω associated with different LWD loads where LWD load is calculated as a function of the riparian vegetation structure.

$$FAI = \frac{\omega_{\text{current\_LWD}}}{\omega_{\text{reference\_LWD}}} \tag{5.12}$$

where $\omega_{\text{current\_LWD}}$ is the stream power at that location in the stream network based on the amount of LWD in the stream at present, and $\omega_{\text{reference\_LWD}}$ is the stream power at that location in the stream network based on the amount of LWD in the stream prior to European settlement. Equation (5.12) can be re-written into Equation (5.13)

$$FAI = \frac{(\rho gRVS)_{\text{current}}}{(\rho gRVS)_{\text{reference}}} \tag{5.13}$$

given that ρ and g are constants, and assuming that the local energy slope S is not effected by the amount of LWD in the channel, then Equation (5.13) can be calculated using R and V values calculated for the current and reference cases. To calculate these R and V values requires information about the following, the amount of LWD present in the channel in both the current and reference cases, and the influence that this LWD has on R and V. This is done in three steps:

1. Estimating the amount of LWD in the channel at any point in the stream network for both the current and reference cases.
2. Calculating R for the current and reference case.

3. Calculating V for the current and reference case.

Calculating the hydraulic radius *R*

The hydraulic radius R is calculated using Equation (5.14)

$$R = \frac{A_b}{P} \tag{5.14}$$

where A_b is the bankfull cross-sectional area and P is the wetted perimeter. If LWD is present in the channel this reduces the hydraulic radius by reducing the cross-sectional area by a factor indicated by the blockage ratio B. B is calculated using Equation (5.15),

$$B = \frac{A_p}{A_b} \tag{5.15}$$

where A_P is the cross-sectional area that the LWD projects into the flow.

So the hydraulic radius with LWD present is given by R_V as calculated in Equation (5.16)

$$R_V = \frac{A_V}{P} \tag{5.16}$$

where A_v can be calculated according to Equation (5.17)

$$A_v = A_b - B \times A_b \tag{5.17}$$

Channel dimensions measured during the fieldwork, described in Section 3.3, were combined with channel dimensions for stream gauging stations surveyed by the Queensland Department of Natural Resources, Mines, to calculate an average set of channel dimensions for each stream order. For example the average third order stream is X metres wide, Y metres deep, have a hydraulic radius of Z m and a cross-sectional area of ZZ m^2.

Comment [l3]: The final stats for these haven't been calculated yet, and will be updated once they have

This use of an average set of channel dimensions for each stream order ignores the fact that streams of a given Strahler order may have a wide range of contributing areas, may pass through different substrates (*i.e.* bedrock controlled reaches and fluvial sediments), and may or may not anastomose into multiple channels but the use average channel dimensions is necessary in order to estimate P and R for each stream order.

The average set of channel dimensions, the values for which are described in Section 0, was used to calculate the channels hydraulic radius with the current load of LWD $R_{vCURRENT}$, and the hydraulic radius of the channel with LWD loads predicted for pre-settlement conditions $R_{vREFERENCE}$. This was done by using the A_p for either case to calculate the blockage ratio for either case $B_{CURRENT}$ and $B_{REFERENCE}$,, which in turn is entered into Equation (5.17) to calculate $A_{vCURRENT}$ and $A_{vREFERENCE}$. These A_v values are then entered into Equation (5.16) to calculate $R_{vCURRENT}$ and $R_{vREFERENCE}$ It is worth noting that if there is no LWD present in the channel, then $B_{CURRENT}$ equals zero and therefore

A_{vCURRENT} equals A_{b} so the hydraulic radius for the channel $R_{vCURRENT}$ would be equal to the hydraulic radius R as calculated in Equation (5.14)

Calculating bankfull flow velocity *V*

From Abernethy and Rutherfurd (1998) we know that the influence of LWD on flow velocity can be expressed in terms of the increase in the Darcy-Weisbach friction factor f due to LWD according to Equation (5.18)

Comment [I4]: Equations 2.51 through to 2.55 come directly from Abernethy and Rutherfurd (1998), is it sufficient to cite the paper as it is at present or should each equation in the original paper be referred to individually?

$$f_v = \frac{4}{\alpha}\chi \tag{5.18}$$

where α is the kinetic energy correction factor (1.15), χ is dimensionless and is derived for a reach averaged projected area A_{p} using Equation (5.19)

$$\chi = \frac{C_{\mathrm{d}} A_{\mathrm{p}}}{CW} \tag{5.19}$$

where CW is the channel width and C_{d} is given by Equation (5.20)

$$C_{\mathrm{d}} = \frac{C_{\mathrm{d}}'}{0.997(1 - B)^{2.06}} \tag{5.20}$$

where C_{d}' is the drag coefficient of LWD in flow with no boundary effects. C_{d}' is dependent on the median angle of LWD pieces to the flow, where the median angle of the LWD pieces is perpendicular to the flow, as was observed for even the largest streams within the study area, C_{d}' is equal to 0.6, and this is the value used for all streams in the study. If we assume that gauging stations in the study area have not been desnagged (Carroll pers com 2005) then the total Darcy-Weisbach friction factor f_t can be calculated using Equation (5.21) (which is Equation 6b in Abernethy and Rutherfurd (1998) rewritten so that the symbols used are consistent with the rest of the thesis).

$$f_{t\mathrm{REFERENCE}} = \frac{8gR_{\mathrm{vREFERENCE}}S}{V_{\mathrm{vREFERENCE}}^2} \tag{5.21}$$

the where $R_{\mathrm{Vreference}}$ is calculated as described above, S is the average slope for a stream of that stream order, and $V_{\mathrm{vREFERENCE}}$ is the velocity of bank full flow for a channel that hasn't been desnagged. The friction due to all other factors aside from the LWD, f_b can be calculated by Equation (5.22)

$$f_b = f_{t\mathrm{REFERENCE}} - f_{v\mathrm{REFERENCE}} \tag{5.22}$$

where $f_{vREFERENCE}$ is the Darcy Weisbach friction values due to LWD, as calculated by Equation (5.18) for the reference case.

If we assume that the friction due to all other factors aside from LWD hasn't changed since pre-settlement, and that the channel geometry has remained constant, then f_b can be considered constant, and $f_{tCURRENT}$ can be calculated using Equation (5.23).

$$f_{tCURRENT} = f_b + f_{vCURRENT} \tag{5.23}$$

where $f_{vCURRENT}$ is the Darcy-Weisbach friction factor due to LWD, as calculated by Equation (5.18) for the current case.

Based on Equation 7a in Abernethy and Rutherfurd (1998) $V_{REFERENCE}$ can be calculated from bank full discharge Q according to Equation (5.24)

$$V_{\text{REFERENCE}} = \frac{Q}{A_{\text{vREFERENCE}}} \tag{5.24}$$

and based on Equation 7b in Abernethy and Rutherfurd (1998) $V_{CURRENT}$ can be calculated using Equation (5.25)

$$V_{\text{CURRENT}} = \sqrt{\frac{8gR_{\text{vCURRENT}}S}{f_{\text{tCURRENT}}}} \tag{5.25}$$

Measurements of Q are only available for higher order (3rd-6th) streams within the study area, consequently Q was estimated for low order streams in the study area by correlating Q against catchment area, and estimating Q for 1st and 2nd order streams based on the average catchment area for each stream order. Using the parameters calculated as described above Equation (5.13) can now be calculated as shown in Equation (5.26).

$$FAI = \frac{\left(\rho g R_{\text{vCURRENT}} V_{\text{CURRENT}} S\right)}{\left(\rho g R_{\text{vREFERENCE}} V_{\text{REFERENCE}} S\right)} \tag{5.26}$$

Given that ρ and g are common to both terms and assuming that the local energy slope S isn't altered by the presence/absence of LWD then Equation (5.26) can be rewritten to Equation (5.27)

$$FAI = \frac{R_{\text{vCURRENT}} V_{\text{CURRENT}}}{R_{\text{vREFERENCE}} V_{\text{REFERENCE}}} \tag{5.27}$$

The FAI as calculated by Equation (5.27) will provide an estimate as to the change in the erosive force of bank full flow between pre-settlement and current day at any given point in the channel (local reference). In terms of identifying areas where the erosive forces are highest throughout the catchment *i.e.* those areas most prone to fluvial attack, based on a global reference, then Equation (5.26) would be used.

It is worth noting that areas with similar FAI values may not necessarily have the same bank erosion rates, this is due to two factors: firstly, two areas with similar FAI values may have different BRI values, and if bank collapse due to mass failure (rather than fluvial attack) is an active process at either site then the bank erosion rates are likely to differ. This is not likely to be a major factor because the FAI and BRI values are positively correlated because both indices are calculated based on vegetation structure, and specifically the number of trees per area (λ); secondly two areas with the same stream power ω may experience different rates of bank erosion depending on the cohesion of the bank material. Data about the spatial distribution of the cohesive strength of bank material are not available for the study area, and consequently areas with the same FAI values may experience different levels of bank erosion.

Comment [I5]: Peter, the FAI as presented up until this point differs to all other indices in this thesis in that it combines information about the riparian vegetation on both banks to describe their influence on an in-stream process, whereas all other indices focus on the influence that an individual stand of RV has on a process. At this point I go on to describe how each stand of veg influences fluvial attack, so that an index can be calculated for a stand on either stream bank (as opposed to the FAI above which is calculated for the channel). I suspect that the FAI calculated so far could provide some very interesting results in terms of bank erosion (which is why I've left the details in) but I could easily move it to an appendix, or omit it all together.

Calculating the reduction in fluvial attack afforded by a stand of riparian vegetation

As described previously riparian vegetation influences fluvial attack by reducing the hydraulic radius of the channel by the blockage ratio B and increasing the Darcy-Weisbach friction factor by an amount described by f_v. The FAI described above integrates the effect of riparian vegetation on either bank by combining inputs from both banks. The calculations detauiled below describe the influence of a stand of vegetation on B and f_v respectively. This is done by calculating B and f_v for half a channel width, based on the assumption that the LWD between the centre line of the channel and the bank comes solely from that bank. This assumption is likely to be violated in narrow streams when the median length of the LWD pieces exceeds half the channel width.

To calculate the influence of the riparian vegetation on one bank on B , let the value of A_{p} for a single bank be (A_{pSB}), then B for a single bank B_{SB} can be calculated using Equation (5.28)

$$B_{SB} = \frac{A_{pSB}}{A_b / 2} \qquad (5.28)$$

Likewise the influence of riparian vegetation on one bank on the Darcy-Weisbach friction factor f_v for a single bank $f_{V\mathrm{sb}}$ can be calculated by combining Equation (5.18) and Equation (5.19) to form Equation (5.29)

$$f_{v\mathrm{SB}} = \frac{4}{\alpha} \bullet \frac{A_{\mathrm{pSB}} C_{\mathrm{d}}}{\mathrm{CW}/2} \qquad (5.29)$$

For a stand of riparian vegetation the reduction in the rate of fluvial attack (FA_{SB}) afforded by that stand of vegetation can be expressed simply by Equation (5.30).

$$FA_{SB} = B_{SB} + f_{vSB} \qquad (5.30)$$

Where both B_{SB} and f_{vSB} are functions of the volume of LWD adjacent to one stream bank, and the volume of LWD in the channel is a function of the volume of standing timber of the bank top vegetation This FA_{SB} term is only meaningful in comparison with a local reference point, such as that shown in Equation (5.31) because it assumes that all other factors such as slope and the Darcy Weisbach friction factor due to non-vegetative elements f_b are equal.

$$FAI_{SB} = \frac{FA_{SB}^{\mathrm{Current}}}{FA_{SB}^{\mathrm{Reference}}} \qquad (5.31).$$

Appendix 3 Estimating bank-average c_r

The material cohesion due to roots, c_r was found to decrease exponentially with depth, and decrease exponentially with distance from the base of the tree as described by Equation (5.32).

$$c_r = e^{k+lC+mD} \tag{5.32}$$

where C is the horizontal distance from the centre of the tree and D is the soil depth.

(Abernethy and Rutherfurd, 2001) present two sets of values for the coefficients k, l, and m based on observations made on two riparian species *Eucalyptus camaldulensis* and *Melaleuca ericifolia* in the LaTrobe valley in Victoria.

The k, l, and m coefficients presented in (Abernethy and Rutherfurd, 2001) enabled the calculation of c_r values as they relate to an average *Eucalyptus camaldulensis* and *Melaleuca ericifolia* in the LaTrobe valley in Victoria. To calculate the BRI it was necessary to calculate c_r values for a stream bank with a vegetation type *vt* on top of the stream bank. In order to do this a number of steps were required.

1. Estimating the c_r for the average tree in a stand of vegetation by calculating the k, l, and m coefficients for that stand of vegetation.
2. Calculating the total c_r for the average tree in a stand of vegetation by integrating Equation (5.32) over soil depth and distance from the centre of the tree
3. Calculating the average c_r for a stream bank based on the total c_r for each tree along the top of the bank and the average distance between the trees.

Estimating the coefficients of the c_r equation for a tree based canopy radius

Canopy dimensions of each vegetation type *vt* were used to calculate the k, l, and m coefficients because the dominant riparian species were different to those described in Abernethy and Rutherfurd (2001), this was done as follows. From Abernethy and Rutherfurd (2001) we know that at the dripline of the vegetation (for both species in that study) the additional cohesion due to root reinforcement is equal to material cohesion ($c = c_r$) at 40cm depth. For *Eucalyptus camaldulensis* $c = c_r$ at a depth of 1.7 metres below the tree trunk $(C = 0)$ and the line of equivalence where $c = c_r$ is shown for *E. camaldulensis* in Figure 0.1.

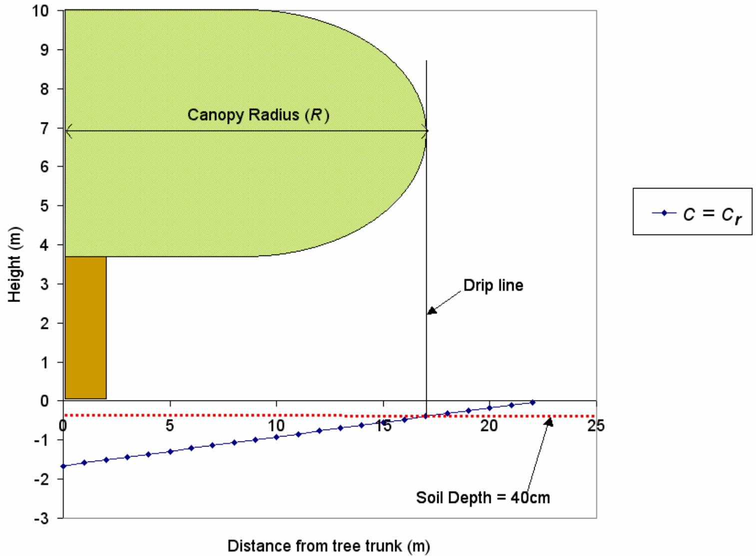

Figure 0.1 Location of the $c = c_r$ line for *Eucalyptus camaldulensis* based on Equation 8 in (Abernethy and Rutherfurd, 2001)

If we assume that for all canopy radii R the line $c = c_r$ occurs at a soil depth of 40cm and passes through the intercept of the two observed $c = c_r$ lines as shown in Figure 0.2. Then it is possible to estimate the location of the line $c = c_r$ for any R. The green line shown in Figure 0.2 represents the average R value of vegetation type vt based on field data. The estimation of the $c = c_r$ line process, shown in Figure 0.2 is based on the assumption that the root distribution of the various riparian tree species in the study area will be the same as the two tree species described in Abernethy and Rutherfurd (2001). This assumption is likely to be violated if the subsoil composition limits root distribution, which has been observed at some locations in the study area (Story *et al*., 1967), but this assumption is necessary in the absence of any c_r measurements from within the study area. If these assumptions are accepted then it is possible to estimate the The k, and l coefficients using Equations (5.33) to (5.37)

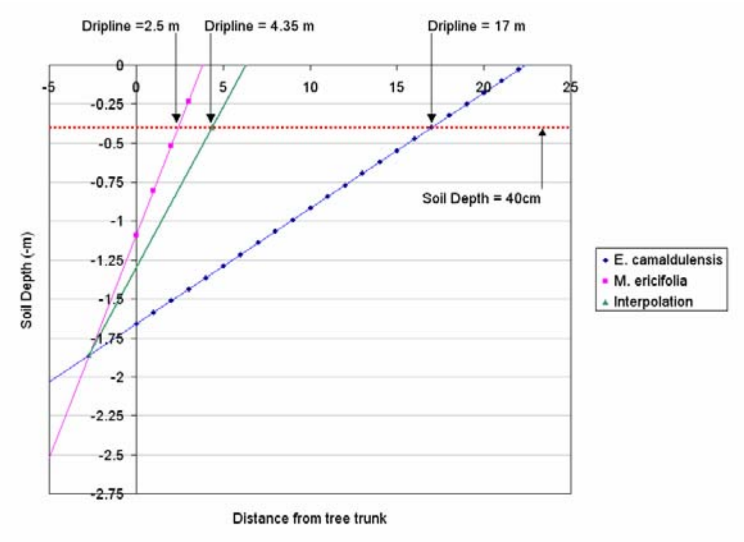

Figure 0.2 Interpolating $c = c_r$ line for the average dripline of trees observed in the field data using equations 8 and 9 contained in (Abernethy and Rutherfurd, 2001)

The coefficients *l* and *m* can be calculated from the interpolated $c = c_r$ line based on the rearrangement of Equation (5.32) contained in Equation (5.33)

$$\ln(c_r) = k + lC + mD \tag{5.33}$$

therefore, rearranging Equation (5.33) to solve for lC

$$lC = \ln(c_r) - k - mD \tag{5.34}$$

and solving for l

$$l = \frac{\ln(c_r) - k - mD}{C} \tag{5.35}$$

and at the point where the line $c = c_r$ intercepts the soil surface, $D = 0$ so

$$l_{(D=0)} = \frac{\ln\left(c_r\right) - k}{C} \tag{5.36}$$

Similarly, directly beneath the tree trunk $C = 0$ and m can be calculated using by rearranging Equation (5.33) using the steps shown above, but this time solving for m as described in Equation (5.37)

$$m_{(C=0)} = \frac{\ln\left(c_r\right) - k}{D} \tag{5.37}$$

The values for k can be calculated using linear interpolation between the two k values reported in Abernethy and Rutherfurd (2001) as shown in Figure 0.3

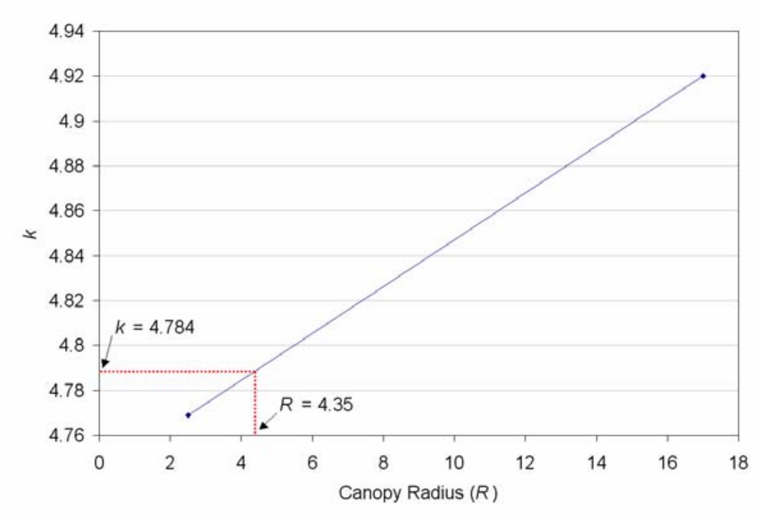

Figure 0.3 Linear interpolation of *k* values for a canopy radius *R*.

Using the steps described above the average canopy radius for each vegetation type observed in the study area $\overline{R}_{VT}$ were used to calculate the *k*,*l*, and *m* coefficients for each vegetation type *vt*. These coefficients were in turn used to describe the c_r equation for individual trees in that vegetation type $c_{r\_VT\_TREE}$ as shown in Equation.

$$c_{r\_VT\_TREE} = e^{k_{VT} + l_{VT}C + m_{VT}D} \tag{5.38}$$

For example for closed forest with an $\overline{R}_{VT}$ of 4.35 metres the $c_{r\_VT\_TREE}$ equation is given by Equation (5.39)

$$c_{r\_VT\_TREE} = e^{4.784 - 0.330C - 1.597D} \tag{5.39}$$

Calculating the total c_r value for an average tree

To calculate the total c_r value for an average tree the following steps were taken.

1. Calculate a maximum value for the C parameter (C_{MAX}) based on the average distance between trees.
2. Calculate a maximum value for the D parameter (D_{MAX}) based on bank height.
3. Integrate Equation (5.38) between 0 and C_{MAX} and 0 and D_{MAX} to calculate the total c_r value for each tree.

If 0 is the base of the channel, and BH is the bank height, then let $D_{MAX} = BH$ The value of c_r can be integrated over soil depth D as shown in Equation (5.40)

$$c_{r\_INT\_D} = \int_0^{D_{MAX}} e^{k_{vt}+l_{vt}C+m_{vt}D} \partial D \tag{5.40}$$

Solving Equation (5.40) gives Equation (5.41)

$$c_{r\_INT\_D} = \frac{e^{(k+l_{vt}C)} \times \left(1-e^{m_{vt}D_{MAX}}\right)}{m_{vt}} \tag{5.41}$$

Which can in turn be integrated between the centre of the tree (0) and a maximum distance from the centre of the tree C_{MAX} as shown in Equation (5.42)

$$c_{r\_INT\_DandC} = \int_0^{C_{MAX}} \frac{e^{(k_{vt}+l_{vt}C)} \times \left(-1+e^{m_{vt}D_{MAX}}\right)}{m_{vt}} \partial C \tag{5.42}$$

Where C_{MAX} is calculated as half the distance to the nearest tree.

If we assume that the root system of one tree will not overlap with the root system of another then C_{MAX} can therefore be calculated using Equation (5.43)

$$C_{MAX} = NND / 2 \tag{5.43}$$

Using C_{MAX} figures calculated from the field data we are then able to solve Equation (5.42) as shown in Equation (5.44)

$$c_{r\_INT\_DandC} = \frac{e^{k_{vt}} \times (-1+e^{m_{vt}D_{MAX}}) \times (-1+e^{l_{vt}C_{MAX}})}{l_{vt} \times m_{vt}} \tag{5.44}$$

The value calculated by Equation (5.44) is shown in Figure 2.2 in dark grey. The total c_r for each tree c_{r_TREE} is calculated as twice this value (both grey areas in Figure 2.2) as according to Equation (5.45)

$$c_{r\_TREE} = 2 \times c_{r\_INT\_DandC} \tag{5.45}$$

Appendix 4: LWD unit conversion

The following steps were used to convert the m3 m^{-1} units used in Marsh *et al.* (2001) to the m3 m^{-3} units used in Abernethy and Rutherfurd (2001) and this thesis

1. Calculate the volume of standing timber per linear metre of channel (VEGd m^3 m^{-1}) for each vegetation class from the fieldwork data.

2. Calculate the volume of LWD adjacent to each linear metre of stream bank based on the density of the bank top vegetation (LWD m^3m^{-1}) using the correlation between VEGd and LWD described in Equation (2.53).

3. Calculate the total volume of LWD per cubic metre of stream channel (m^3 m^{-3}), and dividing by the volume of the channel

4. Calculate the square metres of LWD projected into the channel cross section (m^2 m^{-2}) assuming that the LWD pieces have a random orientation.

Marsh *et al*. (2001) describes the parameter VEGd in terms of the volume of standing timber for the bank-top vegetation per linear metre of channel. So the area from which the VEGd parameter is calculated is given by Equation (5.46)

$$VEGd_{AREA} = \left(\overline{OS} + \overline{DBH}\right) \times L \tag{5.46}$$

where $\overline{OS}$ is the average offset between the edge of the channel and the base of the first tree, and $\overline{DBH}$ is the average diameter at breast height, and L is a length of the stream bank as shown in Figure 0.4

The field work data (described in detail in Chapters 3 and 4) is used to calculate the number of trees per unit area, λ, as given by Equation (5.47) and volume of standing wood for each tree as calculated by Equation (5.48)

$$\lambda = \frac{Ntrees}{Area} \tag{5.47}$$

Where *Ntrees* is the number of trees

$$wood_T = \pi \left(\frac{DBH}{2}\right)^2 \times TH \tag{5.48}$$

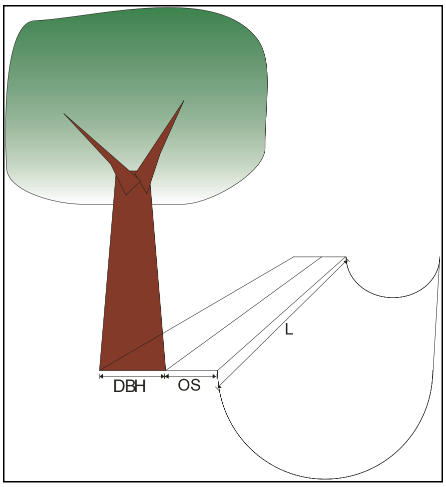

Figure 0.4 Figure showing area calculation to estimate LWD recruitment

Where *DBH* is the diameter at breast height (m), and *TH* is the tree height (m). This formula assumes that the volume of wood for each tree can be described as a cylinder with these dimensions, which is consistent with the calculations for volumes of wood contained in Marsh *et al*. (2001). The volume of wood per unit area (m^3 ha^{-1}) $wood_A$ can be calculated using Equation (5.49)

$$wood_A = \lambda \times \overline{wood_T} \tag{5.49}$$

where $\overline{wood_T}$ is the average volume of wood per tree (m^3). Substituting Equation (5.49) into Equation (5.47) gives Equation (5.50)

$$wood_A = \frac{Ntrees \times \overline{wood_T}}{Area} \tag{5.50}$$

To calculate the volume of wood for the bank top vegetation for a length of stream bank, *l*, substitute Equation (5.50) into Equation (5.46) to give Equation (5.51)

$$wood_A = \frac{Ntrees \times \overline{wood_T}}{\left(\overline{OS} + \overline{DBH}\right) \times l} \tag{5.51}$$

Re-arranging Equation (5.51) gives Equation (5.52)

$$wood_A \times \left(\overline{DBH} + \overline{OS}\right) = \frac{Ntress \times \overline{wood_T}}{l} \tag{5.52}$$

By definition the volume of wood per unit length of stream bank (VEGd) is given by Equation (5.53)

$$VEGd = \frac{Ntrees \times \overline{wood_T}}{l} \tag{5.53}$$

So, based on the terms common to Equations (5.52) and (5.53)

$$VEGd = wood_A \times \left(\overline{OS} + \overline{DBH}\right) \tag{5.54}$$

So the substituting Equation (5.54) into (2.53) the volume of wood in a channel adjacent to a bank with a volume of standing timber $wood_A$ is given by Equation (5.55)

$$LWD = 0.2\left(wood_A \times \left(\overline{OS} + \overline{DBH}\right)\right) - 0.054 \tag{5.55}$$